SEISMIC FRAGILITY AND RETROFITTING FOR

A REINFORCED CONCRETE FLAT-SLAB STRUCTURE

A Thesis

by

JONG-WHA BAI

Submitted to the Office of Graduate Studies of
Texas A&M University
in partial fulfillment of the requirements for the degree of

MASTER OF SCIENCE

May 2004

Major Subject: Civil Engineering

SEISMIC FRAGILITY AND RETROFITTING FOR

A REINFORCED CONCRETE FLAT-SLAB STRUCTURE

A Thesis

by

JONG-WHA BAI

Submitted to Texas A&M University
in partial fulfillment of the requirements
for the degree of

MASTER OF SCIENCE

Approved as to style and content by:

Mary Beth D. Hueste (Chair of Committee)	Joseph M. Bracci (Member)
Terry Kohutek (Member)	Paul Roschke (Head of Department)

May 2004

Major Subject: Civil Engineering

ABSTRACT

Seismic Fragility and Retrofitting for a Reinforced Concrete Flat-Slab Structure.

(May 2004)

Jong-Wha Bai, B.S., Yonsei University

Chair of Advisory Committee: Dr. Mary Beth D. Hueste

The effectiveness of seismic retrofitting applied to enhance seismic performance was assessed for a five-story reinforced concrete (RC) flat-slab building structure in the central United States. In addition to this, an assessment of seismic fragility that relates the probability of exceeding a performance level to the earthquake intensity was conducted. The response of the structure was predicted using nonlinear static and dynamic analyses with synthetic ground motion records for the central U.S. region. In addition, two analytical approaches for nonlinear response analysis were compared.

FEMA 356 (ASCE 2000) criteria were used to evaluate the seismic performance of the case study building. Two approaches of FEMA 356 were used for seismic evaluation: global-level and member-level using three performance levels (Immediate Occupancy, Life Safety and Collapse Prevention). In addition to these limit states, punching shear drift limits were also considered to establish an upper bound drift capacity limit for collapse prevention. Based on the seismic evaluation results, three possible retrofit techniques were applied to improve the seismic performance of the structure, including addition of shear walls, addition of RC column jackets, and confinement of the column plastic hinge zones using externally bonded steel plates.

Finally, fragility relationships were developed for the existing and retrofitted structure using several performance levels. Fragility curves for the retrofitted structure were compared with those for the unretrofitted structure. For various performance levels

to assess the fragility curves, FEMA global drift limits were compared with the drift limits based on the FEMA member-level criteria. In addition to this, performance levels which were based on additional quantitative limits were also considered and compared with FEMA drift limits.

DEDICATION

To my father who went to heaven during my M.S. degree. He was the person who understood me, supported me so that I could continue my study, and encouraged me all the time. He was a model to me for everything in my life. He was a great father.

ACKNOWLEDGMENTS

I would like to gratefully acknowledge my advisor, Dr. Mary Beth D. Hueste, for her guidance and support throughout my graduate studies and the enormous effort she made to revise this document and make possible my graduation. I also wish to sincerely acknowledge the contribution of Dr. Joseph M. Bracci and Terry Kohutek for their guidance and helpful review of this document.

I wish to acknowledge the National Science Foundation and the University of Illinois who funded this research through the Mid-America Earthquake Center under 'CM-4 Structure Retrofit Strategies' project (NSF Grant Number EEC-9701785). I also wish to acknowledge the financial support provided by the Department of Civil Engineering at Texas A&M University. I wish to thank Dr. Amr Elnashai, who is a Co-PI on the same project, and Seong-Hoon Jeong, a graduate student at the University of Illinois at Urbana-Champaign, for their technical guidance.

Special thanks to my wife, Namhee Kim, for her love and encouragement all the time. I would like to thank my family and my friends in Korea for their support and friendship. I also wish to thank all of my friends in College Station and Austin for their prayer, support and encouragement to complete this work. Finally, thanks to God.

TABLE OF CONTENTS

Page

Page

Page

Page

LIST OF FIGURES

Page

Page

Page

Page

Page

Page

LIST OF TABLES

Page

Page

Page

Page

1 INTRODUCTION

1.1 Background

1.1.1 General

Improved understanding of the dynamic behavior and seismic performance of structures has led to new advances in earthquake engineering in recent years. In particular, the performance-based design approach allows for selection of a specific performance objective based on various parameters, including the owner's requirements, the functional utility of the structure, the seismic risk, and the potential economic losses. In spite of these recent advances, many structures in the central United States (U.S.) were not designed for seismic resistance until after the 1989 Loma Prieta earthquake in San Francisco, California and the 1994 Northridge, California earthquake. The presence of the New Madrid seismic zone in the central U.S. led to increased concern for the seismic vulnerability of structures in this area. Because structures in the central U.S. built before the 1990s were not designed according to the current seismic design codes, it is important to evaluate these structures and improve the seismic resistance of systems that are found to be vulnerable. To strengthen structural systems that are found to be deficient, practitioners use various seismic retrofit techniques.

1.1.2 Retrofit of Reinforced Concrete Structures

Many existing structures located in seismic regions are inadequate based on current seismic design codes. In general, buildings that were constructed before the 1970s have significant deficiencies in their overall structural configuration, such as discontinuity of positive reinforcement in beams and slabs, or wide spacing of transverse reinforcement. In addition, a number of major earthquakes during recent years have increased the importance of mitigation to reduce seismic risk. Seismic retrofit of existing

---

This thesis follows the style and format of the *ASCE Journal of Structural Engineering.*

structures is one method to mitigate the risk that currently exists. Recently, a significant amount of research has been devoted to the study of various retrofit techniques to enhance the seismic performance of reinforced concrete (RC) structures.

1.1.3 New Madrid Seismic Zone

The New Madrid Seismic Zone (NMSZ) lies within the central Mississippi Valley, extending from northeast Arkansas, through southeast Missouri, western Tennessee, and western Kentucky to southern Illinois. In North America, the largest series of earthquakes is known as the New Madrid Earthquakes. The New Madrid Earthquakes consisted of three major earthquakes between 1811 and 1812, with magnitude estimates greater than 7.0 in Richter scale, and hundreds of aftershocks that followed over a period of several years (Nuttli 1982).

There are several differences between earthquakes in the NMSZ and those that occur in the western U.S. The most important difference is that the earth's crust in the Midwest region attenuates energy 25% as effectively as the earth's crust in the western U.S. As a result, earthquakes in the central U.S. affect much larger areas than earthquakes of similar magnitude in the western U.S. (Shedlock and Johnston 1994). Another significant difference is the recurrence interval. The estimated recurrence interval for NMSZ earthquakes, such as the New Madrid Earthquakes in 1811-12, is 600 years, while the corresponding estimated recurrence interval for the western U.S. is 100 years. This results in the probability of exceeding a particular ground motion in the NMSZ being smaller than that of the western U.S. by a factor of two to three (McKeown 1982).

1.1.4 Mid-America Earthquake Center

This study is part of the Mid-America Earthquake (MAE) Center project CM-4 "Structure Retrofit Strategies." The MAE Center is developing a new paradigm called Consequence-Based Engineering (CBE) to evaluate the seismic risk across regions or

systems. CBE incorporates identification of uncertainty in all components of seismic risk modeling and quantifies the risk to societal systems and subsystems enabling policy-makers and decision-makers to ultimately develop risk reduction strategies and implement mitigation actions. The core research thrust areas are Damage Synthesis, Hazard Definition, and Consequence Minimization. This project is included in the Consequence Minimization thrust area. More information about the CBE paradigm is provided by Abrams et al. (2002).

1.2 Scope and Purpose

The objectives of this study are to evaluate the seismic vulnerability of a typical 1980s RC building in the central U.S. and to determine the improvement in the seismic performance for various seismic retrofit techniques. Fragility curves were developed to reflect the alteration of response characteristics due to the application of selected intervention techniques to the case study structure. By developing fragility curves that link measures of earthquake intensity to the probability of exceeding specific performance levels for the existing and retrofitted structure, the improvement in seismic performance was evaluated. In order to compute global structural parameters, such as stiffness, strength and deformation capacity; nonlinear static (push-over) analysis and nonlinear dynamic (time history) analysis was conducted for the RC structure. The results of the push-over analysis were compared with nonlinear time-history analysis to evaluate how closely the push-over analysis estimates the dynamic, nonlinear response of the structure.

1.3 Methodology

The particular tasks that were performed to achieve the main objectives of this research are summarized below.

Task 1: Identification of Case Study Structure

Lightly reinforced RC building structures were selected as the structural system of interest for this study. The selected case study building is a five-story RC flat slab structure that is not specially detailed for ductile behavior. Low to moderate rise flat-slab buildings were found to be of particular interest because they are common in the central U.S. and because there is a concern for potential damage to this type of structure during an earthquake of moderate intensity. After the type of structural system and overall dimensions were defined, the structure was designed according to the load requirements in the 1980s building code used in this region.

Task 2: Analytical Studies for Unretrofitted Case Study Building

Push-over and nonlinear dynamic analyses were performed using two different structural analysis programs to investigate the case study building. For the push-over analysis, the distribution of lateral loads over the building height included the typical first mode and rectangular (uniform) load patterns. All push-over analysis results were compared to nonlinear time history analysis results to determine how well the push-over analysis represents the dynamic response of the structure at the system level. Ground motions for the cities of St. Louis, Missouri and Memphis, Tennessee were used in this analysis. Because no recorded strong motion data from New Madrid Seismic Zone earthquakes are available, synthetic ground motions were used.

Task 3: Evaluate Unretrofitted Case Study Building

Based on the analytical results, seismic evaluations were conducted using FEMA 356 performance criteria. FEMA 356 suggests two approaches for seismic evaluation: global-level and member-level using three performance levels (Immediate Occupancy, Life Safety and Collapse Prevention). For global-level evaluation, the maximum interstory drifts for each floor level were determined based on nonlinear dynamic analysis results. The member-level evaluation of FEMA 356 using plastic rotation limits was also performed to determine more detailed information for structural behavior and

seismic performance. The case study building was evaluated to determine if the expected seismic response was acceptable for different performance levels. Nonlinear time-history analysis was performed using sets of synthetic ground motion records corresponding to both two percent and ten percent probabilities of exceedance in 50 years for St. Louis, Missouri and Memphis, Tennessee.

Task 4: Review and Select Relevant Intervention Techniques

The fourth task involved review of relevant seismic retrofit techniques for RC structures, especially flat-slab RC buildings. The goal of this task was to gather information in the literature for the most effective seismic intervention techniques that primarily modify the stiffness, strength or deformation capacity of a structure. Several different intervention techniques were selected and evaluated for the case study structure.

Task 5: Develop Fragility Curves

Fragility curves were developed using global- and member-level performance criteria for the existing and retrofitted structures.

1.4 Outline

This thesis is organized as follows. The introduction in Section 1 presents a brief background, scope, purpose and methodology for this study. Section 2 summarizes previous related research that was useful as guidance for this study. Section 3 describes the case study building. In Section 4, the ground motion data and analytical modeling procedures are discussed. Section 5 presents results from the nonlinear static and dynamic analyses for the unretrofitted case study building. In addition, the seismic evaluation and the fragility analysis performed for the existing building are summarized. Section 6 presents retrofit techniques, analytical results and fragility curves of the retrofitted case study building. Finally, Section 7 summarizes the results of the study, and presents conclusions and recommendations based on this research.

2 LITERATURE REVIEW

2.1 Introduction

This section provides the background of performance-based design, structural analysis, seismic vulnerability evaluation and seismic retrofit techniques for RC buildings. The topics included are general information and a review of previous research related to the above areas.

2.2 Performance-Based Design

Performance-based design means that the general process of the design is based on selective performance objectives. This concept provides a new approach to establishing design objectives and desired performance levels. Recently, ATC-40 (ATC 1996) and FEMA 273 (FEMA 1997a) provided guidelines for the evaluation and more reliable performance-based seismic retrofitting of existing buildings, while the Vision 2000 (SEAOC 1995) report applied this concept to new construction. According to Vision 2000, a performance objective is defined as "an expression of the desired performance level for each earthquake design level." Multiple performance objectives due to the diverse needs of owners should be considered within this performance-based design criteria. These performance objectives could be classified from the state where collapse is prevented to reduce damage and casualties to the state of operation based on the opinion of the group; such as building owners, users, insurance company and others. As a result of this concept, it is possible to predict demand and capacity and then evaluate the seismic performance of structures.

Krawinkler (1999) narrowed down this concept and focused on earthquake engineering, which is called performance-based earthquake engineering. Performance-based earthquake engineering consists of all the required procedures including site

selection, development of conceptual, preliminary and final structural designs, evaluation, and construction. The major procedure includes selection of performance objectives, conceptual design, design evaluation and modification, and socio-economic evaluation.

As the performance-based design paradigm become more accepted for new structures, seismic retrofitting and rehabilitation methods have been affected by this concept. Consequently, retrofitting procedures can be selected and applied so that the performance objective of the retrofit depends upon the importance of the structure and the desired structural performance during a seismic event with a particular recurrence interval.

2.3 Structural Analysis

2.3.1 General

FEMA 356 (ASCE 2000) outlines four different analysis procedures for a performance-based evaluation of a structure: the linear static procedure, the linear dynamic procedure, the nonlinear static procedure (push-over analysis), and the nonlinear dynamic procedure. In this study, push-over analysis and nonlinear dynamic analysis were conducted to estimate the nonlinear response characteristics of a case study structure.

2.3.2 Linear Procedures

The linear analysis procedures provided in FEMA 356 consist of linear static and linear dynamic analysis. When the linear static or dynamic procedures are used for seismic evaluation, the design seismic forces, the distribution of applied loads over the height of the buildings, and the corresponding displacements are determined using a linear elastic analysis. It is difficult to obtain accurate results for structures that undergo

nonlinear response through linear procedures. Therefore, linear procedures may not be used for irregular structures, according to the FEMA 356 guidelines.

2.3.3 Nonlinear Procedures

Nonlinear procedures consist of nonlinear static and nonlinear dynamic analyses. A nonlinear static analysis, also known as a push-over analysis, consists of laterally pushing the structure in one direction with a certain lateral force or displacement distribution until either a specified drift is attained or a numerical instability has occurred. Because linear procedures have limitations and nonlinear dynamic procedures are complicated, nonlinear static analysis is commonly used by many engineers. This procedure has gained popularity in recent years as a relatively simple way to evaluate the design of a structure and predict the sequence of damage in the inelastic range of behavior. Both ATC-40 (ATC 1996) and FEMA 273 (FEMA 1997a) adopted an approach for performance evaluation based on nonlinear static analysis. Hueste and Wight (1999) discussed the concept and detailed the procedure of this analysis.

The nonlinear dynamic procedure (dynamic time history analysis) provides a more accurate estimate of the dynamic response of the structure. However, because the results computed by the nonlinear dynamic procedure can be highly sensitive to characteristics of individual ground motions, the analysis should be carried out with more than one ground motion record. This is also true for the linear dynamic analysis. FEMA 356 provides guidelines regarding the required number of ground motions that should be used for dynamic analysis.

Lew and Kunnath (2002) investigated the effectiveness of nonlinear static analysis in predicting the inelastic behavior of four case study structures: a six-story steel moment frame building, a thirteen-story steel moment-resisting frame building, a seven-story RC moment frame building and a twenty-story RC moment frame building. According to Lew and Kunnath (2002), the maximum displacement profiles predicted by

both nonlinear static and dynamic procedures were similar. However, nonlinear static analysis did not give a good estimate of the interstory drift values compared to nonlinear dynamic analysis. In this study, interstory drifts were generally underestimated at upper levels and overestimated at lower levels.

2.4 Seismic Vulnerability Evaluation

2.4.1 FEMA 356 (ASCE 2000)

2.4.1.1 General

The *Prestandard and Commentary for the Seismic Rehabilitation of Buildings* – FEMA 356 (ASCE 2000) is used to evaluate the expected seismic performance of existing structures using performance levels that are defined qualitatively. The provisions and commentary of this standard are primarily based on FEMA 273 (FEMA 1997a) and FEMA 274 (FEMA 1997b). FEMA 356 covers general information and methodology for seismic rehabilitation of existing building structures. This document begins by introducing rehabilitation objectives according to seismic performance level and discussing the general seismic rehabilitation process. The document also describes general requirements, such as as-built information, and provides an overview of rehabilitation strategies. Finally, the details of the four possible analysis procedures and the methodology for member-level evaluation according to each structural type are explained.

2.4.1.2 Rehabilitation Objectives

The rehabilitation objectives must be selected by the building owner or code official prior to evaluation of the existing building and selection of a retrofit, if needed. FEMA 356 presents many possible rehabilitation objectives that combine different target building performance levels with associated earthquake hazard levels, as shown in Table 2.1. FEMA 356 defines performance levels related to the structural system as follows.

(1) Immediate Occupancy (IO) – Occupants are allowed immediate access into the structure following the earthquake and the pre-earthquake design strength and stiffness are retained.

(2) Life Safety (LS) – Building occupants are protected from loss of life with a significant margin against the onset of partial or total structural collapse.

(3) Collapse Prevention (CP) – Building continues to support gravity loading, but retains no margin against collapse.

Table 2.1. FEMA 356 rehabilitation objectives (adapted from ASCE 2000)

		Target building performance levels			
		Operational performance level (1-A)	Immediate occupancy performance level (1-B)	Life safety performance level (1-C)	Collapse prevention performance level (1-D)
Earthquake hazard level	50% / 50 years	a	b	c	d
	20% / 50 years	e	f	g	h
	BSE - 1 10% / 50 years	i	j	k	l
	BSE - 2 2% / 50 years	m	n	o	p

Notes:

1. Each cell in the above matrix represents a discrete Rehabilitation Objective.
2. The Rehabilitation Objectives in the matrix above may be used to represent the three specific Rehabilitation Objectives defined in Section 1.4.1, 1.4.2, and 1.4.3 of FEMA 356, as follows:

   k+p = Basic Safety Objective (BSO)
   k+p+any of a, e, i, b, j, or n = Enhanced Objectives
   o alone or n alone or m alone = Enhanced Objectives
   k alone or p alone = Limited Objective
   c, g, d, h, l = Limited Objective

2.4.1.3 Global-Level Approach

FEMA 356 defines a wide range of structural performance requirements for the specific limit state. Limits are given for many types of structures including concrete frames, steel moment frames, braced steel frames, concrete walls, unreinforced masonry infill walls, unreinforced masonry walls, reinforced masonry walls, wood stud walls,

precast concrete connections and foundations. Suggested global-level drift limits for concrete frames and concrete walls are in Table 2.2 for three performance levels.

Table 2.2. Structural performance levels and damage – vertical elements (adapted from ASCE 2000)

		Structural performance levels		
Elements	Type	Collapse prevention S-5	Life safety S-3	Immediate occupancy S-1
Concrete frames	Primary	Extensive cracking and hinge formation in ductile elements. Limited cracking and/or splice failure in some nonductile columns. Severe damage in short columns.	Extensive damage to beams. Spalling of cover and shear cracking (<1/8" width) for ductile columns. Minor spalling in nonductile columns. Joint cracks <1/8" wide.	Minor hairline cracking. Limited yielding possible at a few locations. No crushing (strains below 0.003).
	Secondary	Extensive spalling in columns (limited shortening) and beams. Severe joint damage. Some reinforcing buckled.	Extensive cracking and hinge formation in ductile elements. Limited cracking and/or splice failure in some nonductile columns. Severe damage in short columns.	Minor spalling in a few places in ductile columns and beams. Flexural cracking in beams and columns. Shear cracking in joints <1/16" width.
	Drift	4% transient or permanent	2% transient; 1% permanent	1% transient; negligible permanent
Concrete walls	Primary	Major flexural and shear cracks and voids. Extensive crushing and buckling of reinforcement. Failure around openings. Severe boundary element damage. Coupling beams shattered and virtually disintegrated.	Some boundary element stress, including limited buckling of reinforcement. Some sliding at joints. Damage around openings. Some crushing and flexural cracking. Coupling beams: extensive shear and flexural cracks; some crushing, but concrete generally remains in place.	Minor hairline cracking of walls, <1/16" wide. Coupling beams experience cracking <1/8" width.
	Secondary	Panels shattered and virtually disintegrated.	Major flexural and shear cracks. Sliding at joints. Extensive crushing. Failure around openings. Severe boundary element damage. Coupling beams shattered and virtually disintegrated.	Minor hairline cracking of walls. Some evidence of sliding at construc-tion joints. Coupling beams experience cracks <1/8" width. Minor spalling.
	Drift	2% transient or permanent	1% transient; 0.5% permanent	0.5% transient; negligible permanent

2.4.1.4 Member-Level Approach

FEMA 356 classifies the structural types by materials, such as steel, concrete, masonry, wood and light metal framing. For each structural type, FEMA 356 describes the procedure for evaluating seismic performance based on member-level limits. For instance, in Chapter 6, the seismic evaluation of concrete structures includes member-level limits for concrete moment frames, precast concrete frames, concrete frames with infills, concrete shear walls, precast concrete shear walls, concrete-braced frames, cast-in-place concrete diaphragms, precast concrete diaphragms and concrete foundation elements.

Several categories of concrete moment frames are addressed by FEMA 356, including RC beam-column moment frames, prestressed concrete beam-column moment frames, and slab-column moment frames. For concrete moment frames, the plastic rotation of each member is used as a parameter to assess inelastic behavior. Plastic rotation is defined as the amount of rotation beyond the yield rotation of the member. FEMA 356 provides the maximum permissible plastic rotation corresponding to each performance level. Tables 2.3 to 2.7 show the modeling parameters and numerical acceptance criteria for RC beams, RC columns, RC beam-column joints, two-way slabs and slab-column connections, and members controlled by flexure, respectively.

Table 2.3. FEMA 356 modeling parameters and numerical acceptance criteria for nonlinear procedures - RC beams (adapted from ASCE 2000)

Conditions			Modeling parameters[3]			Acceptance criteria[3]				
			Plastic rotation angle, radians		Residual strength ratio	Plastic rotation angle, radians				
						Performance level				
							Component type			
							Primary		Secondary	
			a	b	c	IO	LS	CP	LS	CP
i. Beams controlled by flexure[1]										
$\frac{\rho-\rho'}{\rho_{bal}}$	Transverse Reinforce-ment[2]	$\frac{V}{b_w d\sqrt{f'_c}}$								
≤ 0.0	C	≤ 3	0.025	0.05	0.2	0.01	0.02	0.025	0.02	0.05
≤ 0.0	C	≥ 6	0.02	0.04	0.2	0.005	0.01	0.02	0.02	0.04
≥ 0.5	C	≤ 3	0.02	0.03	0.2	0.005	0.01	0.02	0.02	0.03
≥ 0.5	C	≥ 6	0.015	0.02	0.2	0.005	0.005	0.015	0.015	0.02
≤ 0.0	NC	≤ 3	0.02	0.03	0.2	0.005	0.01	0.02	0.02	0.03
≤ 0.0	NC	≥ 6	0.01	0.015	0.2	0.0015	0.005	0.01	0.01	0.015
≥ 0.5	NC	≤ 3	0.01	0.015	0.2	0.005	0.01	0.01	0.01	0.015
≥ 0.5	NC	≥ 6	0.005	0.01	0.2	0.0015	0.005	0.005	0.005	0.01
ii. Beams controlled by shear[1]										
Stirrup spacing ≤ d/2			0.003	0.02	0.2	0.0015	0.002	0.003	0.1	0.02
Stirrup spacing ≥ d/2			0.003	0.01	0.2	0.0015	0.002	0.003	0.005	0.01
iii. Beams controlled by inadequate development or splicing along the span[1]										
Stirrup spacing ≤ d/2			0.003	0.02	0	0.0015	0.002	0.003	0.1	0.02
Stirrup spacing ≥ d/2			0.003	0.01	0	0.0015	0.002	0.003	0.005	0.01
iv. Beams controlled by inadequate embedment into beam-column joint[1]										
			0.015	0.03	0.2	0.01	0.01	0.015	0.02	0.03

Notes:

1. When more than one of the conditions i, ii, iii, and iv occurs for a given component, use the minimum appropriate numerical value from the table.
2. "C" and "NC" are abbreviations for conforming and nonconforming transverse reinforcement. A component is conforming if, within the flexural plastic hinge region, hoops are spaced at ≤ d/3, and if, for components of moderate and high ductility demand, the strength provided by the hoops (V_s) is at least three-fourths of the design shear. Otherwise, the component is considered nonconforming.
3. Linear interpolation between values listed in the table shall be permitted.

Table 2.4. FEMA 356 modeling parameters and numerical acceptance criteria for nonlinear procedures - RC columns (adapted from ASCE 2000)

Conditions			Modeling parameters[4]			Acceptance criteria[4]				
			Plastic rotation angle, radians		Residual strength ratio	Plastic rotation angle, radians				
						Performance level				
							Component type			
							Primary		Secondary	
			a	b	c	IO	LS	CP	LS	CP
i. Columns controlled by flexure[1]										
$\frac{P}{A_g f'_c}$	Transverse Reinforce-ment[2]	$\frac{V}{b_w d\sqrt{f'_c}}$								
≤ 0.1	C	≤ 3	0.02	0.03	0.2	0.005	0.015	0.02	0.02	0.03
≤ 0.1	C	≥ 6	0.016	0.024	0.2	0.005	0.012	0.016	0.016	0.024
≥ 0.4	C	≤ 3	0.015	0.025	0.2	0.003	0.012	0.015	0.018	0.025
≥ 0.4	C	≥ 6	0.012	0.02	0.2	0.003	0.01	0.012	0.013	0.02
≤ 0.1	NC	≤ 3	0.006	0.015	0.2	0.005	0.005	0.006	0.01	0.015
≤ 0.1	NC	≥ 6	0.005	0.012	0.2	0.005	0.004	0.005	0.008	0.012
≥ 0.4	NC	≤ 3	0.003	0.01	0.2	0.002	0.002	0.003	0.006	0.01
≥ 0.4	NC	≥ 6	0.002	0.008	0.2	0.002	0.002	0.002	0.005	0.008
ii. Columns controlled by shear[1, 3]										
All cases[5]			-	-	-	-	-	-	0.003	0.004
iii. Columns controlled by inadequate development or splicing along the clear height[1, 3]										
Hoop spacing ≤ d/2			0.01	0.02	0.4	0.005	0.005	0.01	0.01	0.02
Hoop spacing ≥ d/2			0	0.01	0.2	0	0	0	0.005	0.01
iv. Columns with axial loads exceeding $0.70P_o$[1, 3]										
Conforming hoops over the entire length			0.015	0.025	0.02	0	0.005	0.01	0.01	0.02
All other cases			0	0	0	0	0	0	0	0

Notes:

1. When more than one of the conditions i, ii, iii, and iv occurs for a given component, use the minimum appropriate numerical value from the table.
2. "C" and "NC" are abbreviations for conforming and nonconforming transverse reinforcement. A component is conforming if, within the flexural plastic hinge region, hoops are spaced at ≤ d/3, and if, for components of moderate and high ductility demand, the strength provided by the hoops (V_s) is at least three-fourths of the design shear. Otherwise, the component is considered nonconforming.
3. To qualify, columns must have transverse reinforcement consisting of hoops. Otherwise, actions shall be treated as force-controlled.
4. Linear interpolation between values listed in the table shall be permitted.
5. For columns controlled by shear, see Section 6.5.2.4.2 for acceptance criteria.

Table 2.5. FEMA 356 modeling parameters and numerical acceptance criteria for nonlinear procedures - RC beam-column joints (adapted from ASCE 2000)

Conditions			Modeling parameters[4]			Acceptance criteria[4]				
			Plastic rotation angle, radians		Residual strength ratio	Plastic rotation angle, radians				
						Performance level				
							Component type			
							Primary		Secondary	
			a	b	c	IO	LS	CP	LS	CP
i. Interior joints[2, 3]										
$\frac{P}{A_g f'_c}$	Transverse Reinforcement	$\frac{V}{V_n}$ [3]								
≤ 0.1	C	≤ 1.2	0.015	0.03	0.2	0	0	0	0.02	0.03
≤ 0.1	C	≥ 1.5	0.015	0.03	0.2	0	0	0	0.015	0.02
≥ 0.4	C	≤ 1.2	0.015	0.025	0.2	0	0	0	0.015	0.025
≥ 0.4	C	≥ 1.5	0.015	0.02	0.2	0	0	0	0.015	0.02
≤ 0.1	NC	≤ 1.2	0.005	0.02	0.2	0	0	0	0.015	0.02
≤ 0.1	NC	≥ 1.5	0.005	0.015	0.2	0	0	0	0.01	0.015
≥ 0.4	NC	≤ 1.2	0.005	0.015	0.2	0	0	0	0.01	0.015
≥ 0.4	NC	≥ 1.5	0.005	0.015	0.2	0	0	0	0.01	0.015
ii. Other joints[2, 3]										
$\frac{P}{A_g f'_c}$	Transverse Reinforce-ment[1]	$\frac{V}{V_n}$								
≤ 0.1	C	≤ 1.2	0.01	0.02	0.2	0	0	0	0.015	0.02
≤ 0.1	C	≥ 1.5	0.01	0.015	0.2	0	0	0	0.01	0.015
≥ 0.4	C	≤ 1.2	0.01	0.02	0.2	0	0	0	0.015	0.02
≥ 0.4	C	≥ 1.5	0.01	0.015	0.2	0	0	0	0.01	0.015
≤ 0.1	NC	≤ 1.2	0.005	0.01	0.2	0	0	0	0.0075	0.01
≤ 0.1	NC	≥ 1.5	0.005	0.01	0.2	0	0	0	0.0075	0.01
≥ 0.4	NC	≤ 1.2	0	0	-	0	0	0	0.005	0.0075
≥ 0.4	NC	≥ 1.5	0	0	-	0	0	0	0.005	0.0075

Notes:

1. "C" and "NC" are abbreviations for conforming and nonconforming transverse reinforcement. A joint is conforming if hoops are spaced at ≤ $h_c/3$ within the joint. Otherwise, the component is considered nonconforming.
2. P is the design axial force on the column above the joint and A_g is the gross cross-sectional area of the joint.
3. V is the design shear force and V_n is the shear strength for the joint. The design shear force and shear strength shall be calculated according to Section 6.5.2.3.
4. Linear interpolation between values listed in the table shall be permitted.

Table 2.6. FEMA 356 modeling parameters and numerical acceptance criteria for nonlinear procedures – two-way slabs and slab-column connections (adapted from ASCE 2000)

Conditions		Modeling parameters[4]			Acceptance criteria[4]				
		Plastic rotation angle, radians		Residual strength ratio	Plastic rotation angle, radians				
					Performance level				
						Component type			
						Primary		Secondary	
		a	b	c	IO	LS	CP	LS	CP
i. Slabs controlled by flexure, and slab-column connections[1]									
$\frac{V_g}{V_o}$ [2]	Continuity Reinforce-ment[3]								
≤ 0.2	Yes	0.02	0.05	0.2	0.01	0.015	0.02	0.03	0.05
≥ 0.4	Yes	0	0.04	0.2	0	0	0	0.03	0.04
≤ 0.2	No	0.02	0.02	-	0.01	0.015	0.02	0.015	0.02
≥ 0.4	No	0	0	-	0	0	0	0	0
ii. Slabs controlled by inadequate development or splicing along the span[1]									
		0	0.02	0	0	0	0	0.01	0.02
iii. Slabs controlled by inadequate embedment into slab-column joint[1]									
		0.015	0.03	0.2	0.01	0.01	0.015	0.02	0.03

Notes:

1. When more than one of the conditions i, ii, iii, and iv occurs for a given component, use the minimum appropriate numerical value from the table.
2. V_g = the gravity shear acting on the slab critical section as defined by ACI 318; V_o = the direct punching shear strength as defined by ACI 318
3. Under the heading "Continuity Reinforcement," use "Yes" where at least one of the main bottom bars in each direction is effectively continuous through the column cage. Where the slab is post-tensioned, use "Yes" where at least one of the post-tensioning tendons in each direction passes through the column cage. Otherwise, use "No."
4. Linear interpolation between values listed in the table shall be permitted.

Table 2.7. FEMA 356 modeling parameters and numerical acceptance criteria for nonlinear procedures – member controlled by flexure (adapted from ASCE 2000)

Conditions			Modeling Parameters			Acceptance Criteria				
			Plastic Rotation Angle, radians		Residual Strength Ratio	Plastic Rotation Angle, radians				
						Performance Level				
							Component Type			
							Primary		Secondary[4]	
			a	b	c	IO	LS	CP	LS	CP
i. Shear walls and wall segments										
$\frac{(A_s - A_s')f_y + P}{t_w l_w f_c'}$	$\frac{Shear}{t_w l_w \sqrt{f_c'}}$	Confined Boundary[1]								
≤ 0.1	≤ 3	Yes	0.015	0.02	0.75	0.005	0.01	0.015	0.015	0.02
≤ 0.1	≥ 6	Yes	0.01	0.015	0.4	0.004	0.008	0.01	0.01	0.015
≥ 0.25	≤ 3	Yes	0.009	0.012	0.6	0.003	0.006	0.009	0.009	0.012
≥ 0.25	≥ 6	Yes	0.005	0.01	0.3	0.0015	0.003	0.005	0.005	0.01
≤ 0.1	≤ 3	No	0.008	0.015	0.6	0.002	0.004	0.008	0.008	0.015
≤ 0.1	≥ 6	No	0.006	0.01	0.3	0.002	0.004	0.006	0.006	0.01
≥ 0.25	≤ 3	No	0.003	0.005	0.25	0.001	0.002	0.003	0.003	0.005
≥ 0.25	≥ 6	No	0.002	0.004	0.2	0.001	0.001	0.002	0.002	0.004
ii. Columns supporting discontinuous shear walls										
Transverse reinforcement[2]										
Conforming			0.01	0.015	0.2	0.003	0.007	0.01	n.a.	n.a.
Nonconforming			0	0.01	0.2	0	0	0	n.a.	n.a.
iii. Shear wall coupling beams										
Longitudinal reinforcement and transverse reinforcement[3]	$\frac{Shear}{t_w l_w \sqrt{f_c'}}$									
Conventional longitudinal reinforcement with conforming transverse reinforcement	≤ 3		0.025	0.05	0.75	0.01	0.02	0.025	0.025	0.05
	≥ 6		0.02	0.04	0.5	0.005	0.01	0.02	0.02	0.04
Conventional longitudinal reinforcement with nonconforming transverse reinforcement	≤ 3		0.02	0.035	0.5	0.006	0.012	0.02	0.02	0.035
	≥ 6		0.01	0.025	0.25	0.005	0.008	0.01	0.01	0.025
Diagonal reinforcement	n.a.		0.03	0.05	0.8	0.006	0.018	0.03	0.03	0.05

Notes:

1. Requirements for a confined boundary are the same as those given in ACI 318.
2. Requirements for conforming transverse reinforcement in columns are: (a) hoops over the entire length of the column at a spacing ≤ d/2, and (b) strength of hoops $V_s \geq$ required shear strength of column.
3. Conventional longitudinal reinforcement consists of top and bottom steel parallel to the longitudinal axis of the coupling beam. Conforming transverse reinforcement consists of: (a) closed stirrups over the entire length of the coupling beam at a spacing ≤ d/3, and (b) strength of closed stirrups $V_s \geq 3/4$ of required shear strength of the coupling beam.
4. For secondary coupling beams spanning < 8'-0", with bottom reinforcement continuous into the supporting walls, secondary values shall be permitted to be doubled.

2.4.2 Fragility Curves

According to Wen et al. (2003), a fragility curve is defined as "the probability of entering a specified limit state conditioned on the occurrence of a specific hazard, among the spectrum of hazards." Wen et al. (2003) defines a vulnerability function as "the probability of incurring losses equal to (or greater than) a specified monetary unit, conditioned on the occurrence of an earthquake with a specified intensity."

The vulnerability of a structure is determined by a probabilistic relation between the predicted limit state and some measure of the earthquake demand, such as spectral acceleration (S_a), peak ground acceleration (PGA) probability of recurrence, or a specified ground motion magnitude. Therefore, the evaluation of the seismic vulnerability of a building requires knowledge of the dynamic response of the structure and potential for damage under a certain seismic demand.

Limit state probability, $P_t[LS]$, is defined as the probability of a set of given limit states of a system being reached at a given location over a given period of time (0, t), calculated as follows (Wen et al. 2003).

$$P_t[LS] = \Sigma\, P[LS|D=d]\, P[D=d] \qquad (2.1)$$

where:

$P_t[LS]$	=	Probability of a given limit state (LS) for a system being reached over a given period of time (0,t).
D	=	Spectrum of uncertain hazards.
d	=	Control of interface variable, such as occurrence of a specific hazard intensity.
P[LS|D=d]	=	*fragility* = Conditional limit state probability, given that D=d, and the summation is taken over all values of D.
P[D=d]	=	Defines the hazard in terms of a probabilistic density function (or cumulative distribution function, P[D>d]).

For estimating the fragility of the structure, if demand is a prescribed excitation intensity measure, such as spectral acceleration, then identical systems located in different seismic regions will have different fragility curves because of varying degrees of nonlinear structural behavior due to differences in representative ground motions. Therefore, the structural fragility has uncertainty in both the seismic demand and the capacity.

2.4.3 Additional Literature

Many research studies related to seismic evaluation have been conducted. In particular, after developing the performance-based design concept, the methodology of seismic evaluation for existing buildings that are inadequate based on current seismic design codes was developed. Recently, research related to seismic vulnerability and the methodology of developing fragility curves has been actively conducted.

Hassan and Sozen (1997) described the seismic vulnerability of low-rise buildings with and without masonry infilled walls damaged by the 1992 Erzincan earthquake in Turkey. In addition, Gulkan and Sozen (1999) proposed a method to select buildings with higher seismic vulnerability based on wall and column indices relating the effective cross-sectional area to the total area of each member.

Shinozuka et al. (2000a) developed empirical fragility curves for the Hanshin Expressway Public Corporations' (HEPC's) bridges for the 1995 Kobe earthquake. In addition, analytical fragility curves were obtained for bridges in Memphis, Tennessee and these fragility curves were estimated by statistical procedures. In addition, Shinozuka et al. (2000b) applied nonlinear static procedures to develop fragility curves for the bridges in Memphis. Synthetic ground motion generated by Hwang and Huo (1996) were used in this study. A fragility curve developed using the capacity spectrum method (CSM), which is a simplified approach, was compared with a fragility curve developed using nonlinear dynamic analysis. The fragility curve developed using the

CSM showed good agreement for the region of minor damage, but the comparison was not as good for the region of major damage where nonlinear effects control structural systems.

Dumova-Jovanoska (2000) developed fragility curves for two RC structures (6-story and 16-story frame structures) in Skopje, Macedonia using 240 synthetic ground motion data for this region. The fragility curves were developed using discrete damage states from the damage index defined by Park et al. (1985).

Shama et al. (2002) investigated seismic vulnerability analysis for bridges supported by steel pile bents. They developed fragility curves for the original and retrofitted bridge probabilistically based on the uncertainties in demand and capacity. This curve showed that the retrofitting was effective for this bridge type.

Reinhorn et al. (2002) introduced a method for developing global seismic fragility of a RC structure with shear walls by a simplified approach in which fragility is evaluated from the spectral capacity curve and the seismic demand spectrum. The performance limit states which were investigated by Hwang and Huo (1994) were used to evaluate the seismic fragility of the structure. The investigation showed that the inelastic response was influenced by structural parameters such as yield strength, damping ratio and post-yielding stiffness ratio. In addition, they investigated the influence between the fragility of structure and structural parameters including strength, stiffness and damping. While the effect for strength and stiffness were not very significant, the influence of variation of damping significantly affected the fragility.

2.5 Seismic Retrofit Techniques for RC Structures

2.5.1 General

Generally, there are two ways to enhance the seismic capacity of existing structures. The first approach is based on strength and stiffness, which involves global modifications to the structural system (see Fig. 2.1). Common global modifications include the addition of structural walls, steel braces, or base isolators. The second approach is based on deformation capacity (see Fig. 2.2). In this approach, the ductility of components with inadequate capacities is increased to satisfy their specific limit states. The member-level retrofit includes methods such as the addition of concrete, steel, or fiber reinforced polymer (FRP) jackets to columns for confinement.

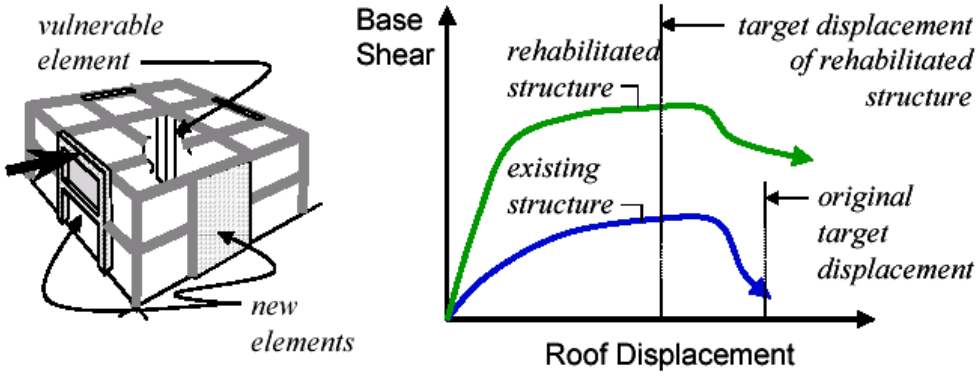

Fig. 2.1. Global modification of the structural system (Moehle 2000)

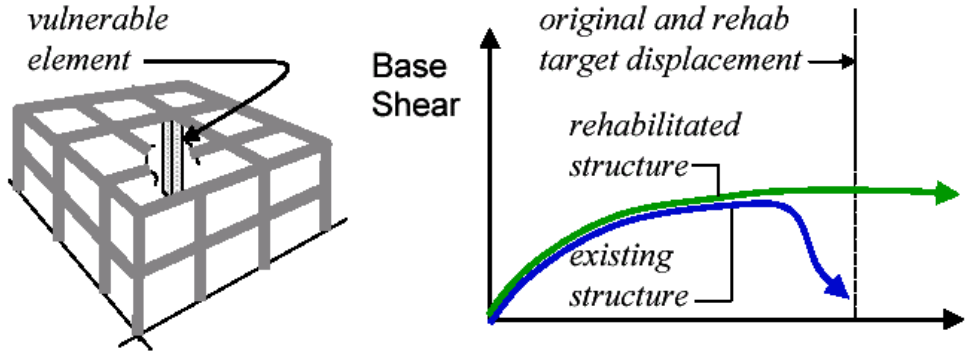

Fig. 2.2. Local modification of structural components (Moehle 2000)

There are many seismic retrofit techniques available, depending upon the various types and conditions of structures. Therefore, the selection of the type of intervention is a complex process, and is governed by technical as well as financial and sociological considerations. The following are some factors affecting the choice of various intervention techniques (Thermou and Elnashai 2002).

- Cost versus importance of the structure
- Available workmanship
- Duration of work/disruption of use
- Fulfillment of the performance goals of the owner
- Functionally and aesthetically compatible and complementary to the existing building
- Reversibility of the intervention
- Level of quality control
- Political and/or historical significance
- Structural compatibility with the existing structural system
- Irregularity of stiffness, strength and ductility
- Adequacy of local stiffness, strength and ductility
- Controlled damage to non-structural components
- Sufficient capacity of foundation system
- Repair materials and technology available

2.5.2 Structure-Level Retrofit

Structure-level retrofits are commonly used to enhance the lateral resistance of existing structures. Such retrofits for RC buildings include steel braces, post-tensioned cables, infill walls, shear walls, masonry infills, and base isolators. The methods described below are commonly used when implementing a structure-level retrofit technique.

2.5.2.1 Addition of RC Structural Walls

Adding structural walls is one of the most common structure-level retrofitting methods to strengthen existing structures. This approach is effective for controlling global lateral drifts and for reducing damage in frame members. Generally, repair of an existing shear wall or infilling one of the bays in the frame structure is used. In order to reduce time and cost, shotcrete or precast panels can be used.

Many research studies have been conducted for structural walls, and findings corresponding to detailed interventions have been reported (Altin et al. 1992, Pincheira and Jirsa 1995, Lombard et al. 2000, Inukai and Kaminosono 2000). The research shows that with the infilling process, details play an important role in the response of panels and the overall structure. The infilling process tends to stiffen the structure such that the base shear can increase. The overturning effects and base shear are concentrated at the stiffer infill locations. Therefore, strengthening of the foundation is typically required at these locations.

Jirsa and Kreger (1989) tested one-story infill walls using four specimens. In their experiment, they used three one-bay, single-story, non-ductile RC frames that were designed to represent 1950s construction techniques. These included wide spacing in the column shear reinforcement and compression splices that were inadequate to develop the required tensile yield strength. In their experiment, the first three walls varied in their opening locations. Longitudinal reinforcement was added adjacent to the existing columns to improve the continuity of the steel in the fourth specimen. The first three experiments had brittles failures due to the deficient column lap splices, even though the infill strengthened the frame. The fourth specimen enhanced both the strength and ductility of the frame (see Fig. 2.3).

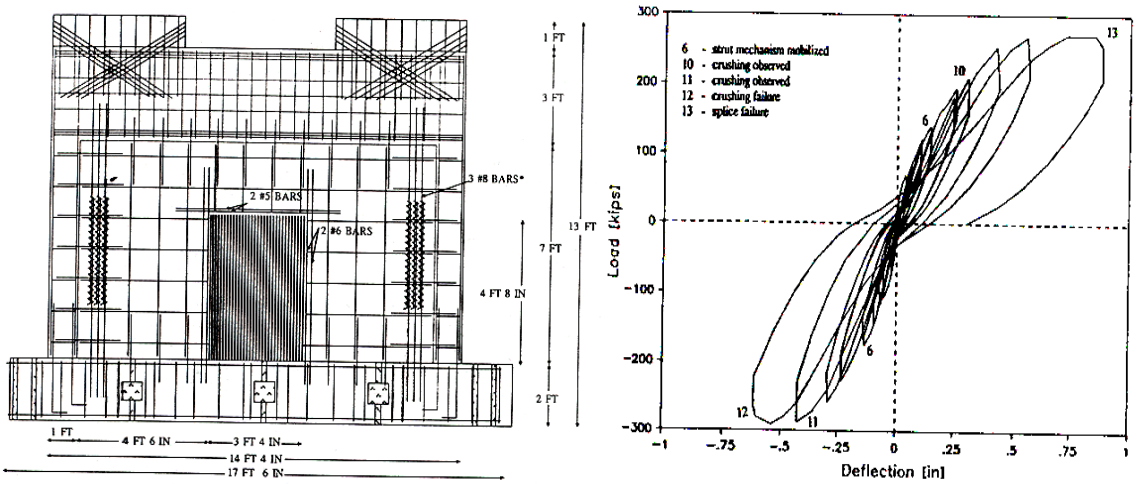

Fig. 2.3. Infill wall and load-deflection history of the specimen (Jirsa and Kreger 1989)

2.5.2.2 Use of Steel Bracing

The addition of steel bracing can be effective for the global strengthening and stiffening of existing buildings. Concentric or eccentric bracing schemes can be used in selected bays of an RC frame to increase the lateral resistance of the structure. The advantage of this method is that an intervention of the foundation may not be required because steel bracings are usually installed between existing members. Increased loading on the existing foundation is possible at the bracing locations and so the foundation still must be evaluated. In addition, the connection between the existing concrete frame and the bracing elements should be carefully treated because the connection is vulnerable during earthquakes.

Several researchers have reported successful results when using steel bracing to upgrade RC structures (Badoux and Jirsa 1990, Bush et al. 1991, Teran-Gilmore et al. 1995). Furthermore, post-tensioned steel bracing was investigated by Miranda and Bertero (1990) to upgrade the response of low-rise school buildings in Mexico.

Braces in tension tend to stretch and become slack when the load is removed. Subsequent loading cycles may be applied abruptly and may cause the premature failure of the braces. This condition can be alleviated by using high strength materials, such as

alloy steel strands, and/or initially prestressing the braces. Prestressed high slenderness ratio braces, also referred to as post-tensioned bracing systems, increase the initial lateral stiffness of the frame and allow the braces to yield in tension without becoming slack upon removal of the load (Pincheira 1992).

Pincheira and Jirsa (1995) investigated an analytical study for three-, seven-, and twelve-story RC frames using the computer program DRAIN-2D (Kannan and Powell 1973). They applied several retrofit techniques including post-tensioned bracing, structural steel bracing systems (X-bracing), and infill wall as rehabilitation schemes for low- and medium-rise RC frames. Nonlinear static and dynamic analyses were performed and five earthquake records on firm and soft soils were used for dynamic analysis. The bracing systems and infill walls were added only to the perimeter frames. Fig. 2.4 shows the comparison of base shear coefficient and drift for original and retrofitted twelve-story RC frame.

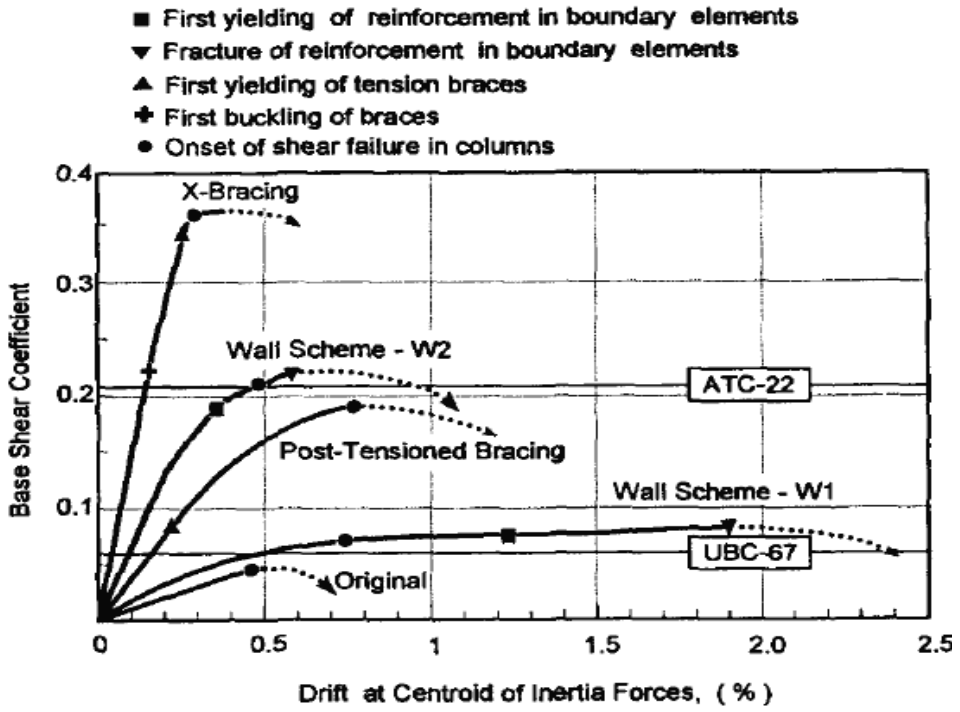

Fig. 2.4. Comparison of base shear coefficient and drift relationships for original and retrofitted 12-story building (Pincheira and Jirsa 1995)

Goel and Masri (1996) tested a weak slab-column building structure using a one-third scale, two-bay, two-story RC slab-column frame specimen. They tested two different phases of the steel bracing on both the exterior and interior bays, respectively, and compared them with the original RC frame. Fig. 2.5 shows the layout of the braced frame specimen. Fig 2.6 compares the hysteretic loops for the unretrofitted and retrofitted frame, showing the increase in strength, stiffness and energy dissipation due to retrofit. This observation was true for both retrofitted specimens. In particular, the results after applying the concrete-filled braces showed that the frame behaved in a very ductile manner through all fifteen cycles, with no failures.

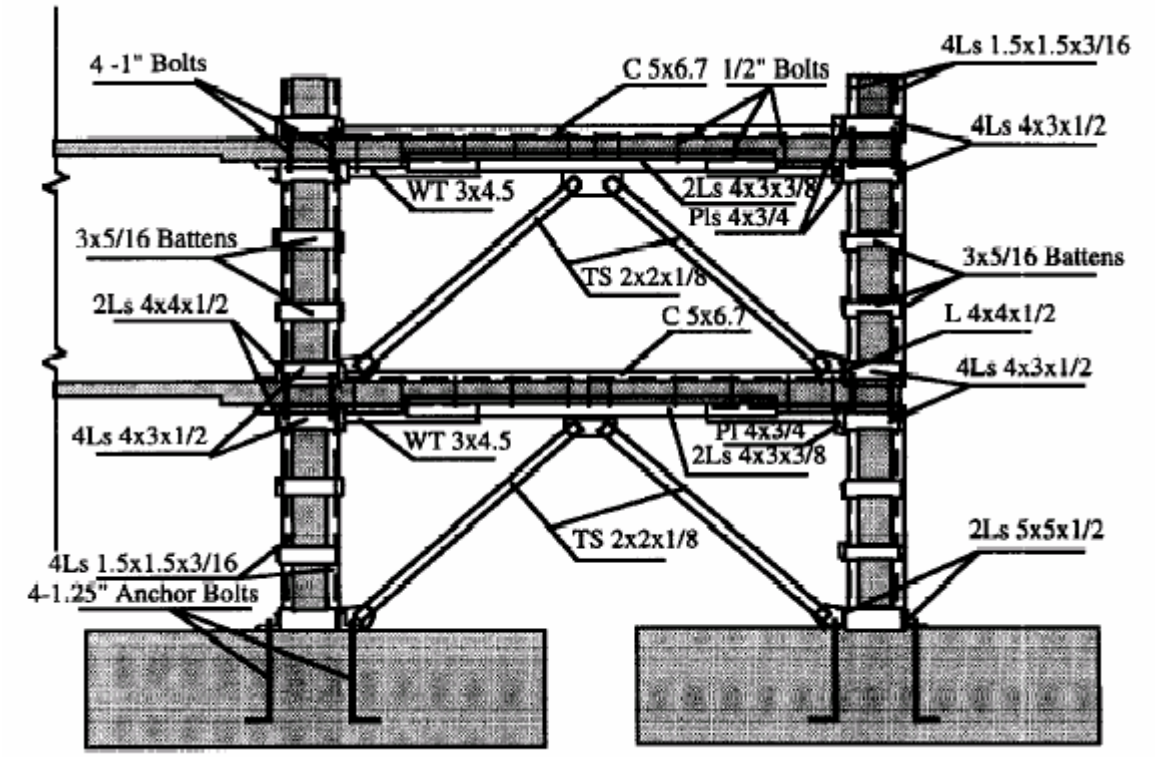

Fig. 2.5. Layout of the braced frame (Goel and Masri 1996)

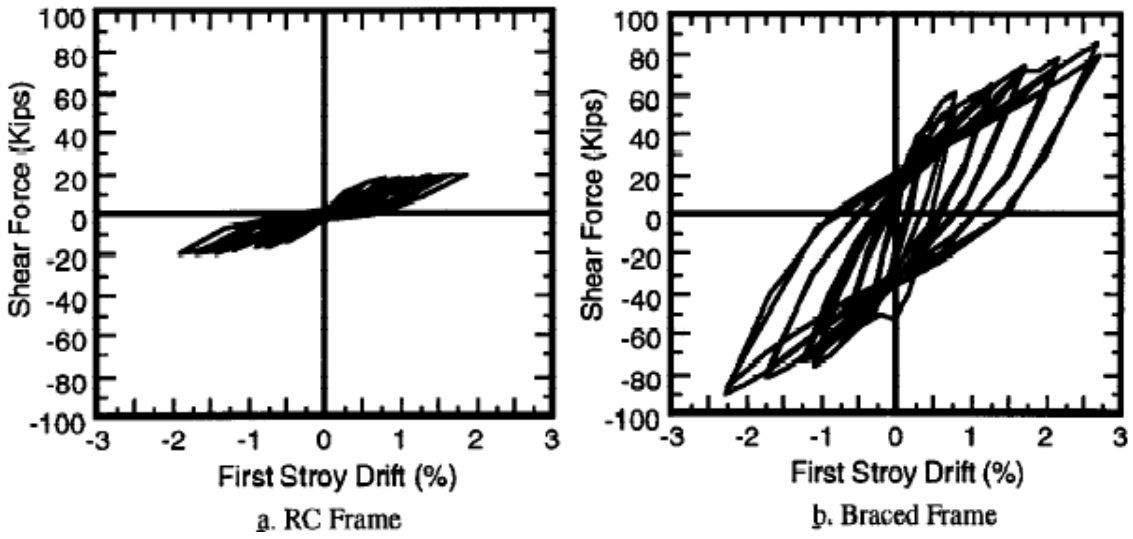

Fig. 2.6. Hysteretic loops of the RC and braced frames (Goel and Masri 1996)

2.5.2.3 Seismic Isolation

Recently, many researchers have studied seismic isolation as a possible retrofit method (Gates et al. 1990, Kawamura et al. 2000, Tena-Colunga et al. 1997, Constantinou et al. 1992). The objective of this type of retrofit is to isolate the structure from the ground motion during earthquake events. The bearings are installed between the superstructure and its foundations. Because most bearings have excellent energy dissipation characteristics, this technique is most effective for relatively stiff low-rise buildings with heavy loads.

2.5.2.4 Supplemental Energy Dissipation

The most commonly used approaches to add energy dissipation to a structure include installing frictional, hysteretic, viscoelastic, or magnetorheological (MR) dampers as components of the braced frames. A number of researchers have studied supplemental energy dissipation methods (Pekcan et al. 1995, Kunisue et al. 2000, Fu 1996, Munshi 1998, Yang et al. 2002). On the other hand, FEMA 356 discusses some negative aspects. While lateral displacements are reduced through the use of supplemental energy dissipation, the forces in the structure can increase not really if designed properly (ASCE 2000).

2.5.3 Member-Level Retrofit

The member-level retrofit approach can provide a more cost-effective strategy than structure-level retrofit because only those components needed to enhance the seismic performance of the existing structure are selected and upgraded. The member-level retrofit approaches include the addition of concrete, steel, or fiber reinforced polymer (FRP) jackets for use in confining RC columns and joints. In particular, in flat-slab structures, punching shear failures are likely to occur if the slab is not designed for the combined effects of lateral and gravity loads. Therefore, local retrofits are mainly performed on slab-column connections. Recently, research related to member-level retrofits in the U.S. has actively investigated columns, beam-column joints, and slab-column joints (Harries et al. 1998, Luo and Durrani 1994, Farhey et al. 1993, Martinez et al. 1994).

2.5.3.1 Column Jacketing

Column retrofitting is often critical to the seismic performance of a structure. To prevent a story mechanism during an earthquake, columns should never be the weakest components in the building structure. The response of a column in a building structure is controlled by its combined axial load, flexure, and shear. Therefore, column jacketing may be used to increase strength so that columns are not damaged (Bracci et al. 1995).

Recently, research has emphasized the applications of composite materials. In particular, carbon fiber reinforced polymer composite (FRPC) material may be used for jackets when retrofitting columns. Because these jackets sufficiently confine the columns, column failure through the formation of a plastic hinge zone can be prevented (see Fig. 2.7).

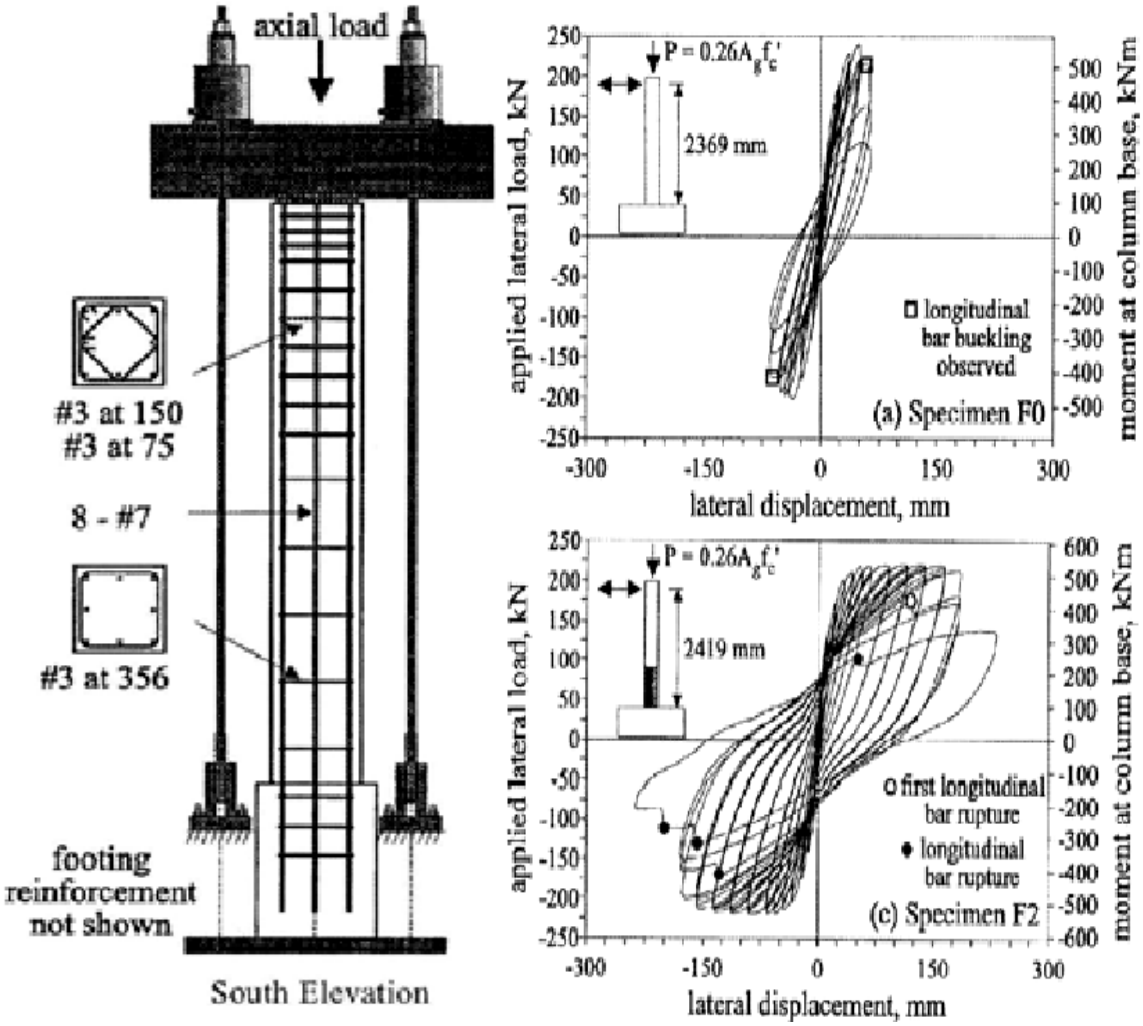

Fig. 2.7. Column retrofitting by carbon FRPC (Harries et al. 1998)

2.5.3.2 Slab-Column Connection Retrofits

In slab-column connections, punching shear failure due to the transfer of unbalanced moments is the most critical type of structural damage. The retrofitting of slab-column connections is beneficial for the prevention of punching shear failures and much research into retrofitting slab-column connections has been conducted (Luo and Durrani 1994, Farhey et al. 1993, Martinez et al. 1994) reported that adding concrete capitals or steel plates on both sides of the slab can prevent punching shear failures. Both solutions showed improvement in strength along the perimeter. The details of this method are shown in Fig 2.8.

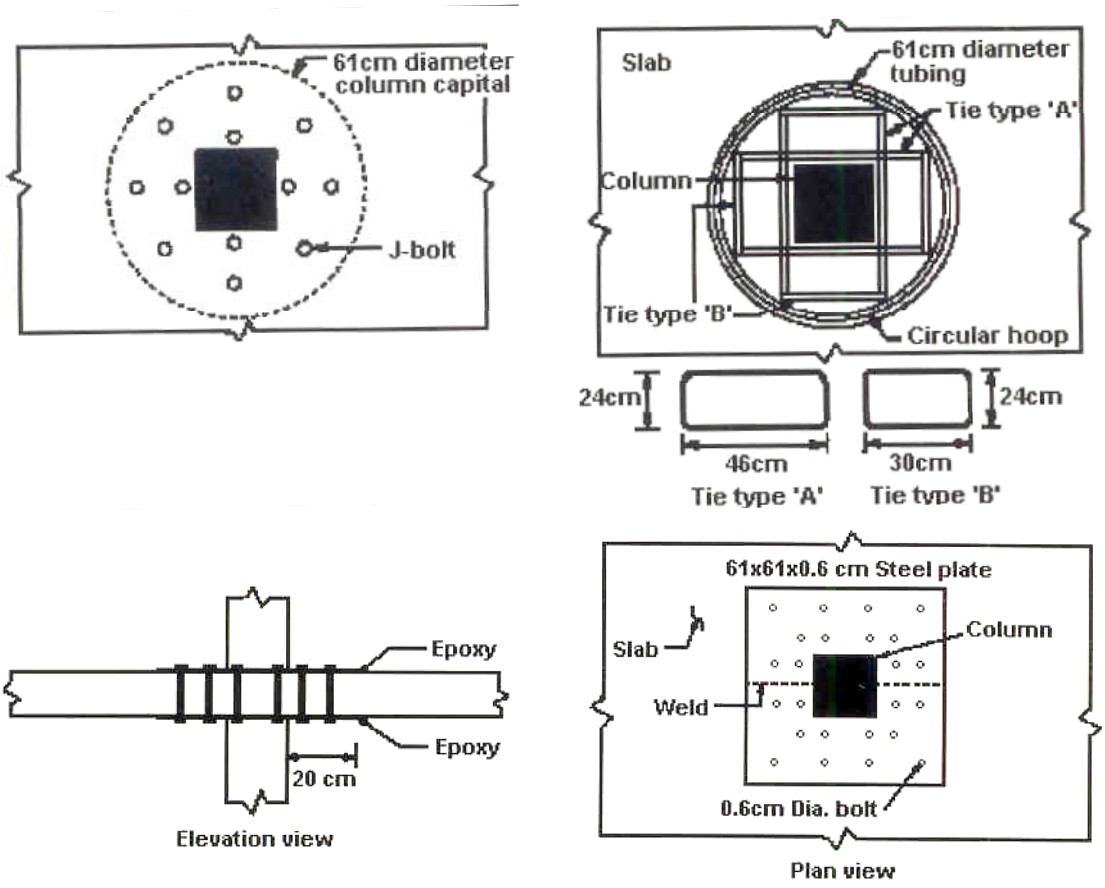

Fig. 2.8. Retrofit of slab-column connections (Martinez et al. 1994)

2.5.4 Selective Techniques

Elnashai and Pinho (1998) suggest another approach where retrofitting techniques are classified by their impact on structural response characteristics. This theory represents an economical approach because only the necessary structural characteristics are modified. The experimental program was conducted by Elnashai and Salama (1992) at Imperial College. This theory was tested by individually increasing the three design response parameters: stiffness, strength and ductility. Concrete walls were used for the experimental program, and the experimental data were compared with computer analysis results. The influence of selective intervention techniques on the global behavior was determined. Fig 2.9 shows the elevation and cross-section of the specimen.

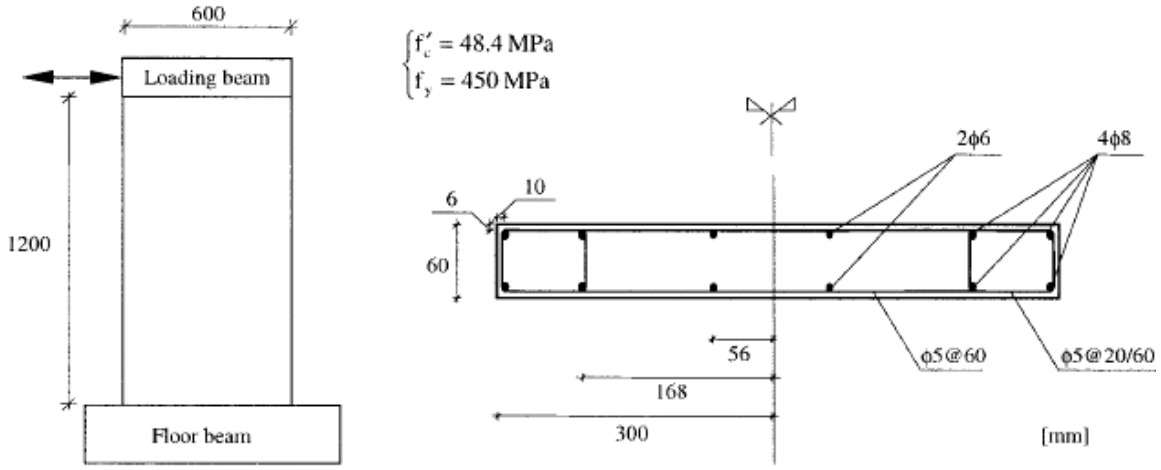

Fig. 2.9. Elevation and cross-section of the specimen (Elnashai and Pinho 1998)

For the stiffness-only scenario, external bonded steel plates were used to increase stiffness without any change in strength and ductility. In this approach, the height, width and thickness of the plate were important parameters to control the level of increase in the stiffness. To get the best results, the plates were placed as near to the edges as possible. External unbonded reinforcement bars or external unbonded steel plates could be used to increase only strength. Using a longer lever arm and smaller plates or smaller yield strength gave the best results. Finally, for the ductility-only scenario, U-shaped external confinement steel plates were used. This was most effective when the plates were close together and the total height of the plates was maximized. The details of the test specimens are shown in Figs. 2.10 to 2.12.

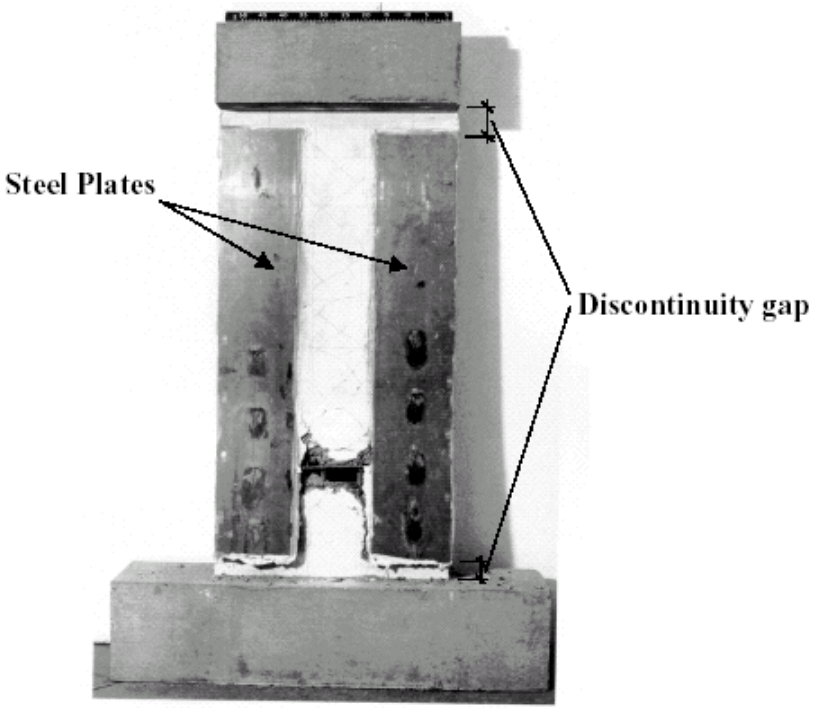

Fig. 2.10. Stiffness-only intervention test specimen (Elnashai and Salama 1992)

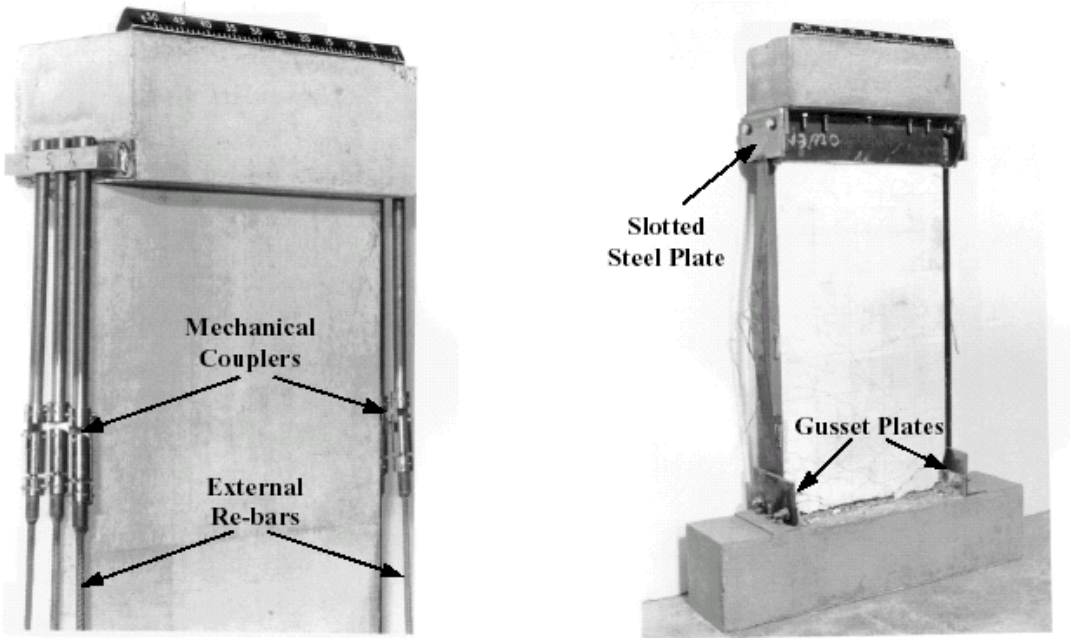

(a) External Unbonded Reinforcement Bars (b) External Unbonded Steel Plates

Fig. 2.11. Strength-only intervention test specimens (Elnashai and Salama 1992)

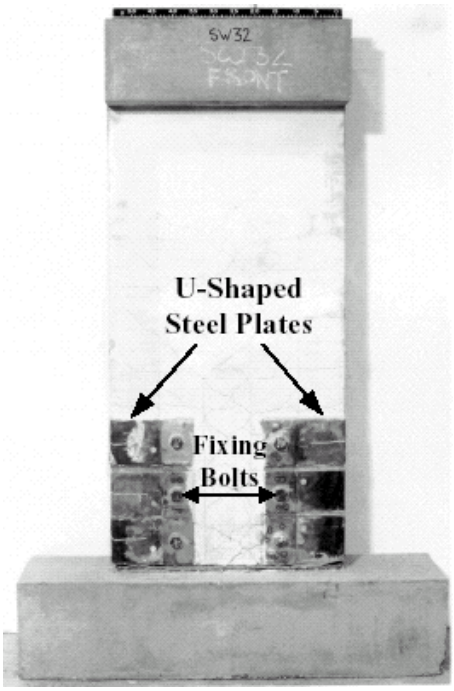

Fig. 2.12. Ductility-only intervention test specimen (Elnashai and Salama 1992)

3 CASE STUDY BUILDING

3.1 Introduction

Lightly reinforced RC building structures were selected as the structural system of interest for this study. The case study building is a five-story RC flat-slab structure with a perimeter frame that is based on a building layout developed by Hart (2000). The building is a frame system that is not detailed for ductile behavior and is designed based on codes used in the central U.S. in the mid-1980s. Hart (2000) surveyed several practicing engineers to determine typical structural systems used for office buildings in the central U.S. Low to moderate rise flat-slab buildings were found to be of particular interest because they are very common in the central U.S. and because there is a concern for potential damage to this type of structure during an earthquake of moderate intensity.

3.2 Building Description

The case study building is a five story RC flat-slab building with an overall height of 20.4 m (67 ft.) and a perimeter moment resisting frame. The first story is 4.58 m (15 ft.) high and the height of each of the remaining four stories is 3.97 m (13 ft.). The building is essentially rectangular in shape and is 42.7 m (140 ft.) long by 34.2 m (112 ft.) wide. The bay size is 8.54 m (28 ft.) by 8.54 m (28 ft.). Figs. 3.1 and 3.2 show the plan and elevation views of the case study building.

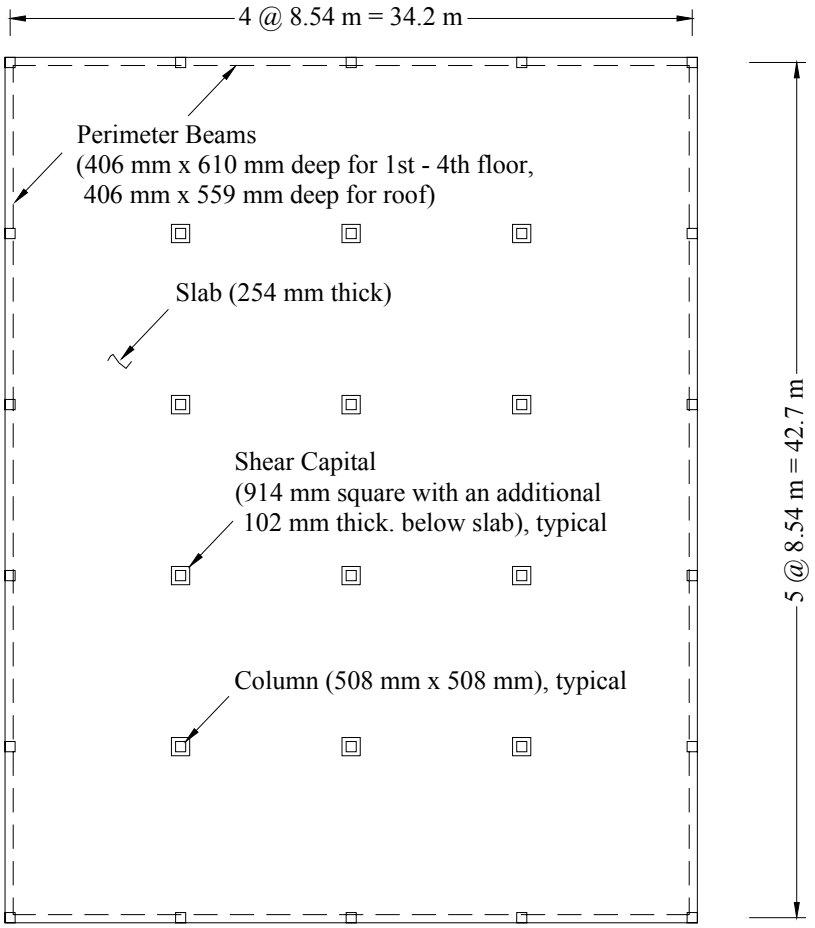

Fig. 3.1. Plan view of case study building

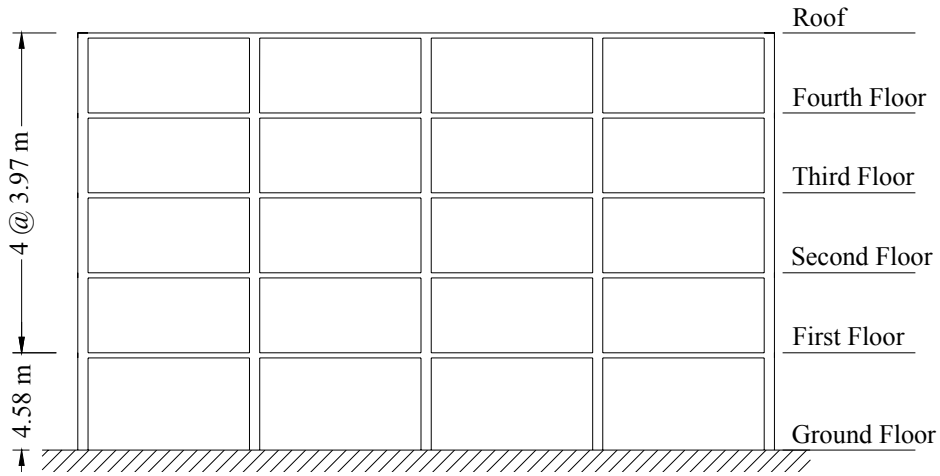

Fig. 3.2. Elevation view of case study building

3.3 Building Design

3.3.1 Design Codes

The case study building was designed according to the load requirements in the ninth edition of the *Building Officials and Code Administrators (BOCA) Basic/National Code* (BOCA 1984). This building was designed to be representative of those constructed in St. Louis, Missouri and Memphis, Tennessee in the mid-1980s. According to 1984 *BOCA* code, St. Louis, Missouri and Memphis, Tennessee have the same design wind loads and seismic zone factor (Zone 1). The design of structural components was carried out according to the provisions of the *American Concrete Institute (ACI) Building Code Requirements for Reinforced Concrete, ACI 318-83* (ACI Comm. 318 1983).

3.3.2 Loading

All design loads were determined according to Chapter 9 of the 1984 *BOCA* code. Dead loads included the self-weight of the structure, the partition load and the cladding load. The self-weight of reinforced concrete was assumed to be 23.6 kN/m^3 (150 pcf) and a partition loading of 958 N/m^2 (20 psf) was considered. For the exterior frames, a cladding loading of 719 N/m^2 (15 psf) was applied to each perimeter beam as a uniform load based on the vertical tributary area. The design live load for this office building is 2400 N/m^2 (50 psf) on each floor. The roof live load was calculated as the larger value of the roof loads and snow loads. The roof load for interior frame members is 575 N/m^2 (12 psf), which is for structural members with tributary area larger than 55.7 m^2 (600 ft.^{2}). The roof load for exterior frame members is 766 N/m^2 (16 psf), which is for buildings with tributary area between 18.6 m^2 (200 ft.^{2}) and 55.7 m^2 (600 ft.^{2}). The snow load for this structure is 814 N/m^2 (17 psf). The wind load was applied as a uniform load distributed vertically on the windward and leeward sides of the building and horizontally on the building's roof. Fig. 3.3 and Table 3.1 describe the wind load applied to the case study building.

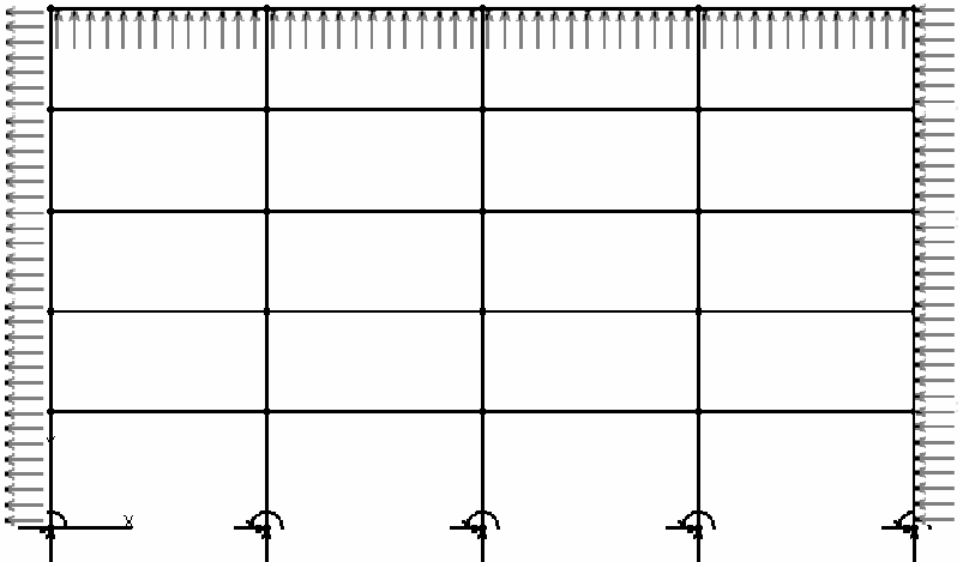

Fig. 3.3. Load pattern for wind load

Table 3.1. Wind load

Load type	WL_E (kN/m)	WL_I (kN/m)
Windward Wall	1.96	3.93
Leeward Wall	1.23	2.45
Roof	2.45	4.91

Notes:
WL_E = Wind load for exterior frame
WL_I = Wind load for interior frame
1 kN/m = 0.0685 kips/ft.

The 1984 *BOCA* specifies the total design seismic base shear as follows.

$$V = ZKCW \tag{3.1}$$

where:

Z = Seismic zone factor = 0.25 for Zone 1 in Figure 916 of 1984 *BOCA*
K = Horizontal force factor for buildings = 1.0
C = Coefficient based on fundamental period of building = $0.05 \div \sqrt[3]{T}$ = 0.063

T = Fundamental period of vibration of the building or structure in seconds in the direction under consideration, estimated as $0.10N$ = 0.5 s
W = Weight of structure = 55,100 kN (includes self-weight, cladding and partition load)

Based on the above equation, the base shear of this case study building is 868 kN (195 kips). This is 1.6 percent of the building's seismic weight, W. The design seismic loads at each level are calculated using the following expression.

$$F_x = \frac{(V - F_t)w_x h_x}{\sum w_i h_i} \tag{3.2}$$

where:

F_x = Lateral force applied to level x
V = Design seismic base shear, as calculated using Eq. 3.1
F_t = That portion of V considered concentrated at the top of the structure at level n, not exceeding $0.15V$ and may be considered as 0 for values of h_n / D_s of 3 or less, where h_n =20.4 m and D_s =42.7 m
w_x, w_i = Weight of a given floor level x or i measured from the base
h_x, h_i = Height of a given floor level x or i measured from the base

The factored load combinations of *ACI 318-83,* listed in Eqs. 3.3 through 3.7, were used to compute the factored design forces. Fig. 3.4 shows the four live load patterns for the frame in the short direction.

(i) $U = 1.4D + 1.7L$ (3.3)
(ii) $U = 0.75\ (1.4D + 1.7L + 1.7W)$ (3.4)
(iii) $U = 0.9D \pm 1.3W$ (3.5)
(iv) $U = 0.75\ (1.4D + 1.7L \pm 1.7\ (1.1E))$ (3.6)
(v) $U = 0.9D \pm 1.3\ (1.1E)$ (3.7)

where:

D = Dead load
L = Live load
W = Wind load
E = Earthquake load

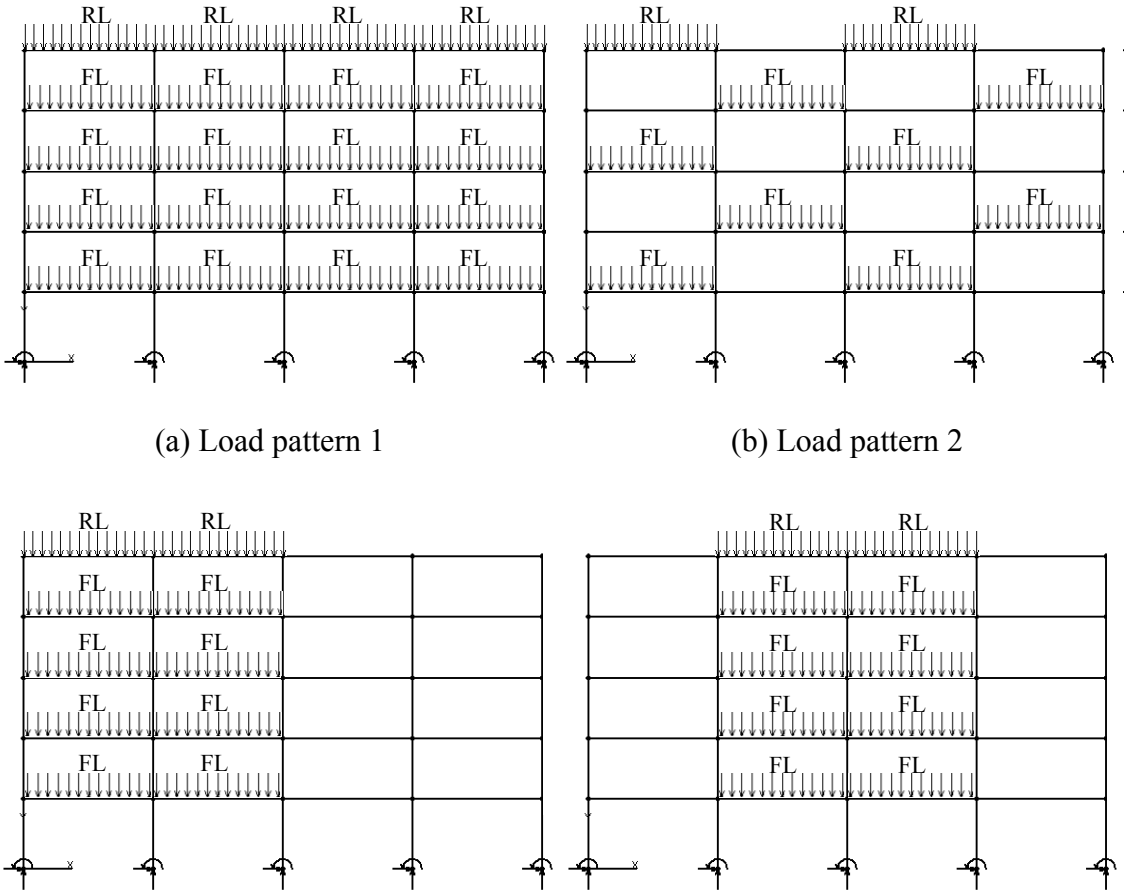

Fig. 3.4. Live load patterns

A structural analysis of the building was conducted using Visual Analysis 3.5 (IES 1998). Because the case study building has a symmetrical configuration and no irregularities, half of the building as a two-dimensional analytical model, was analyzed.

The perimeter beams and columns were designed based on the results of structural analysis using the above factored load combinations. The perimeter frames were designed to resist the full design lateral loads, including wind and seismic loads, based on design practices that were common and generally accepted during the 1980s. Based on the analytical results, the perimeter beams and columns were mostly controlled by load combinations including earthquake loads.

3.3.3 Structural Member Details

Normal weight concrete having a specified compressive strength of 27.6 MPa (4000 psi) was used for the design of the beams, slabs and columns. Grade 60 reinforcement was used for the longitudinal and transverse reinforcement in all major structural members. The perimeter beams are 406 mm (16 in.) wide by 610 mm (24 in.) deep for the first through the fourth floors, and the roof perimeter beams are 406 mm (16 in.) wide by 559 mm (22 in.) deep. The two-way slab is 254 mm (10 in.) thick. The minimum thickness of the slab was calculated using the following equations from *ACI 318-83*:

$$h = \frac{l_n(800 + 0.005 f_y)}{36,000 + 5000\beta\left[\alpha_m - 0.5(1-\beta_s)\left(1+\frac{1}{\beta}\right)\right]} \tag{3.8}$$

but not less than

$$h = \frac{l_n(800 + 0.005 f_y)}{36,000 + 5000\beta(1+\beta_s)} \tag{3.9}$$

and need not be more than

$$h = \frac{l_n(800 + 0.005 f_y)}{36,000} \tag{3.10}$$

where:

h = Overall thickness of two-way slab member, in.
l_n = Length of clear span in long direction of two-way construction, measured face-to-face of supports in slabs without beams and face-to-face of beams or other supports in other cases
f_y = Specified yield strength of nonprestressed reinforcement, psi
α_m = Average value of α for all beams on edges of a panel
β = Ratio of clear spans in long to short direction of two-way slabs
β_s = Ratio of length of continuous edges to total perimeter of a slab panel

The slabs were designed for gravity loads using the direct design method for two-way slab design, which is described in Chapter 11 of *ACI 318-83*. Shear capitals that are 914 mm (36 in.) square and provide an additional 102 mm (4 in.) of thickness below the slab are used at all interior slab-column connections, except at the roof level. The shear capitals were needed because the two-way shear strength at the slab-column connections was not adequate for gravity loads when only a 254 mm (10 in.) thick slab is used. The columns are 508 mm (20 in.) square. The transverse reinforcement in the beam and column members was selected to meet the minimum requirements in Chapter 7of *ACI 318-83*. According to *ACI 318-83*, the maximum permissible spacing of the transverse reinforcement for the perimeter beams and columns are 279 mm (11 in.) and 457 mm (18 in.), respectively. For the beam members, 254 mm (10 in.) spacing was selected. Tables 3.2 to 3.5 summarize the reinforcement in the perimeter beams, slabs for the specific floor levels and columns, respectively.

Table 3.2. Reinforcement in perimeter beams

Floor level	Beam width (mm)	Beam depth (mm)	Number of reinforcing bars		Bar size (US)	Stirrups (US)
1st – 2nd	406	610	Top	7	#8	#4 @ 254 mm c/c
			Bottom	3		
3rd	406	610	Top	6	#8	#4 @ 254 mm c/c
			Bottom	3		
4th	406	610	Top	5	#8	#4 @ 254 mm c/c
			Bottom	3		
Roof	406	559	Top	5	#8	#4 @ 254 mm c/c
			Bottom	3		

Note: 1 in. = 25.4 mm

Table 3.3. Reinforcement in slabs (1st – 4th floor level)

Frame	Span	Strip		Reinforcement (US)
Edge	End	Column	Exterior negative	#5 @ 432 mm
			Positive	
			Interior negative	
		Middle	Exterior negative	#5 @ 432 mm
			Positive	
			Interior negative	#5 @ 406 mm
	Interior	Column	Positive	#5 @ 432 mm
			Interior negative	
		Middle	Positive	#5 @ 432 mm
			Interior negative	
Interior	End	Column	Exterior negative	#5 @ 254 mm
			Positive	#5 @ 229 mm
			Interior negative	#5 @ 127 mm
		Middle	Exterior negative	#5 @ 432 mm
			Positive	#5 @ 356 mm
			Interior negative	#5 @ 406 mm
	Interior	Column	Positive	#5 @ 330 mm
			Interior negative	#5 @ 127 mm
		Middle	Positive	#5 @ 432 mm
			Interior negative	

Note: 1 in. = 25.4 mm

Table 3.4. Reinforcement in slabs (roof level)

Frame	Span	Strip		Reinforcement (US)
Edge	End	Column	Exterior negative	#5 @ 318 mm
			Positive	
			Interior negative	
		Middle	Exterior negative	#5 @ 406 mm
			Positive	
			Interior negative	
	Interior	Column	Positive	#5 @ 318 mm
			Interior negative	
		Middle	Positive	#5 @ 406 mm
			Interior negative	
Interior	End	Column	Exterior negative	#5 @ 305 mm
			Positive	#5 @ 229 mm
			Interior negative	#5 @ 152 mm
		Middle	Exterior negative	#5 @ 368 mm
			Positive	
			Interior negative	
	Interior	Column	Positive	#5 @ 368 mm
			Interior negative	#5 @ 165 mm
		Middle	Positive	#5 @ 368 mm
			Interior negative	

Note: 1 in. = 25.4 mm

Table 3.5. Reinforcement in columns

Column location	Story	Column width (mm)	Number of reinforcing bars	Bar size (US)	Tie bar size (US)
Exterior	$1^{st} - 5^{th}$	508	8	#9	#3 @ 457 mm c/c
Interior	1^{st}	508	16	#9	#3 @ 457 mm c/c
Interior	2^{nd} - 5^{th}	508	8	#9	#3 @ 457 mm c/c

Note: 1 in. = 25.4 mm

Typical details for the columns and perimeter beams are shown in Figs. 3.5 and 3.6. Figs. 3.7 and 3.8 show details for the slab reinforcement and Fig. 3.9 show details for the beam reinforcement.

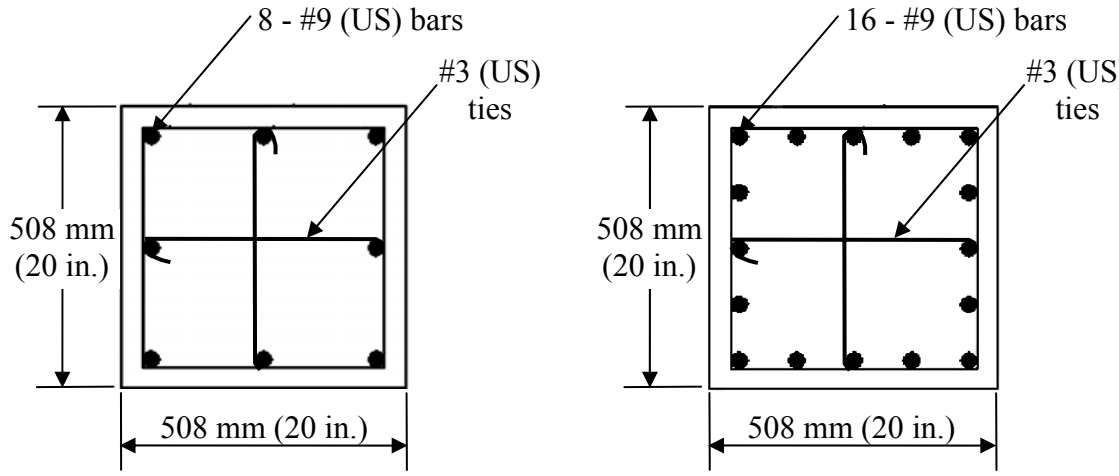

(a) 1st ~ 5th Story for External Frame
2nd ~ 5th Story for Interior Frame

(b) 1st Story for Interior Frame

Fig. 3.5. Typical column cross sections

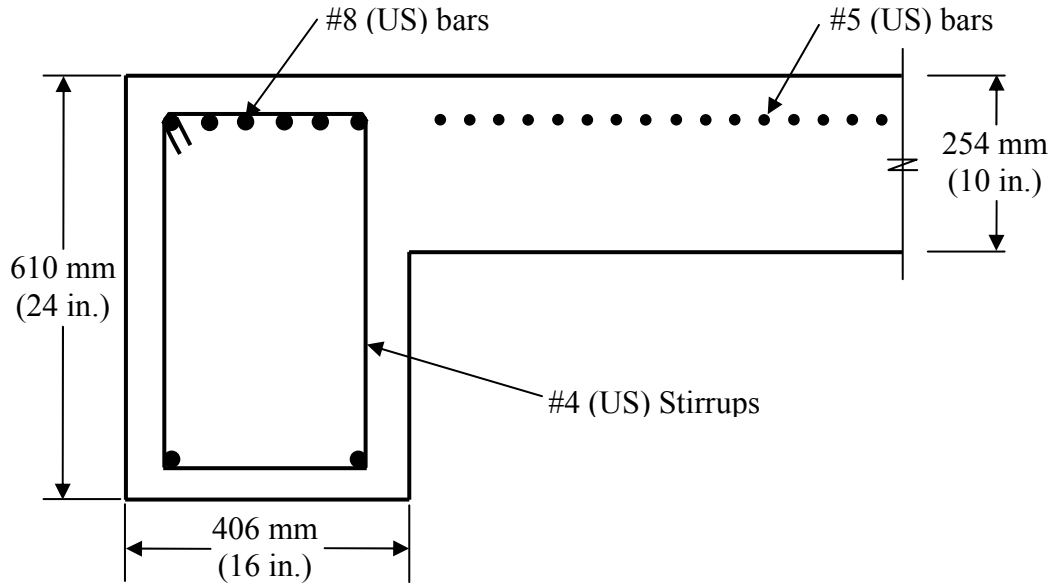

Fig. 3.6. Typical first floor beam cross section

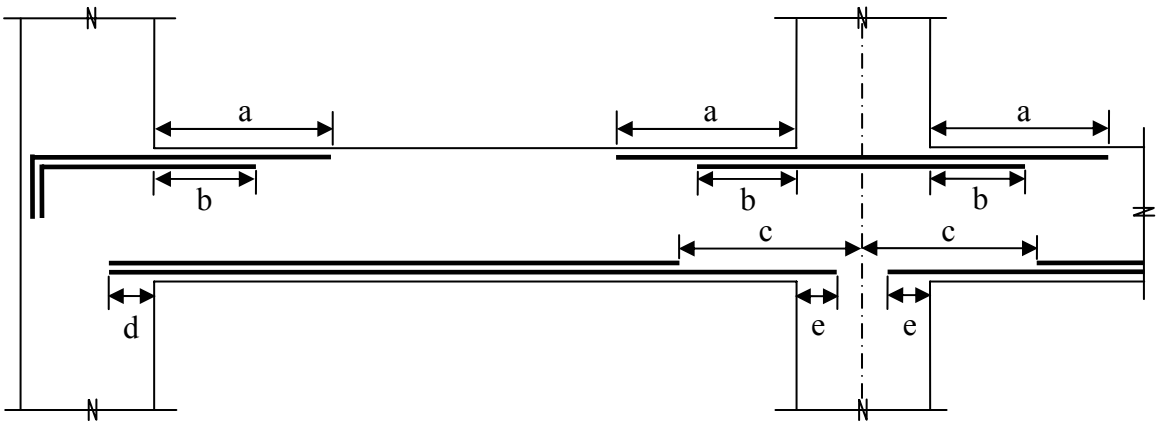

a: 241 cm (95 in.) - 50% of negative moment reinforcement
b: 163 cm (64 in.) - 50% of negative moment reinforcement
c: 107 cm (42 in.) - 50% of positive moment reinforcement
d: 15.2 cm (6 in.) - positive moment reinforcement embedded at exterior support
e: 17.8 cm (7 in.) - 50% of positive moment reinforcement embedded at interior support

Fig. 3.7. Details of slab reinforcement for column strip of case study building

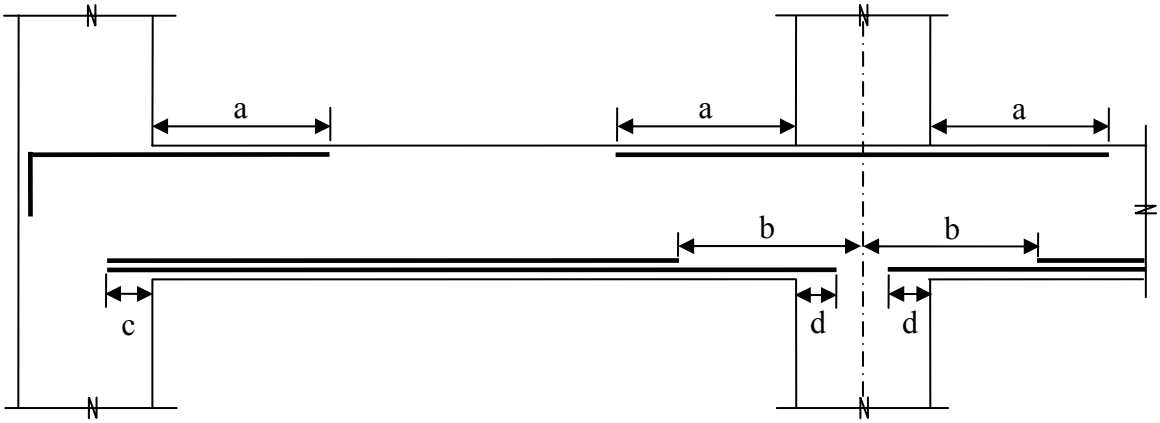

a: 178 cm (70 in.) - 100% of negative moment reinforcement
b: 127 cm (50 in.) - 50% of positive moment reinforcement
c: 15.2 cm (6 in.) - positive moment reinforcement embedded at exterior support
d: 17.8 cm (7 in.) - 50% of positive moment reinforcement embedded at interior support

Fig. 3.8. Details of slab reinforcement for middle strip of case study building

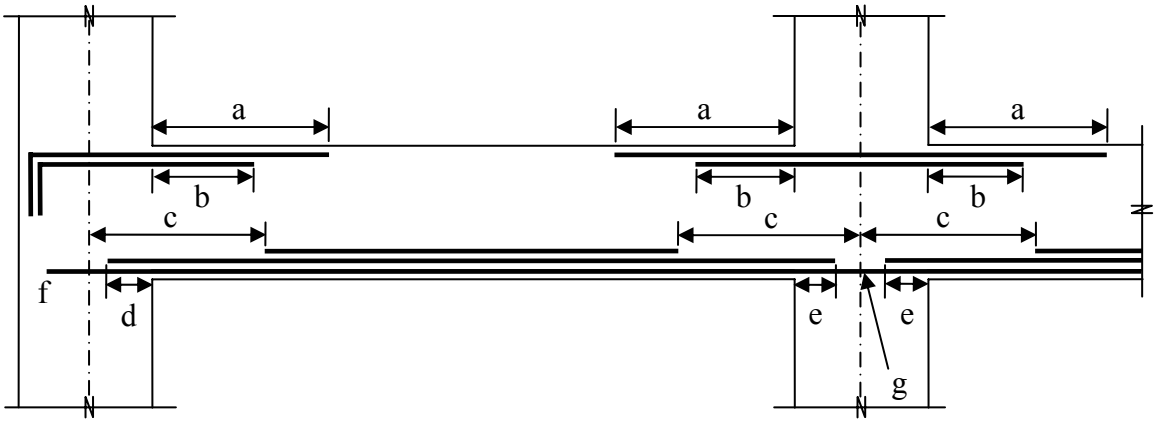

a: 345 cm (136 in.) - 1 bar of negative moment reinforcement at 1st and 2nd floors
b: 178 cm (70 in.) - 4 bars of negative moment reinforcement at 1st and 2nd floors
208 cm (82 in.) - 4 bars of negative moment reinforcement at 3rd floor
178 cm (70 in.) - 3 bars of negative moment reinforcement at 4th floor and roof
c: 127 cm (50 in.) - 1 bar of positive moment reinforcement at 1st - 4th floors
224 cm (88 in.) - 1 bar of positive moment reinforcement at roof
d: 15.2 cm (6 in.) - positive moment reinforcement except 2 bars that are fully-developed at exterior support
e: 17.8 cm (7 in.) - positive moment reinforcement except 2 bars that are continuous at interior support
f: 2 bars of positive moment reinforcement fully-developed at exterior support
g: 2 bars of positive moment reinforcement continuous at interior support

Fig. 3.9. Details of beam reinforcement for case study building

4 MODELING OF CASE STUDY BUILDING

4.1 Introduction

This section presents the modeling procedures for the case study building. In this study, two different approaches for modeling and analyzing the case study building were evaluated and compared: a fiber model and a macromodel. The ZEUS-NL program (Elnashai et al. 2002) was selected for the fiber model and DRAIN-2DM program (Al-Haddad and Wight 1986, Tang and Goel 1988, Raffaelle and Wight 1992, Soubra et al. 1992, Hueste and Wight 1997) was used for the macromodel. The synthetic ground motion data developed by Wen and Wu (2000) for St. Louis, Missouri and Memphis, Tennessee were used for the dynamic analysis. The following sections describe the analytical models, modeling assumptions and synthetic ground motions.

4.2 Description of Nonlinear Analysis Tools

4.2.1 General

In this study, the ZEUS-NL and DRAIN-2DM programs were used for the nonlinear structural analysis. The fundamental equation of motion used to determine the dynamic response for the structural models is given in Eq. 4.1.

$$[M]\{a\} + [C]\{v\} + [K]\{u\} = -[M]\,a_g \tag{4.1}$$

where:

[M] = Mass matrix
{a} = Acceleration vector
[C] = Viscous damping matrix
{v} = Velocity vector
[K] = Structural stiffness matrix
{u} = Displacement vector
a_g = Ground acceleration

Both programs use the Newmark integration method to solve the equation of motion for each time step. An integration factor of 0.5, corresponding to an average acceleration during the time step, was selected for this study. The programs have significant differences in the formulation of the structural elements, as described below. The time step of 0.005 seconds for DRAIN-2DM was used for dynamic time history analysis. However, in order to reduce the size of output files, a time step of 0.01 seconds which is the same as the time step for ground motion data, was used for the ZEUS-NL analysis.

4.2.2 ZEUS-NL Program

4.2.2.1 General

ZEUS-NL is a finite element structural analysis program developed for nonlinear dynamic, conventional and adaptive push-over, and eigenvalue analysis. The program can be used to model two-dimensional and three-dimensional steel, RC and composite structures, taking into account the effects of geometric nonlinearities and material inelasticity. The program uses the fiber element approach to model these nonlinearities. Fiber models are widely used because of their suitability for describing the interaction between the flexural behavior and the axial force. Fig. 4.1 presents a decomposition of a rectangular RC section. As shown below, the response of elements is computed by assembling the responses of individual fibers that consist of many monitoring points. Each fiber is classified by the appropriate material stress-strain relationship.

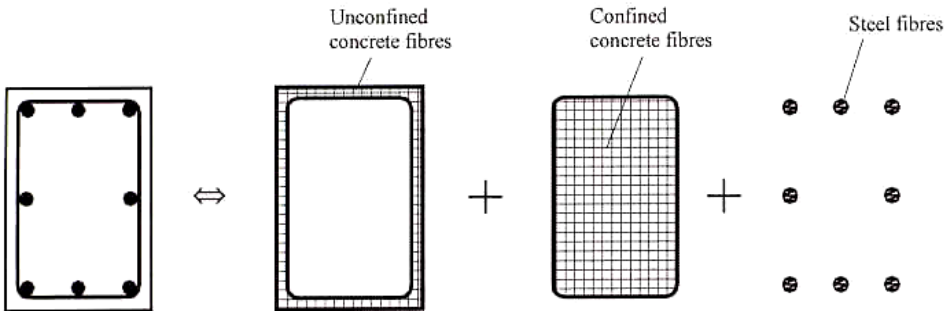

Fig. 4.1. Decomposition of a rectangular RC section (Elnashai et al. 2000)

For the numerical integration of the governing equation, two Gauss points are used in the cubic formulation, with the location given in Fig. 4.2.

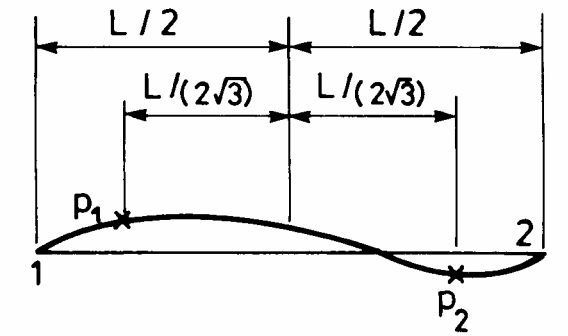

Fig. 4.2. Location of gauss points (Elnashai et al. 2000)

4.2.2.2 Element and Cross Section Types

There are six element types in ZEUS-NL, as shown in Table 4.1. The cubic element is used to model structural elements. The cubic element is an elasto-plastic three-dimensional (3D) beam-column element used for detailed inelastic modeling. To compute the element forces, the stress-strain relationship of monitoring areas is computed by numerical integration at the two Gauss points. For instance, 100 monitoring points may be used for an rss (rectangular solid section) section, which is a single-material section, but more complicated sections such as an rcts (RC T-section) section, may require 200 monitoring points. Several elements are available to include mass and damping (Lmass, Dmass, Ddamp and Rdamp). The joint element is used for modeling supports and joints.

Fourteen cross-section types are available in the ZEUS-NL program (see Table 4.2). The cross-section types include single-material sections, RC sections and composite sections.

Table 4.1. Element types in ZEUS-NL

Type	Description
Cubic	Cubic elasto-plastic 3D beam-column element
Joint	3D joint element with uncoupled axial, shear and moment actions
Lmass	Lumped mass element
Dmass	Cubic distributed mass element
Ddamp	Dashpot viscous damping element
Rdamp	Rayleigh damping element

Table 4.2. Cross-section types in ZEUS-NL

Type	Description
rss	Rectangular solid section
css	Circular solid section
chs	Circular hollow section
sits	Symmetric I- or T-section
alcs	Asymmetric L- or C-section
pecs	Partially encased composite I-section
fecs	Fully encased composite I-section
rcrs	RC rectangular section
rccs	RC circular section
rcts	RC T-section
rcfws	RC flexural wall section
rchrs	RC hollow rectangular section
rchcs	RC hollow circular section
rcjrs	RC jacket rectangular section

4.2.2.3 Material Models

There are four material models in the ZEUS-NL program. Stl1 is a bilinear elasto-plastic model with kinematic strain-hardening. This material model is used for steel and includes definition of Young's modulus, the yield strength and a strain-hardening parameter. Con1 is the simplified model for uniaxial modeling of concrete where the initial stiffness, compressive strength, degradation stiffness and residual strength are defined. Con2 is applied for uniaxial modeling of concrete assuming constant confinement with a confinement factor. Con3 is a uniaxial variable

confinement concrete model. Descriptions of each material model are shown in Table 4.3. Fig. 4.3 shows typical stress-strain curves for each material model, respectively.

Table 4.3. Material models in ZEUS-NL

Type	Description
stl1	Bilinear elasto-plastic model with kinematic strain-hardening
con1	Trilinear concrete model
con2	Uniaxial constant confinement concrete model
con3	Uniaxial variable confinement concrete model

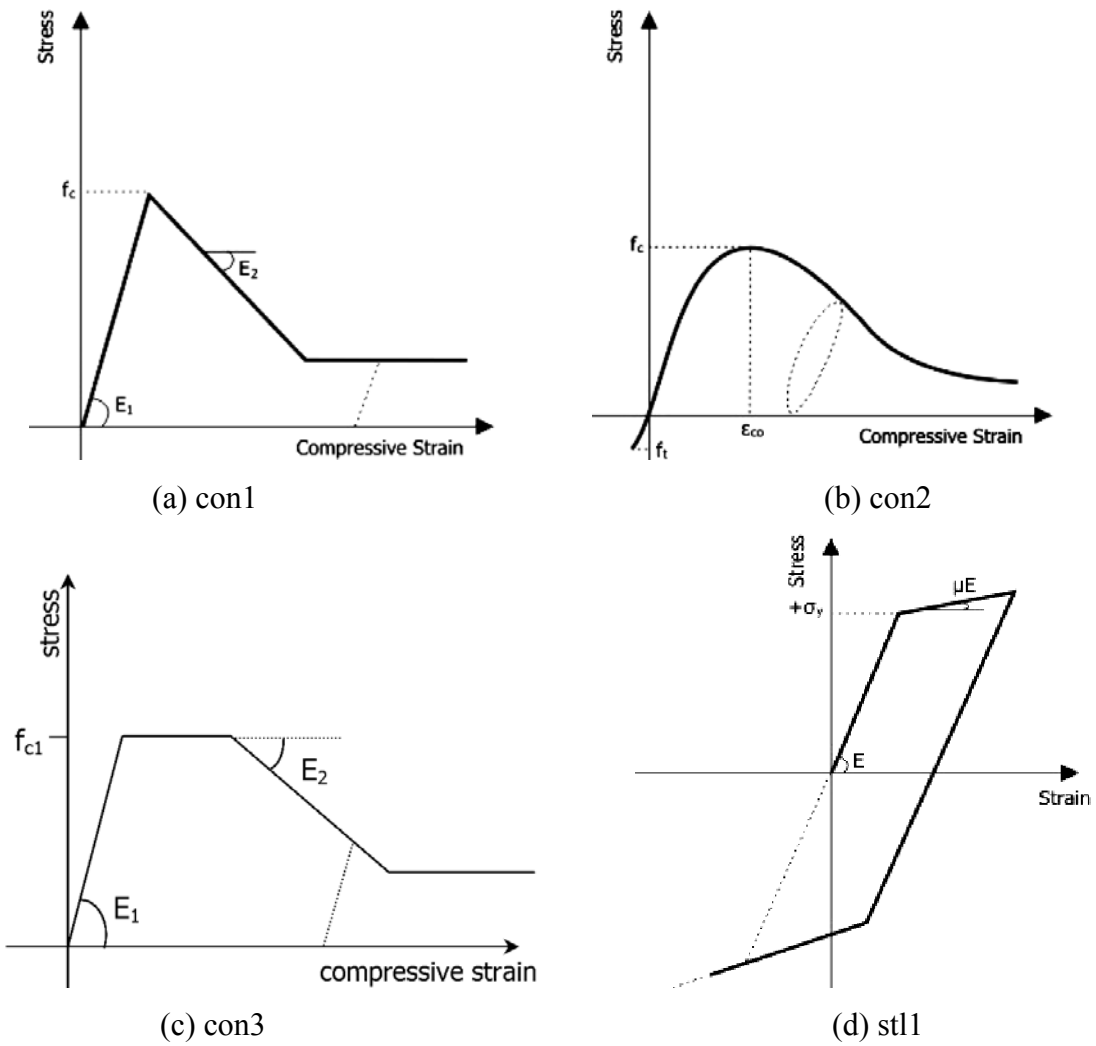

Fig. 4.3. Material models for ZEUS-NL analysis (Elnashai et al. 2002)

4.2.3 DRAIN-2DM Program

4.2.3.1 General

The original program DRAIN-2D was developed at the University of California, Berkeley (Kanaan and Powell 1973, Powell 1973). This program is capable of modeling the behavior of structures in the elastic and inelastic ranges for static and dynamic analysis. In this study, a modified version of the program called DRAIN-2DM, which was developed at the University of Michigan, was used. DRAIN-2DM performs nonlinear analysis of frame structure with the capability of predicting punching shear behavior of RC slab members (Al-Haddad and Wight 1986, Tang and Goel 1988, Raffaelle and Wight 1992, Soubra et al. 1992, Hueste and Wight 1997).

4.2.3.2 Element and Cross Section Types

Table 4.4 shows ten element types available in DRAIN-2DM. In most cases for RC structures, the beam-column element, RC beam element and RC slab element are used for structural analysis.

Table 4.4. Element types in DRAIN-2DM

Type	Description
Element 1	Truss element
Element 2	Beam-column element
Element 3	Infill panel element
Element 4	Semi-rigid connection element
Element 5	Beam element
Element 6	Shear link element
Element 8	RC beam element
Element 9	Buckling element
Element 10	End moment-buckling element
Element 11	RC slab element

The beam-column element (Element 2) has both flexural and axial stiffness. Yielding may occur only in concentrated plastic hinges at the element ends. A plastic hinge is formed within the elasto-plastic element when the combination of axial force

and moment falls outside the axial load versus moment interaction envelope, which describes yield conditions for the member cross-section. Strain hardening is assumed such that the element consists of elastic and elasto-plastic components in parallel, as describes by the moment versus rotation relationship shown in Fig. 4.4.

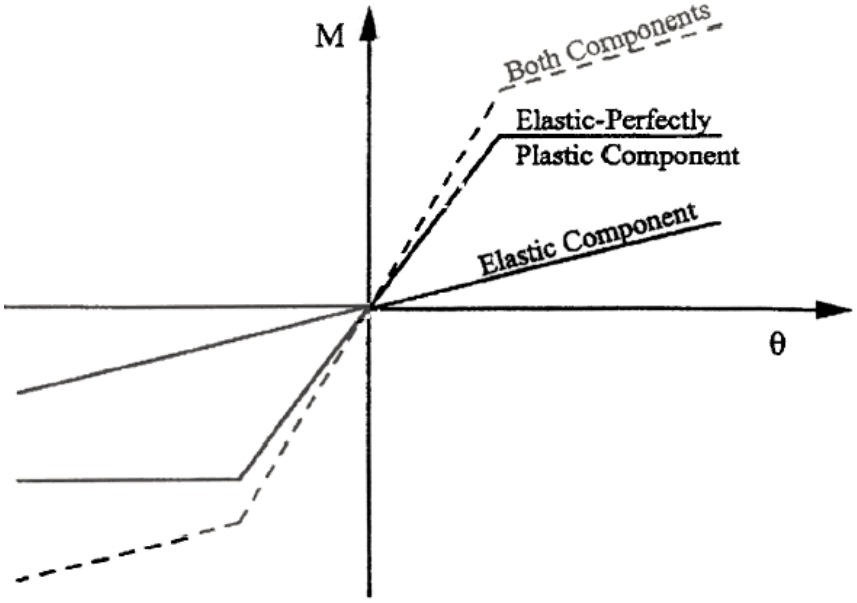

Fig. 4.4. Bilinear moment-rotation relationship for beam-column element (Element 2) (Soubra et al. 1992)

Element 8 is a RC beam element that yields under flexure only. This element consists of an elastic line element and two nonlinear flexural springs. The nonlinear behavior is concentrated in the springs, which can be located at some distance from the column face. The hysteretic model for this element includes the effects of stiffness degradation, strength deterioration and pinching (see Fig. 4.5).

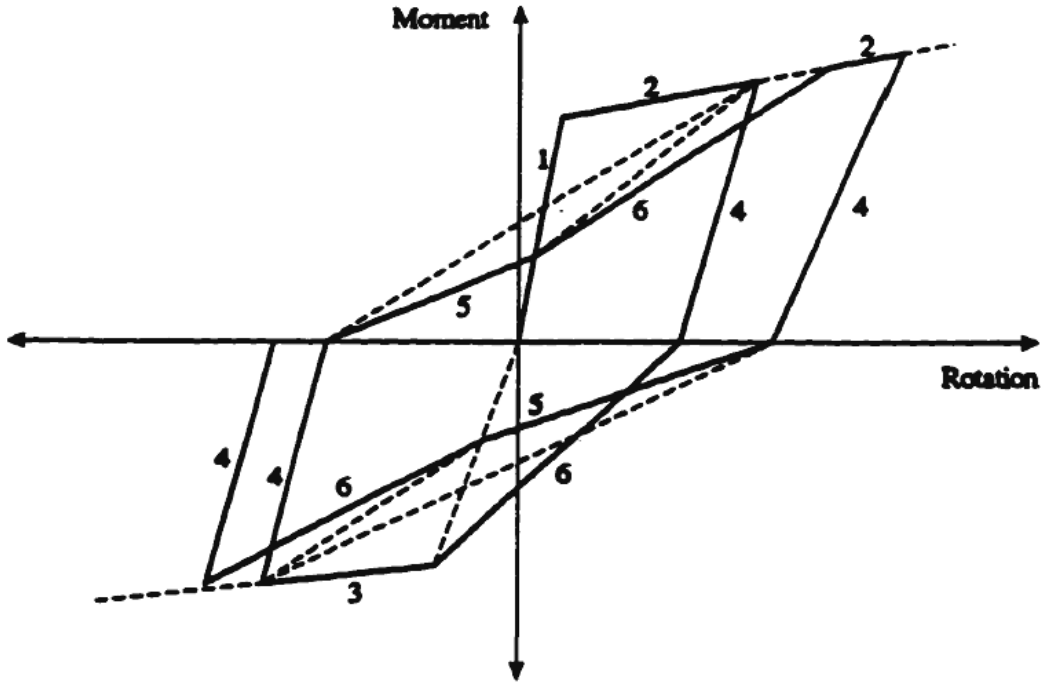

Fig. 4.5. Generalized model for the hysteretic behavior of the RC beam element (Element 8) (Raffaelle and Wight 1992)

Element 11 is a RC slab element that allows inelastic rotation at the member ends and also includes a punching shear failure prediction. This element behaves exactly like the RC beam element (Element 8) until a punching shear failure is predicted. The punching shear model, developed by Hueste and Wight (1999), monitors the member-end rotations for each time step. In order to detect the punching shear failure in Element 11, the gravity shear ratio (V_g/V_o) and critical rotation (θ_{cr}) are defined by the user. The gravity shear ratio is the ratio of the shear at a slab-column joint due to gravity loads and the shear strength of the critical section around the column, described in Chapter 11 of ACI 318-02. Fig. 4.6 shows the response model used for Element 11 when punching shear is predicted. The response prior to the prediction of punching shear is the same as that for Element 8, shown in Fig. 4.5.

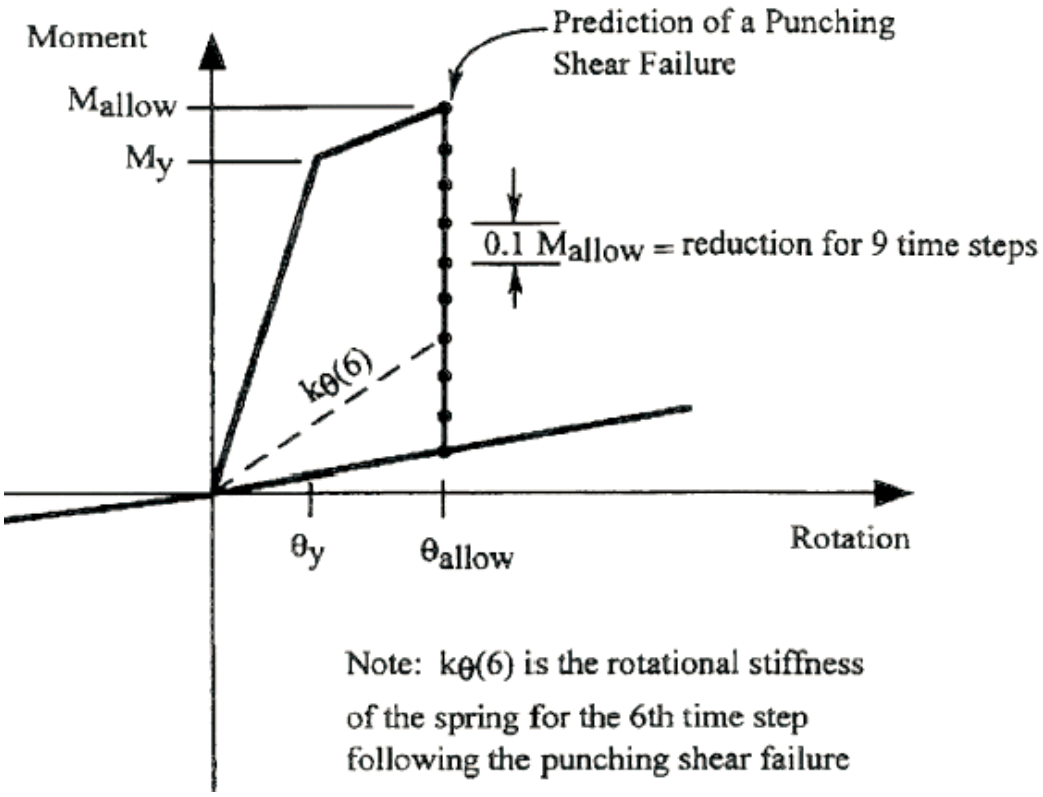

Fig. 4.6. Hysteretic response model used for the RC slab element (Element 11) (Hueste and Wight 1999)

4.3 Description of Analytical Models for Case Study Building

4.3.1 ZEUS-NL Model

4.3.1.1 Model Geometry

The building has a symmetrical configuration and so only half of the building was analyzed. Because there are no irregularities, a two-dimensional analytical model of the case study building is adequate to simulate the structural behavior under lateral forces. One exterior and two interior frames were linked at each floor level using rigid elements with no moment transfer between frames (see Fig. 4.7).

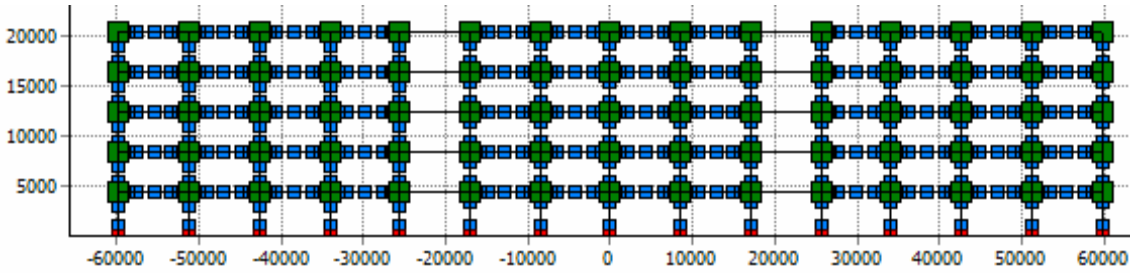

Fig. 4.7. Model of case study building used in ZEUS-NL analysis (units in mm)

As shown in Fig. 4.8, rigid elements were placed at every beam-column and slab-column joint. This prevents plastic hinges from forming inside the joints and moves the inelastic behavior outside the joint region where it is expected to occur.

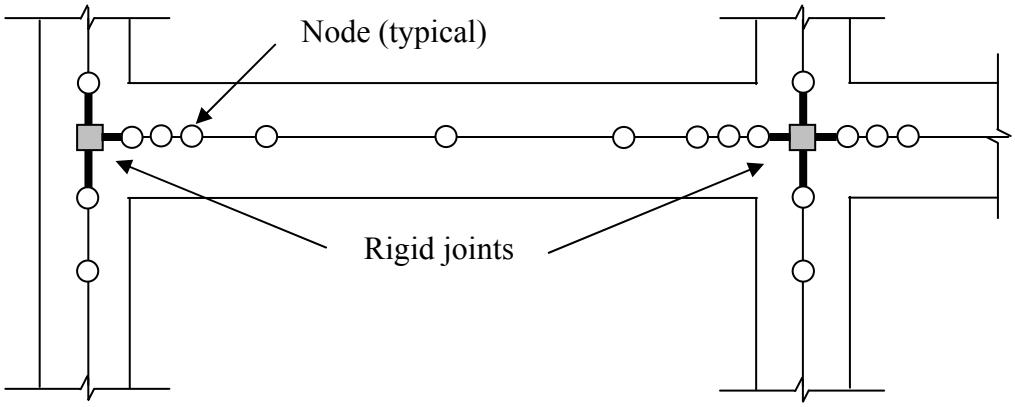

Fig. 4.8. Definition of rigid joints

The effective width of beam and slab members is also an important issue for two-dimensional modeling. Because the ZEUS-NL program calculates and updates various section properties at every time-step during analysis, it is not necessary to define cracked section properties. The uncracked section properties were defined based on the recommendations by Hueste and Wight (1997). To define the stiffness of the spandrel beam members, an effective width of 1120 mm was used based on the effective flange width defined in Section 8.10.3 of *ACI 318-02* (ACI Comm. 318 2002). Tables 4.5 and 4.6 present the parameters used to model the exterior and interior frame members, respectively.

Table 4.5. Parameters for exterior frame

Parameter	Description	Expression	Value, mm (in.)
Effective beam width for stiffness	I_g	$b_w + 1/12\ l_2$	1120 (44)
	A_g		
Effective beam width for strength	Compression zone for positive bending [ACI 318, Sec. 8.10.3]	$b_w + 1/12\ l_2$	1120 (44)
	Compression zone for negative bending	b_w	406 (16)
	Tension zone for negative bending	$b_w + 1/4\ l_2$	2540 (100)

Notes:
I_g = Gross moment of inertia
A_g = Gross area
l_2 = Length of slab span in transverse direction (center-to-center of supports)
b_w = Width of beam section projecting below the slab
h_w = Distance beam projects below the slab

Table 4.6. Parameters for interior frame

Parameter	Description	Value
Slab-Beam Effective Width	Strength	Full Width, l_2
	Stiffness	$1/2\ l_2$

Notes:
l_2 = Length of slab span in transverse direction (center-to-center of supports)

To obtain more accurate results from the analysis, all the beam and slab members were divided into ten-sub elements. To apply the gravity loads using point loads, three nodes were defined at the quarter points, dividing the beams and slabs into four sub elements. For modeling of the rigid zone within the joints, a node was added at each column face. In order to reflect the cut-off of reinforcement, a node was added at 914 mm (3 ft.) from each column face. In addition to this, the closest members from each column face were divided by two sub elements so that the location of Gauss points is close enough to calculate the forces more accurately. Columns were divided into five-sub elements using a similar approach where more refinement is used at the element ends. Fig. 4.9 shows the overall node geometry for a typical frame and Fig. 4.10 shows

the details of the boxed area in Fig. 4.9. For the nonlinear dynamic analysis, masses were lumped at the beam-column and slab-column joints.

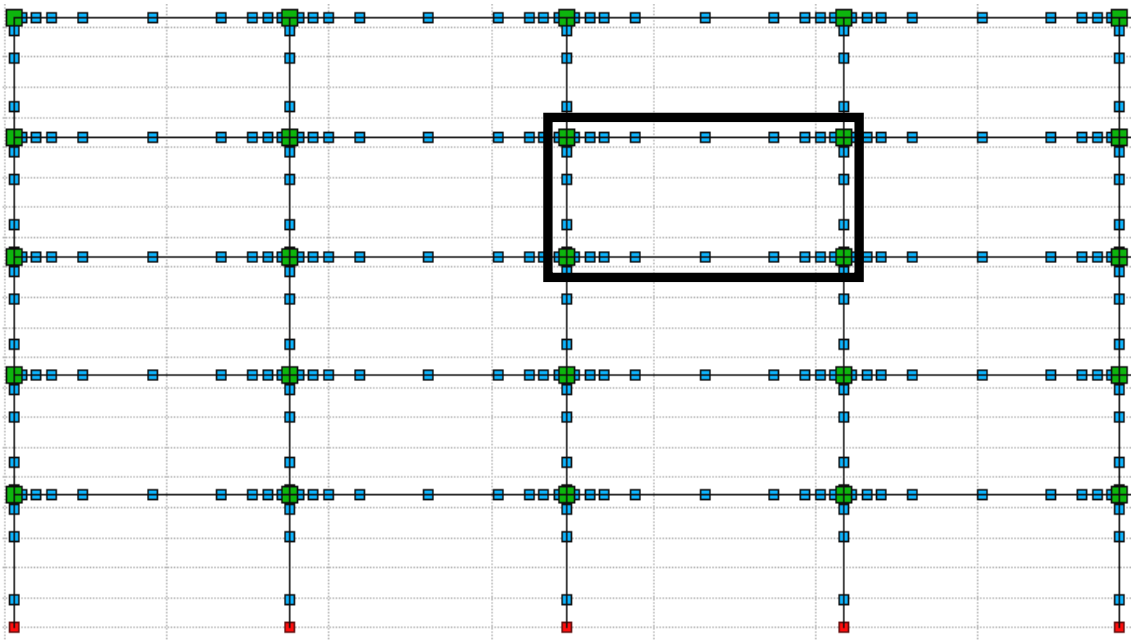

Fig. 4.9. Modeling of case study building in ZEUS-NL – typical frame geometry

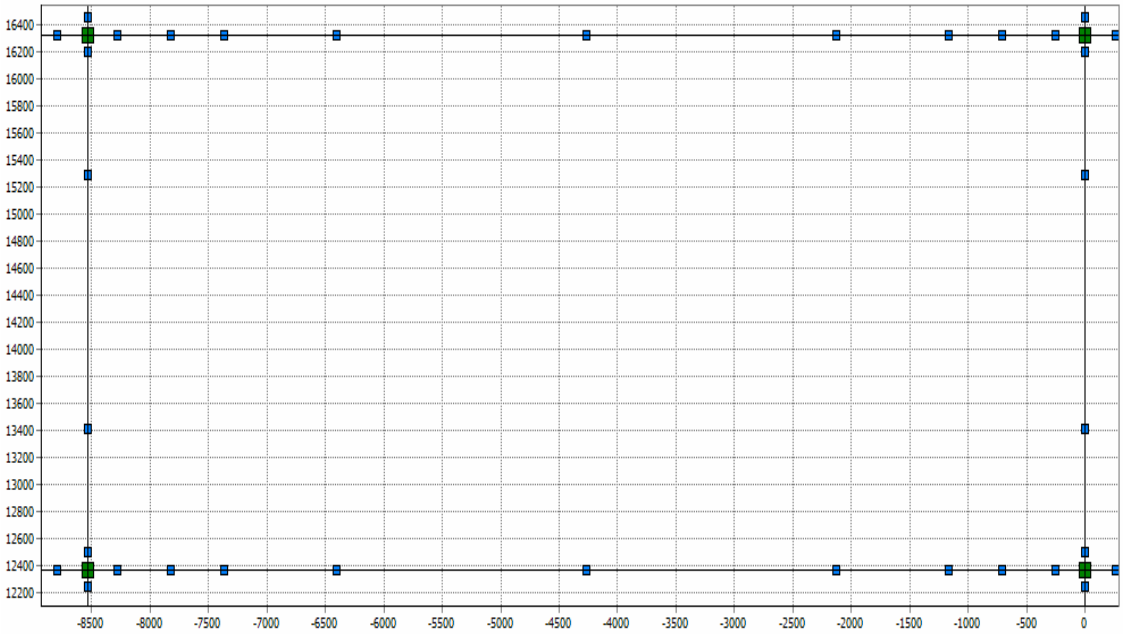

Fig. 4.10. Details of typical modeling of frame members (units in mm)

4.3.1.2 Material Models

Two material models were used in the ZEUS-NL model of the case study building. The bilinear elasto-plastic model with kinematic strain-hardening model (stl1) was used for the reinforcement and rigid connections, and the uniaxial constant confinement concrete model (conc2) was used for the concrete.

Three parameters are required for the stl1 model: Young's modulus (E), yield strength (σ_y) and a strain-hardening parameter (μ). For the conc2 model, four parameters are required: compressive strength (f'_c), tensile strength (f_t), maximum strain (ε_{co}) corresponding to f'_c, and a confinement factor (k). Table 4.7 shows the values for the parameters used in this study. For the rigid connections, the values of the Young's modulus and yield strength were chosen to be very large to prevent yielding. The parameter k is discussed below.

Table 4.7. Values for material modeling parameters in ZEUS-NL

Material type	Parameter	Values
stl1 (Steel)	E	200,000 N/mm^2 (29,000 ksi)
	σ_y	413 N/mm^2 (60,000 psi)
	μ	0.02
stl1 (Rigid connection)	E	6,890,000 N/mm^2 (1,000,000 ksi)
	σ_y	34,500 N/mm^2 (5,000,000 psi)
	μ	0.02
conc2 (Concrete for columns)	f'_c	27.6 N/mm^2 (4000 psi)
	f_t	2.76 N/mm^2 (400 psi)
	ε_{co}	0.002
	k	1.02
conc2 (Concrete for beams and slabs)	f'_c	27.6 N/mm^2 (4000 psi)
	f_t	2.76 N/mm^2 (400 psi)
	ε_{co}	0.002
	k	1.0

Note: See Fig. 4.3 for graphical description of variables.

Based on the material stress-strain relationships, moment-curvature analysis is conducted to predict the ductility and expected member behavior under varying loads. The confinement factor (k) for a rectangular concrete section with axial compression forces is based on the model of Mander et al. (1988) and is calculated as follows:

$$k = \frac{f'_{cc}}{f'_{co}} \tag{4.2}$$

where f'_{cc} is the confined concrete compressive strength and f'_{co} is the unconfined concrete compressive strength. These are calculated using the following equations.

$$f'_{cc} = f'_{co}\left(-1.254 + 2.254\sqrt{1 + \frac{7.94 f'_l}{f'_{co}}} - 2\frac{f'_l}{f'_{co}}\right) \tag{4.3}$$

$$f'_l = k_e \rho f_{yh} \tag{4.4}$$

$$k_e = \frac{A_e}{A_{cc}} \tag{4.5}$$

$$A_e = \left(b_c d_c - \sum_{i=1}^{n} \frac{(w_i')^2}{6}\right)\left(1 - \frac{s'}{2b_c}\right)\left(1 - \frac{s'}{2d_c}\right) \tag{4.6}$$

$$A_{cc} = A_c\left(1 - \rho_{cc}\right) \tag{4.7}$$

where:

f'_l = Effective lateral confining stresses
k_e = Confinement effectiveness coefficient
f_{yh} = Yield strength of transverse reinforcement
A_e = Area of effectively confined core concrete
A_{cc} = Area of core within center lines of perimeter spiral or hoops excluding area of longitudinal steel
A_c = Area of core of section within center lines of perimeter spiral
b_c = Concrete core dimension to center line of perimeter hoop in x-direction

d_c = Concrete core dimension to center line of perimeter hoop in y-direction
w_i' = i^{th} clear transverse spacing between adjacent longitudinal bars
s' = Clear spacing between spiral or hoop bars
ρ_{cc} = Ratio of area of longitudinal steel to area of core of section

For this model, the nominal values for the steel yield strength and concrete compressive strength were used. The minimum value of k is 1.0, which indicates an unconfined section. In this case, for the columns, where the transverse reinforcement is placed at every 457 mm (18 in.), the confinement factor is only 1.02 based on the above calculation.

4.3.1.3 Element and Cross-Section Types

For column, beam, slab and rigid elements, a cubic elasto-plastic three-dimensional element (cubic) was used. The lumped mass element (Lmass) was used to define the lumped masses at the joints for the dynamic and eigenvalue analysis. For the rigid joints, a three-dimensional joint element with uncoupled axial, shear and moment actions (joint) was used. The force-displacement characteristics for the axial forces, shear forces, and moments in the joint elements were determined by the joint curves that describe joint action, such as an elastic or elasto-plastic behavior.

For the cross-sections in the ZEUS-NL analysis, the RC rectangular section (rcrs) was selected to model the column members and the RC T-section (rcts) was selected to model the beam and slab members in the frame. Because there is no typical section for slab member, the rcts section was used with a negligible flange width and length. The input parameters for rcrs are section height, stirrup height, section width and stirrup width. The rcts section requires eight dimensional parameters: slab thickness, beam height, confined height in slab, confined height in beam, slab effective width, beam width, confined width in slab and confined width in beam. Fig. 4.11 shows cross sections used in the case study building analysis and Table 4.8 shows the values used in this analysis.

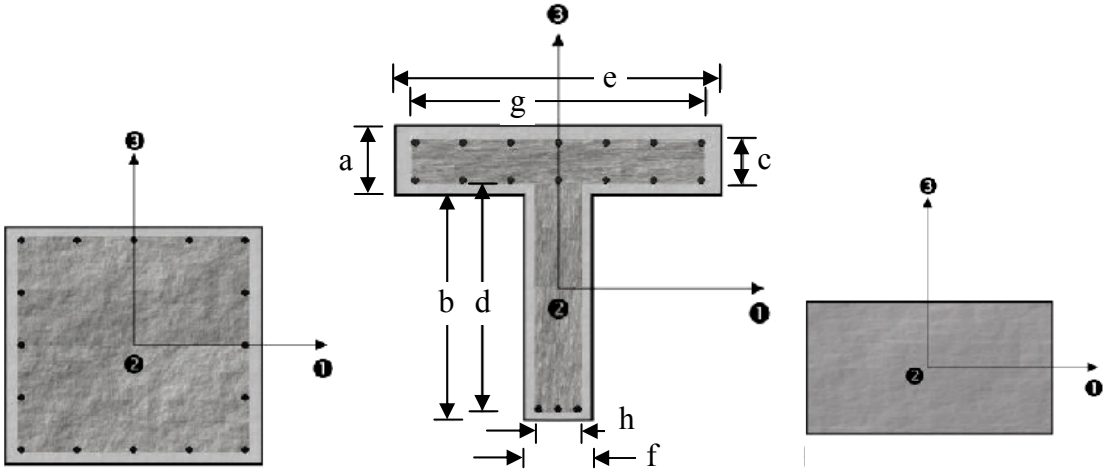

(a) rcrs (RC rectangular) (b) rcts (RC T-section) (c) rss (Rectangular solid)

Fig. 4.11. Sections for the case study building analysis (Elnashai et al. 2002)

In addition, the reinforcement for the short member in beam and slab elements which is located near the joints, were reduced to reflect bar cutoffs and discontinuous bottom bars that had reduced embedment lengths. The available tensile force was calculated based on the proportional relationship of embedment length and development length of the bottom bars, using the following equations (Aycardi et al. 1994).

$$F_t = \frac{l_{embedment}}{l_{development}} A_s f_y \tag{4.8}$$

where:

F_t = Tensile force that can be developed by reinforcement with reduced embedment length

$l_{embedment}$ = Embedment length of a reinforcing bar

$l_{development}$ = Development length of a reinforcing bar (from *ACI 318-02*)

A_s = Area of steel reinforcement

The reduced reinforcement area, *As(red)*, for bars that are not fully developed was then found using the following relationship.

$$As(red) = \frac{F_t}{f_y} \tag{4.9}$$

This reduced reinforcement area was then modeled in ZEUS-NL.

Table 4.8. Values for section modeling parameters in ZEUS-NL

Section type	Dimensional parameter	Values, mm (in.)
Column	Section height and width	508 (20)
	Stirrup height and width	384 (15.1)
Beam (Ground floor - 4th floor)	a. Slab thickness	254 (10)
	b. Beam web height	356 (14)
	c. Confined height in slab	178 (7)
	d. Confined height in beam web	356 (14)
	e. Slab effective width	1120 (44)
	f. Beam web width	406 (16)
	g. Confined width in slab	1090 (43)
	h. Confined width in beam web	330 (13)
Beam (Roof level)	a. Slab thickness	254 (10)
	b. Beam web height	305 (12)
	c. Confined height in slab	178 (7)
	d. Confined height in beam web	305 (12)
	e. Slab effective width	1120 (44)
	f. Beam web width	406 (16)
	g. Confined width in slab	1090 (43)
	h. Confined width in beam web	330 (13)
Slab	a. Slab thickness	254 (10)
	b. Beam web height	0.01*
	c. Confined height in slab	216 (8.5)
	d. Confined height in beam web	0.01*
	e. Slab effective width	4270 (168)
	f. Beam web width	4270 (168)
	g. Confined width in slab	4230 (167)
	h. Confined width in beam web	4230 (167)
Rigid element	Height	254 (10)
	Width	254 (10)

* To model slab members using the rcts (RC T-Section), a very small value was used for the beam web height.

4.3.1.4 Loads, Masses and Damping

The gravity loads consist of distributed loads (*w*) due to the weight of beams and slabs, and point loads due to the column weight. Point loads were applied to the beam-column and slab-column joints to include the column weight. Because there is no distributed load definition in the ZEUS-NL program, beams and slabs were divided into four sub-elements and three equivalent point loads were applied to the nodes between sub elements. Equivalent point loads were calculated using the concentrated load equivalents factors in the Table 5-16 of the third edition of *LRFD* (AISC 2001). Fig. 4.12 shows the equivalent point loads applied on beams and slabs. For the nonlinear dynamic analysis, masses were lumped at beam-column or slab-column joints.

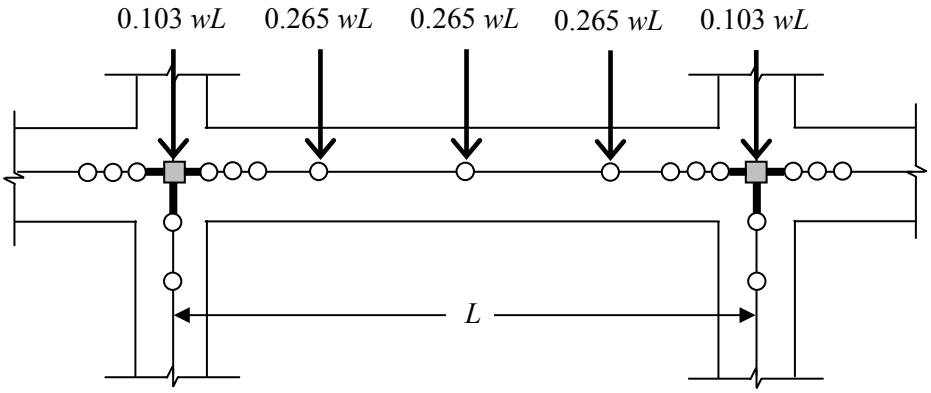

Fig. 4.12. Equivalent point loads applied on beam and slab members

4.3.2 DRAIN-2DM Model

4.3.2.1 Model Geometry and Material Models

Fig. 4.13 shows the analytical model used in the DRAIN-2DM analysis. Half of the case study building was analyzed with a two-dimensional analytical model, which is the same as the ZEUS-NL model geometry. Rigid zones within the beam-column and slab-column joints were also defined, as described by Fig. 4.14.

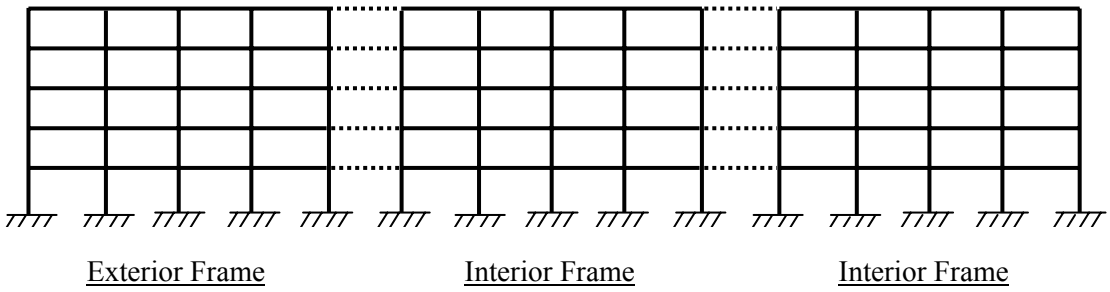

Fig. 4.13. Model of case study building used in DRAIN-2DM analysis

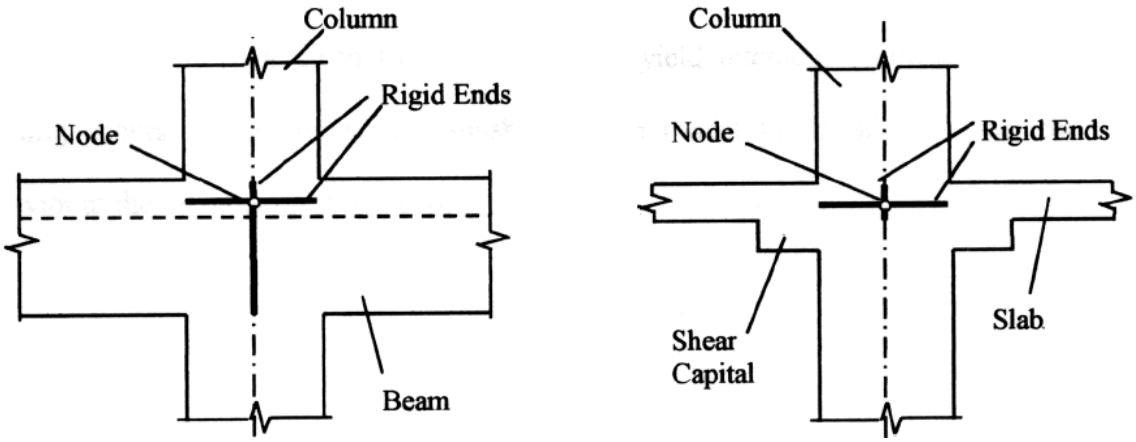

(a) Beam-column connection (b) Slab-column connection

Fig. 4.14. Rigid end zones for connections (Hueste and Wight 1997)

All material properties, including the Young's modulus, yield strength and strain-hardening modulus for the reinforcement and the concrete compressive strength were defined as the same values used for the ZEUS-NL model.

4.3.2.2 Element and Cross-Section Types

The beam-column element (Element 2) was selected to model the column members, and the buckling element (Element 9), which carries axial load only, was used to model the rigid links. The RC beam element (Element 8) was selected to model the beam members in the exterior frame. The slab members were modeled using the RC slab element (Element 11), which allows punching shear failure prediction.

The hysteretic behavior modeled at the member ends required a pinching factor, which describe slippage of bars and crack closure within the beam-column joint. A pinching factor of 0.75 was selected for all beam and slab members, to correspond to a moderate level of pinching (Hueste and Wight 1997). The unloading stiffness factor of 0.30 and no strength deterioration factor were used for this analysis. To define the punching shear model for Element 11, the critical rotation (θ_{cr}) was determined from a push-over analysis. The procedure to determine appropriate rotation values followed the methodology suggested by Hueste and Wight (1999). In this study, the critical rotation was calculated as the average member-end rotation in the slab elements when the building drift reaches 1.25%.

For the initial stiffness for beam and slab members, the cracked section properties are used in the DRAIN-2DM model. For beams, the cracked moment of inertia is the gross moment of inertia multiplied by a factor of 0.35. The corresponding factors for column and slab members are 0.70 and 0.25, respectively. These factors are based on those recommended by *ACI 318-02* (ACI Comm. 318 2002). The gross moment of inertia for slab members in Table 4.9 was calculated based on full length of a slab span in transverse direction. Table 4.9 summarizes the parameters for section modeling in DRAIN-2DM.

Table 4.9. Parameters for section modeling in DRAIN-2DM

Section type	Parameter	Value
Beam	Cracked stiffness	$0.35*I_g$
	Pinching factor	0.75
	Unloading stiffness factor	0.30
	Strength deterioration factor	0
Column	Cracked stiffness	$0.70*I_g$
Slab	Cracked stiffness	$0.25*I_g$
	Pinching factor	0.75
	Unloading stiffness factor	0.30
	Strength deterioration factor	0
Floor slabs	Gravity shear ratio	0.29
	Average yield rotation	0.0151 rad.
	Average critical rotation	0.0173 rad.
	Average allowable rotation	0.0399 rad.
Roof slab	Gravity shear ratio	0.39
	Average yield rotation	0.0111 rad.
	Average critical rotation	0.00646 rad.
	Average allowable rotation	0.0128 rad.

4.3.2.3 Loads, Masses and Damping

In order to account for gravity loads, fixed end forces were applied to the beam and slab member ends. These were computed based on the results from an analysis for the applied gravity loads using the Visual Analysis program (IES 1998). For dynamic analysis, the viscous damping [C] was assumed to be proportional to the mass matrix [M] and the initial elastic stiffness [K_0], as follows:

$$[C] = \alpha_0 [M] + \beta_0 [K_0] \tag{4.10}$$

where α_0 and β_0 are the mass proportional damping factor and stiffness proportional damping factor, respectively. These proportional factors are calculated using the following equations (Raffaelle and Wight 1992). The periods of the first and second modes were found from the eigenvalue analysis with uncracked section properties using

the ZEUS-NL program. The results for this case study building were α_0 = 0.167 and β_0 = 0.0018.

$$\alpha_0 = \frac{4\pi(T_1\xi_1 - T_2\xi_2)}{T_1^2 - T_2^2} \tag{4.11}$$

$$\beta_0 = \frac{T_1T_2(T_1\xi_1 - T_2\xi_2)}{\pi(T_1^2 - T_2^2)} \tag{4.12}$$

where:

T_1 = Natural period for the 1st mode of vibration = 1.14 s
T_2 = Natural period for the 2nd mode of vibration = 0.367 s
ζ_1 = Target critical damping ratio for the 1st mode of vibration = 2%
ζ_2 = Target critical damping ratio for the 2nd mode of vibration = 2%

4.4 Synthetic Ground Motion Data

In order to predict the response of structures during an earthquake, representative ground motion data for that location should be used. However, there is not adequate recorded strong motion data to characterize the seismicity for specific locations in the Mid-America region. Therefore, synthetic ground motions have been developed for cities in the region impacted by the New Madrid Seismic Zone (NMSZ).

Synthetic ground motions developed by Wen and Wu (2000) for the cities of St. Louis, Missouri and Memphis, Tennessee were used in this study. These motions include suites of ten ground motion records for each of two probabilities of exceedance levels: 2% and 10% in 50 years. In addition, the ground motions are available for representative soil and for bedrock. In this study ground motions for representative soil were selected because soil can affect the ground motion of an earthquake by amplifying the accelerations and the structural model does not include a soil model. To reduce the

computational time, the ground motions were shortened for the nonlinear dynamic analysis at the time point where the energy reaches 95% of the total energy imparted by a particular ground motion record. This procedure was based on the methodology developed by Trifunac and Brady (1975). The equation to compute the total energy of a strong ground motion record is given in Eq. 4.13. Based on this relationship, Trifunac and Brady suggested the duration of the strong ground motion to be the time interval remaining between the low and high 5% cut-off of the total energy. For this study, only the high 5% cut-off of the ground motion was used to reduce the record.

$$E_{Total} = \int_0^t a^2(t)dt \tag{4.13}$$

where:

E_{Total} = Total energy of a ground motion record
$a(t)$ = Acceleration at a time, t

Figs. 4.15 and 4.16 show the response spectra for the ground motion sets. Details of each ground motion record are shown in Tables 4.10 to 4.13. Plots of each ground motion record are shown in Figs. 4.17 to 4.20.

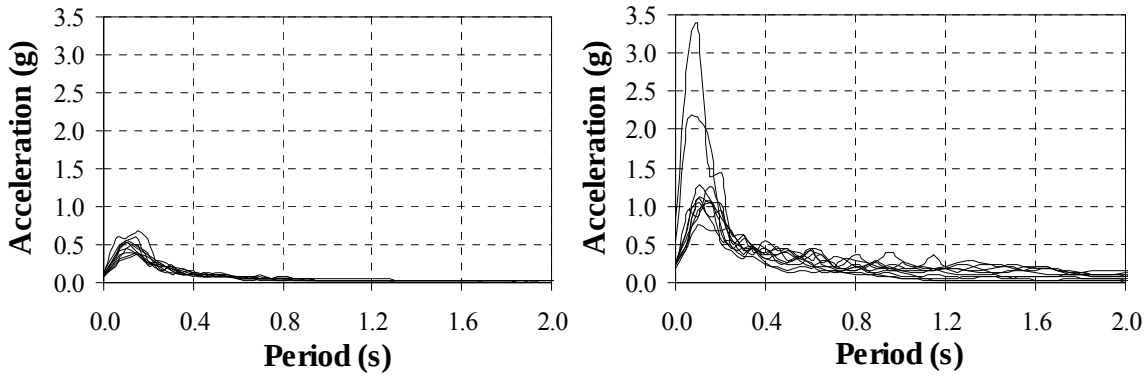

(a) 10% in 50 years (b) 2% in 50 years

Fig. 4.15. Response spectra for St. Louis ground motions (2% critical damping)

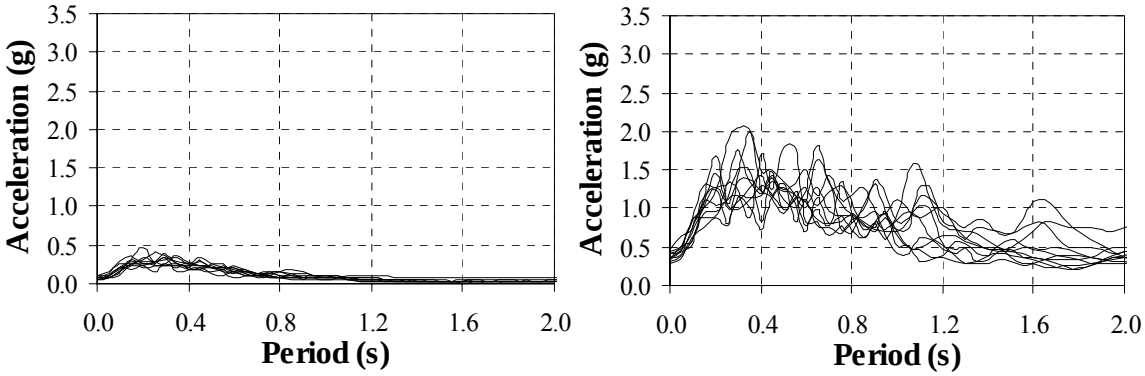

(a) 10% in 50 years (b) 2% in 50 years

Fig. 4.16. Response spectra for Memphis ground motions (2% critical damping)

Table 4.10. 10% probability of exceedance in 50 years ground motions for St. Louis, Missouri (from Wen and Wu 2000)

Ground motion record ID	Peak ground acceleration (g)	Duration (s)	Duration of 95% energy (s)	Body-wave magnitude	Focal depth (km)	Epicentral distance from St. Louis (km)
l10_01s	0.127	41.0	18.9	6.0	2.7	76.4
l10_02s	0.097	81.9	27.0	6.9	9.3	202
l10_03s	0.091	81.9	34.4	7.2	4.4	238
l10_04s	0.111	41.0	23.6	6.3	9.8	252
l10_05s	0.129	41.0	16.0	5.5	2.9	123
l10_06s	0.113	41.0	22.0	6.2	7.7	208
l10_07s	0.097	81.9	27.2	6.9	1.7	194
l10_08s	0.118	41.0	20.6	6.2	27.6	175
l10_09s	0.106	41.0	21.6	6.2	6.5	221
l10_10s	0.085	81.9	28.8	6.9	2.7	237

Table 4.11. 2% probability of exceedance in 50 years ground motions for St. Louis, Missouri (from Wen and Wu 2000)

Ground motion record ID	Peak ground acceleration (g)	Duration (s)	Duration of 95% energy (s)	Body-wave magnitude	Focal depth (km)	Epicentral distance from St. Louis (km)
l02_01s	0.230	150	48.9	8.0	17.4	267
l02_02s	0.246	150	49.9	8.0	9.1	230
l02_03s	0.830	20.5	9.8	5.4	2.1	28.7
l02_04s	0.249	81.9	31.9	7.1	5.5	253
l02_05s	0.190	150	40.2	8.0	17.4	254
l02_06s	0.243	81.9	26.7	6.8	5.8	225
l02_07s	0.244	150	56.9	8.0	33.9	196
l02_08s	0.239	150	28.2	8.0	9.1	261
l02_09s	0.245	150	30.4	8.0	9.1	281
l02_10s	0.544	41.0	14.9	5.9	4.4	47.7

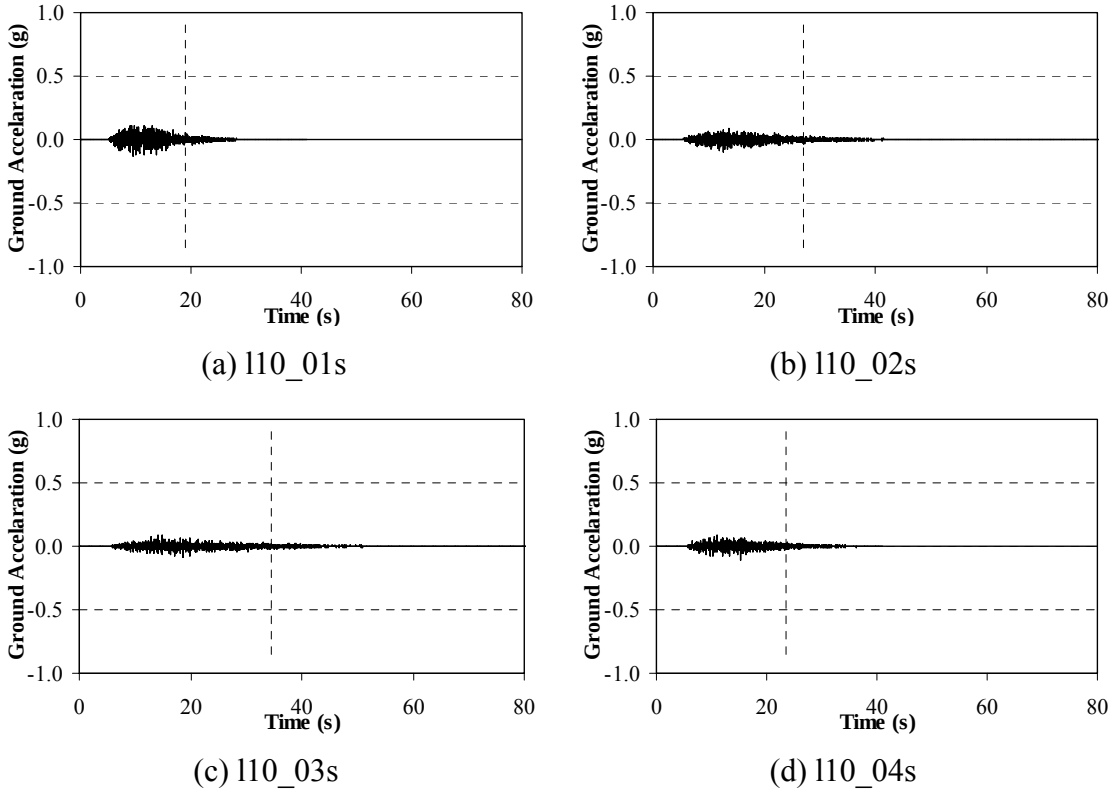

(a) l10_01s (b) l10_02s

(c) l10_03s (d) l10_04s

Fig. 4.17. Acceleration time histories for 10% in 50 years St. Louis Motions [from Wen and Wu (2000)]

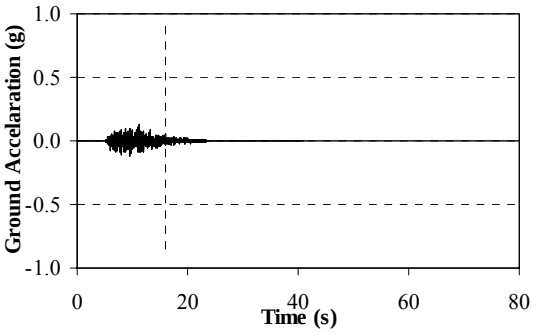

(e) l10_05s

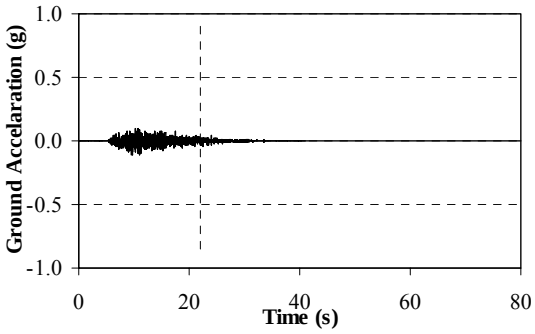

(f) l10_06s

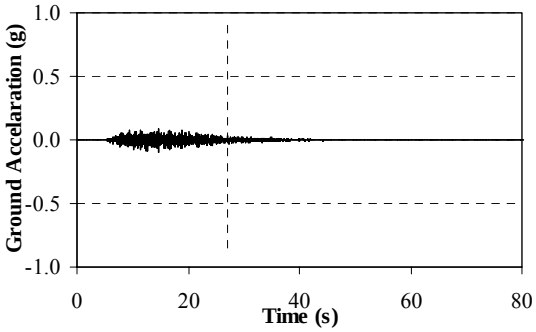

(g) l10_07s

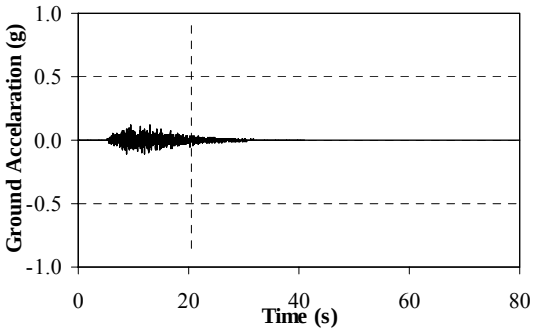

(h) l10_08s

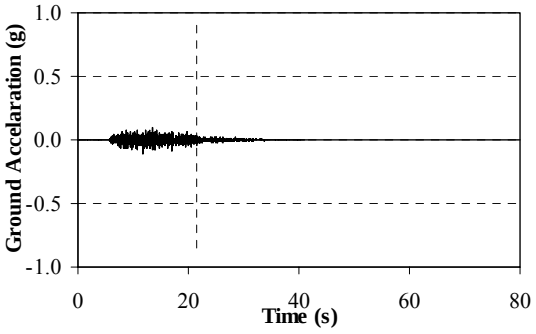

(i) l10_09s

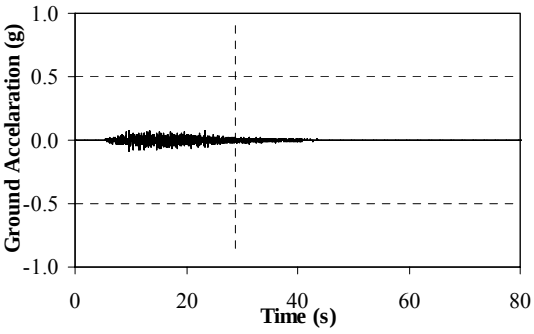

(j) l10_10s

Fig. 4.17. Continued

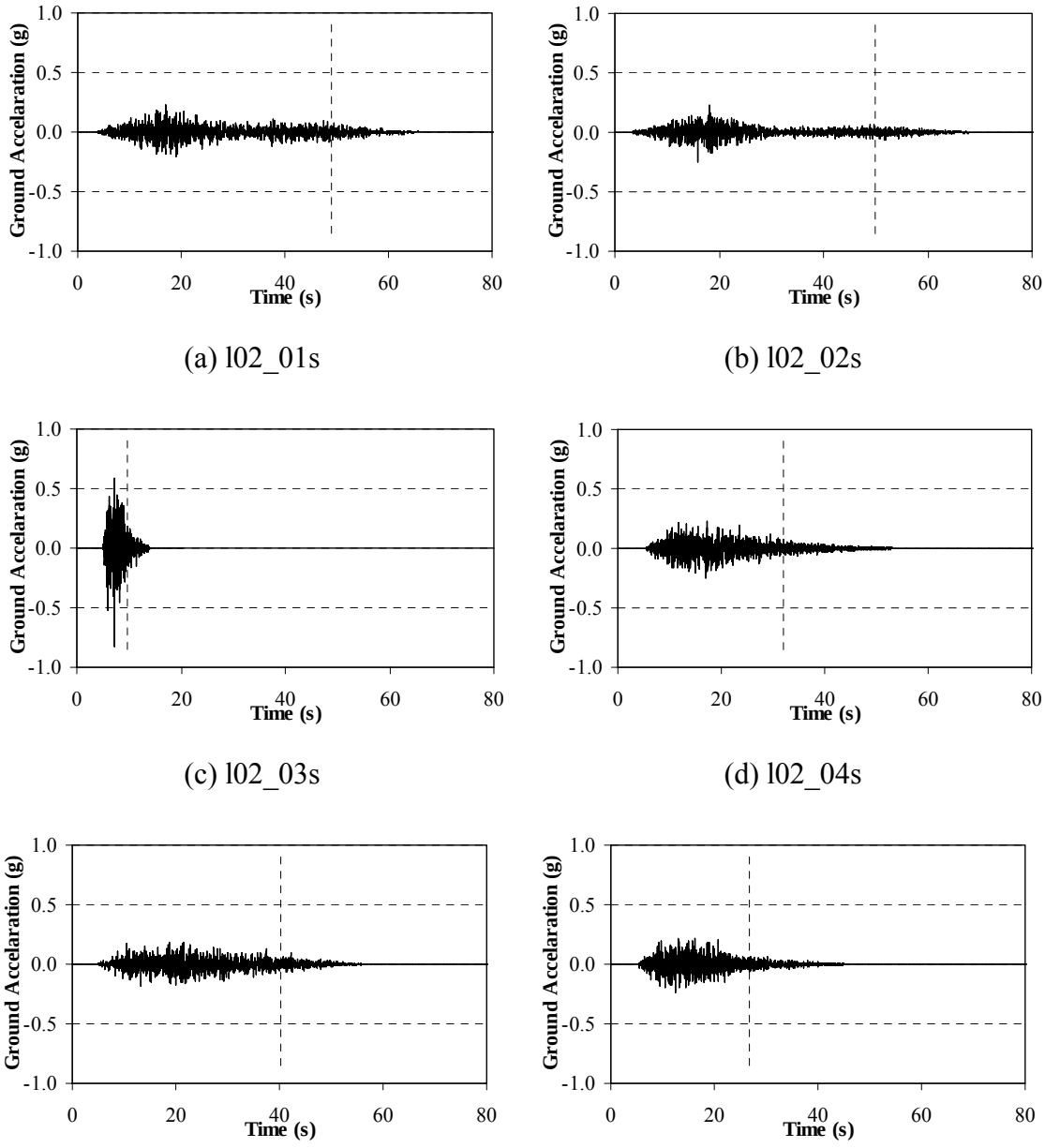

Fig. 4.18. Acceleration time histories for 2% in 50 years St. Louis motions [from Wen and Wu (2000)]

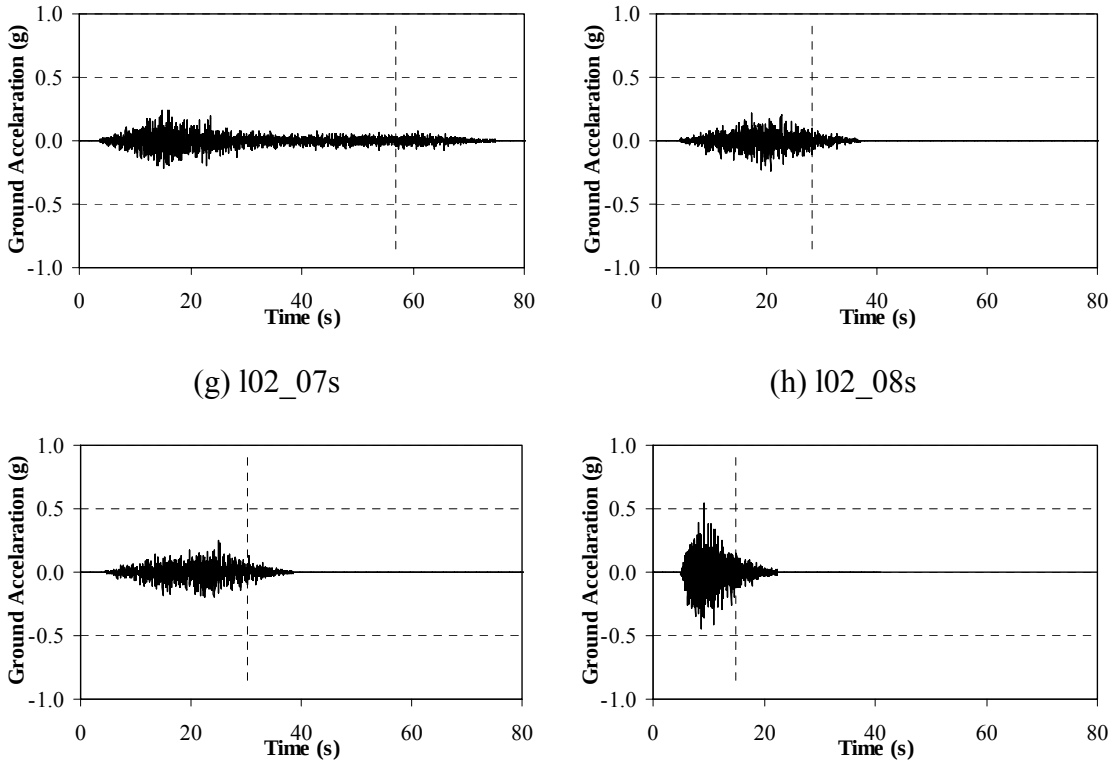

(g) l02_07s (h) l02_08s

(i) l02_09s (j) l02_10s

FIG. 4.18. Continued

Table 4.12. 10% probability of exceedance in 50 years ground motions for Memphis, Tennessee (from Wen and Wu 2000)

Ground motion record ID	Peak ground acceleration (g)	Duration (s)	Duration of 95% energy (s)	Body-wave magnitude	Focal depth (km)	Epicentral distance from Memphis (km)
m10_01s	0.059	41.0	22.2	6.3	5.2	121
m10_02s	0.075	41.0	19.7	6.4	6.7	57.5
m10_03s	0.070	41.0	17.5	6.8	18.1	125
m10_04s	0.068	41.0	23.4	6.8	2.1	92.4
m10_05s	0.108	41.0	14.9	6.2	27.0	107
m10_06s	0.054	150	48.9	6.2	3.2	41.2
m10_07s	0.070	41.0	20.3	6.5	11.5	58.8
m10_08s	0.088	20.5	12.4	6.5	23.9	129
m10_09s	0.093	20.5	10.2	6.3	9.5	166
m10_10s	0.064	41.0	18.5	6.8	8.7	35.6

Table 4.13. 2% probability of exceedance in 50 years ground motions for Memphis, Tennessee (from Wen and Wu 2000)

Ground motion record ID	Peak ground acceleration (g)	Duration (s)	Duration of 95% energy (s)	Body-wave magnitude	Focal depth (km)	Epicentral distance from Memphis (km)
m02_01s	0.439	150	29.2	8.0	25.6	148
m02_02s	0.333	150	23.5	8.0	33.9	186
m02_03s	0.360	150	23.7	8.0	25.6	163
m02_04s	0.323	150	52.8	8.0	9.10	170
m02_05s	0.476	150	36.2	8.0	9.10	97.6
m02_06s	0.416	150	37.1	8.0	17.4	118
m02_07s	0.365	150	24.8	8.0	17.4	119
m02_08s	0.292	150	20.9	8.0	9.10	146
m02_09s	0.335	150	26.0	8.0	9.10	171
m02_10s	0.412	150	22.2	8.0	17.4	188

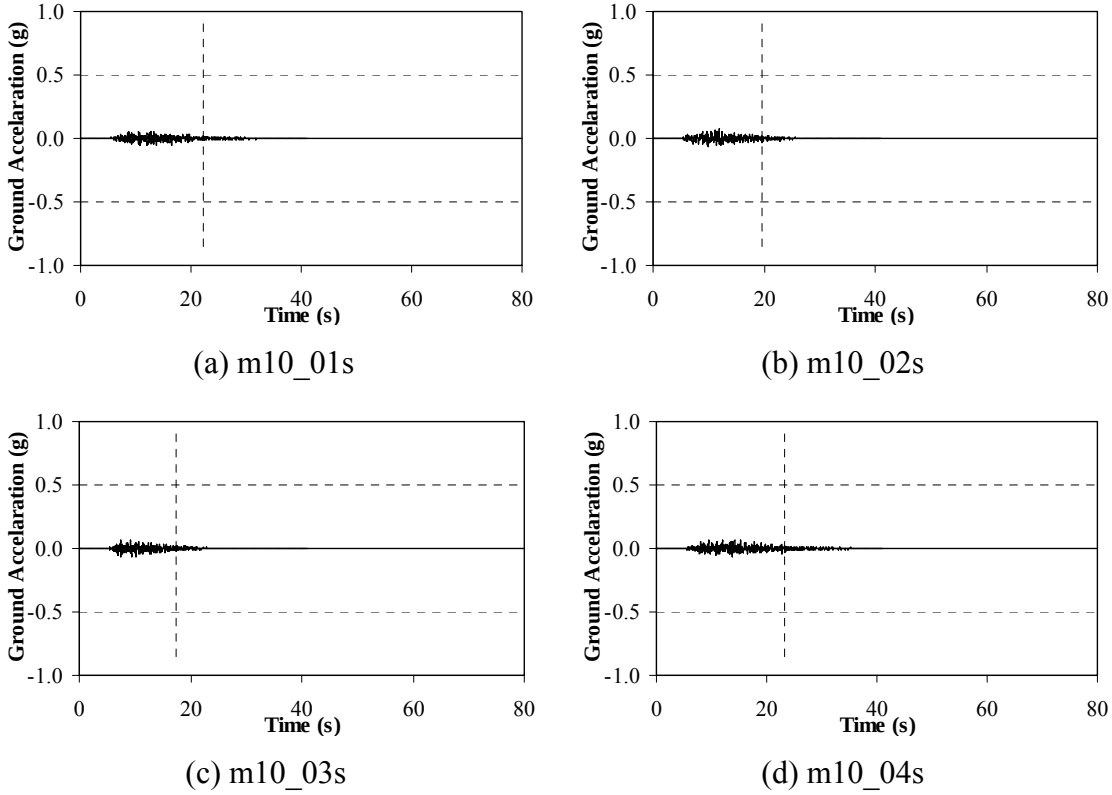

(a) m10_01s (b) m10_02s

(c) m10_03s (d) m10_04s

Fig. 4.19. Acceleration time histories for 10% in 50 years Memphis motions [from Wen and Wu (2000)]

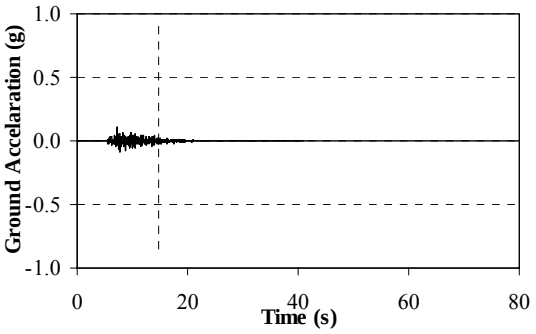

(e) m10_05s

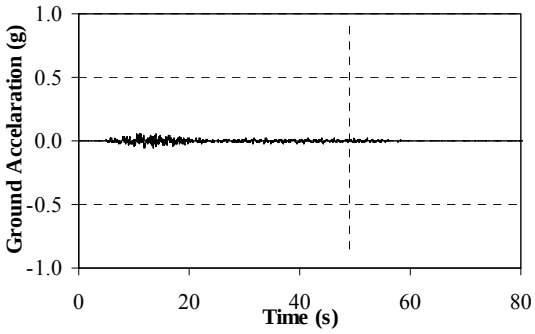

(f) m10_06s

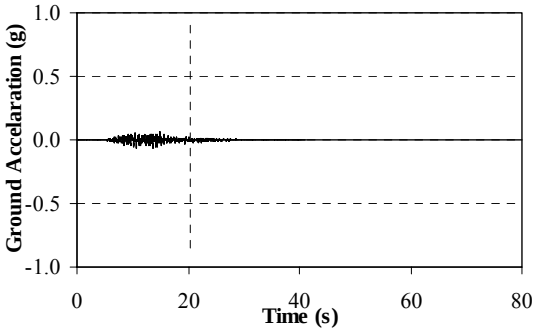

(g) m10_07s

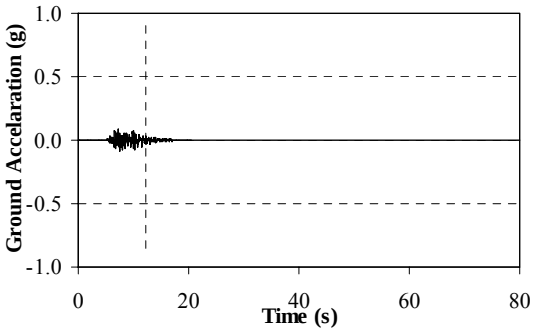

(h) m10_08s

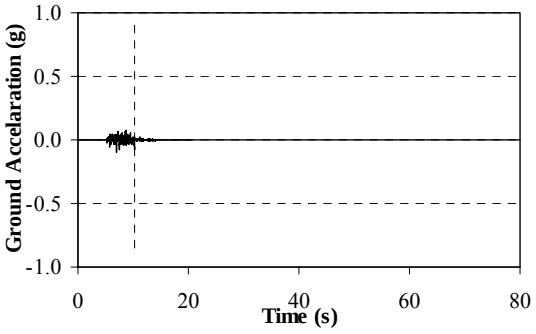

(i) m10_09s

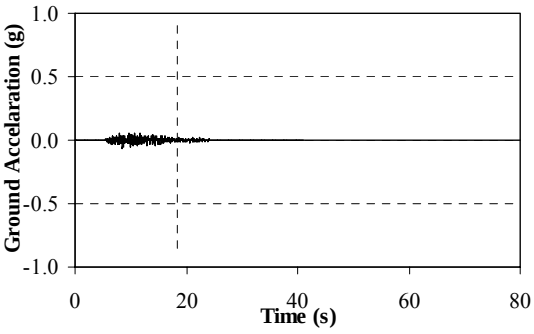

(j) m10_10s

FIG. 4.19. Continued

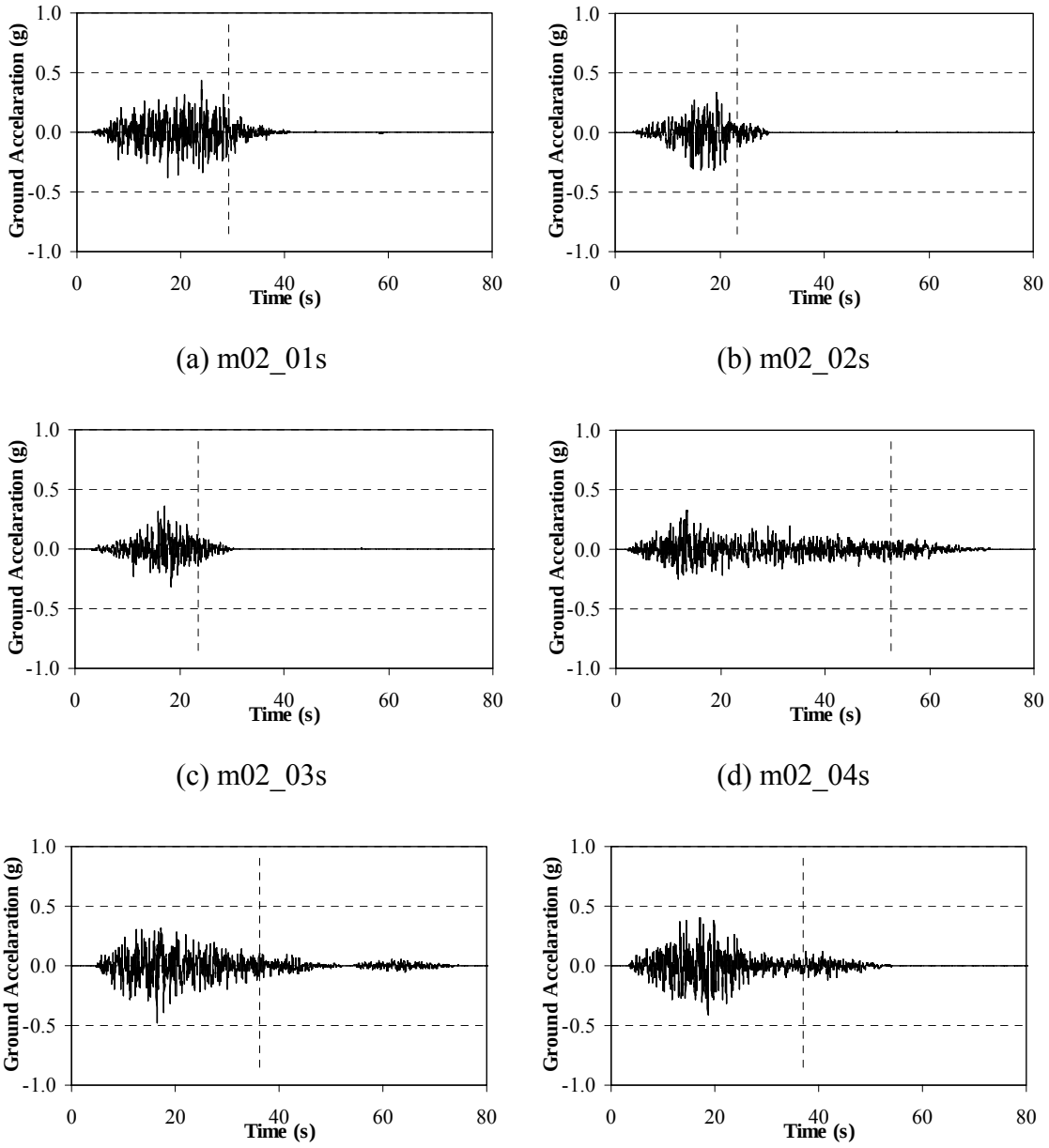

(a) m02_01s (b) m02_02s

(c) m02_03s (d) m02_04s

(e) m02_05s (f) m02_06s

Fig. 4.20. Acceleration time histories for 2% in 50 years Memphis motions [from Wen and Wu (2000)]

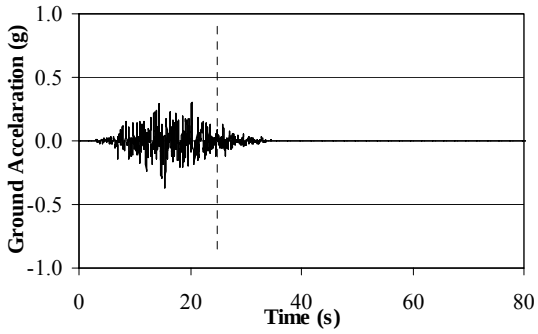

(g) m02_07s

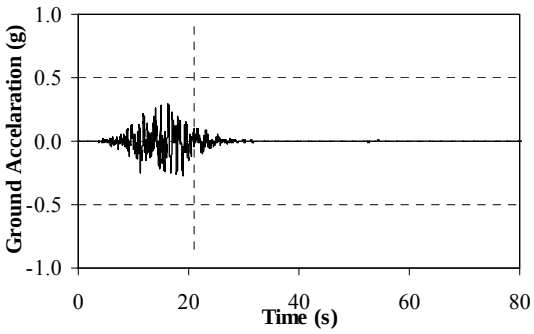

(h) m02_08s

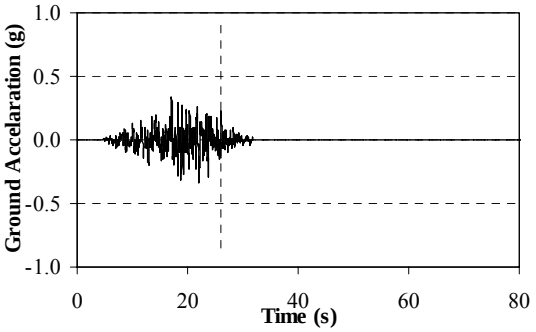

(i) m02_09s

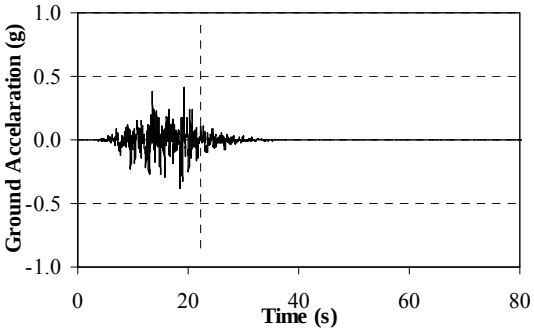

(j) m02_10s

FIG. 4.20. Continued

5 ANALYSIS OF UNRETROFITTED CASE STUDY BUILDING

5.1 Introduction

This section presents the analysis of the unretrofitted case study building. Two structural analysis methods, nonlinear static analysis and nonlinear dynamic analysis, were used to predict the seismic behavior of the building under lateral forces. A comparison of these analysis results is provided. In addition, results from two structural nonlinear analysis programs (ZEUS-NL and DRAIN-2DM) are compared. The ZEUS-NL program was selected for additional analytical studies to evaluate the expected seismic performance of the structure for St. Louis and Memphis synthetic ground motions. Based on the analytical results, fragility curves were developed using the FEMA 356 performance criteria and additional limit states. FEMA 356 provides global-level and member-level criteria for three performance levels for seismic evaluation. In this study, both global-level and member-level criteria were used for seismic evaluation of the unretrofitted and retrofitted case study building.

5.2 Comparison of ZEUS-NL and DRAIN-2DM

5.2.1 Nonlinear Static Analysis

Two different load patterns for conventional push-over analysis were used: uniform (rectangular) and inverted triangular cases. The inverted triangular load case is based on first mode shape from an eigenvalue analysis of the case study building (see Fig. 5.1). The results of the push-over analyses using the ZEUS-NL and DRAIN-2DM programs are shown in Fig. 5.2. In addition to this, a comparison of push-over analysis from these two programs is shown in Fig. 5.3.

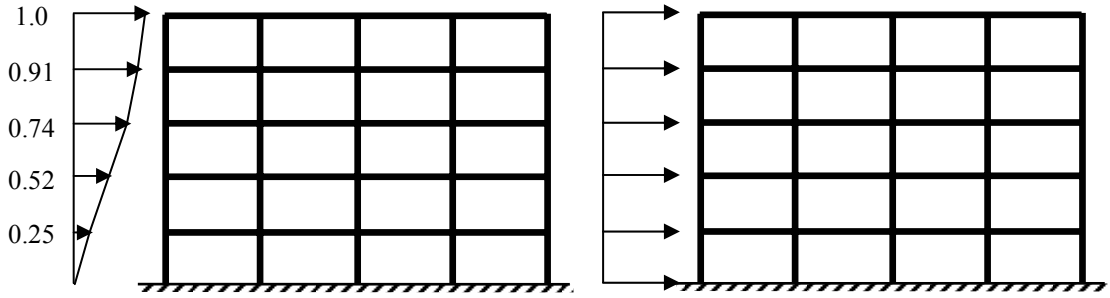

(a) Inverted triangular load pattern (b) Rectangular load pattern

Fig. 5.1. Load patterns for conventional push-over analysis

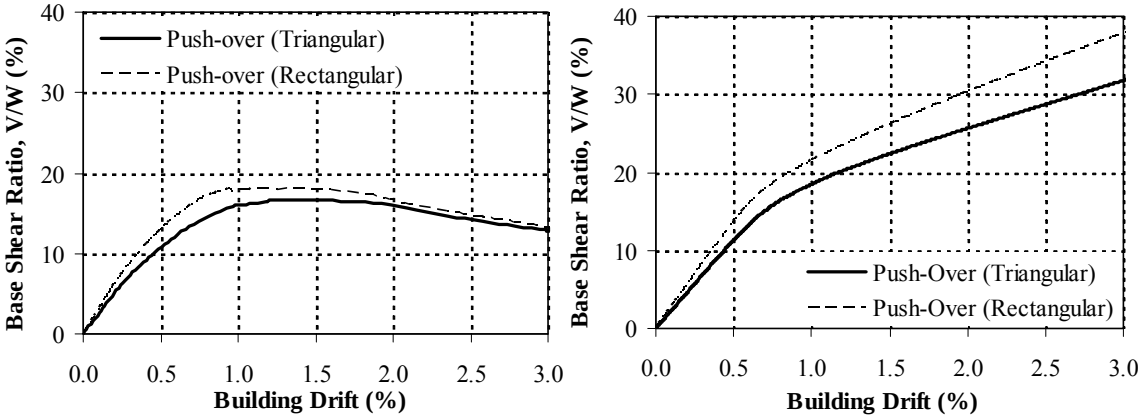

(a) ZEUS-NL (b) DRAIN-2DM

Fig. 5.2. Push-over curves

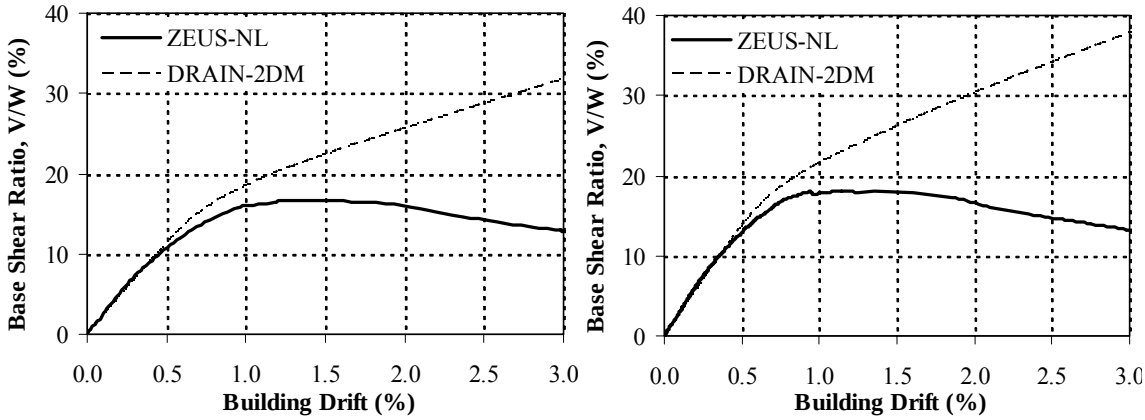

(a) Inverted triangular load pattern (b) Rectangular load pattern

Fig. 5.3. Comparison of push-over curves from ZEUS-NL and DRAIN-2DM

As shown in Fig. 5.2, the overall responses for the two load patterns have a similar shape. For both programs, however, the rectangular load case gave a slightly larger base shear ratio at a certain building drift. A comparison of the response predictions from the two programs shows some significant differences (see Fig. 5.3). From 0.0% to 0.5% building drift, the results from both programs match quite well. However, after 0.5% drift, the ZEUS-NL model had a peak value at about 1.2% building drift, while the DRAIN-2DM model had a yielding point around 0.8% building drift, but continued to take on significant load for both load patterns. Based on the above comparison, ZEUS-NL seems to more appropriately take into account P-delta effects and stiffness degradation.

The comparison of interstory drift profiles for both 1% and 2% average building drifts are shown in Fig. 5.4. At 1% building drift, both models gave a similar shape for the interstory drift profile. However, at 2% building drift, ZEUS-NL gives higher interstory drift values for the lower story levels and lower drifts for the upper story levels.

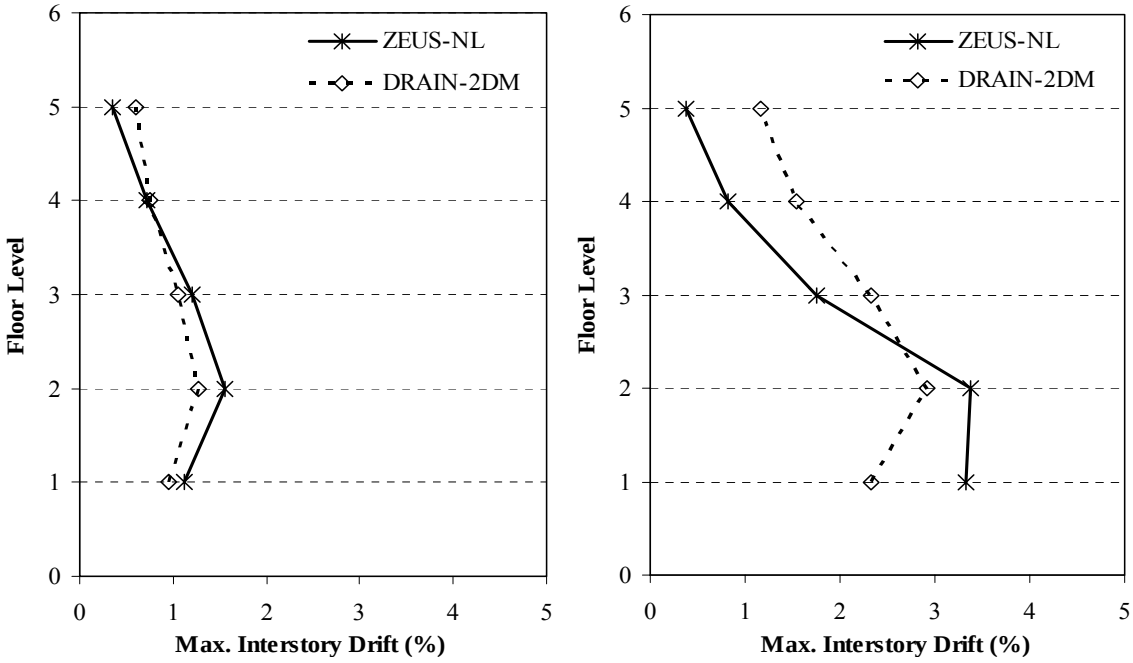

(a) 1% Building Drift (b) 2% Building Drift

Fig. 5.4. Comparison of interstory drifts for push-over analysis

5.2.2 Nonlinear Dynamic Analysis

Nonlinear dynamic analysis was performed using the ZEUS-NL and DRAIN-2DM program for twenty St. Louis ground motions (see Tables 4.9 and 4.10) to compare the predicted behavior of the case study building under dynamic loads. Modeling of seismic action was achieved by applying the ground acceleration history at the column supports. Tables 5.1 and 5.2 show the results of the nonlinear dynamic analysis for the St. Louis motions. Fig. 5.5 provides a comparison of the building drift versus time for the two models. According to Tables 5.1 and 5.2, the maximum values of building drifts are quite similar for the two models. However, as shown in Fig. 5.5, the overall response is not very close. The ground motions shown are those that gave a maximum building drift closest to the median value of the maximum building drift for each ground motion set. Because the synthetic ground motion data were developed with the lognormally distributed parameters, the median values of the maximum building drift and maximum base shear ratio were calculated based on the natural log of these values (see Eq. 5.1).

$$Y_M = e^{average\_\ln(x_i)} \tag{5.1}$$

where:

Y_M = Median response
x_i = Response for a given ground motion record *i*

Table 5.1. Maximum building drift and maximum base shear ratio for St. Louis motions (10% in 50 years)

Ground motion	Max. building drift (%)		Max. base shear ratio, V/W (%)	
	ZEUS-NL	DRAIN-2DM	ZEUS-NL	DRAIN-2DM
l10_01s	0.039	0.0387	3.2	1.27
l10_02s	0.0768	0.0763	4.33	1.52
l10_03s	0.0654	0.112	3.35	2.08
l10_04s	0.0849	0.0753	3.61	1.67
l10_05s	0.0411	0.0538	2.67	1.73
l10_06s	0.0635	0.0763	3.56	2.02
l10_07s	0.094	0.079	4.41	1.46
l10_08s	0.0711	0.109	3.93	2.15
l10_09s	0.0567	0.0637	4.26	1.79
l10_10s	0.0787	0.105	3.63	1.91
Median	0.0688	0.0753	3.66	1.74

Table 5.2. Maximum building drift and maximum base shear ratio for St. Louis motions (2% in 50 years)

Ground motion	Max. building drift (%)		Max. base shear ratio, V/W (%)	
	ZEUS-NL	DRAIN-2DM	ZEUS-NL	DRAIN-2DM
l02_01s	0.774	0.686	13.2	11.9
l02_02s	0.722	0.539	14.1	10.7
l02_03s	0.0714	0.107	6.63	4.88
l02_04s	0.227	0.306	8.76	7.42
l02_05s	0.725	0.644	14.3	9.61
l02_06s	0.212	0.24	8.71	5.9
l02_07s	0.502	0.488	12.1	9.78
l02_08s	0.253	0.597	8.2	9.58
l02_09s	0.72	0.498	14.2	10.5
l02_10s	0.0808	0.115	4.99	3.49
Median	0.377	0.352	9.95	7.86

The modeling assumptions for the case study building using both programs were taken to be as consistent as possible. However, the programs use different element formulations and computing procedures, and so the results are not exactly the same for the two models. However, the maximum building drift results are reasonably close to each other.

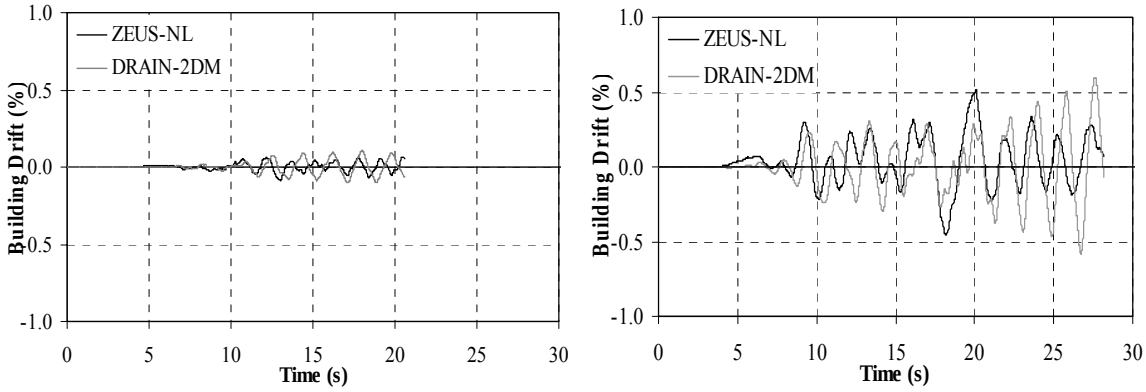

(a) l10_08s (b) l02_08s

Fig. 5.5. Comparison of building drifts for St. Louis motions

Fig. 5.6 provides a comparison of the building drift versus time for the two models using the median motion of the 2% in 50 years Memphis motions. Based on the comparison of push-over analysis results, there was a significant difference between the ZEUS-NL and DRAIN-2DM models at about 2.0% building drift. However, as shown in Fig. 5.6, the maximum building drift for the dynamic analysis are reasonably close to each other, although the response versus time varies.

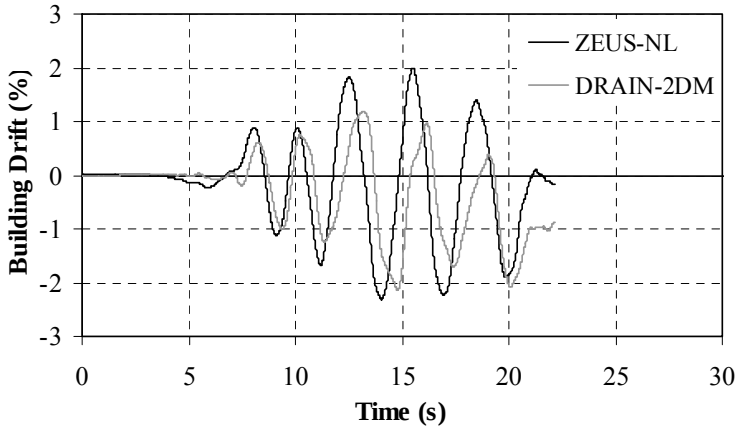

Fig. 5.6. Comparison of building drifts for Memphis motions (m02_10s)

5.3 Further Analysis Using ZEUS-NL Program

The ZEUS-NL program was selected for further analysis of the case study building. To compute the fundamental period of the case study building, an eigenvalue analysis was performed. To further understand the dynamic behavior of the structure, nonlinear dynamic analysis was also conducted using the Memphis motions. Finally, the results of push-over analysis and nonlinear dynamic analysis using ZEUS-NL were compared.

5.3.1 Eigenvalue Analysis

Based on an eigenvalue analysis, the fundamental period of the case study building is 1.14 seconds. It should be noted that ZEUS-NL initially models members as uncracked and so this value corresponds to the fundamental period based on uncracked section properties. Mode shapes determined by eigenvalue analysis with the ZEUS-NL program are shown in Fig. 5.7. The first four mode shapes and profiles developed from combining mode shapes on the basis of the Square-Root-of-Sum-of-Squares (SRSS) rule are shown. These mode shapes were used to determine the lateral load pattern for additional push-over analysis.

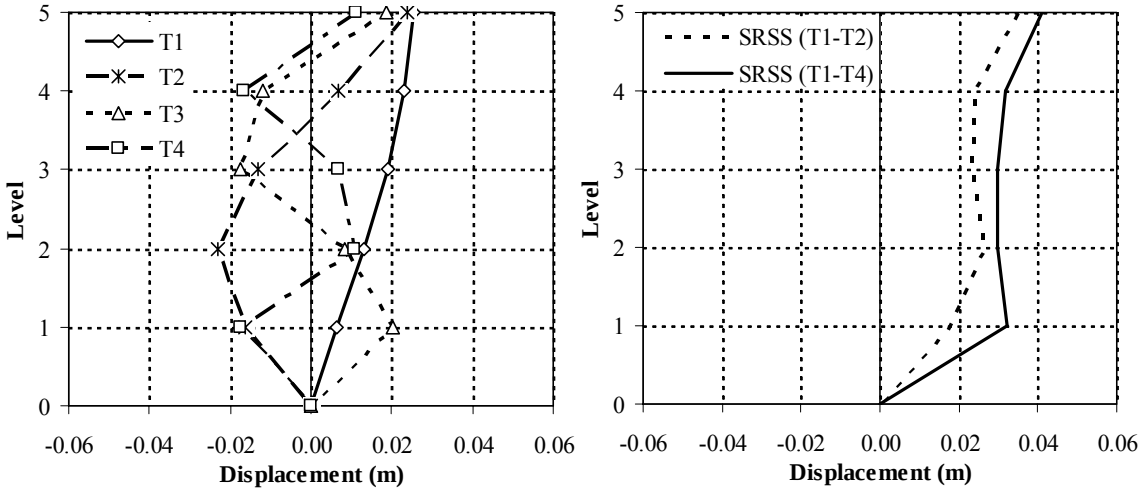

(a) First four mode shapes (b) SRSS shapes

Fig. 5.7. Mode shapes from eigenvalue analysis

Fig. 5.8 shows a comparison of the structural response from the push-over analysis with different load patterns. As shown in Fig. 5.8, the push-over results for the load patterns of SRSS are bounded between the inverted triangular and rectangular case.

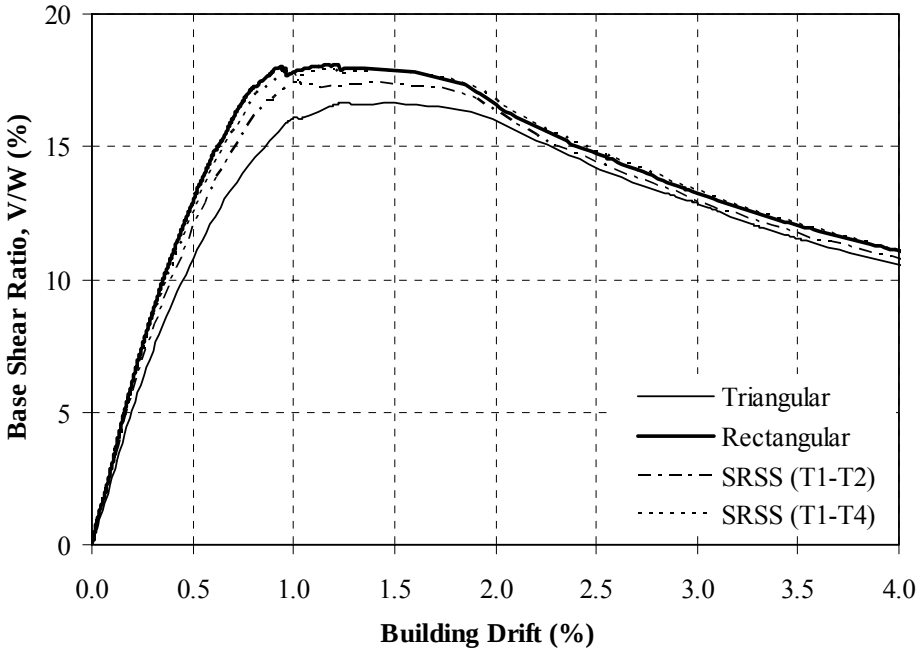

Fig. 5.8. Push-over analysis using SRSS shapes from eigenvalue analysis

5.3.2 Nonlinear Dynamic Analysis

Synthetic ground motion records from both St. Louis and Memphis were used to evaluate the dynamic behavior of the case study building. The results from the nonlinear analyses using the St. Louis motions were provided in Tables 5.1 and 5.2. The results for the twenty Memphis motions are shown in Tables 5.3 and 5.4. (The building drift time histories for the St. Louis and Memphis motions are provided in Appendix A.)

Table 5.3. Maximum building drift and maximum base shear ratio for Memphis motions (10% in 50 years, ZEUS-NL)

Ground motion	Max. building drift (%)	Max. base shear ratio, V/W (%)
m10_01s	0.142	4.54
m10_02s	0.122	5.29
m10_03s	0.164	4.97
m10_04s	0.153	4.54
m10_05s	0.129	4.99
m10_06s	0.425	7.81
m10_07s	0.134	4.65
m10_08s	0.155	5.97
m10_09s	0.0800	4.84
m10_10s	0.0950	4.21
Median	0.144	5.10

Table 5.4. Maximum building drift and maximum base shear ratio for Memphis motions (2% in 50 years, ZEUS-NL)

Ground motion	Max. building drift (%)	Max. base shear ratio, V/W (%)
m02_01s	1.99	18.4
m02_02s	2.36	19.1
m02_03s	1.94	18.8
m02_04s	1.92	18.9
m02_05s	2.64	18.5
m02_06s	2.47	18.2
m02_07s	1.99	19.6
m02_08s	2.74	17.9
m02_09s	1.88	18.7
m02_10s	2.31	18.1
Median	2.20	18.6

As shown in Tables 5.3 and 5.4, the median value of the maximum building drifts for the 10% in 50 years Memphis motions is quite small and maximum base shear ratios are less than the design shear. In addition to this, the median values of the maximum building drifts and maximum base shear ratios for the 2% in 50 years Memphis motions are significantly increased due to the larger magnitude of the ground motions.

5.3.3 Comparison of Push-Over and Dynamic Analysis

A comparison of the overall structural response from the push-over and nonlinear dynamic analyses using ZEUS-NL are shown in Fig. 5.9. As shown, the points from the dynamic analyses representing the maximum building drift and base shear for each ground motion show a reasonable match with the push-over curves. The global responses of the structure from the static and dynamic analyses show relatively similar values for lower amplitudes of motion and diverge for greater demands. In particular, the base shear ratios from the 2% in 50 years Memphis motions are a bit underestimated by the push-over analysis curve.

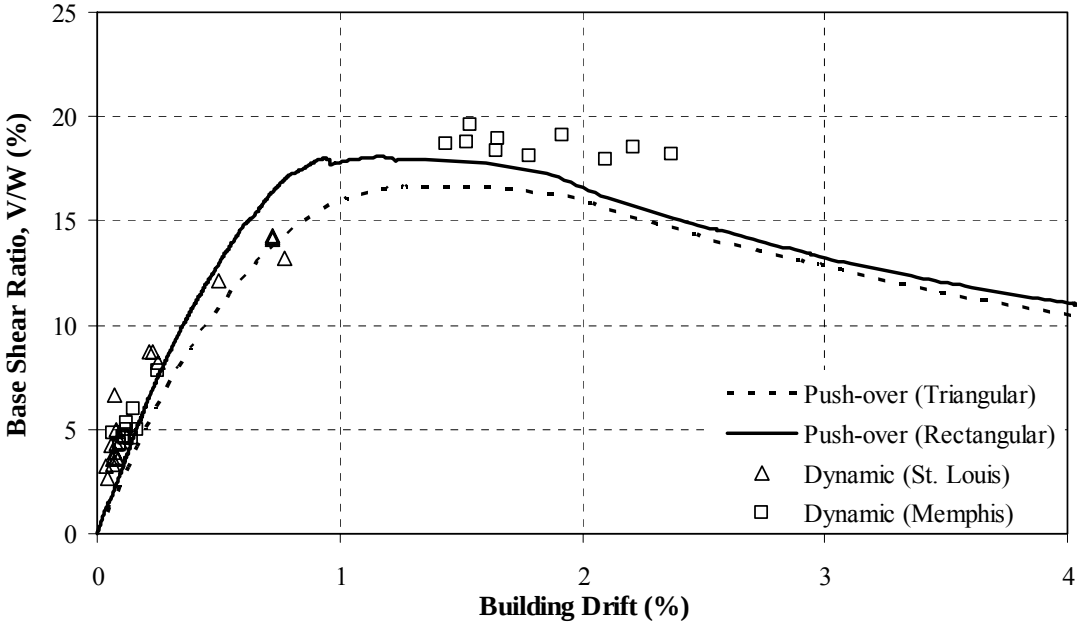

Fig. 5.9. Comparison of push-over and dynamic analysis

5.4 Seismic Evaluation for Unretrofitted Case Study Building

5.4.1 Global-Level Evaluation

The performance criteria for the global-level approach are defined by the maximum interstory drift. This approach may not be appropriate for predicting member-level performance. However, it is useful for a first approximation of structural behavior

under seismic demands. It is necessary to conduct a member-level evaluation to determine specific member performance. Table 5.5 shows the global-level interstory drift limits for three performance levels for concrete frame elements in FEMA 356 (ASCE 2000).

Table 5.5. Drift limits for concrete frame elements in FEMA 356 (ASCE 2000)

Structural performance levels	Drift (%)
Immediate occupancy	1
Life safety	2
Collapse prevention	4

Fig. 5.10 shows the maximum interstory drift profiles for the unretrofitted case study building from the analyses using the St. Louis motions. The median value is also indicated. According to FEMA 356, the Basic Safety Objective (BSO) is defined as LS performance for the Basic Safety Earthquake 1 (BSE-1) earthquake hazard level and CP performance for the BSE-2 earthquake hazard level. BSE-1 is defined as the smaller of an event corresponding to 10% probability of exceedance in 50 years (10% in 50 years) and 2/3 of BSE-2, which is the 2% probability of exceedance in 50 years (2% in 50 years) event.

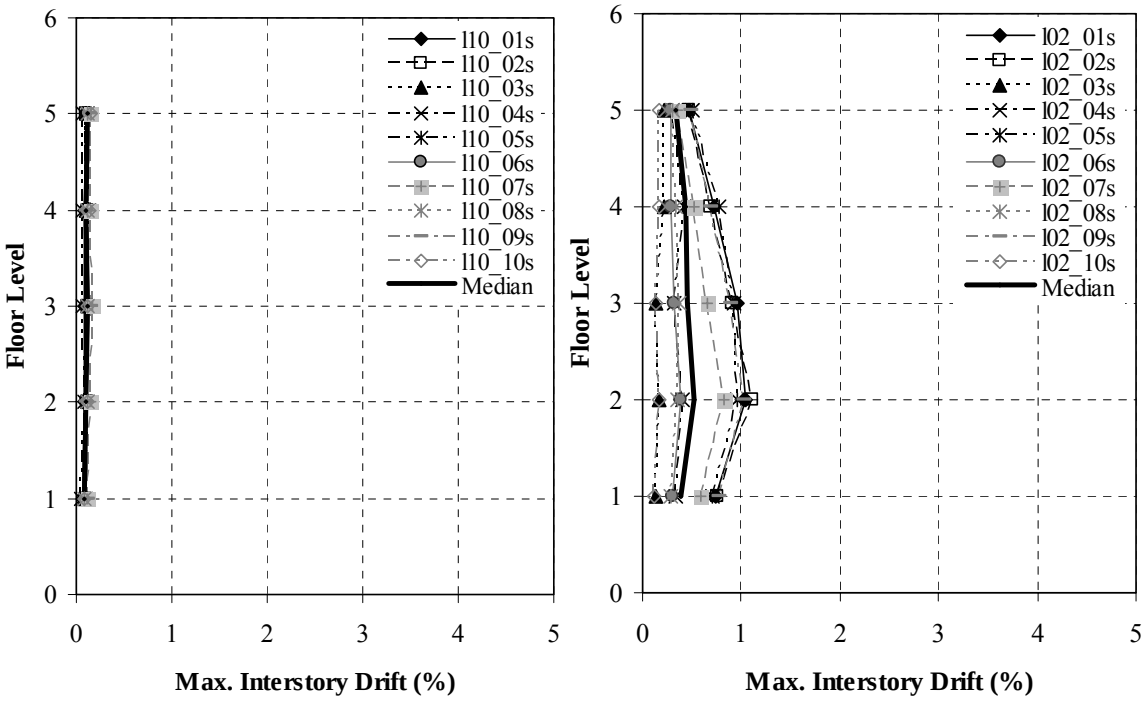

(a) 10% in 50 years (b) 2% in 50 years

Fig. 5.10. Maximum interstory drifts for St. Louis motions

As seen in Fig. 5.10, because all the maximum interstory drift values are less than 1% maximum interstory drift, the structural response is within the FEMA 356 global-level limit of 2% for LS for the 10% in 50 years motions. For the 2% in 50 years motions, the median interstory drifts are much less than the CP limit of 4%. Therefore, the case study building meets the BSO under St. Louis motions based on a global-level evaluation.

Fig. 5.11 shows the global-level evaluation of the case study building for the Memphis motions. Similar to the St. Louis motions, the maximum interstory drift values for 10% in 50 years motions are less than 1%. For the 2% in 50 years motions, the median response of the structure is less than 4%, which is the limit for CP performance. Therefore, based on a global-level evaluation, the case study building does not require retrofitting to meet the BSO for both the Memphis and St. Louis motions.

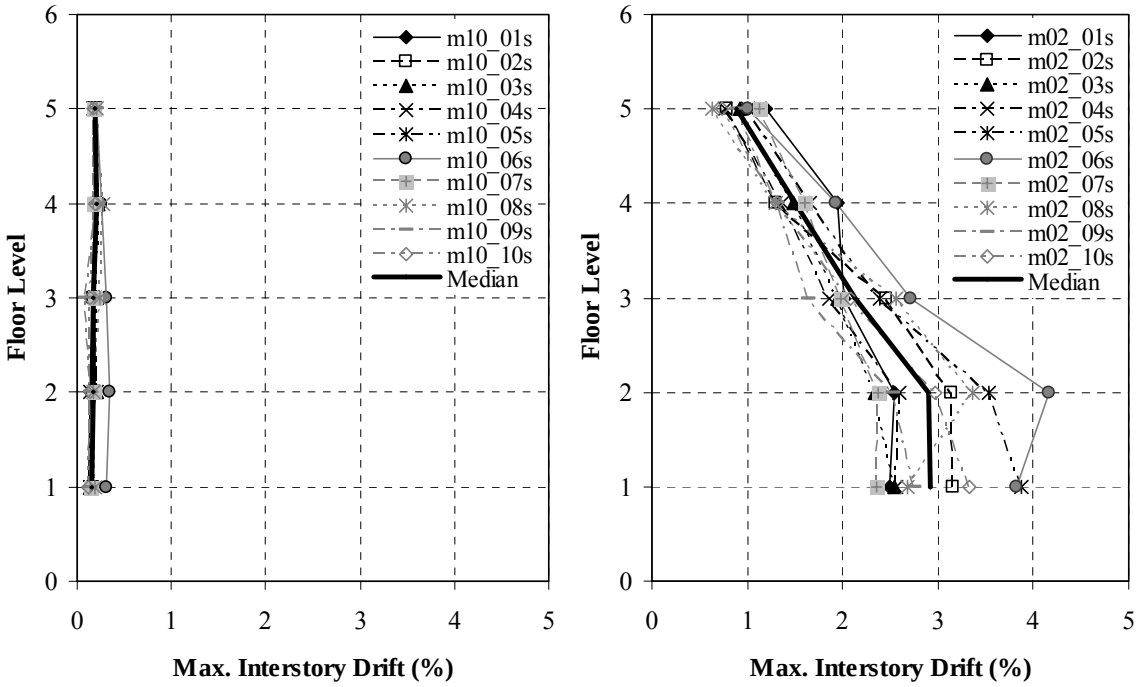

(a) 10% in 50 years (b) 2% in 50 years

Fig. 5.11. Maximum interstory drifts for Memphis motions

5.4.2 Member-Level Evaluation

The global-level evaluation provides a general assessment of the seismic performance of a structure. However, it does not identify member deficiencies and a vulnerable member, which is necessary to select appropriate member-level retrofit techniques. Therefore, in this study, the member-level evaluation of FEMA 356 was also performed to determine more detailed information for structural behavior and seismic performance. Based on this evaluation, several retrofit techniques were selected and applied to the case study structure.

Plastic rotation limits are provided by FEMA 356 for a member-level evaluation of the structural components. Plastic rotation is defined as the difference between the maximum rotation at a member end and the yield rotation for that member. Fig. 5.12 provides an example of the determination of the plastic rotation for a beam member.

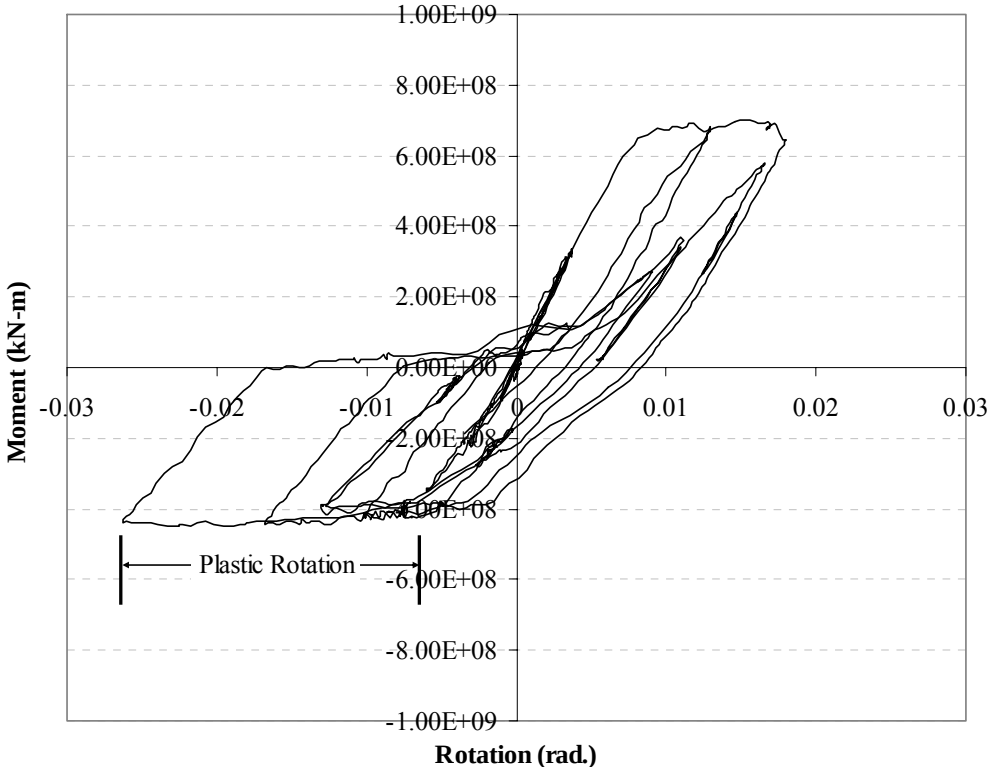

Fig. 5.12. Plastic rotation for a first floor beam member

Three member types were evaluated: beams, columns, and slabs. For the global-level approach, the median ground motions were selected as those that caused an interstory drift closest to the median interstory drift for each story. The FEMA limitations of plastic rotation values for each member were described in the Tables 2.3 to 2.7 in Section 2.4.1.4. Specific limits for this case study structure are given in Table 5.6. The analysis for the 10% in 50 years and 2% in 50 years St. Louis motions and the 10% in 50 years Memphis motions resulted in no plastic rotations. Therefore, those events met the FEMA 356 criteria for the BSO, like the global-level evaluation. However, there was a difference for the 2% in 50 years Memphis motions. Table 5.7 summarizes the results of the member-level evaluation for the 2% in 50 years Memphis motions. For the 2% in 50 years events, the BSO is met when the plastic rotations are within the limits for CP. As shown in Table 5.7, the BSO of CP is not satisfied because the CP limits for plastic rotation are exceeded in several members (noted with bold font). According to

this result, the first and second floor level may experience significant damage and all the columns, except the fifth story, may be vulnerable under the expected earthquake event.

Table 5.6. FEMA 356 plastic rotation limits for the unretrofitted case study building

Story	Performance Level	Beams	Columns	Beam-Column Joints	Slabs and Slab-Column Joints
1	IO	0.00500	0.00418	0	0.00550
	LS	0.0100	0.00418	0	0.00825
	CP	0.0100	0.00518	0	0.0110
2	IO	0.00500	0.00453	0	0.00550
	LS	0.0100	0.00453	0	0.00825
	CP	0.0100	0.00553	0	0.0110
3	IO	0.00500	0.00481	0	0.00550
	LS	0.0100	0.00481	0	0.00825
	CP	0.0153	0.00581	0	0.0110
4	IO	0.00500	0.00500	0	0.00550
	LS	0.0100	0.00500	0	0.00825
	CP	0.0161	0.00600	0	0.0110
5	IO	0.00500	0.00500	0	0.000500
	LS	0.0100	0.00500	0	0.000750
	CP	0.0157	0.00600	0	0.00100

Table 5.7. Maximum plastic rotations for 2% in 50 years Memphis motions

Story	Median Ground Motion	Beams	Columns	Slabs
1	m02_09s	**0.0179**	**0.0286**	**0.0179**
2	m02_10s	**0.0168**	**0.0222**	**0.0127**
3	m02_10s	0.0110	**0.0175**	0.00768
4	m02_03s	0.00487	**0.0112**	0
5	m02_09s	0	0.00507	0

Fig. 5.13 shows the locations of inelastic behavior in the unretrofitted structure where the plastic rotations exceed the limits for each performance level (IO, LS, and CP) under the median ground motion for the 2% in 50 years Memphis event. Locations where the rotations exceeded the FEMA 356 member-level criteria for each limit state are shown with black circles. These figures demonstrate that most columns in the

external frame, and beams and some of slab members at the 1st and 2nd floors are vulnerable.

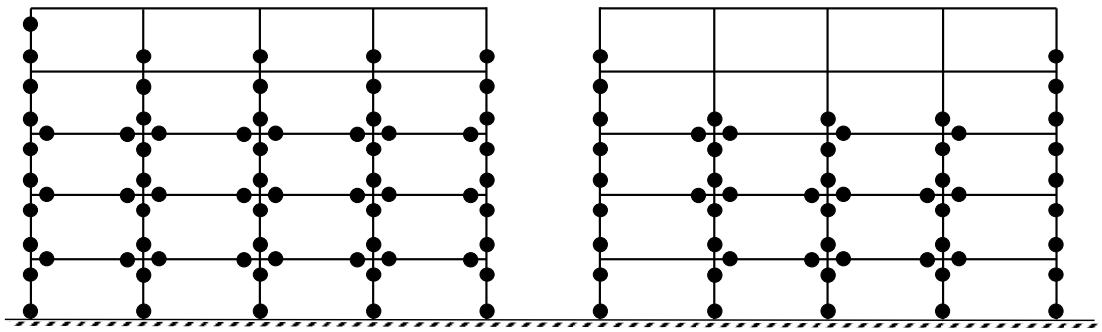

(a) IO

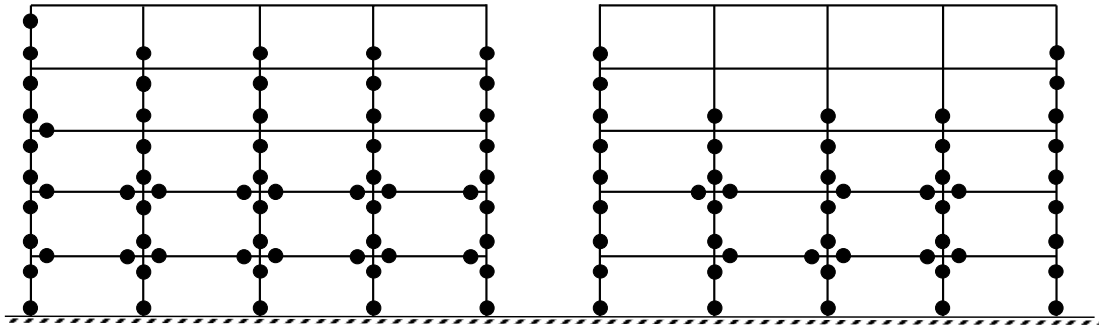

(b) LS

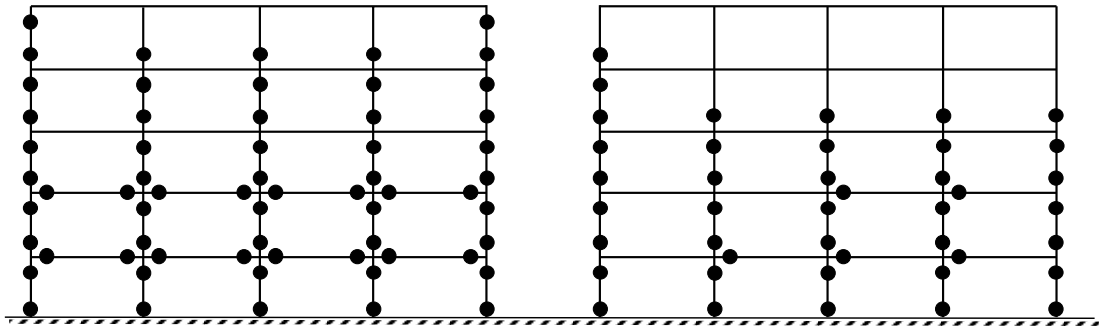

(c) CP

● = Exceedance of plastic rotation limit

Fig. 5.13. Locations in unretrofitted building where FEMA 356 plastic rotation limits are exceeded (2% in 50 years Memphis event)

5.4.3 Additional Evaluation

5.4.3.1 Column-to-Beam Strength Ratio

During strong earthquake events, RC frame buildings are often subjected to story mechanism or column sidesway. Theses failure mechanisms are associated with the development of plastic hinges at column and beam members. Therefore, it is important to determine the column-to-beam strength ratio to identify the structure's seismic performance. For the unretrofitted structure, the column-to-beam strength ratio of the 1st floor level was 0.92, which is less than the minimum requirement in the current code. The current ACI 318 code requires a minimum column-to-beam ratio of 1.2 (ACI Comm. 318 2002).

5.4.3.2 Column Shear and Punching Shear

Because the analytical results from ZEUS-NL did not include a shear failure, the shear strength of the columns at the base was calculated and compared with the current requirement. According to the *ACI 318-02*, a shear strength provided by concrete members subjected to axial compression was defined using the following equation.

$$V_c = 2\left(1+\frac{N_u}{2000A_g}\right)\sqrt{f'_c}\,b_w d \qquad (5.2)$$

where:

V_c = Nominal shear strength provided by concrete, lb

N_u = Factored axial load normal to cross section occurring simultaneously with *Vu* or *Tu*; to be taken as positive for compression, lb

A_g = Gross area of section, $in.^2$

f'_c = Specified compressive strength of concrete, psi

b_w = Web width, in.

d = Distance from extreme compression fiber to centroid of longitudinal tension reinforcement

Based on the results from nonlinear dynamic analysis, the maximum values of base shear were less than the shear capacity of columns.

In addition to this, punching shear failure was checked with the relationship between the maximum interstory drift and the gravity shear ratio (V_g/V_o). This relationship was established based on experimental data from a member of researchers (Hueste and Wight 1999). The gravity shear ratio (V_g/V_o) is the ratio of the two-way shear demand from gravity loads to the nominal two-way shear strength at the slab-column connection. It is defined the value of the vertical gravity shear (V_g) divided by the nominal punching shear strength (V_o) for the connection without moment transfer. For the case study building, V_g/V_o is 0.29 at the floor levels and 0.39 at the roof level. Fig. 5.14 shows the prediction of punching shear failure based on this relationship.

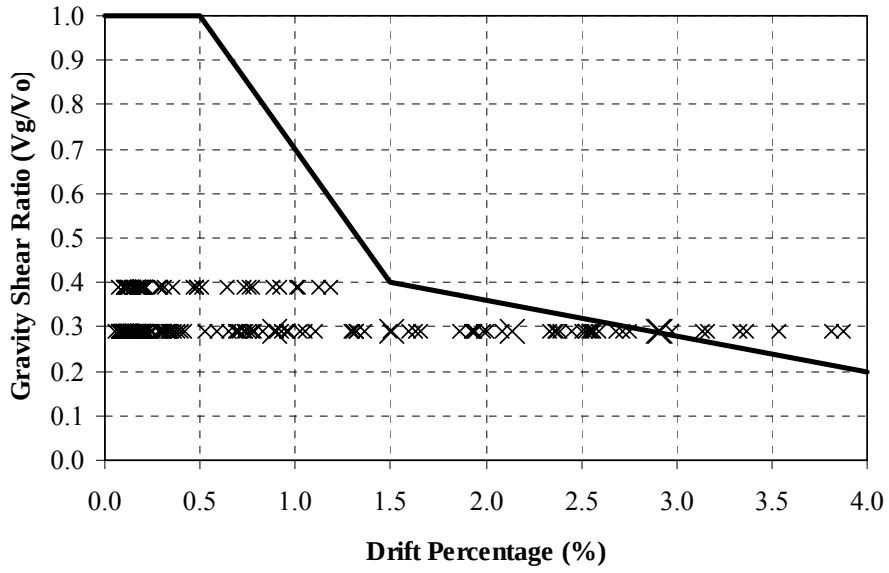

Fig. 5.14. Prediction model for punching shear and flexural punching shear failures with analytical results

As shown in Fig. 5.14, several results from the 2% in 50 years Memphis motions were exceed the limit. Therefore, the punching shear failure may be expected under the large magnitude of seismic events.

5.5 Fragility Curves for Unretrofitted Case Study Building

5.5.1 Methodology

In this study, the objective of the seismic fragility analysis was to assess the effectiveness of retrofit by estimating the reduction in the probability of exceeding a certain limit state, as compared to the unretrofitted structure. To develop the desired fragility curves, several parameters were needed, including structural characteristics, earthquake intensities, and uncertainties for capacity and demand. The seismic demand was determined from the twenty synthetic Memphis ground motions summarized in Tables 4.11 and 4.12. The desired fragility curves were developed using the following equation (Wen et al. 2004).

$$P(LS/S_a) = 1 - \Phi\left(\frac{\lambda_{CL} - \lambda_{D/S_a}}{\sqrt{\beta_{D/S_a}{}^2 + \beta_{CL}{}^2 + \beta_M{}^2}}\right) \tag{5.3}$$

where:

$P(LS/S_a)$ = Probability of exceeding a limit state given spectral acceleration

Φ = Standard normal cumulative distribution function

λ_{CL} = ln(*median of drift capacity*), where drift capacity is expressed as a percentage of the story height

λ_{D/S_a} = ln(*calculated median demand drift*), where demand drift is determined from a fitted power law equation

β_{D/S_a} = Uncertainty associated with the fitted power law equation used to estimated demand drift = $\sqrt{\ln(1+s^2)}$

β_{CL} = Uncertainty associated with the drift capacity criteria, taken as 0.3 for this study

β_M = Uncertainty associated with analytical modeling of the structure, taken as 0.3 for this study

s^2 = Square of the standard error

$= \frac{\sum\left[\ln(Y_i) - \ln(Y_p)\right]^2}{n-2}$, where Y_i, Y_p are the observed and power law predicted demand drift, respectively, given the spectral acceleration

5.5.2 Global-Level Limits

The λ_{CL} term for the fragility analysis was calculated with the natural log of the specified limit state in percentile. For example, according to the FEMA 356 global-level drift limits for concrete frame structures, 1, 2 and 4 were used for IO, LS, and CP, respectively.

The case study building is a RC flat slab building which is very vulnerable to punching shear failure under significant lateral displacements during seismic loadings. For this reason, the punching shear model based on the gravity shear ratio (V_g/V_o) and interstory drift proposed by Hueste and Wight (1999) was used to establish an upper bound drift limit for CP. Fig. 5.15 shows the proposed relationship between interstory drift and the gravity shear ratio under seismic loads. For the case study building, V_g/V_o is 0.29 at the floor levels and 0.39 at the roof level. Because the maximum interstory drift occurred at the lower stories for the push-over and dynamic analyses, a gravity shear ratio of 0.29 was used to find corresponding drift limit for the prediction of punching shear failure. As shown in Fig. 5.15, the corresponding drift limit at which punching shear is predicted at the interior slab-column connections is 2.9%. Therefore, this drift limit was used for derivation of the CP fragility curve for the unretrofitted building. Table 5.8 summarizes the drift limits based on global-level criteria.

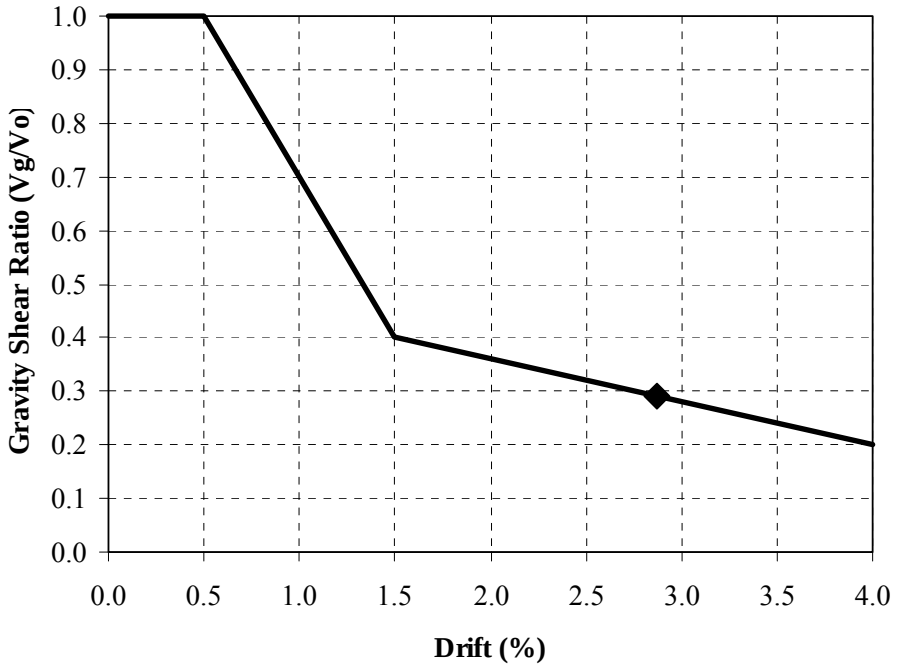

Fig. 5.15. Prediction model for punching shear and flexural punching shear failures at interior slab-column connections [adapted from Hueste and Wight (1999)]

Table 5.8. Limits based on global-level criteria

Structural performance levels	Drift (%)
IO	1
LS	2
CP	2.9*

* 2.9% was used for CP based on punching shear model.

To demonstrate the methodology for derivation of the fragility curves, the unretrofitted case study building is considered. Fig. 5.16 provides the relationship between maximum interstory drift and the corresponding spectral acceleration for both the 10% in 50 years and the 2% in 50 years Memphis motions. A total of twenty points are plotted, where each data point represents the demand relationship for one ground motion record. The spectral acceleration (S_a) for a given ground motion record is the value corresponding to the fundamental period of the structure based on cracked section properties (T_1 = 1.62 s) and 2 percent damping. The drift demand value is the maximum

interstory drift determined during the nonlinear time history analysis of the structure when subject to that ground motion record. The best-fit power law equation is also provided in the graph. This equation is used to describe the demand drift when constructing the fragility curves for the unretrofitted structure. The corresponding value of s^2 for the unretrofitted case is 0.144, which gives a β_{D/S_a} value of 0.367. The fragility curves developed using FEMA global-level performance criteria are shown in Fig. 5.17.

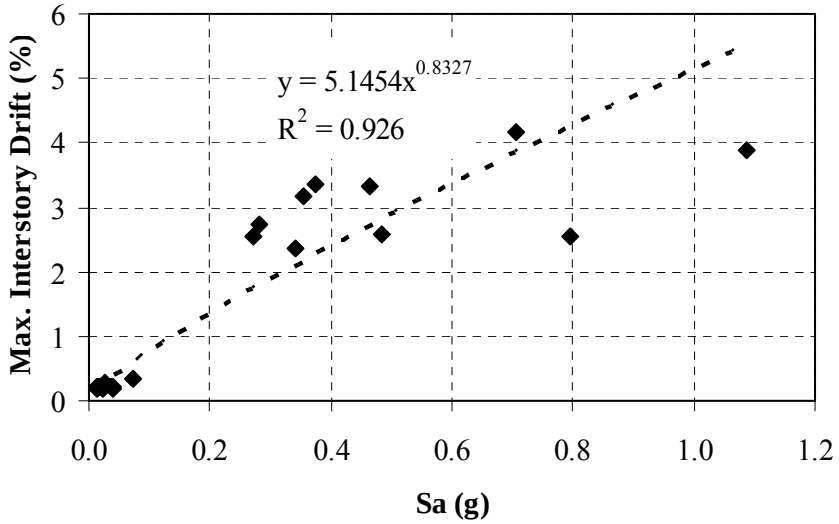

Fig. 5.16. Development of power law equation for unretrofitted structure (Memphis motions)

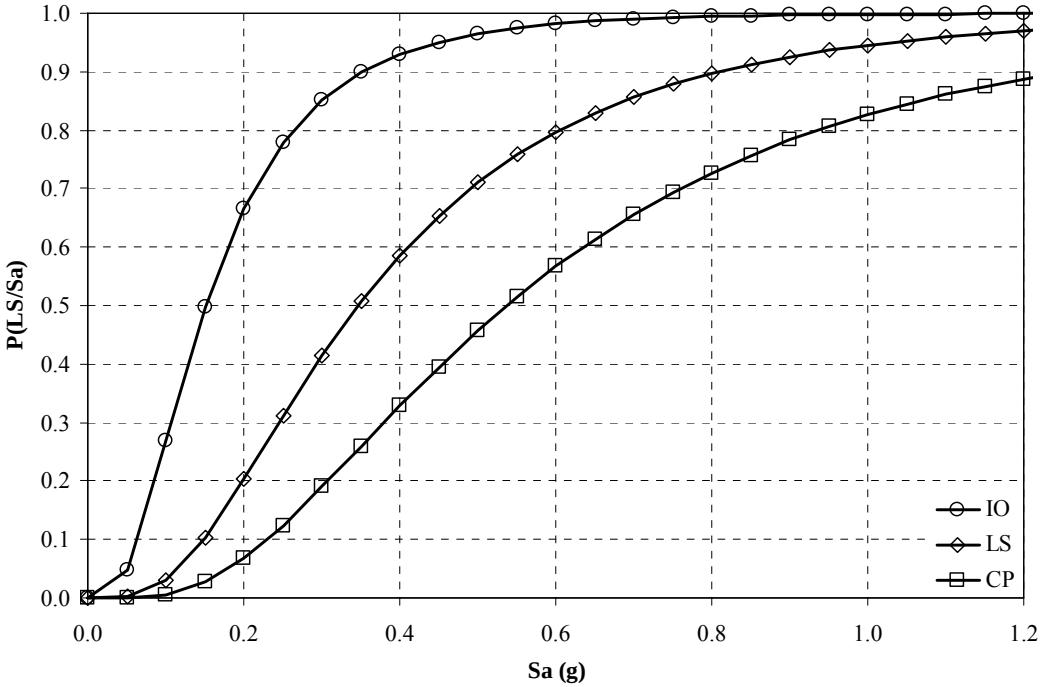

Fig. 5.17. Global-level fragility curves of the unretrofitted structure for Memphis motions

5.5.3 Member-Level Limits

To develop fragility curves based on the FEMA 356 member-level criteria, drift limits corresponding to those criteria were determined. In this study, two different analyses were used for determining the most critical interstory drift corresponding to the member-level criteria: regular push-over analysis and the method developed by Dooley and Bracci (2001). For regular push-over analysis, the inverted triangular load pattern was used. The second method, which was suggested by Dooley and Bracci (2001), was used to find critical drifts based on the development of a plastic mechanism within a story. Fig. 5.18 shows a comparison between a regular push-over analysis and a push-over analysis to evaluate the critical response of a story. As shown in Fig. 5.18, in order to determine the drift capacity of a story, the x-direction deformation of the level below is restrained to create the most critical story mechanism.

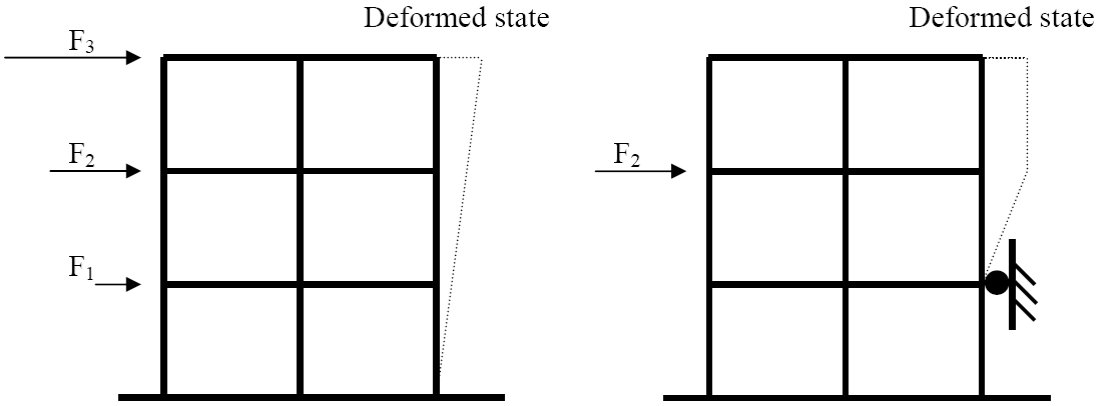

(a) Inverted triangular loading (first mode response) (b) Critical second story response

Fig. 5.18. Example loading patterns for push-over analysis (Wen et al. 2003)

First of all, the FEMA 356 member-level limit states were determined using a regular push-over analysis. Push-over analysis with the inverted triangular load pattern was performed to define the drift limit at which a member-level rotation limit is exceeded. The drift limits corresponding to the exceedance of FEMA 356 member-level criteria are provided in Table 5.9 and Fig. 5.19.

Table 5.9. FEMA 356 limits based on member-level criteria

Structural performance levels	Drift (%)
Immediate occupancy	0.88
Life safety	0.88
Collapse prevention	1.07

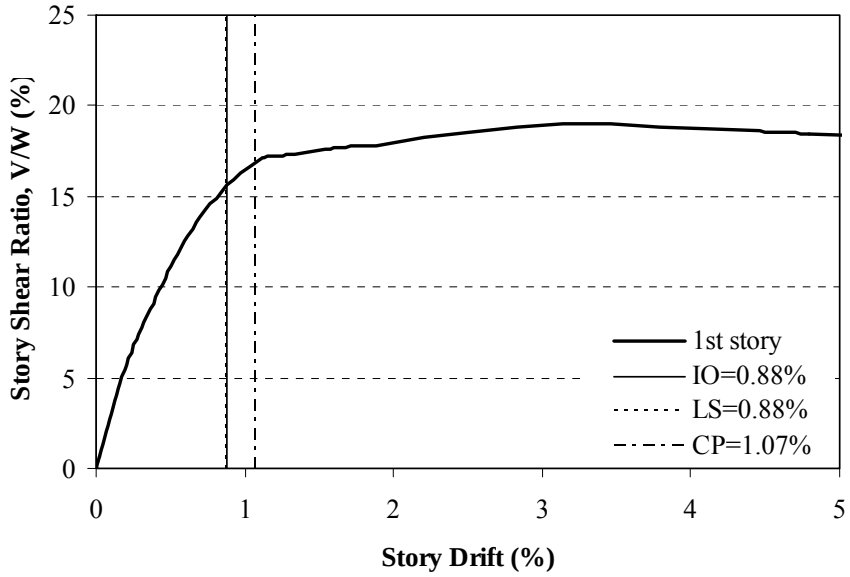

Fig. 5.19. FEMA limits based on member-level criteria with push-over curve for the 1st story

The response of the first story provided the minimum value for drift limits. As shown in Table 5.9, the drift limits between FEMA global-level and member-level criteria provided some differences. Using the member-level criteria, all the drift limits are much less than global-level drifts. In particular, the drifts for LS and CP are close each other. Since plastic rotation limits of RC column member for IO and LS limit states had the same values in this study, the corresponding drift limits for IO and LS are the same values. Fig. 5.20 shows the fragility curves using the drift limits based on the FEMA 356 member-level criteria. For comparison, the fragility curves using the global drift limits are represented on each graph with dotted lines. As shown in Fig. 5.20, the probability of exceeding each limit for the FEMA member-level criteria gave larger values than that for the FEMA global-level criteria.

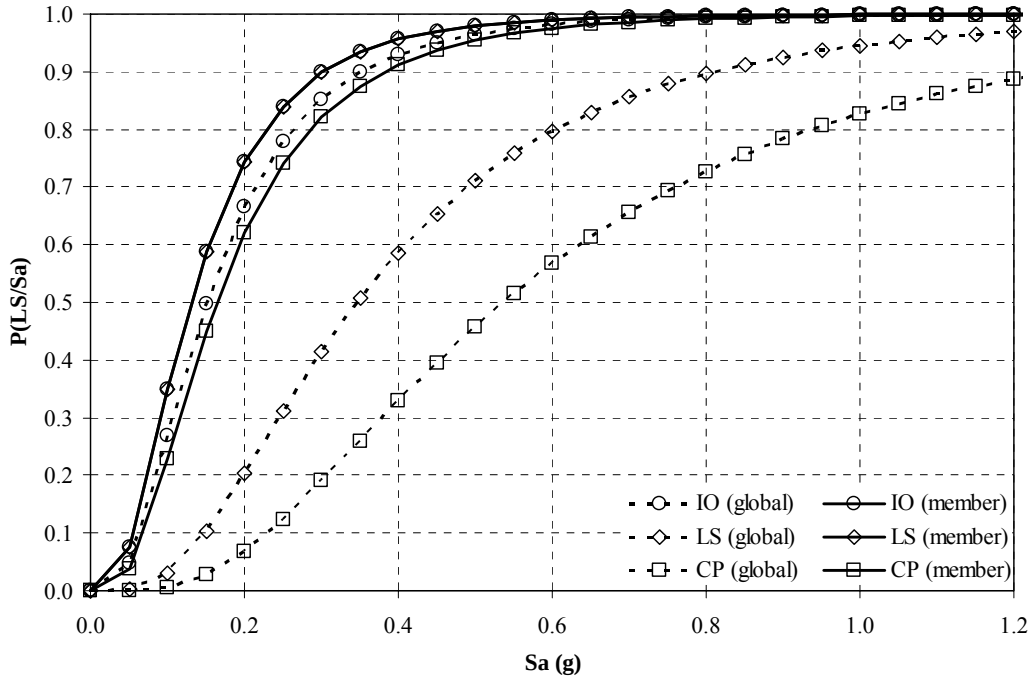

Fig. 5.20. Fragility curves for the FEMA member-level criteria from a regular push-over analysis

A second method, suggested by Dooley and Bracci (2001), was used to find more critical drifts based on the plastic mechanism of each story. Push-over analysis using a story-by-story procedure (see Fig. 5.18) was performed for each story to define the drift limits. In order to obtain more accurate results, displacements were controlled during the push-over analysis. The drift limits corresponding to the first exceedance of the FEMA member-level criteria are provided in Table 5.10 and Fig. 5.21.

Table 5.10. FEMA limits based on member-level criteria for the critical response

Structural performance levels	Drift (%)
Immediate occupancy	0.62
Life safety	0.62
Collapse prevention	0.69

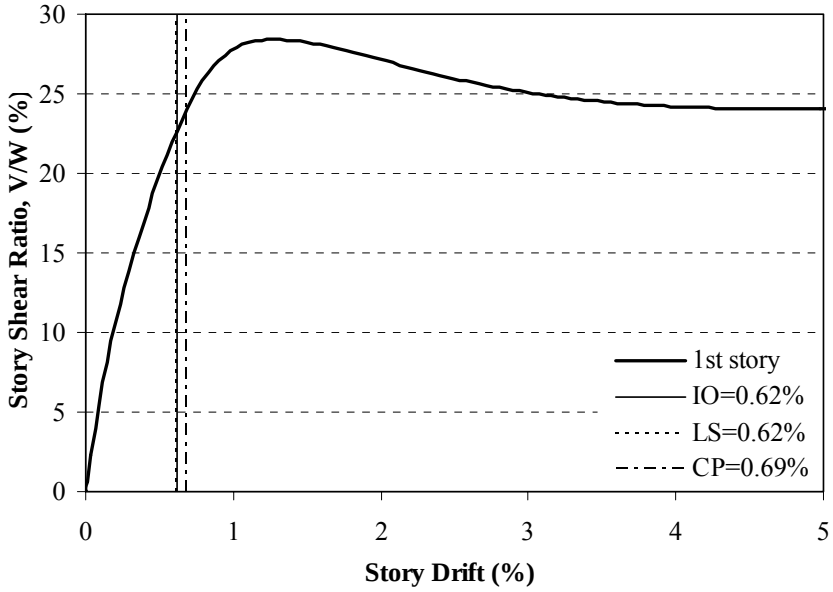

Fig. 5.21. FEMA limits based on member-level criteria with critical response push-over curve for the 1st story

In this case, the response of the 1st story also provided the minimum value for drift limits. As shown in Table 5.10, the drift limits are much less than FEMA global-level and even less than member-level criteria with a regular push-over analysis. Fig. 5.22 shows the fragility curves for the FEMA member-level criteria based on limits from the critical response push-over analysis. For comparison, the fragility curves using the FEMA 356 global-level drift limits are also represented on each graph with dotted lines.

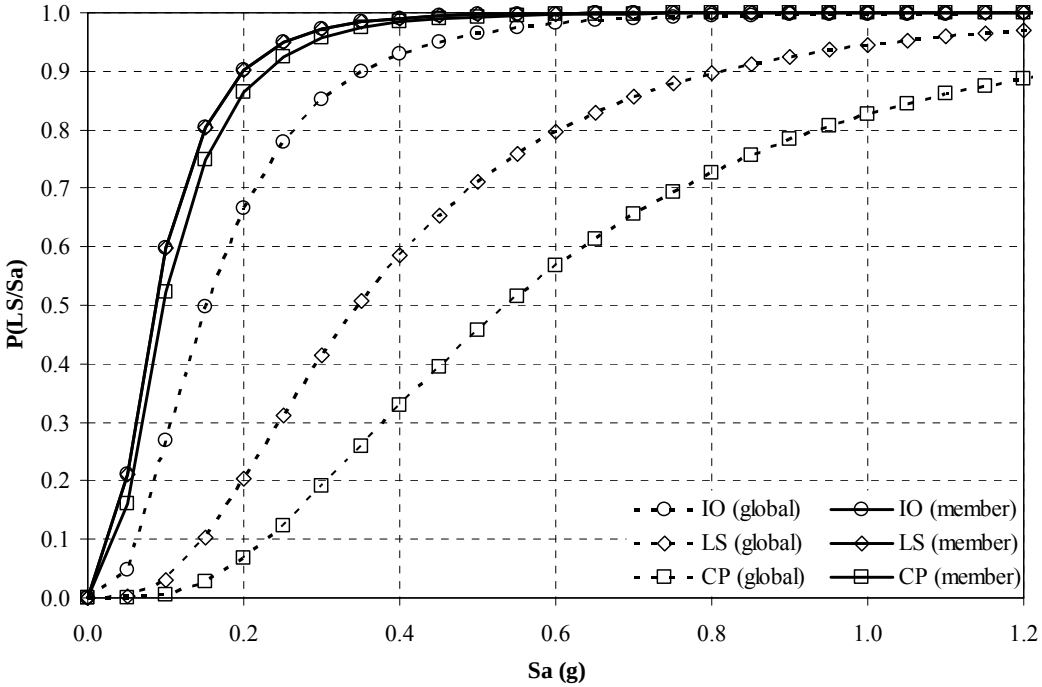

Fig. 5.22. Fragility curves for the FEMA member-level criteria from a regular push-over analysis

5.5.4 Additional Quantitative Limits

Additional quantitative limit states were evaluated based on limits described by Wen et al. (2003), as follows.

(1) First Yield (FY) – Interstory drift at which a member of a story or a structure initiates yielding under an imposed lateral loading.

(2) Plastic Mechanism Initiation (PMI) – Interstory drift at which a story mechanism (typical of a column sidesway mechanism), an overall beam sidesway mechanism, or a hybrid mechanism initiates under an imposed lateral loading.

(3) Strength Degradation (SD) – Interstory drift at which the story strength (resistance) has degraded by more than a certain percentage of the maximum strength (usually about 20 percent). Note that strength degradation can occur

due to material nonlinearities in the analytical models and also due to geometric nonlinearities from P-delta effects.

First of all, the drift limits corresponding to the above limit states were determined using a regular push-over analysis. Push-over analysis with the inverted triangular load pattern was performed to define the drift limits. The drift limits for the quantitative limit states are provided in Table 5.11 and Fig. 5.23. In addition, Fig. 5.24 shows the locations of inelastic rotation when the PMI limit state occurred for the 1st story.

Table 5.11. Drift limits for quantitative limit states (regular push-over analysis)

Structural performance levels	Drift (%)
First yield	0.66
Plastic mechanism initiation	0.81

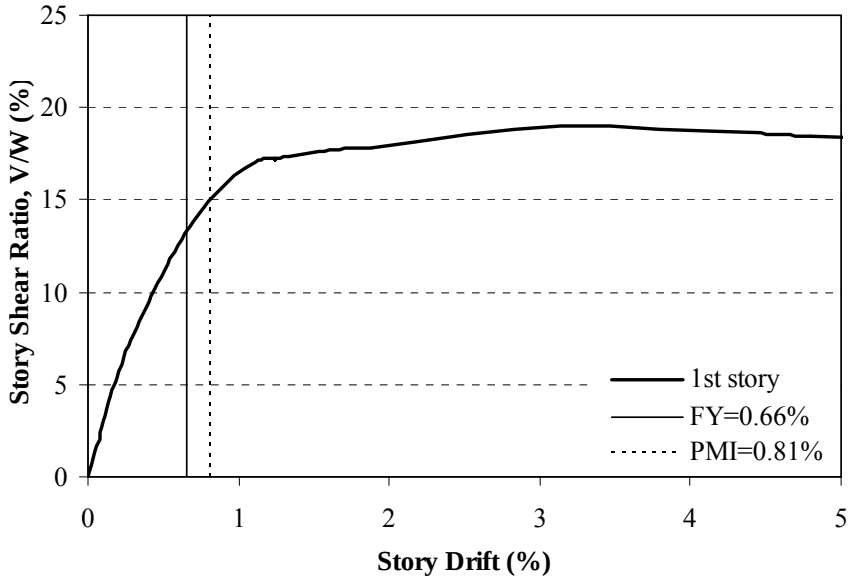

Fig. 5.23. Drift limits for quantitative limit states with push-over curve for the 1st story (regular push-over analysis)

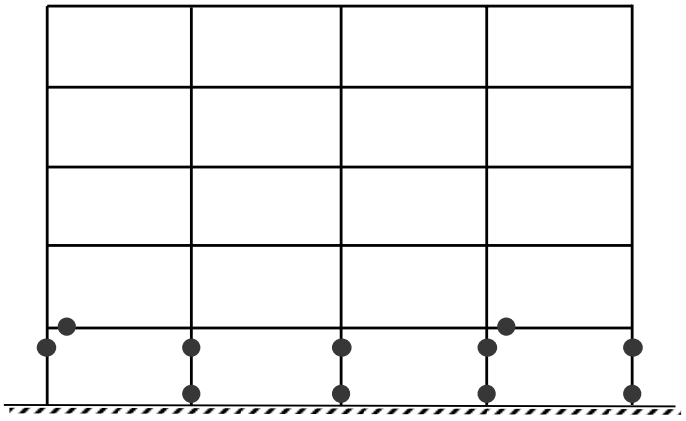

Fig. 5.24. Locations of inelastic rotation at PMI limit state based on the quantitative approach with push-over curve for the 1st story

As shown in Table 5.11, drift limits based on the quantitative limit states are even less than those found for the FEMA member-level criteria. In this case, the SD limit state was not detected because the strength did not fall to 20% of the maximum strength. Fig. 5.25 shows the fragility curves using these limit state definitions. For comparison, the fragility curves using the global drift limits are represented on each graph with dotted lines. As shown, the drift limits from the additional quantitative limits gave a much higher probability of failure than the drifts for the FEMA global-level criteria.

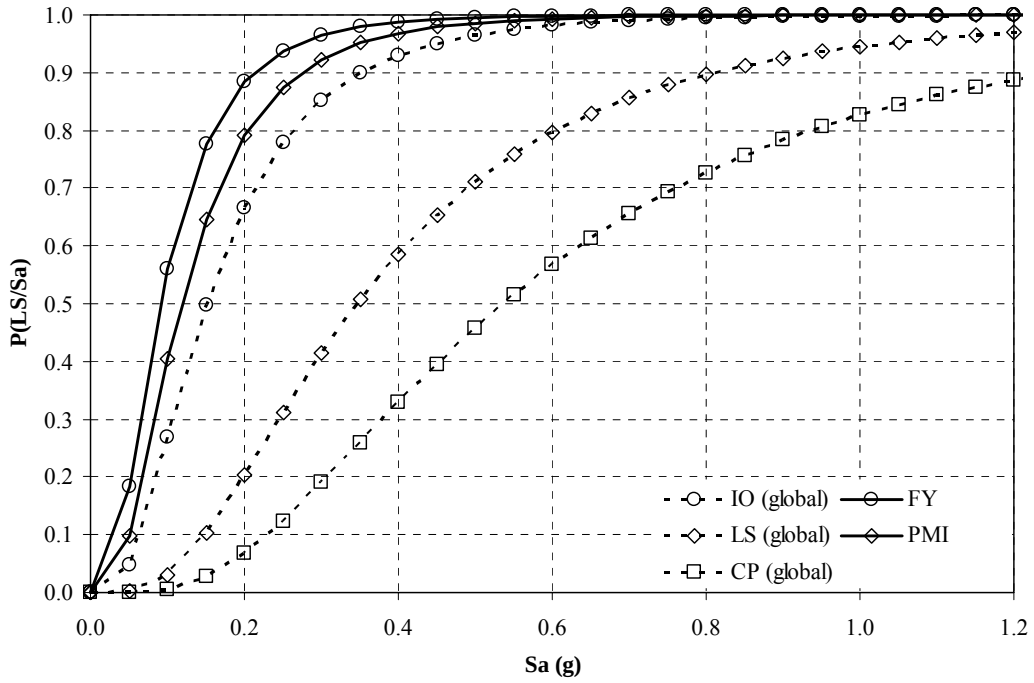

Fig. 5.25. Fragility curves for the FEMA member-level criteria from a regular push-over analysis

The method suggested by Dooley and Bracci (2001) was used to find more critical drifts based on the story-by-story push-over analysis. The corresponding drift limits for the quantitative limit states are provided in Table 5.12 and Fig. 5.26. In Table 5.12, the minimum drifts for each limit state are noted with bold font. In addition, Fig. 5.27 shows the locations of inelastic rotation when the PMI limit state occurred for the 1st story.

Table 5.12. Drift limits for the limit states based on the quantitative approach

	Interstory drift (%)		
	FY	PMI	SD
1st story	**0.36**	**0.66**	·
2nd story	0.51	0.86	**2.81**
3rd story	0.52	0.89	3.27
4th story	0.61	0.91	4.23
5th story	0.49	0.82	·

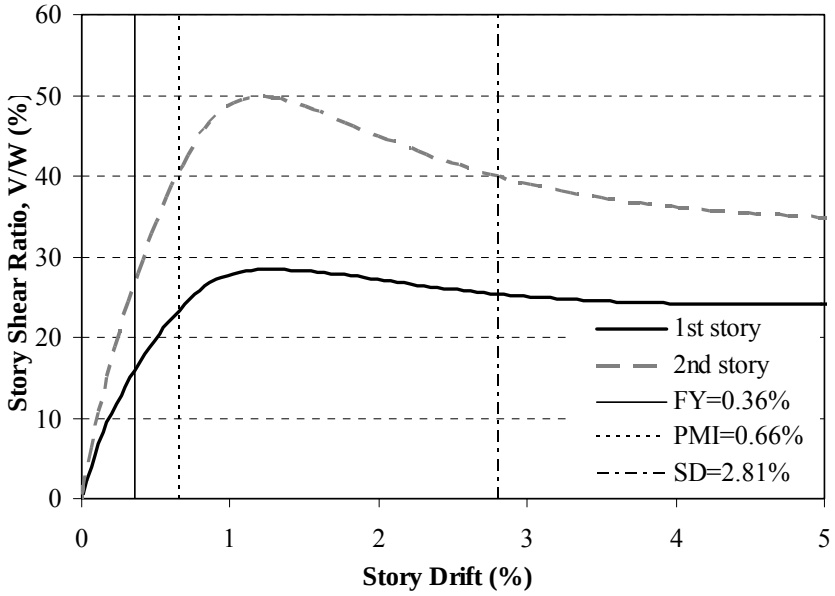

Fig. 5.26. Drift limits for the limit states based on the quantitative approach with critical response push-over curve for the 1st and 2nd stories

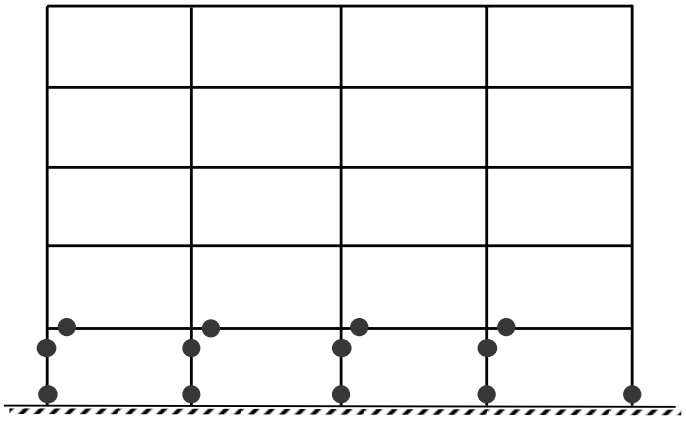

Fig. 5.27. Locations of inelastic rotation at PMI limit state based on the quantitative approach with push-over curve for the 1st story

As shown in Fig. 5.26, the minimum drifts for the FY and PMI limit states were provided by the 1st story push-over curve while SD limit state was given by the response of the 2nd story. The drift for SD limit state is similar in magnitude to the global-level drift limit assigned to CP which is associated with punching shear failure.

Fig. 5.28 shows the fragility curves with the critical response push-over analysis. For comparison, the fragility curves using the global drift limits are also represented on each graph with dotted lines.

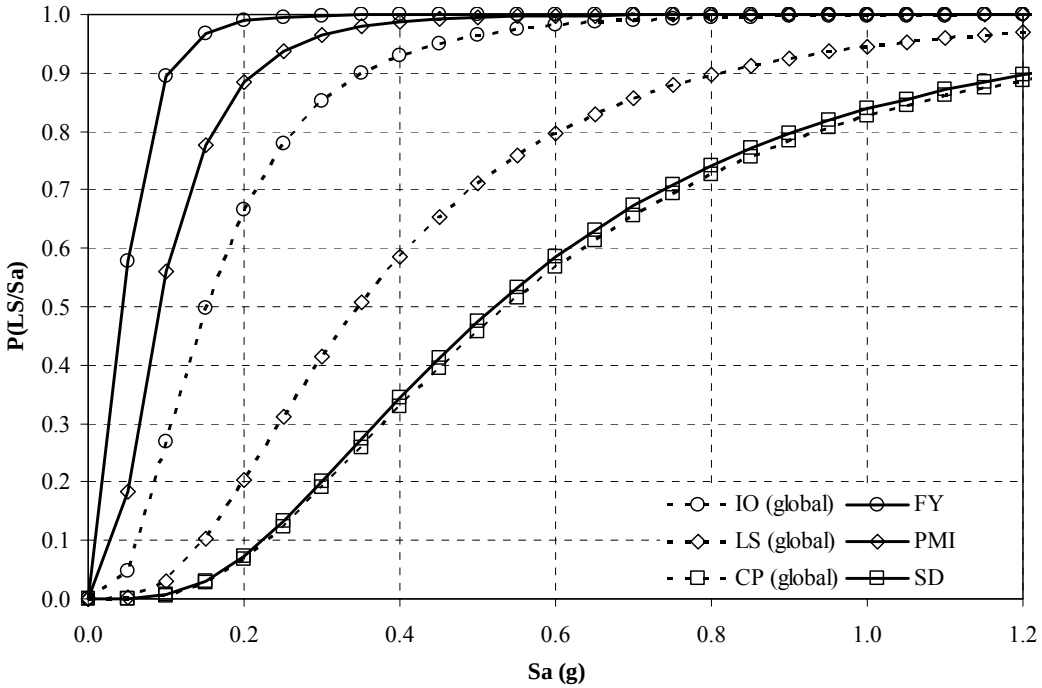

Fig. 5.28. Fragility curves for the FEMA member-level criteria from a regular push-over analysis

5.6 Summary

In this section, the analysis of the unretrofitted case study building was described. Results from two structural analysis methods (nonlinear static analysis and nonlinear dynamic analysis) and two structural nonlinear analysis programs (ZEUS-NL and DRAIN-2DM) were compared. The ZEUS-NL program was selected for additional analytical studies to evaluate the expected seismic performance of the structure for St. Louis and Memphis synthetic ground motions. Based on the analytical results, fragility curves were developed using the FEMA 356 performance criteria and additional limit states. The fragility curves developed based on FEMA global-level drift limits and member-level plastic rotation limits were compared. In addition to this, additional quantitative limit states, described by Wen et al. (2003), were determined and compared to the limits based on the FEMA 356 criteria.

6 RETROFIT DESIGN AND ANALYSIS OF RETROFITTED CASE STUDY BUILDING

6.1 Introduction

This section presents the analytical results of the retrofitted case study building. Three seismic retrofit techniques were applied to enhance the seismic performance of the structure. The seismic behavior of the retrofitted structure and seismic evaluation using FEMA 356 were conducted through nonlinear analyses. In addition, the probabilistic fragility curves for the retrofitted structure were developed and compared with the original structure.

6.2 Retrofit Strategies

6.2.1 General

From the structural design point of view, the selection of the most appropriate strategy depends on the structural characteristics of the building and the inelastic behavior of each member. This implies that the most vulnerable structural characteristic and the weakest part of the structure should be considered prior to others. It is also important to consider the effects of different retrofit techniques on the seismic performance, including dynamic response of the structure and each member, after applying the retrofit schemes.

As discussed in Section 5, the member-level evaluation for the unretrofitted structure did not satisfy the FEMA 356 BSO in several structural members for the 2% in 50 years Memphis motions. Based on this result, three retrofit schemes were selected. The application of retrofits that modified different structural response parameters was of interest. Because IO performance is mainly related to stiffness, shear walls were added to the external frame to increase the lateral stiffness of the structure. To impact LS

performance, the existing columns were encased with RC jackets to increase their strength. Finally, to impact CP performance, the expected plastic hinge zones of the existing columns were confined with external steel plates to increase ductility. Table 6.1 summarizes the rehabilitation objectives and retrofit techniques corresponding to each limit state (performance level). It is noted that for the shear wall and column jacketing retrofit, both stiffness and strength would increase.

Table 6.1. Rehabilitation objectives for each limit state criteria

Limit state	Rehabilitation objective	Retrofit technique
IO	Increase stiffness (& strength)	Add shear walls to external frame
LS	Increase strength (& stiffness)	Add RC column jacketing
CP	Increase ductility	Confine columns plastic hinge zones with steel plates

6.2.2 Retrofit 1: Addition of Shear Walls

The first retrofit strategy consisted of adding RC shear walls to the two center bays of the exterior frame. The addition of shear walls is a common seismic retrofit technique for RC frame structures. This technique increases both the stiffness and strength of the structure. Because lateral stiffness has the most significant change from this retrofit technique, the IO limit state was considered to select a target drift limit. Therefore, the size of walls was determined based on the IO of 1% for the FEMA 356 global-level evaluation. The shear walls are 406 mm (16 in.) thick. The reinforcement was designed using *ACI 318-02* (ACI Comm. 318 2002). Two layers of #6 (US) reinforcing bars at 305 mm (12 in.) spacing were selected for the shear walls. For modeling purposes, the minimum thickness for concrete jackets was applied to the existing columns. Fig. 6.1 shows the elevation view of the external frame after adding shear walls.

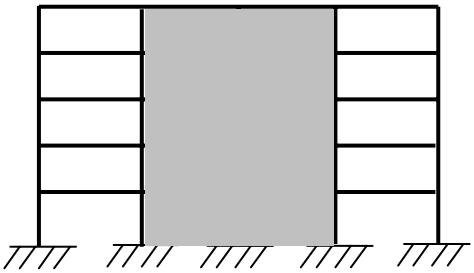

Fig. 6.1. Retrofit 1: Shear walls added to exterior frame

6.2.3 Retrofit 2: Column Jacketing

Based on the FEMA 356 member-level evaluation of the unretrofitted case study building (Chapter 5), the columns had the most deficiencies in meeting the BSO of CP for the 2% in 50 years Memphis events. To strengthen these vulnerable members, the column jacketing technique was selected as the second retrofit scheme. Based on the member-level seismic evaluation, the columns that did not satisfy the FEMA 356 CP criteria were selected and retrofitted with additional reinforcement and concrete jackets. Because this is primarily a strengthening technique, it best corresponds to improving to LS performance. Therefore, the size of the RC jackets and the amount of reinforcement were determined based on the 2% LS drift global-level drift limit. Fig. 6.2 shows the location of jacketed members and Fig. 6.3 shows typical details of the jacketed columns.

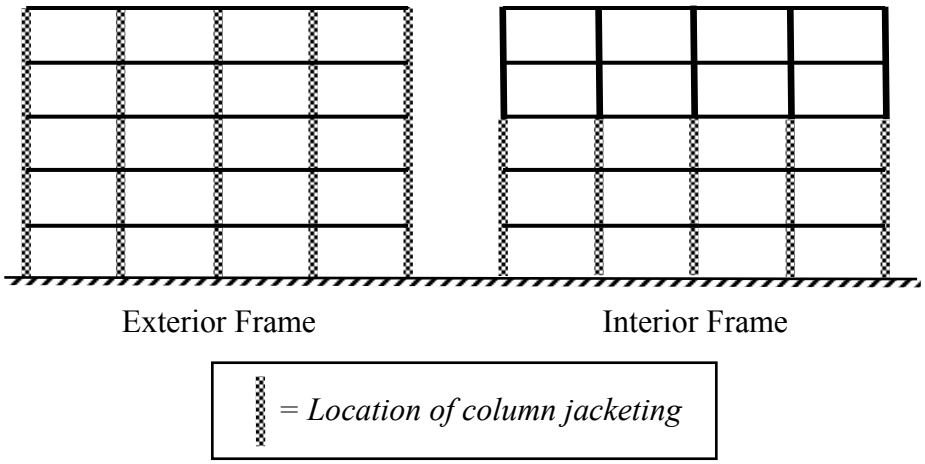

Fig. 6.2. Retrofit 2: Addition of RC column jackets

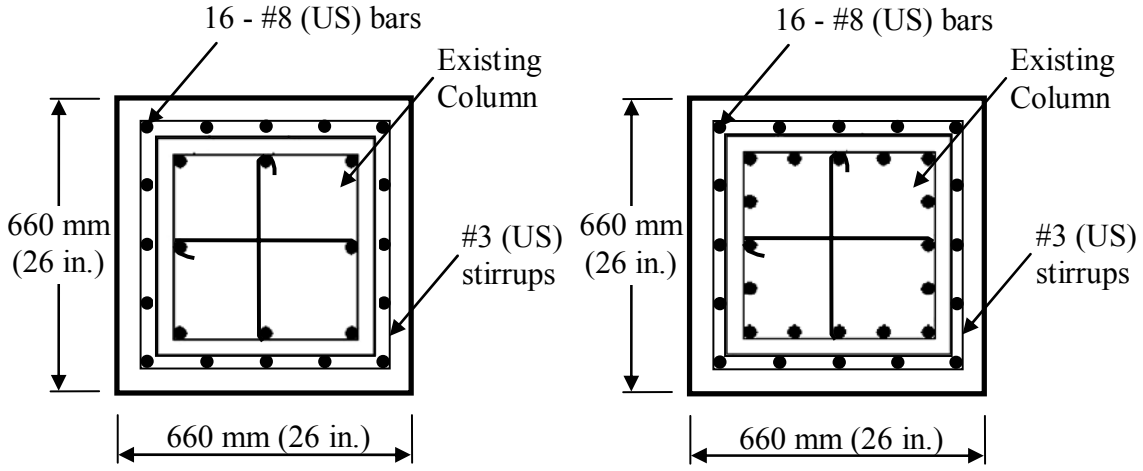

(a) 1st - 5th story for external frame
2nd - 3rd story for interior frame

(b) 1st story for interior frame

Fig. 6.3. Cross-sectional details of RC column jacket retrofit

6.2.4 Retrofit 3: Confinement of Column Plastic Hinge Zones

The third retrofit scheme was to add external steel plates to confine the expected plastic hinge zones of the columns to increase the ductility of the members. This technique was suggested by Elnashai and Pinho (1998) for the ductility-only scenario of selective techniques described in Section 2. When the member ends of columns are vulnerable, failure mechanisms, such as a soft story mechanism can occur. In order to prevent this serious failure mechanism, external confinement steel plates were utilized to confine the columns. The column ends that were confined with steel plates are shown in Fig. 6.4. These correspond to the locations in the unretrofitted structure where the plastic rotations exceeded the CP limits for the 2% in 50 years Memphis motions.

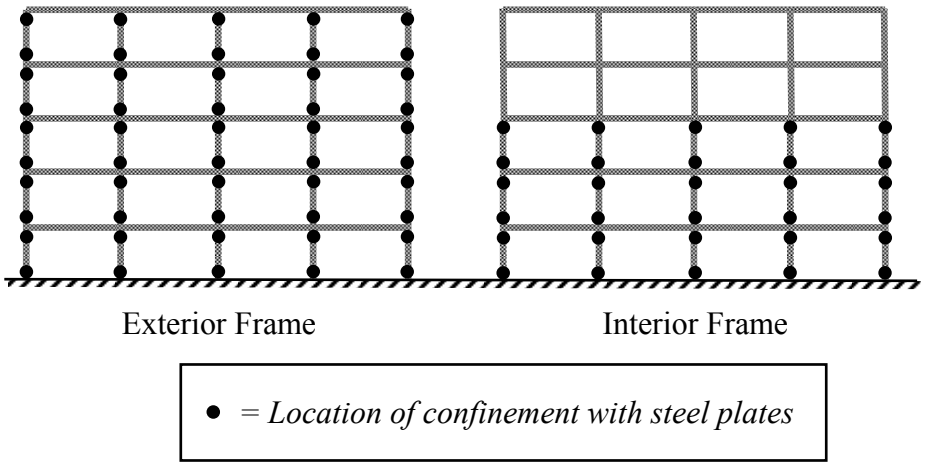

Fig. 6.4. Retrofit 3: Confinement of column plastic hinge zones

6.3 Analytical Modeling of Retrofitted Case Study Building

6.3.1 General

ZEUS-NL was also used for the structural analysis of the retrofitted structure. For the nonlinear dynamic analysis, the twenty ground motions for Memphis, Tennessee were used (see Tables 4.11 and 4.12). To model the selected retrofit techniques, several sections and material properties developed in ZEUS-NL were utilized.

6.3.2 Retrofit 1: Addition of Shear Walls

To model the shear walls, the RC flexure wall section (rcfws) in the ZEUS-NL program library was used. Fig. 6.5 shows a cross-section of the rcfws member and Table 6.2 provides the values used for each parameter in this analysis. The fully confined region of the rcfws section (labeled as "e") is for a boundary element, such as an existing column, but the thickness of the wall was less than the width of existing columns in this study. Therefore, a very small value was used for "e" to model the wall members properly.

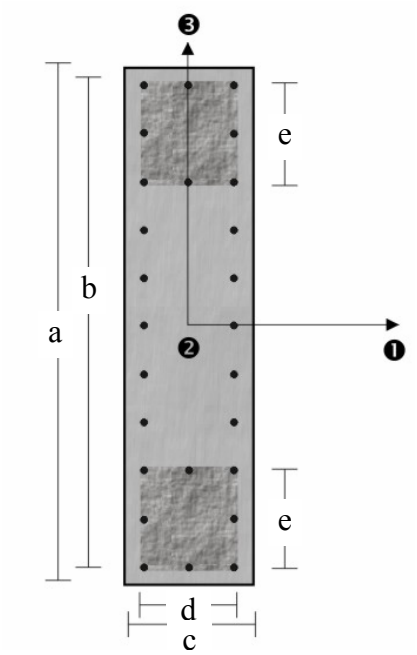

Fig. 6.5. RC flexural wall section in ZEUS-NL (Elnashai et al. 2002)

Table 6.2. Values for modeling parameters of RC flexural wall section

Dimensional parameter	Values, mm (in.)
a. Wall width	7670 (310)
b. Confined width	7320 (288)
c. Wall thickness	406 (16)
d. Confined area thickness	330 (13)
e. Height of fully confined region	1*

* To model the different thickness of the wall members and column width, a very small value was used for the height of the fully confined region (e).

6.3.3 Retrofit 2: Addition of RC Column Jackets

For modeling of the RC jacketed columns, RC jacket rectangular section (rcjrs) in ZEUS-NL was used. Fig. 6.6 shows a cross-section of the rcjrs member and Table 6.3 provides the values used for each parameter in this analysis.

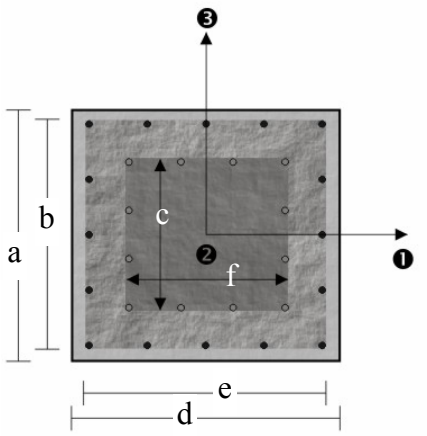

Fig. 6.6. RC jacket rectangular section in ZEUS-NL

Table 6.3. Values for modeling parameters of RC jacket rectangular section

Dimensional parameter	Values, mm (in.)
a. Section height	660 (26)
b. External stirrup height	584 (23)
c. Internal stirrup height	384 (15.1)
d. Section width	660 (26)
e. External stirrup width	584 (23)
f. Internal stirrup width	384 (15.1)

For comparison, the column-to-beam strength ratios for the unretrofitted structure and the retrofitted structure by adding RC jackets were calculated. The current ACI 318 code requires a minimum column-to-beam ratio of 1.2 (ACI Comm. 318 2002). The column-to-beam strength ratio of the 1st floor level for the unretrofitted structure is 0.92 and that for the retrofitted structure by adding RC jackets is 2.66. According to Dooley and Bracci (2001), a minimum strength ratio of 2.0 is more appropriate to prevent the formation of a story mechanism under design seismic loading.

6.3.4 Retrofit 3: Confinement of Column Plastic Hinge Zones

For modeling of the third retrofit scheme, the confinement factor (k), which was discussed in Sec. 4.3.1.2, was increased for the expected plastic hinge zones of the vulnerable columns. This gave the same result as physically confining the columns with

external steel plates. To find the proper value of k, the FEMA 356 requirements for ductile column detailing were used. Based on the minimum transverse reinforcement for ductile behavior, a confinement factor k of 1.3 was adopted. The external steel plates were assumed to be applied over a 910 mm (36 in.) length at the column ends indicated in Fig. 6.4. This length was selected to exceed the expected flexural plastic hinge length of 625 mm (24.6 in.) for the first story columns based on the following equation (Paulay and Priestly 1992).

$$L_p = 0.15 d_b f_y + 0.08 L \tag{6.1}$$

where:

L_p = Plastic hinge length (inches)
d_b = Longitudinal bar diameter (inches)
f_y = Yield strength of reinforcement (ksi)
L = Member length (inches)

6.4 Comparison of Analytical Results between Unretrofitted and Retrofitted Case Study Building

6.4.1 Push-Over Analysis

Push-over analysis were conducted with an inverted triangular load pattern for the retrofitted case study building and compared with the original structure. The inverted triangular load pattern is based on the first mode shape from an eigenvalue analysis of each retrofitted structure. Fig. 6.7 shows the load patterns for each structure. The push-over curves, relating base shear to building drift, for each retrofitted structure are shown in Fig. 6.8. As seen in Fig. 6.8, the results from the three retrofit schemes demonstrate that each retrofit method affects the global structural response characteristics differently.

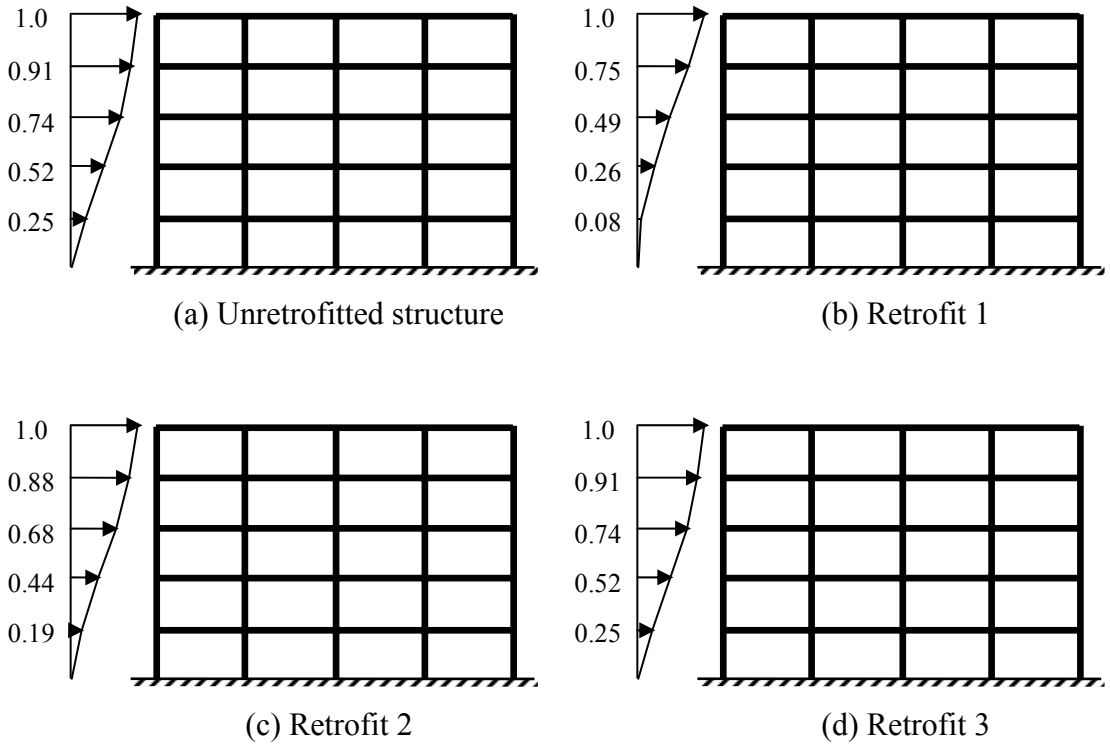

Fig. 6.7. Inverted triangle load patterns for push-over analysis

Table 6.4 summarizes the values of the weight for half of each structure as modeled. First, the retrofitted structure by adding shear walls provided much stiffer behavior than the original structure, but also increased the strength with a maximum base shear ratio of 34.3% of the seismic weight, *W*. This was a 105% increase compared to the unretrofitted building. With this retrofit technique, most of the lateral resistance of the building was provided by the shear walls of the exterior frame. Due to the concrete jackets applied to the existing columns adjacent to shear walls, strength degradation occurred slowly. However, 5% building drift for the retrofitted structure by adding shear walls seems too high since shear failure is not considered in this result. Column jacketing provided 53.0% increase of the maximum base shear ratio compared to the original structure. In addition to this, it gave more ductile behavior during the analysis, such as a slow process for transforming from the linear to nonlinear range, and enhancement of the deformation capacity due to the confinement of the jacketed columns. For the structure retrofitted by confining the column plastic hinge zones with

external steel plates, the initial stiffness and change of strength up to the peak base shear were almost the same as for the unretrofitted structure. This retrofit did not significantly affect the strength or stiffness of the original structure. However, strength degradation occurred more slowly due to the increase of ductility in the columns.

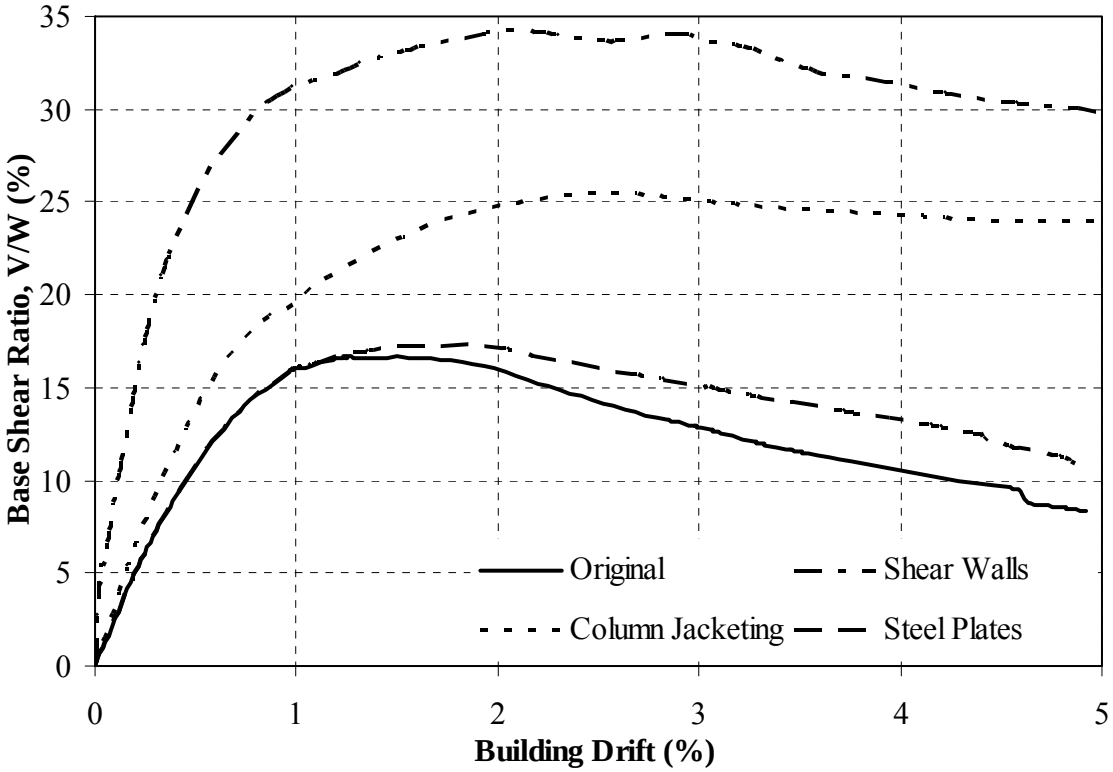

Fig. 6.8. Comparison of push-over curves from the original structure and retrofitted structures

Table 6.4. Weight for half of structure

Model	Weight (kN)
Unretrofitted structure	27,513
Retrofit 1: Addition of shear walls	30,981
Retrofit 2: Addition of RC column jackets	27,852
Retrofit 3: Confinement of column plastic hinge zones	27,513

Note: 1 kN = 4.45 kips

6.4.2 Fundamental Periods

Eigenvalue analyses were performed to find the fundamental periods of the retrofitted structure. The fundamental period of the unretrofitted structure was 1.14 seconds based on uncracked (gross section) member properties. Table 6.5 shows the fundamental periods for the unretrofitted and retrofitted structures after applying each retrofitting scheme. As seen in Table 6.5, the addition of shear walls and column jacketing reduced the value of the fundamental period. However, the retrofit using confinement with steel plates gave the same fundamental period because the stiffness and strength were not changed in this case.

Table 6.5. Fundamental periods for each retrofit scheme

Model	Uncracked T_1 (s)	Cracked T_1 (s)
Unretrofitted structure	1.14	1.62
Retrofit 1: Addition of shear walls	0.43	0.80
Retrofit 2: Addition of RC column jackets	0.96	1.42
Retrofit 3: Confinement of column plastic hinge zones	1.14	1.62

The results from the ZEUS-NL program were based on the fundamental period only reflecting load effects due to gravity loads. To better understand the dynamic behavior of the structure under lateral loadings, the fundamental period should be calculated after the structural members are damaged. Therefore, an impulse load with magnitude 0.5g was applied to each structure and the resulting fundamental period was determined for the damaged structure. Fundamental periods should be considered carefully because the response of a structure is significantly affected by the spectral acceleration corresponding to the fundamental period of the structure. Fig. 6.9 shows the difference of spectral acceleration values for 2% in 50 years Memphis motions corresponding to the two different fundamental period values determined for the unretrofitted case building structure.

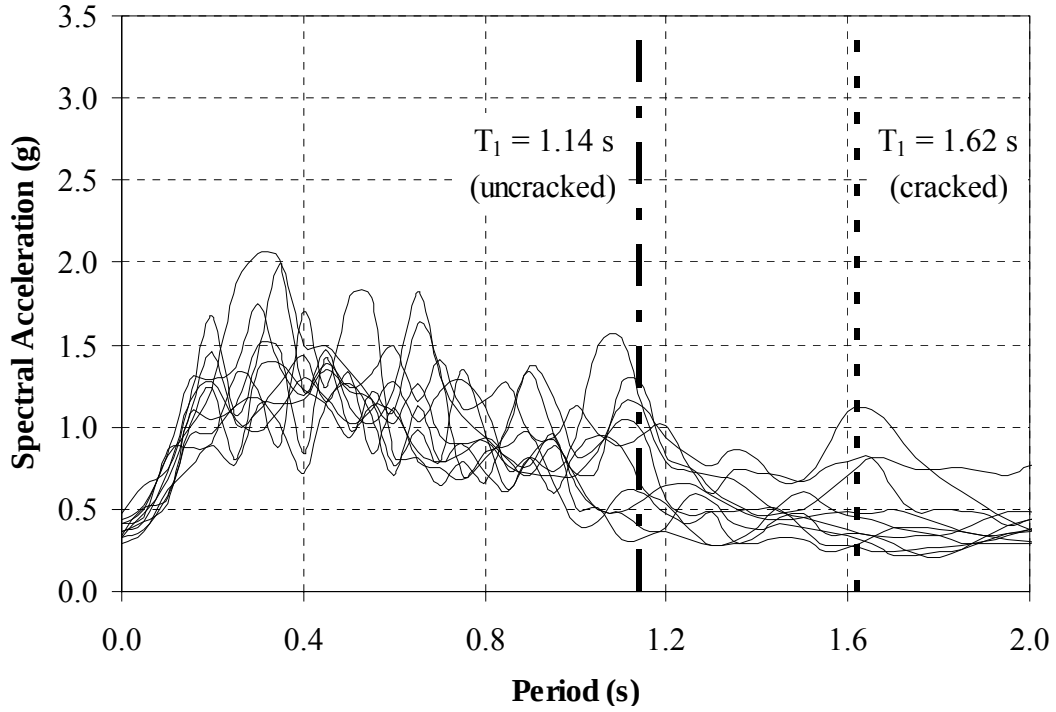

Fig. 6.9. Difference of the spectral acceleration values corresponding to fundamental periods for unretrofitted building (2% in 50 years Memphis motions)

The fundamental periods for the unretrofitted and retrofitted structures after damage are also shown in Table 6.5. For comparison, the fundamental period computed with cracked section properties using DRAIN-2DM was 1.70 seconds for the unretrofitted structure. This is very close to 1.62 seconds computed using the impulse analysis in ZEUS-NL. As seen in Table 6.5, the fundamental periods based on cracked sections are larger than for the uncracked properties. This means that the damaged structure is more flexible so that the fundamental periods from the eigenvalue analysis overestimate the stiffness of the structures.

6.4.3 Dynamic Analysis

The dynamic behavior of the retrofitted case study building was investigated using the Memphis synthetic ground motions. The results from the nonlinear analyses were compared between before and after applying retrofit techniques to verify the effectiveness of retrofitting under the dynamic loadings. The results from the nonlinear

analyses for three retrofit schemes using Memphis motions are provided in Tables 6.6 to 6.9.

Table 6.6. Maximum building drift (%) for retrofitted structure (10% in 50 years Memphis motions)

Ground motion	Unretrofitted	Retrofit 1	Retrofit 2	Retrofit 3
m10_01s	0.142	0.105	0.210	0.112
m10_02s	0.122	0.106	0.146	0.126
m10_03s	0.164	0.151	0.144	0.164
m10_04s	0.153	0.156	0.130	0.146
m10_05s	0.129	0.115	0.147	0.124
m10_06s	0.425	0.117	0.247	0.255
m10_07s	0.134	0.178	0.139	0.112
m10_08s	0.155	0.122	0.115	0.152
m10_09s	0.0800	0.155	0.0906	0.0680
m10_10s	0.0950	0.104	0.0920	0.0956
Median	0.144	0.129	0.139	0.128

Table 6.7. Maximum building drift (%) for retrofitted structure (2% in 50 years Memphis motions)

Ground motion	Unretrofitted	Retrofit 1	Retrofit 2	Retrofit 3
m02_01s	1.99	1.17	1.63	1.88
m02_02s	2.36	0.867	1.63	2.00
m02_03s	1.94	1.21	0.955	1.54
m02_04s	1.92	0.825	1.82	1.74
m02_05s	2.64	1.29	2.56	2.26
m02_06s	2.47	1.24	2.54	2.42
m02_07s	1.99	0.672	1.14	1.58
m02_08s	2.74	1.16	1.61	2.12
m02_09s	1.88	0.753	1.04	1.45
m02_10s	2.31	0.939	1.48	1.81
Median	2.20	0.989	1.56	1.86

Table 6.8. Maximum base shear ratio, V/W (%) for retrofitted structure (10% in 50 years Memphis motions)

Ground motion	Unretrofitted	Retrofit 1	Retrofit 2	Retrofit 3
m10_01s	4.54	11.5	10.2	4.58
m10_02s	5.29	12.9	6.49	5.28
m10_03s	4.97	17.2	7.81	5.00
m10_04s	4.54	22.5	7.33	4.57
m10_05s	4.99	12.7	7.41	5.00
m10_06s	7.81	24.0	9.11	7.89
m10_07s	4.65	20.7	8.20	4.60
m10_08s	5.97	21.3	6.43	5.95
m10_09s	4.84	15.7	6.80	4.84
m10_10s	4.21	12.2	7.55	4.20
Median	5.10	16.5	7.66	5.11

Table 6.9. Maximum base shear ratio, V/W (%) for retrofitted structure (2% in 50 years Memphis motions)

Ground motion	Unretrofitted	Retrofit 1	Retrofit 2	Retrofit 3
m02_01s	18.4	36.8	30.1	18.9
m02_02s	19.1	48.7	27.7	19.8
m02_03s	18.8	39.8	23.3	19.6
m02_04s	18.9	37.9	27.7	19.8
m02_05s	18.5	50.2	25.7	19.0
m02_06s	18.2	48.3	28.6	18.8
m02_07s	19.6	45.6	23.4	20.2
m02_08s	17.9	41.3	26.1	18.3
m02_09s	18.7	39.9	21.3	19.2
m02_10s	18.1	40.9	30.2	19.2
Median	18.6	42.7	26.2	19.3

Fig. 6.10 provides comparisons of the building drift between the original structure and three retrofitted structures. The ground motions to represent the median demand were selected based on the median maximum building drift for the original structure. The median values of the maximum building drift were calculated based on the natural log of each value, as discussed in Section 5.

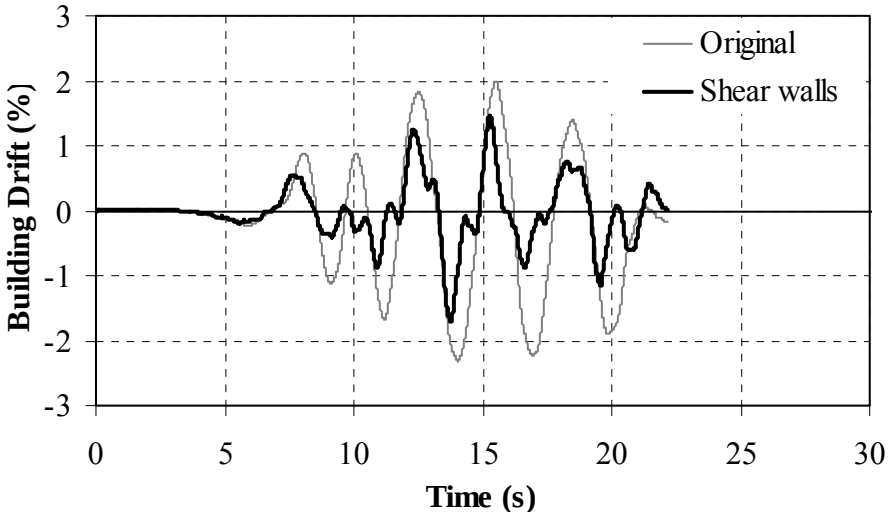

(a) Retrofit 1: Addition of shear walls

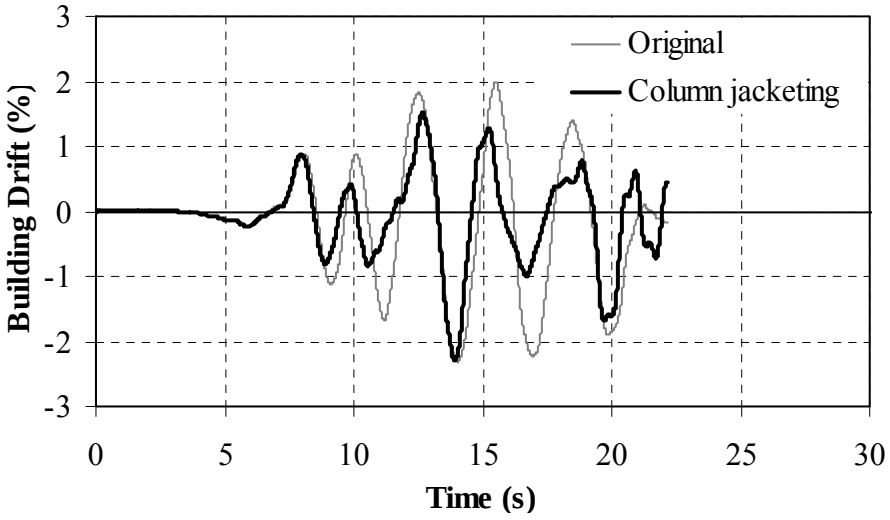

(b) Retrofit 2: Addition of RC column jackets

Fig. 6.10. Comparison of building drifts for the median motion (m02_10s) of 2% in 50 years Memphis data

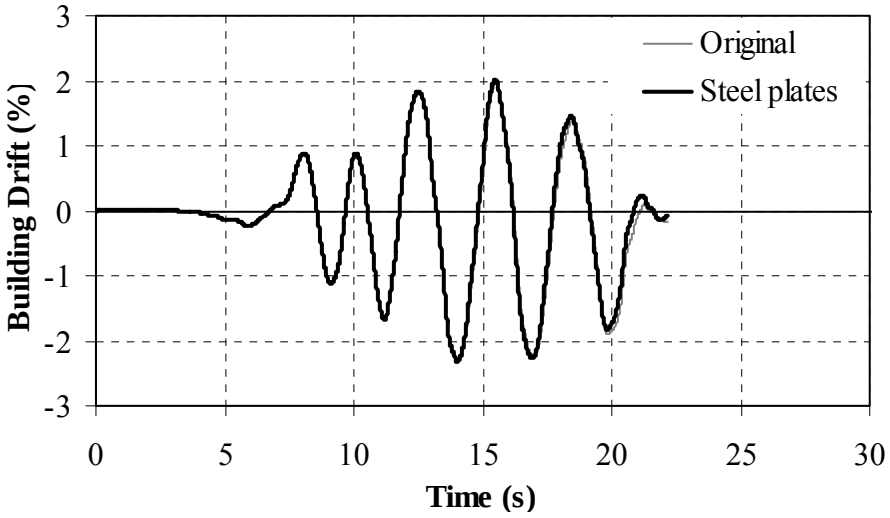

(c) Retrofit 3: Confinement of column plastic hinge zones

Fig. 6.10. Continued

As seen in Tables 6.6 to 6.9, the median values of the maximum building drift were reduced for all retrofit schemes. In particular, shear wall retrofitting was most effective to reduce the building drift, as shown in Fig. 6.10a. For retrofitting by confining with steel plates, the building drift values were not very different from those of the unretrofitted structure.

6.5 Seismic Evaluation for Retrofitted Case Study Building

6.5.1 Global-Level Evaluation

For evaluating the retrofitted structure based on the FEMA 356 global-level criteria, the maximum interstory drift values were taken from the nonlinear dynamic analyses. Table 6.10 provides the interstory drift limits for three structural performance levels for concrete frame and concrete wall elements were suggested by FEMA 356 (ASCE 2000).

Table 6.10. Global-level drift limits in FEMA 356 (ASCE 2000)

	Drift limits (%)		
	IO	LS	CP
Concrete frame	1	2	4
Concrete wall	0.5	1	2

The BSO was satisfied for the 10% and 2% in 50 years St. Louis motions and for the 10% in 50 years Memphis motions based on the global-level evaluation for the unretrofitted case study building. Therefore, the 2% in 50 years Memphis motions were used to evaluate the retrofitted structure. Figs. 6.11 to 6.13 show the maximum interstory drift profiles for the three retrofitted structures based on the analyses using the 2% in 50 years Memphis motions. The median values for the unretrofitted case is also indicated and compared with the median drifts of the retrofitted structures.

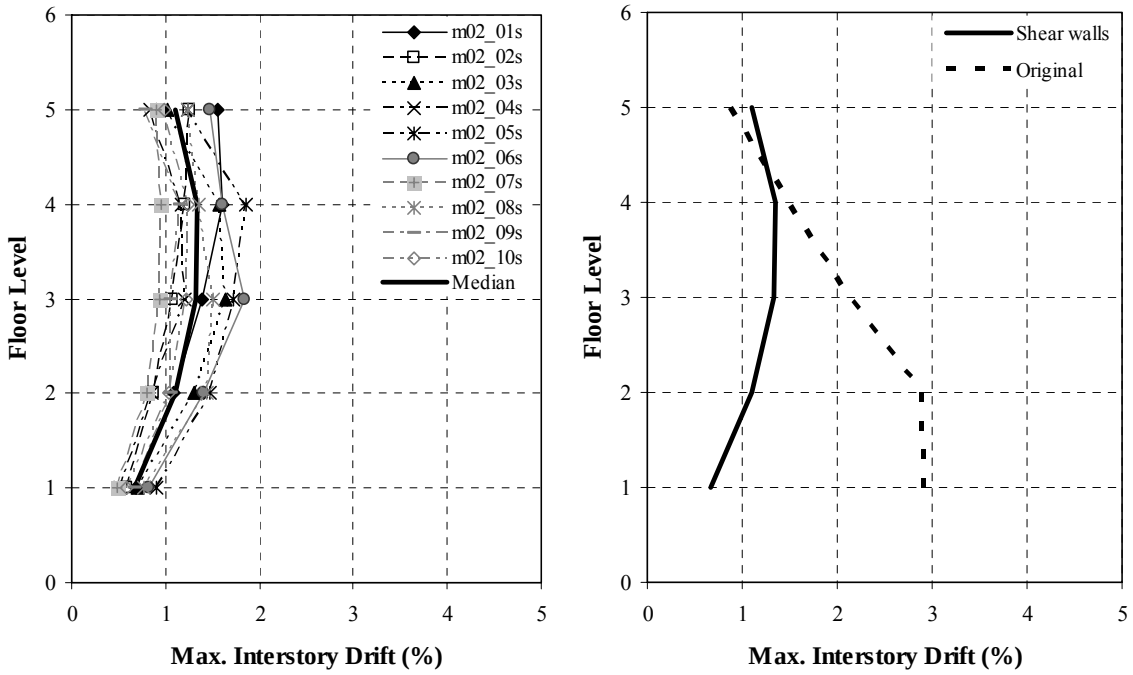

(a) Retrofitted structure (b) Comparison with unretrofitted structure

Fig. 6.11. Maximum interstory drifts for retrofitted structure with shear walls (2% in 50 years Memphis motions)

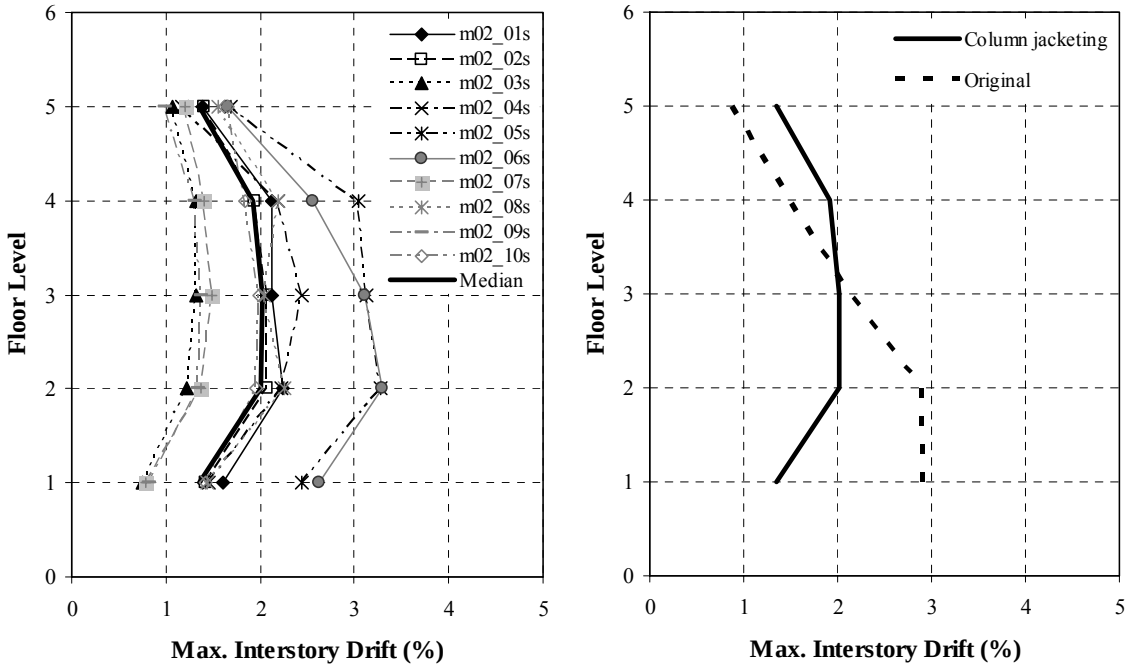

(a) Retrofitted structure (b) Comparison with unretrofitted structure

Fig. 6.12. Maximum interstory drifts for retrofitted structure with RC column jackets (2% in 50 years Memphis motions)

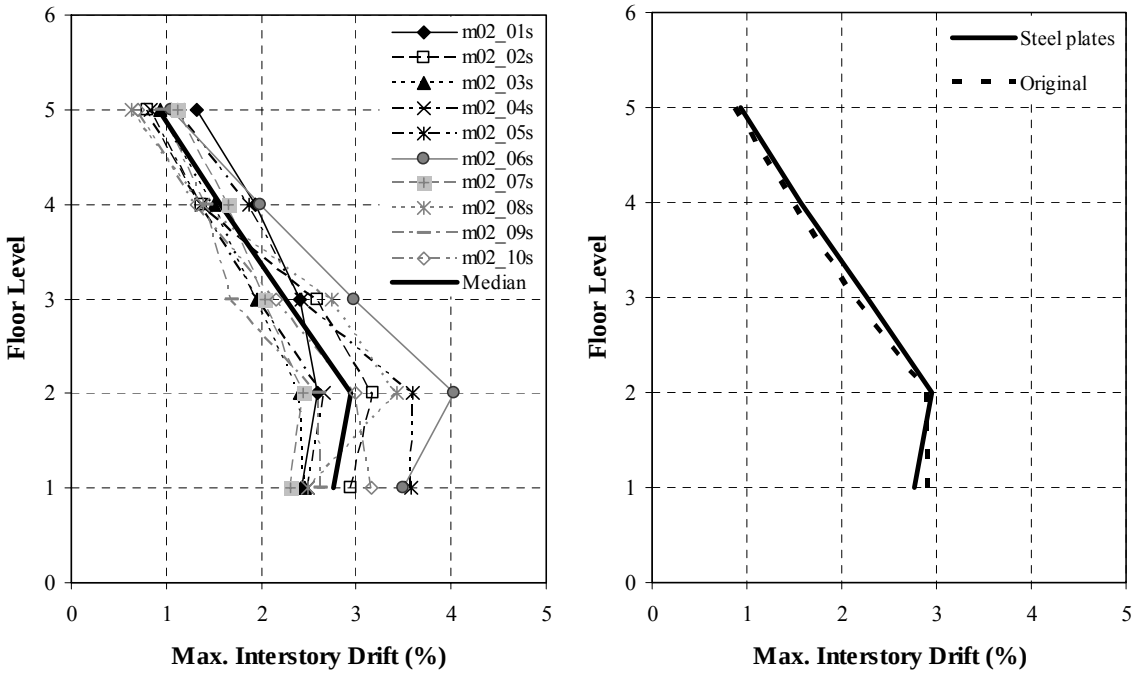

(a) Retrofitted structure (b) Comparison with unretrofitted structure

Fig. 6.13. Maximum interstory drifts for retrofitted structure with plastic hinge zone confinement (2% in 50 years)

For the shear wall retrofit, the performance of the building based on a global-level evaluation showed a significant improvement. As shown in Fig. 6.11, the maximum interstory drifts for each story were reduced, in general. In particular, the drifts of the lower stories were more reduced substantially. Second, the maximum interstory drifts for the RC column jacketing retrofit shown in Fig. 6.12, were also reduced at the lower stories. However, for the fourth and fifth stories where the retrofit was not applied, the maximum interstory drifts increased slightly. Finally, for the retrofit involving confinement of the column plastic hinge zones, no major change occurred in the median drift profile. As shown in Fig. 6.13b, the overall profiles for the unretrofitted and retrofitted structures have a similar shape. Like the unretrofitted structure, the three retrofitted structures satisfied the BSO suggested by FEMA 356 based on the global-level evaluation.

6.5.2 Member-Level Evaluation

The member-level evaluation of FEMA 356 was performed for each retrofitted structure. For shear wall retrofitting, the plastic rotations limits for the members controlled by flexure in FEMA 356, was used (see Table 2.7). The results of the member-level evaluation for each retrofitted structure are shown in Table 6.11 to 6.13. In these tables, the FEMA 356 criteria are listed vertically in the order of the IO, LS and CP limit states.

Table 6.11. Member-level evaluation for Retrofit 1 (2% in 50 years Memphis motions)

Floor level	Median motion	Beams		Columns		Slabs		Shear walls	
		FEMA 356 limits (rad.)	Max. plastic rotation (rad.)	FEMA 356 limits (rad.)	Max. plastic rotation (rad.)	FEMA 356 limits (rad.)	Max. plastic rotation (rad.)	FEMA 356 limits (rad.)	Max. plastic rotation (rad.)
1	m02_09s	0.00500	0.00214	0.00481	0.00231	0.00550	0	0.00500	0
		0.0100		0.0147		0.00825		0.0100	
		0.0100		0.0195		0.0110		0.0150	
2	m02_01s	0.00500	0.00542	0.00506	0.00463	0.00550	0	0.00500	0
		0.0100		0.0150		0.00825		0.0100	
		0.0100		0.0200		0.0110		0.0150	
3	m02_01s	0.00500	0.00480	0.00531	0.00434	0.00550	0	0.00500	0
		0.0100		0.0153		0.00825		0.0100	
		0.0153		0.0204		0.0110		0.0150	
4	m02_08s	0.00500	0.00487	0.00522	0.00421	0.00550	0	0.00500	0
		0.0100		0.0153		0.00825		0.0100	
		0.0161		0.0206		0.0110		0.0150	
5	m02_05s	0.00500	0.00377	0.00500	0.00207	0.000500	0	0.00500	0
		0.0100		0.0150		0.000750		0.0100	
		0.0157		0.0200		0.00100		0.0150	

Table 6.12. Member-level evaluation for Retrofit 2 (2% in 50 years Memphis motions)

Floor level	Median motion	Beams		Columns		Slabs	
		FEMA 356 limits (rad.)	Max. plastic rotation (rad.)	FEMA 356 limits (rad.)	Max. plastic rotation (rad.)	FEMA 356 limits (rad.)	Max. plastic rotation (rad.)
1	m02_09s	0.00500	**0.0138**	0.00485	**0.0207**	0.00550	**0.0179**
		0.0100		0.0148		0.00830	
		0.0100		0.0196		0.0110	
2	m02_10s	0.00500	**0.0114**	0.00496	0.0183	0.00550	**0.0116**
		0.0100		0.0149		0.00830	
		0.0100		0.0199		0.0110	
3	m02_10s	0.00500	0.0114	0.005	0.0166	0.00550	0.00768
		0.0100		0.015		0.00830	
		0.0153		0.02		0.0110	
4	m02_03s	0.00500	0.0114	0.005	0.0158	0.00550	0
		0.0100		0.015		0.00830	
		0.0161		0.02		0.0110	
5	m02_09s	0.00500	0.00619	0.005	0.00861	0.000500	0
		0.0100		0.015		0.000800	
		0.0157		0.02		0.00100	

Table 6.13. Member-level evaluation for Retrofit 3 (2% in 50 years Memphis motions)

Floor level	Median motion	Beams		Columns		Slabs	
		FEMA 356 limits (rad.)	Max. plastic rotation (rad.)	FEMA 356 limits (rad.)	Max. plastic rotation (rad.)	FEMA 356 limits (rad.)	Max. plastic rotation (rad.)
1	m02_09s	0.00500	**0.0194**	0.00445	**0.0264**	0.00550	**0.0179**
		0.0100		0.0142		0.00830	
		0.0100		0.0186		0.0110	
2	m02_10s	0.00500	**0.0179**	0.00469	**0.0233**	0.00550	**0.0137**
		0.0100		0.0145		0.00830	
		0.0100		0.0192		0.0110	
3	m02_10s	0.00500	0.0127	0.00487	0.0182	0.00550	0.00768
		0.0100		0.0148		0.00830	
		0.0153		0.0197		0.0110	
4	m02_03s	0.00500	0.00614	0.00500	0.0113	0.00550	0
		0.0100		0.0150		0.00830	
		0.0161		0.0200		0.0110	
5	m02_03s	0.00500	0	0.00500	0.00468	0.000500	0
		0.0100		0.0150		0.000800	
		0.0157		0.0200		0.00100	

For all the retrofit schemes, except Retrofit 1, member-level evaluations did not perfectly meet the suggested FEMA BSO of CP for the 2% in 50 years event. However, the evaluation shows that the retrofits improve the seismic performance. Retrofitting resulted in a reduction of plastic rotations, or increase of member capacity. For instance, the plastic rotations for Retrofit 3 are very similar to the unretrofitted structure. However, the columns at the third and fourth stories are within the FEMA limit due to an increase in column ductility. Consequently, the overall seismic performance was enhanced.

Fig. 6.14 shows the locations of inelastic behavior in the unretrofitted structure and retrofitted structure where the plastic rotations exceed the limits for CP performance level under the median ground motion for the 2% in 50 years Memphis event. Locations where the rotations exceeded the FEMA 356 member-level criteria for each limit state are shown with black circles. These figures demonstrate the effectiveness after applying

retrofit techniques. The figure for Retrofit 1 is not shown because the rotations were not exceeded CP limits Retrofit 1.

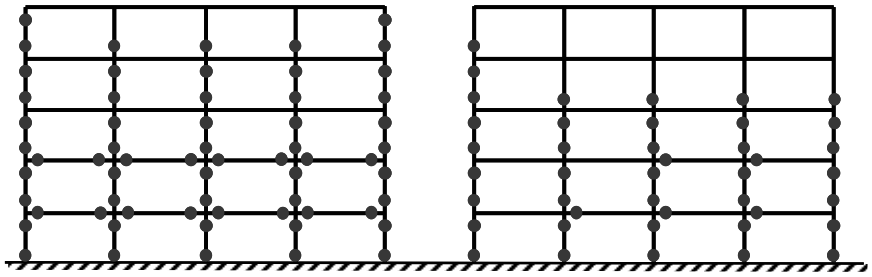

(a) Unretrofitted structure

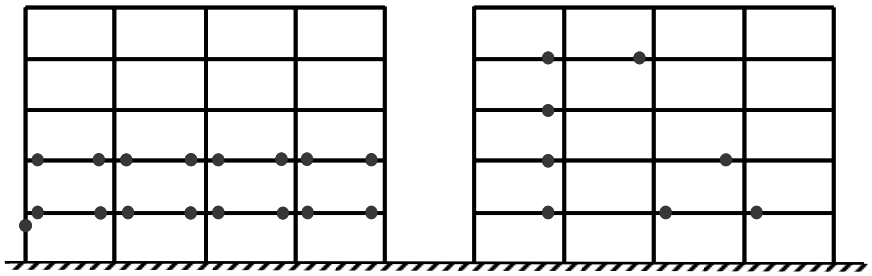

(b) Retrofit 2: Addition of RC column jackets

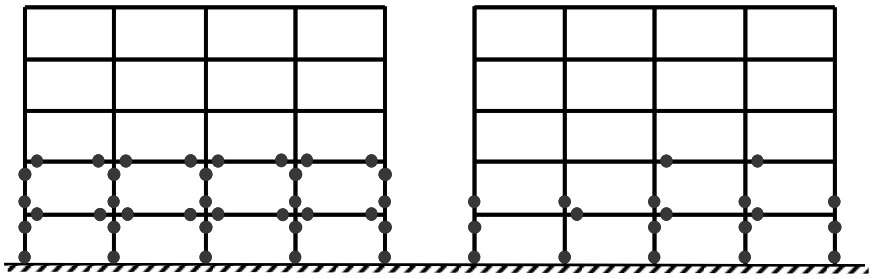

(c) Retrofit 3: Confinement of column plastic hinge zones

● = Exceedance of plastic rotation limit

Fig. 6.14. Locations in unretrofitted and retrofitted building where CP plastic rotation limits are exceeded (2% in 50 years Memphis event)

6.6 Fragility Curves for Retrofitted Case Study Building

6.6.1 Global-Level Limits

To compare the enhancement of seismic performance of the structure, probabilistic fragility curves were also developed for the retrofitted structures and compared to those for the unretrofitted structure. As discussed in Section 5, spectral acceleration values from each ground motion record were used to develop the relationship between demand and structural response (drift), and fragility curves were developed using Eq. 5.1. Fig. 6.15 shows the fitted power law equations for each retrofitted structure reflecting the maximum interstory drift and spectral acceleration for the twenty synthetic Memphis motions. The spectral acceleration (S_a) for a given ground motion record is the value corresponding to the fundamental period of the structure based on cracked section properties and 2 percent damping.

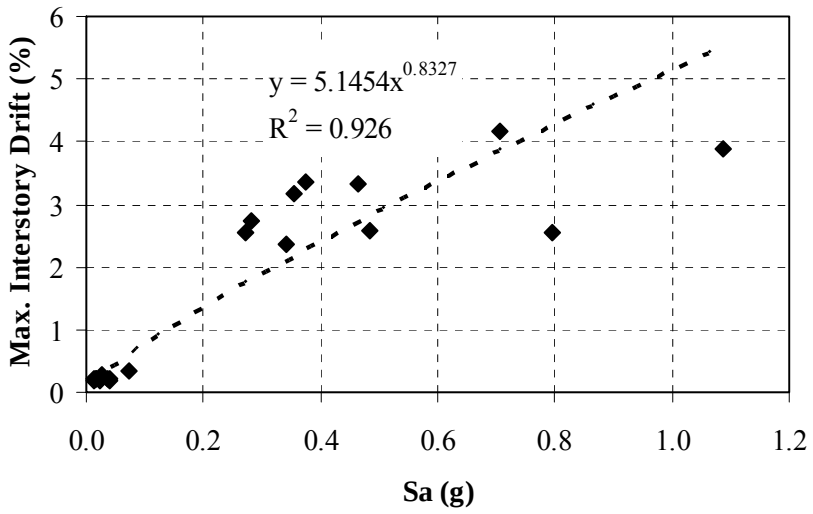

(a) Unretrofitted structure

Fig. 6.15. Development of power law equation for demand drift for retrofitted structures

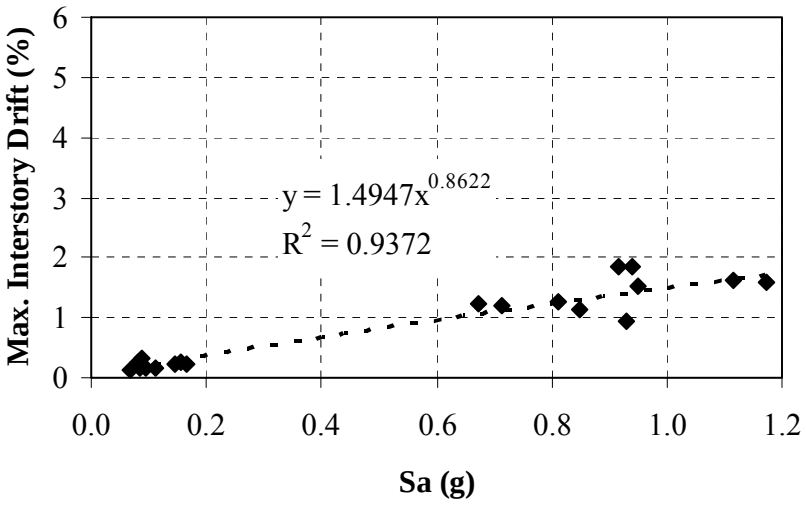

(b) Retrofit 1: Addition of shear walls

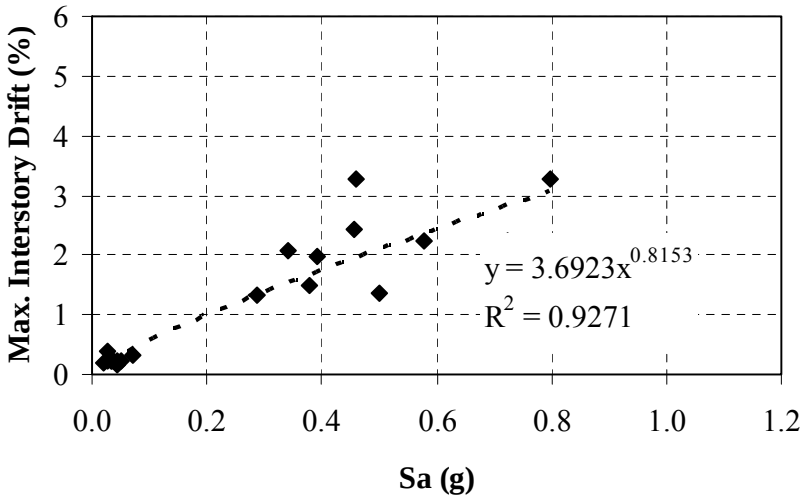

(c) Retrofit 2: Addition of RC column jackets

Fig. 6.15. Continued

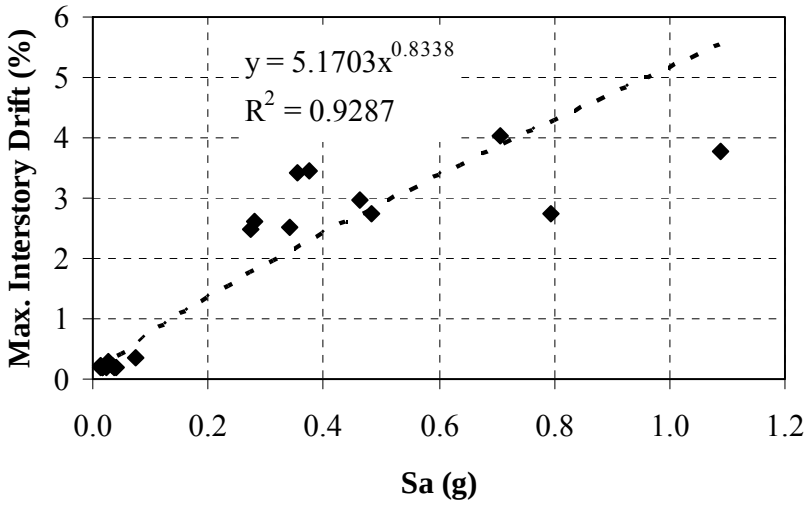

(d) Retrofit 3: Confinement of column plastic hinge zones

Fig. 6.15. Continued

Table 6.14 provides the parameters for Eq. 5.1 used in developing the global-level fragility curves for the retrofitted structures

Table 6.14. Parameters for developing the global-level fragility curves for retrofit

Model	Parameter	Value
Retrofit 1: Addition of shear walls	s^2	0.0679
	β_{D/S_a}	0.256
	β_{CL}	0.3
	β_M	0.3
Retrofit 2: Addition of RC column jackets	s^2	0.101
	β_{D/S_a}	0.310
	β_{CL}	0.3
	β_M	0.3
Retrofit 3: Confinement of column plastic hinge zones	s^2	0.139
	β_{D/S_a}	0.360
	β_{CL}	0.3
	β_M	0.3

The fragility curves developed using the three retrofit techniques are provided in Fig. 6.16. For comparison, the fragility curves for the unretrofitted structure are represented on each graph with dotted lines. Based on the global drift limits of FEMA 356, the IO, LS and CP performance levels are defined differently for concrete wall elements; with drift limits of 0.5, 1 and 2 percent, respectively. Therefore, these values were used to define drift capacity for the shear wall retrofit fragility curves. As discussed in Section 5, the punching shear failure was included as an upper bound of CP limit state. However, the FEMA 356 limit of 2% for CP was less than the drift limit for punching shear taken to as 2.9% for the case study building. Therefore, 2% was used for the CP drift capacity for the shear wall retrofit.

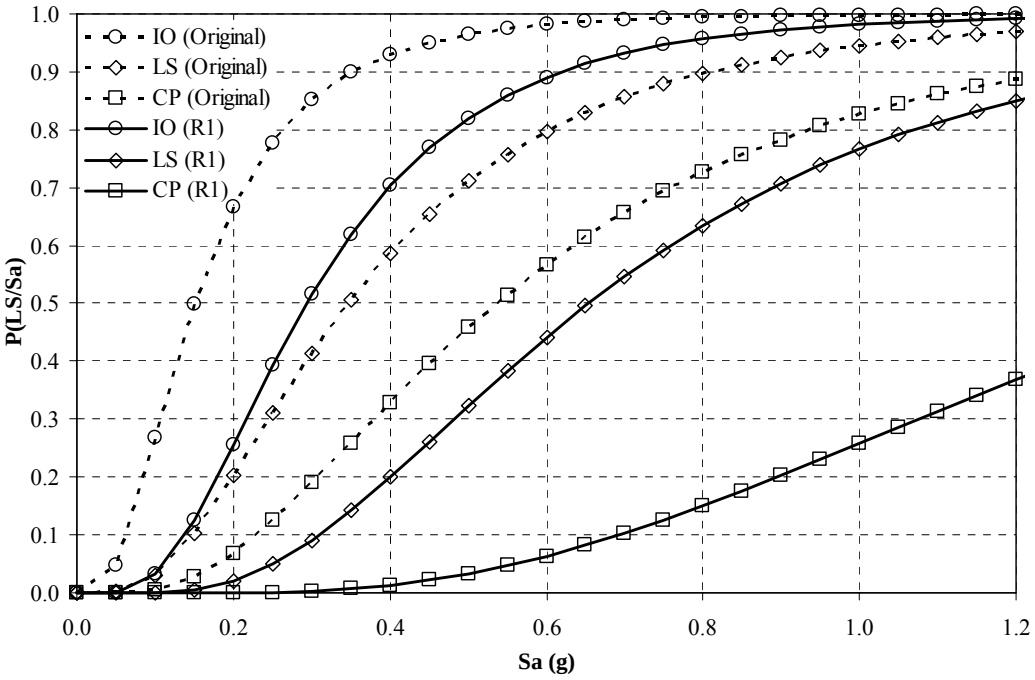

(a) Retrofit 1: Addition of shear walls

Fig. 6.16. Global-level fragility curves for the retrofitted structure

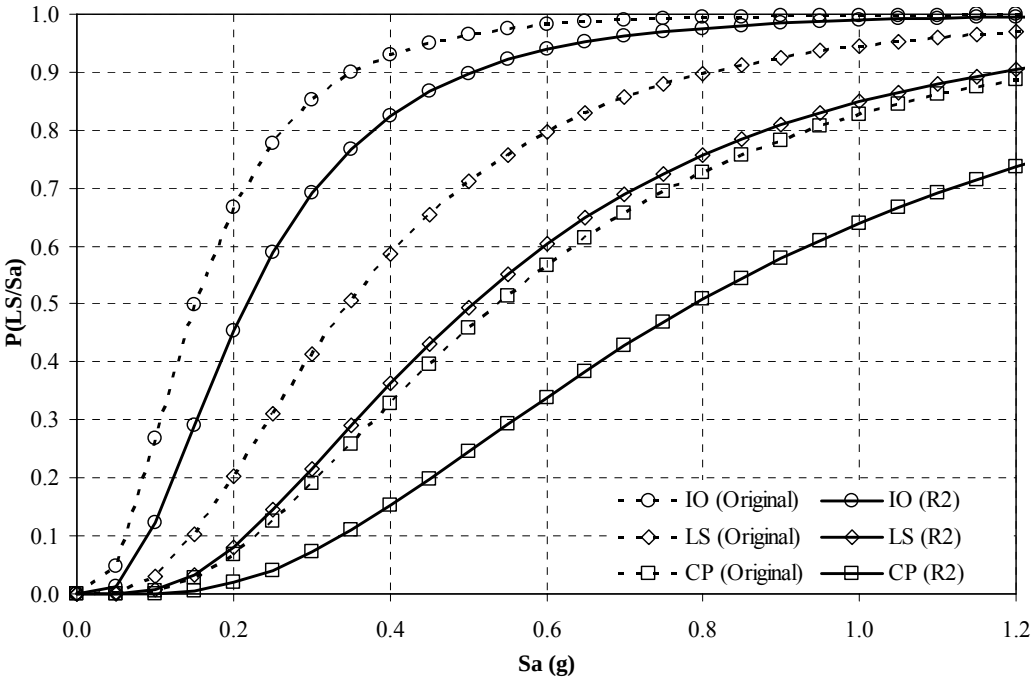

(b) Retrofit 2: Addition of RC column jackets

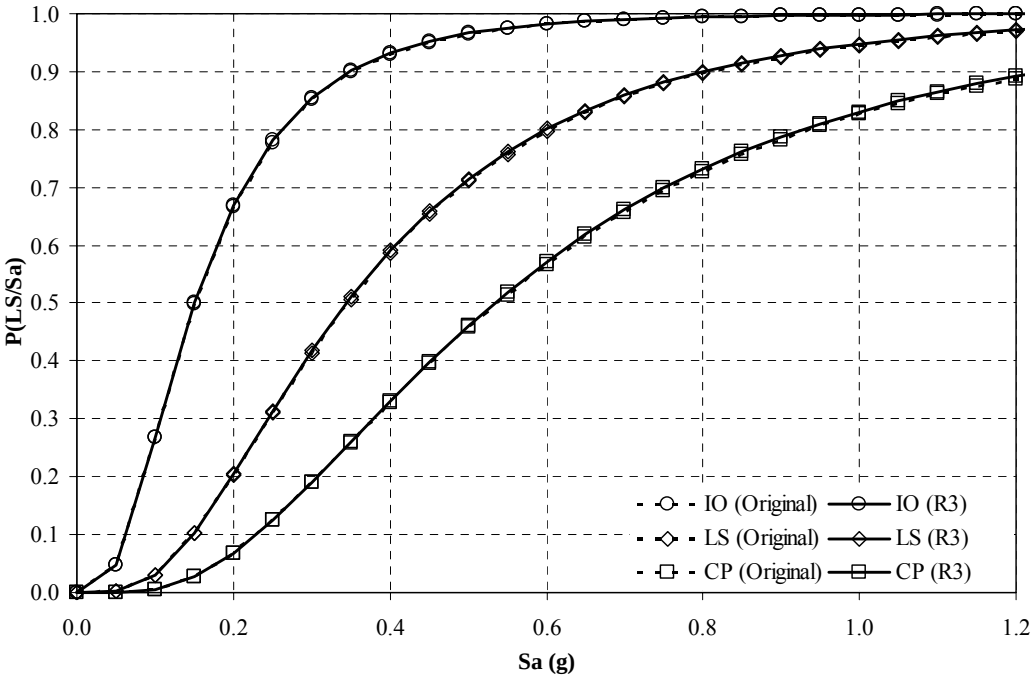

(c) Retrofit 3: Confinement of column plastic hinge zones

Fig. 6.16. Continued

As shown in Figs. 6.16b and 6.16c, the addition of shear walls and RC column jackets were effective in decreasing the probability of exceeding each limit state. However, for the case of confining the plastic hinge zones (Retrofit 3), the fragility curves for each limit state are the same as those for the unretrofitted structure. This is because the same global-level capacity drift limits are used for both the unretrofitted and Retrofit 3 structures. In addition, the demand drifts are nearly the same because the added confinement of Retrofit 3 does not modify the global structural response. Fig. 6.17 shows the fragility curves for each limit state. As shown in Fig. 6.17, the probabilities of exceeding each limit state for the addition of shear walls and RC column jackets were reduced while those for the confinement of column plastic hinge zones were the same with the unretrofitted structure.

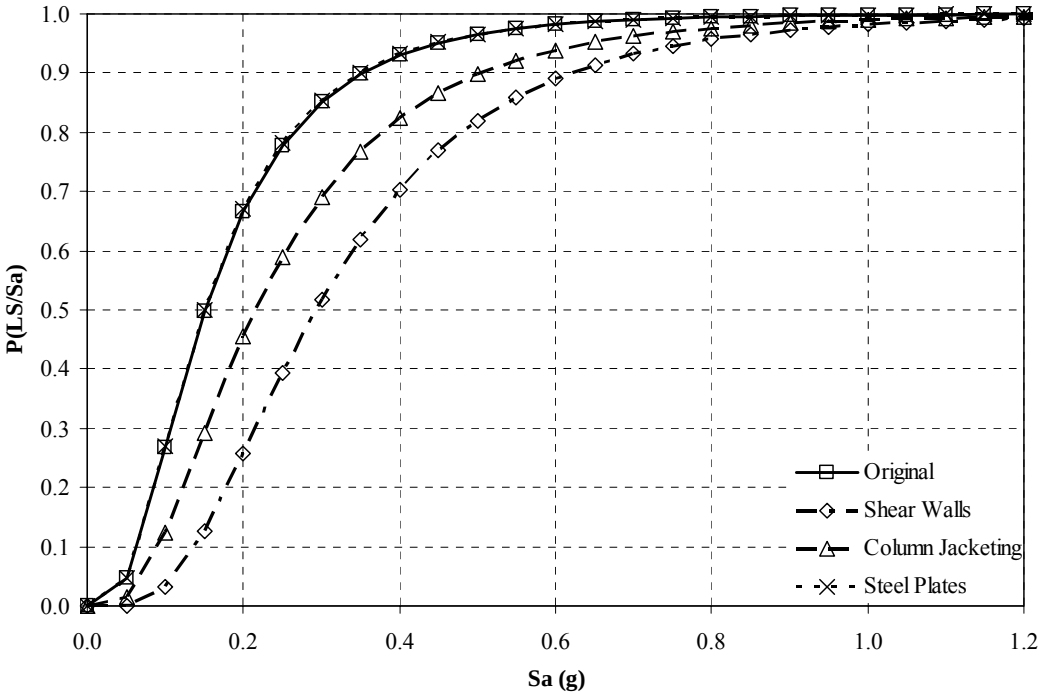

(a) IO

Fig. 6.17. Comparisons of global-level fragility curves for each limit state

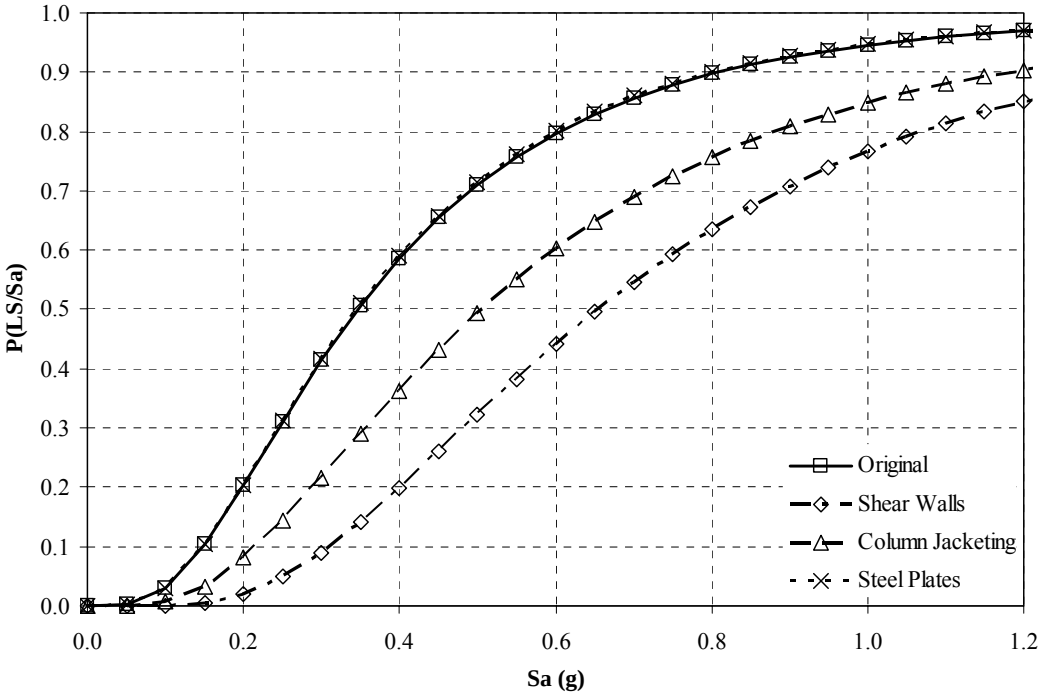

(b) LS

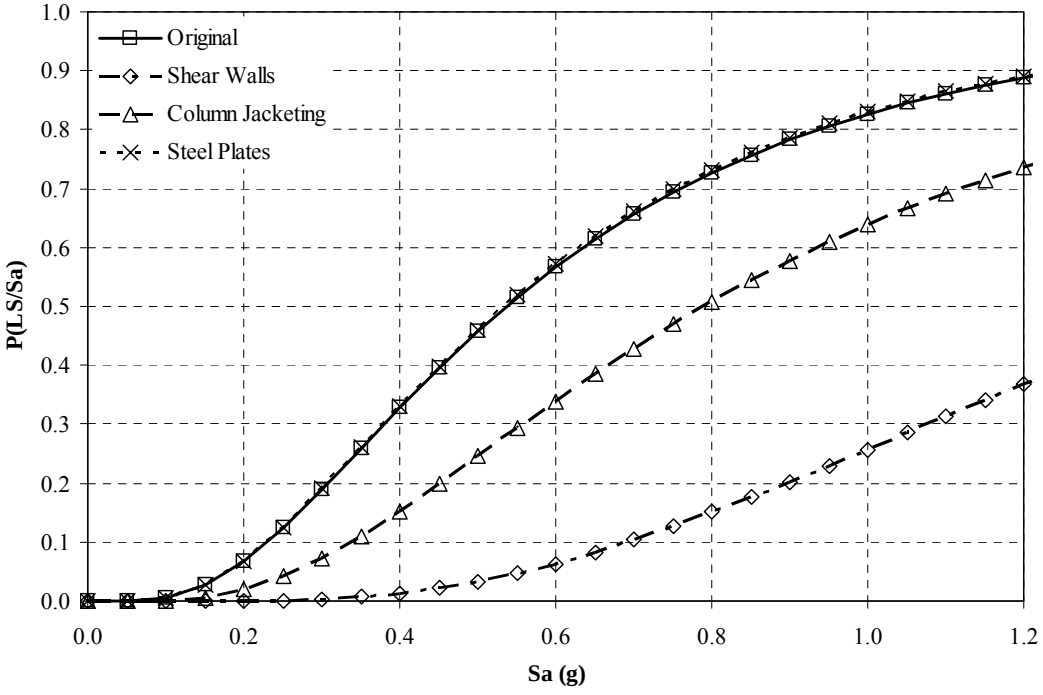

(c) CP

Fig. 6.17. Continued

6.6.2 Member-Level Limits

As discussed in Section 5, member-level fragility curves were developed based on drift capacities determined from a regular push-over analysis with an inverted triangular load pattern and a critical response push-over analysis.

First, drift limits based for each the retrofitted structure, were determined using a regular push-over analysis. Push-over analysis with the inverted triangular load pattern was performed to define the drift limits. The inverted triangular load patterns were shown in Fig. 6.7. The push-over analysis method to determine the critical response, suggested by Dooley and Bracci (2001), was also performed for the retrofitted structures. The drift limits for FEMA member-level criteria are summarized in Table 6.15.

Table 6.15. Interstory drift (%) limits based on FEMA 356 member-level criteria

Structure	Regular push-over			Critical response push-over		
	IO	LS	CP	IO	LS	CP
Unretrofitted	0.88	0.88	1.07	0.62	0.62	0.69
Retrofit 1	0.72	1.24	1.67	0.65	1.24	1.42
Retrofit 2	1.10	1.81	2.12	0.81	1.38	1.69
Retrofit 3	1.07	1.74	1.89	0.83	1.46	1.81

As shown in Table 6.15, the drift limits for IO limit state are larger than the FEMA global drift limits for retrofitted cases. However, the drift limits for LS and CP limit states are less than the FEMA global drift limits. By comparison to the unretrofitted structure, drift limits are increased according to enhance structural characteristics by retrofitting. Figs. 6.18 to 6.20 show the fragility curves based on these criteria for each retrofitted structure. For comparison, the fragility curves using the global drift limits are represented on each graph with dotted lines.

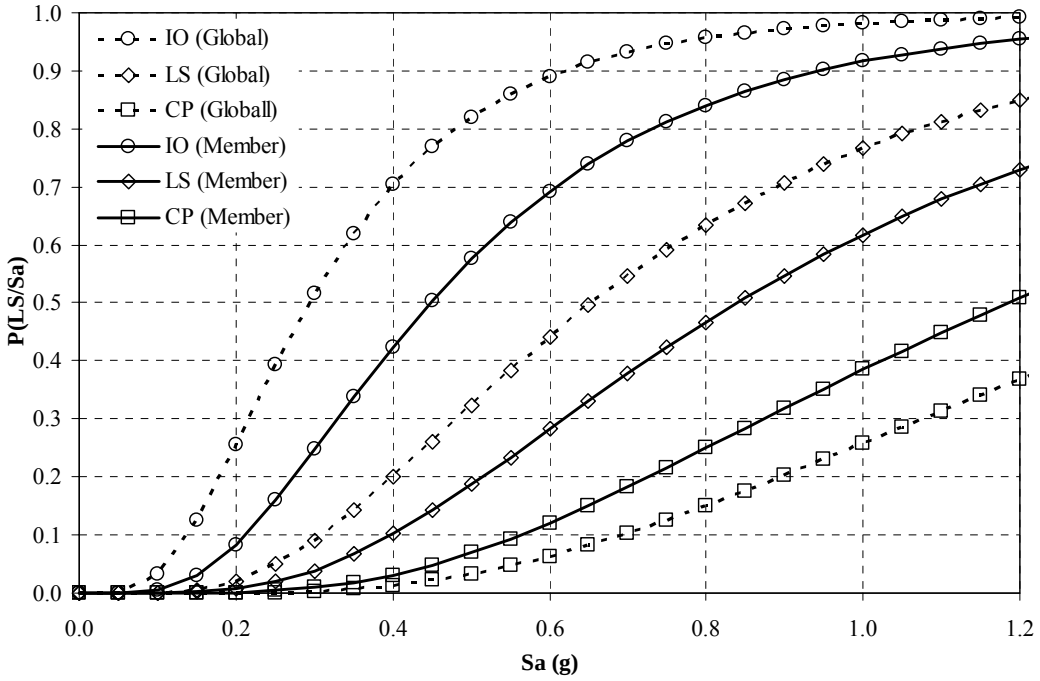

(a) Regular push-over analysis

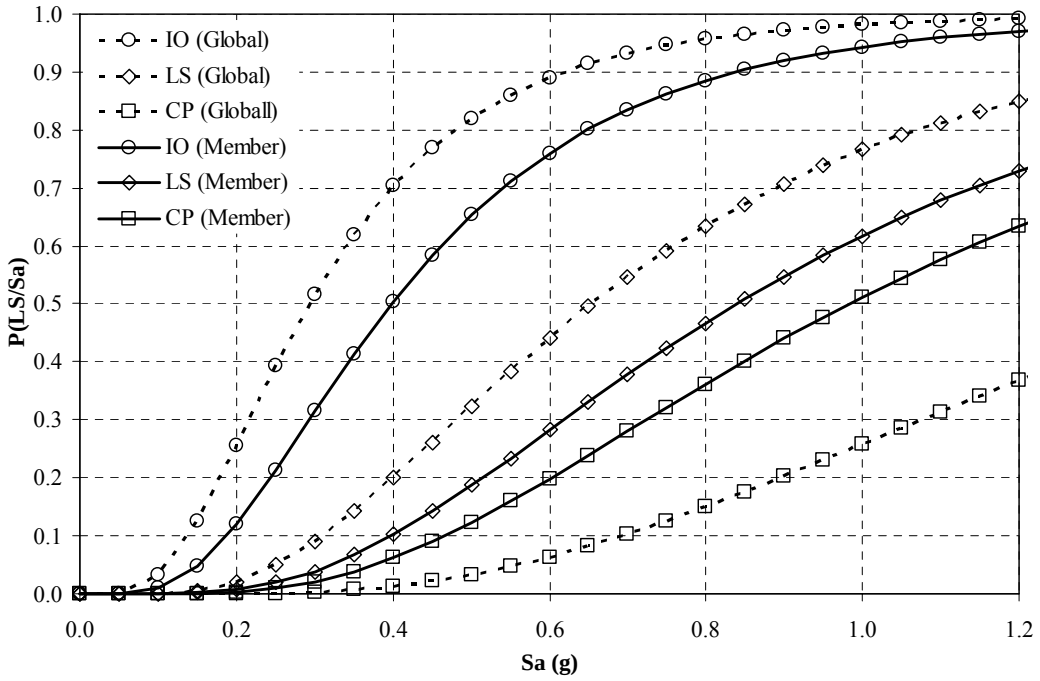

(b) Critical response push-over analysis

Fig. 6.18. Fragility curves for Retrofit 1 based on FEMA member-level limits

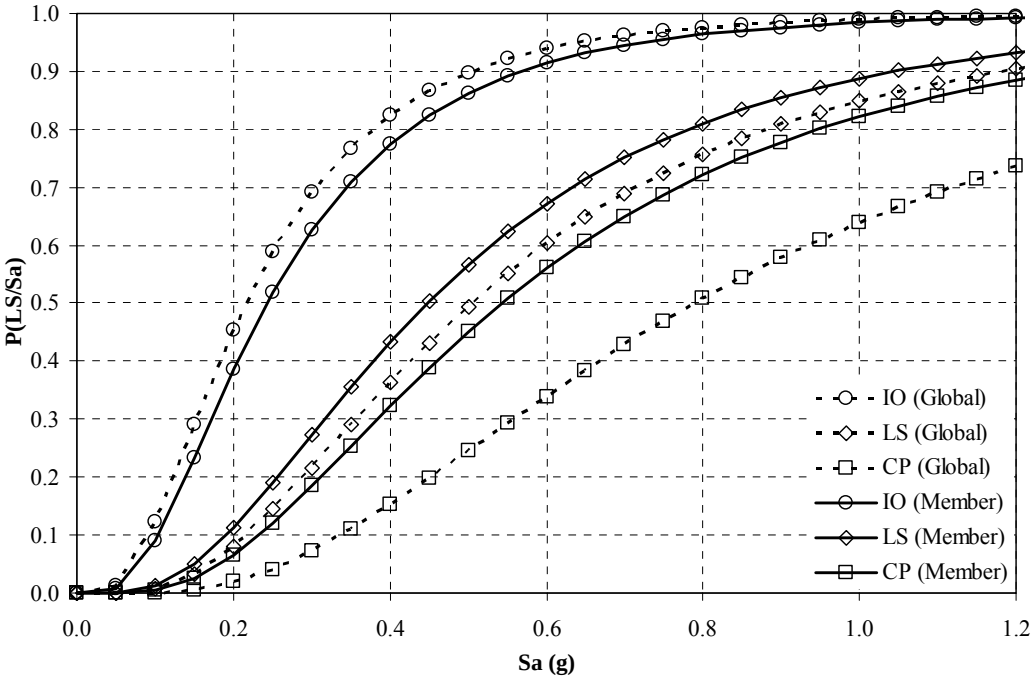

(a) Regular push-over analysis

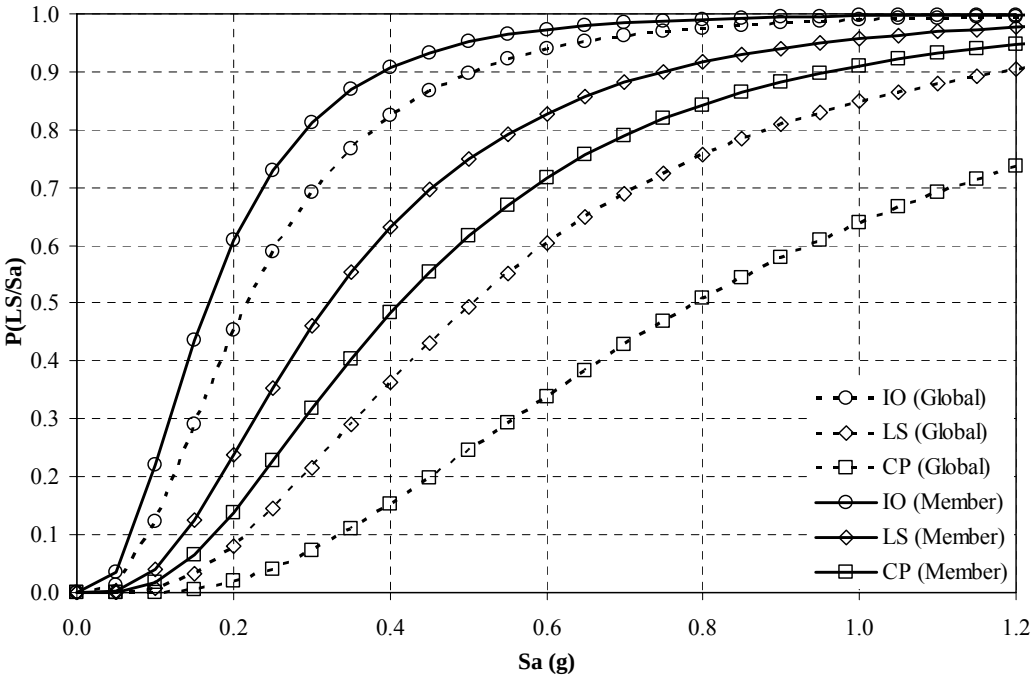

(b) Critical response push-over analysis

Fig. 6.19. Fragility curves for Retrofit 2 based on FEMA member-level limits

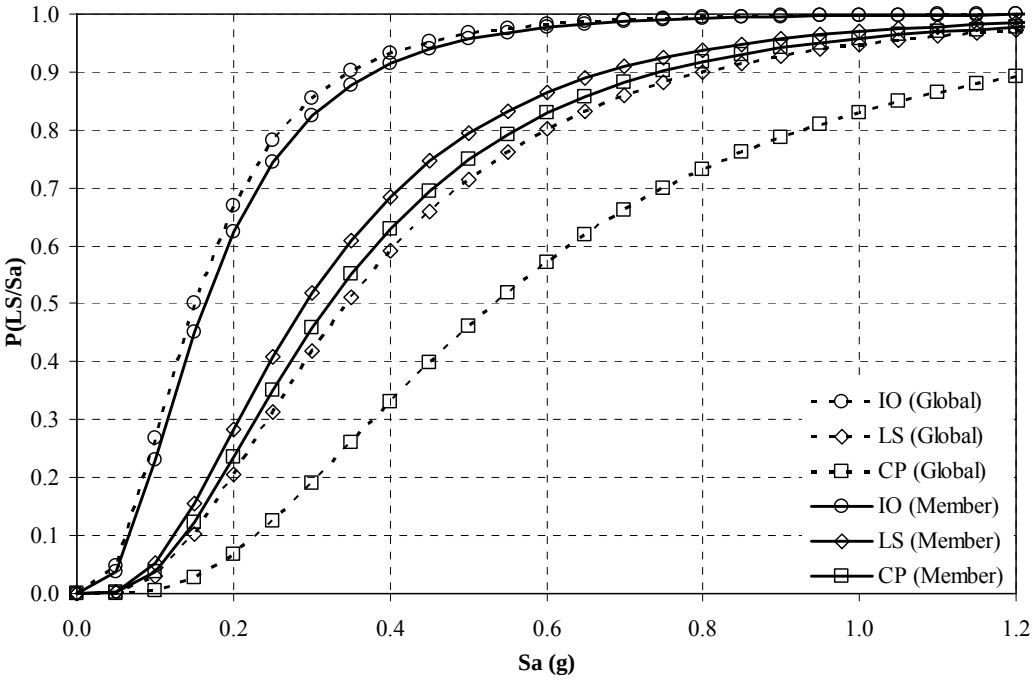

(a) Regular push-over analysis

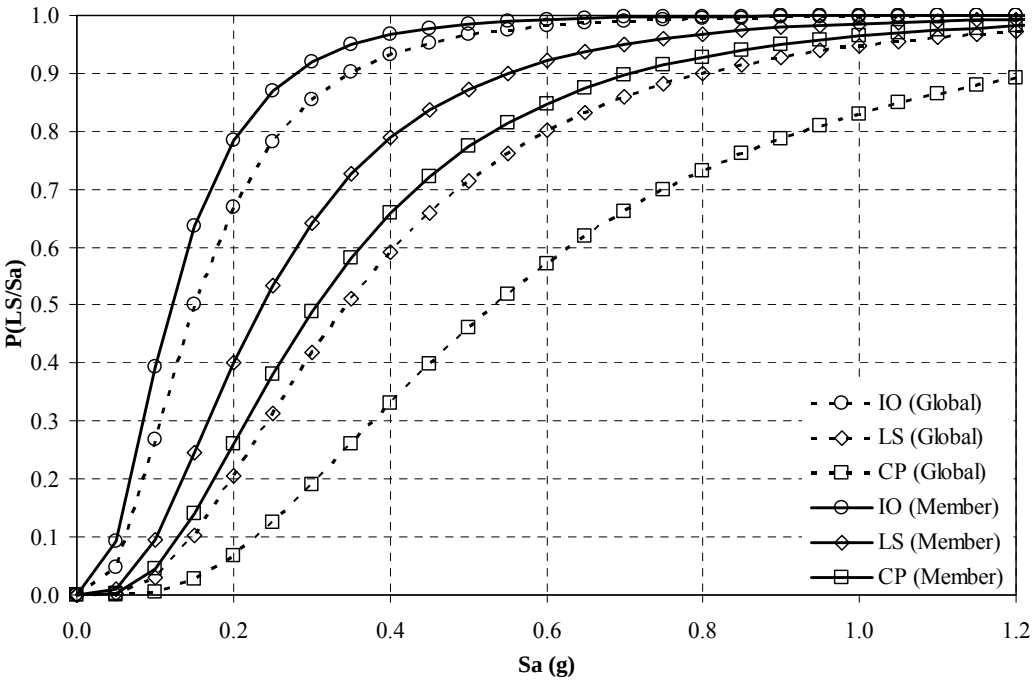

(b) Critical response push-over analysis

Fig. 6.20. Fragility curves for Retrofit 3 based on FEMA member-level limits

Table 6.16 summarizes the probability of exceeding CP limit state corresponding to a spectral acceleration value for FEMA member-level criteria with a critical response push-over analysis. As shown, the probabilities of exceeding CP limit state for each retrofitted structure were significantly reduced.

Table 6.16. Probability of exceeding CP limit state with a critical response push-over analysis

Structure	Spectral acceleration (S_a)						
	0.0	0.2	0.4	0.6	0.8	1.0	1.2
Unretrofitted	0	0.884	0.987	0.998	0.999	1	1
Retrofit 1	0	0.004	0.068	0.216	0.388	0.541	0.663
Retrofit 2	0	0.156	0.526	0.756	0.873	0.932	0.962
Retrofit 3	0	0.300	0.696	0.869	0.940	0.970	0.985

Fig. 6.21 shows the fragility curves for each limit state based on FEMA 356 member-level criteria with a critical response push-over analysis. As shown in Fig. 6.21, the probabilities of exceeding each limit state for each retrofitted structure were reduced.

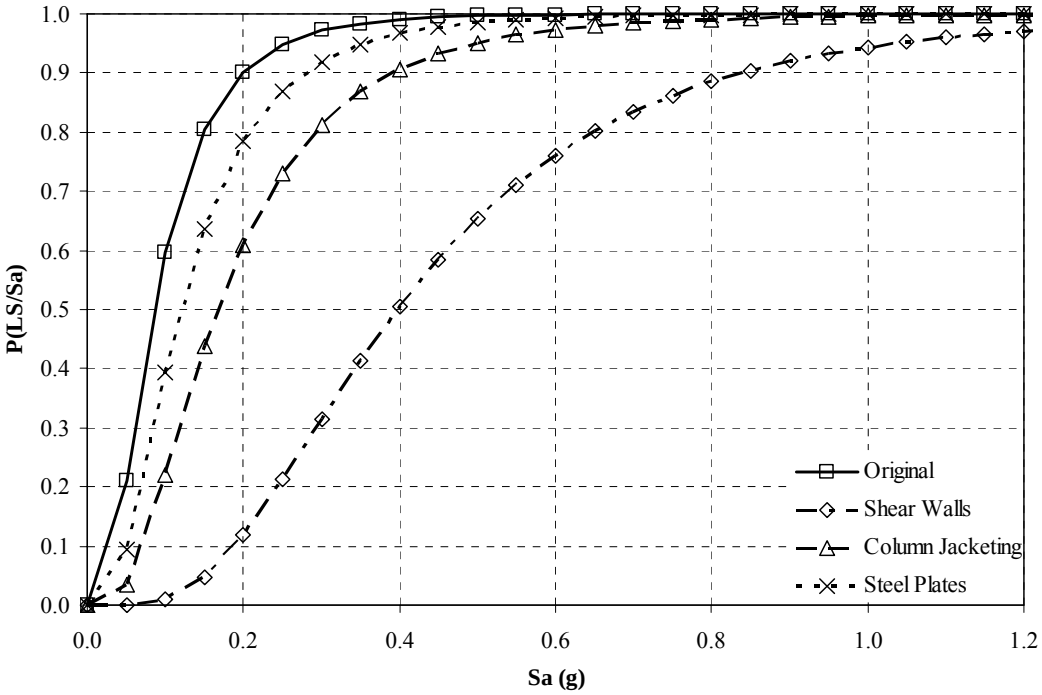

(a) IO

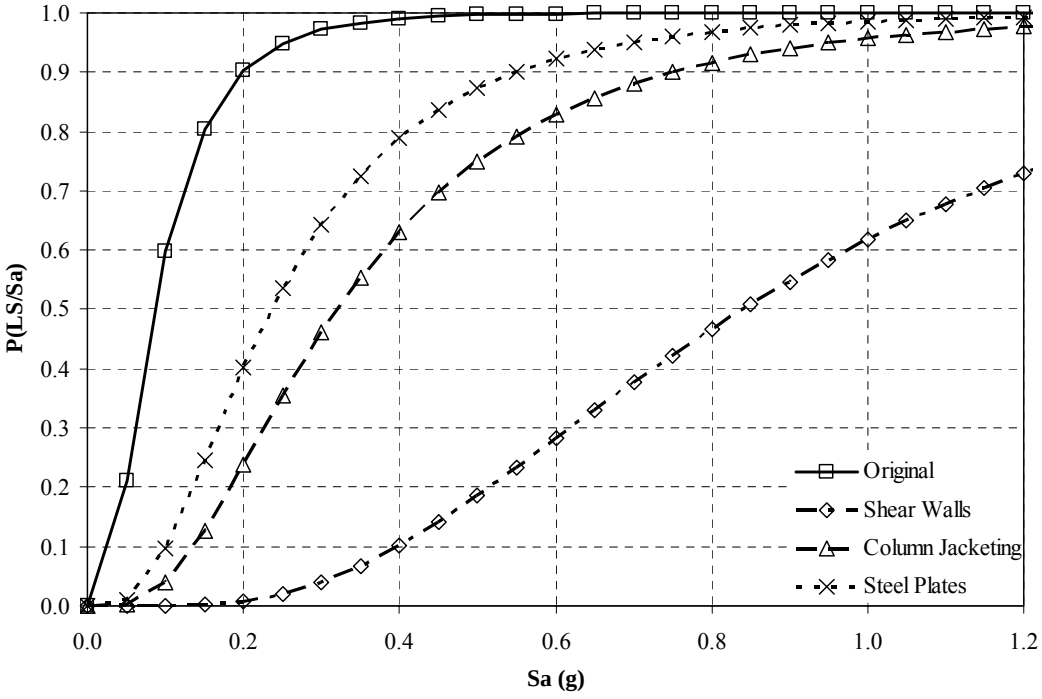

(b) LS

Fig. 6.21. Comparisons of FEMA member-level fragility curves

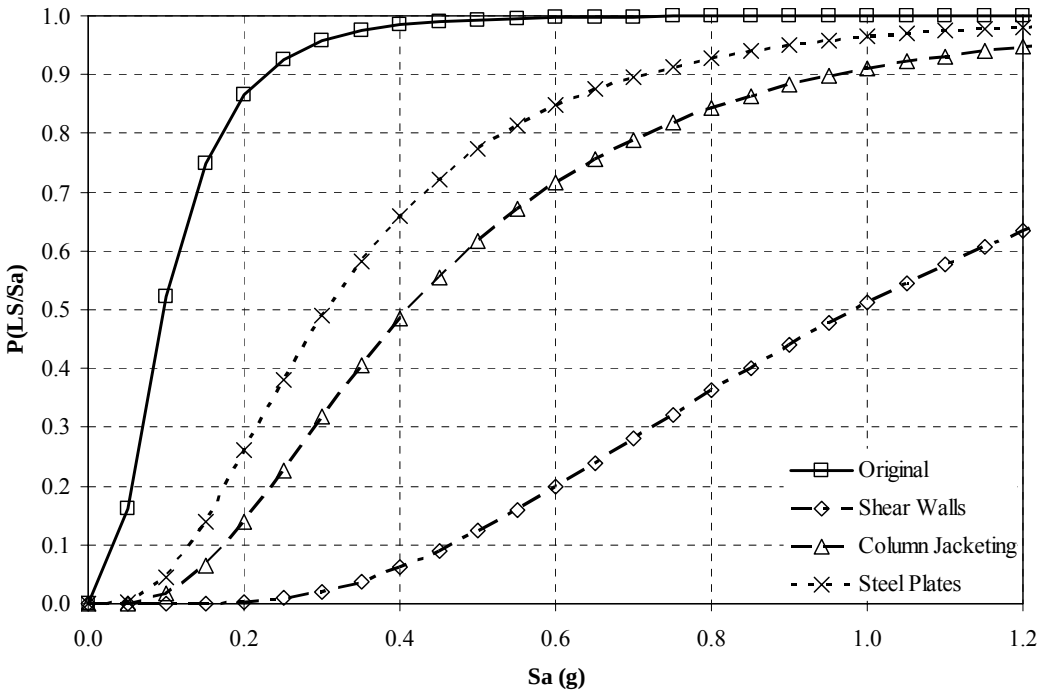

(c) CP

Fig. 6.21. Continued

6.6.3 Additional Quantitative Limits

The drift limits based on the quantitative limits described in Sec. 5.4.3.4 are provided in Table 6.17 for each retrofitted structure. For the case of the addition of shear walls, PMI limit state was obtained at the interior frame because there was no plastic mechanism occurred at the exterior frame.

Table 6.17. Interstory drift (%) limits based on additional quantitative limits

Structure	Regular push-over			Critical response push-over		
	FY	PMI	SD	FY	PMI	SD
Unretrofitted	0.66	0.81	·	0.36	0.66	2.81
Retrofit 1	0.93	2.66*	·	0.90	3.65*	·
Retrofit 2	0.75	1.71		0.64	1.38	
Retrofit 3	0.78	1.01	·	0.55	0.79	·

* PMI at the interior frame

Because the first and second story of the unretrofitted structure were most vulnerable, drift limits were provided at those stories. For the retrofitted structure, the seismic capacity of lower stories was increased. Therefore, the drift limits for a critical story mechanism were increased due to the applied retrofit techniques. In this case, SD limit state was not detected because strength did not fall to 20% of the maximum strength. Figs. 6.22 to 6.24 show the push-over curves of the weak story using these two limit states definition for each retrofitted structure.

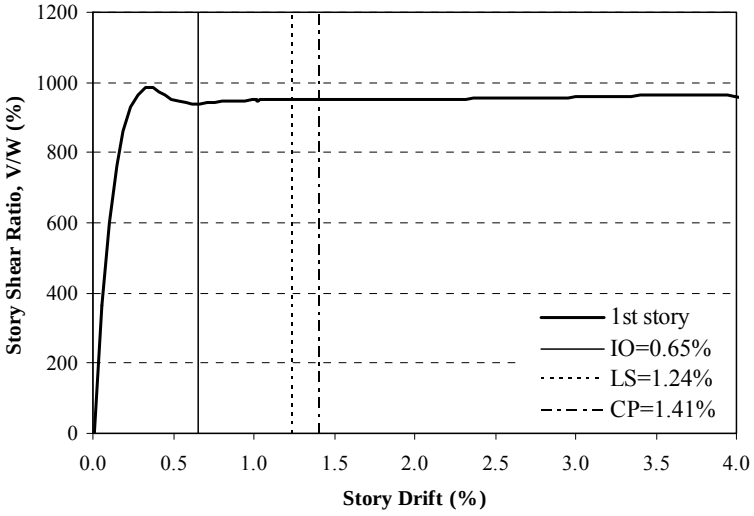

(a) FEMA limits based on member-level criteria (1st story)

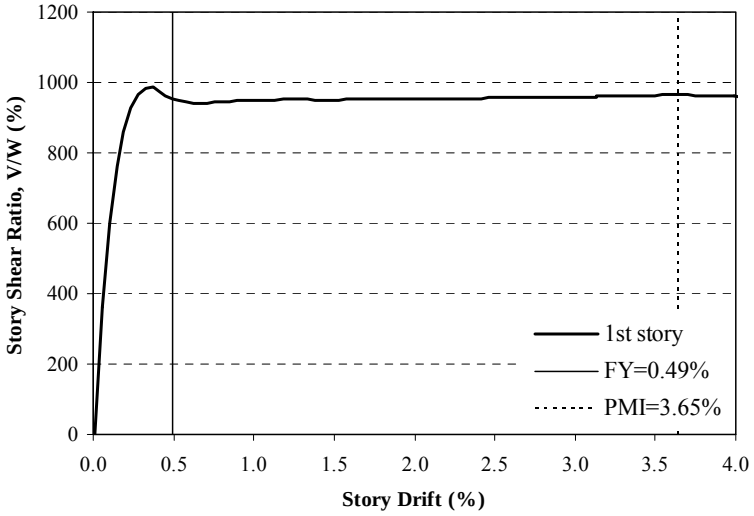

(b) Drift limits for quantitative limit states (1st story)

Fig. 6.22. Push-over curve for Retrofit 1 with critical response push-over analysis

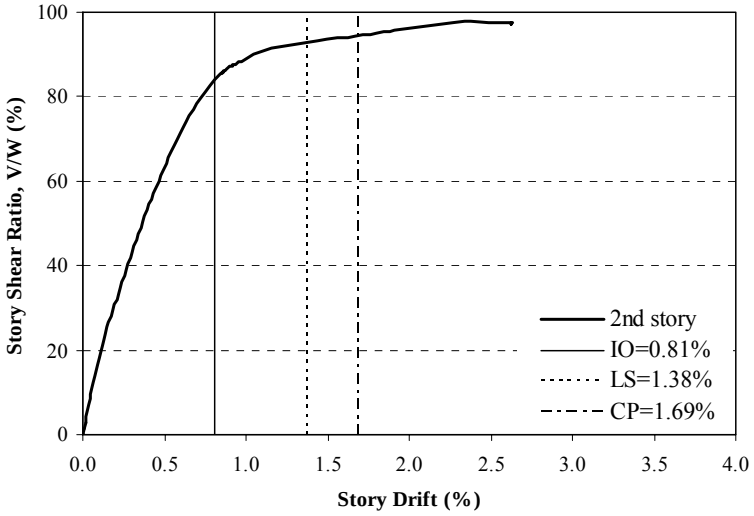

(a) FEMA limits based on member-level criteria (2nd story)

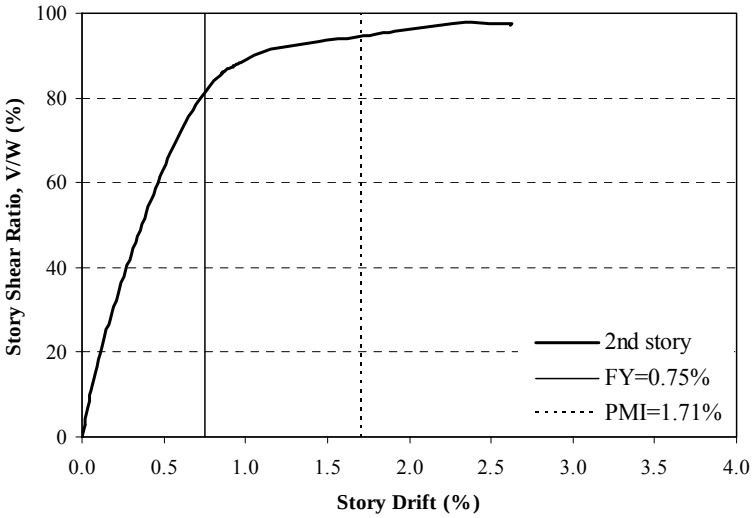

(b) Drift limits for quantitative limit states (2nd story)

Fig. 6.23. Push-over curve for Retrofit 2 with critical response push-over analysis

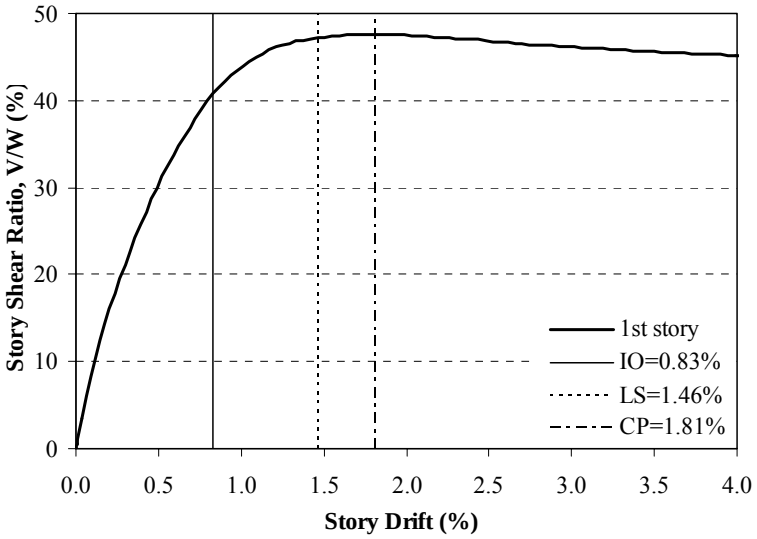

(a) FEMA limits based on member-level criteria (1st story)

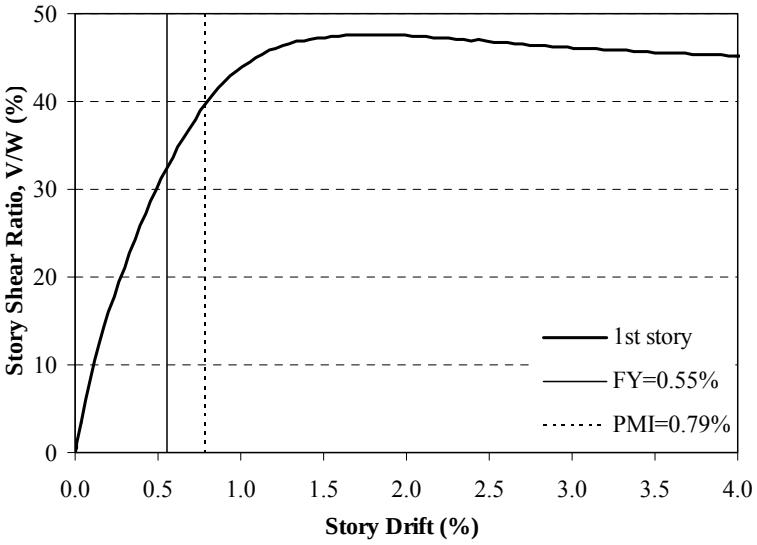

(b) Drift limits for quantitative limit states (1st story)

Fig. 6.24. Push-over curve for Retrofit 3 with critical response push-over analysis

Figs. 6.25 to 6.27 show the fragility curves using these two limit states with the critical response push-over analysis. For comparison, the fragility curves using the global drift limits for each case are also represented on each graph with dotted lines.

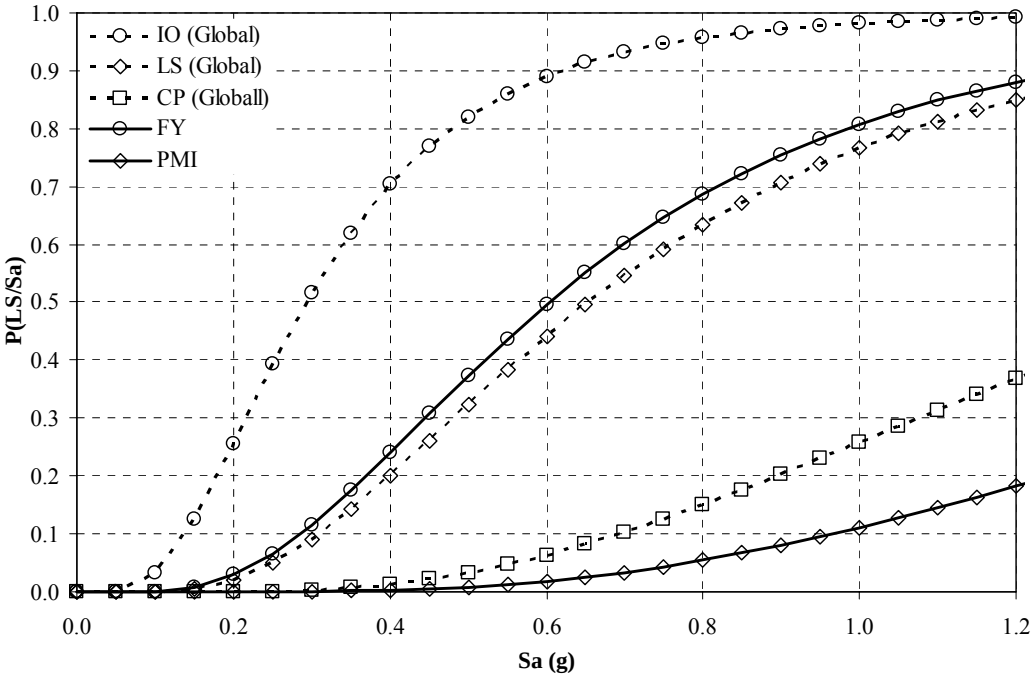

(a) Regular push-over analysis

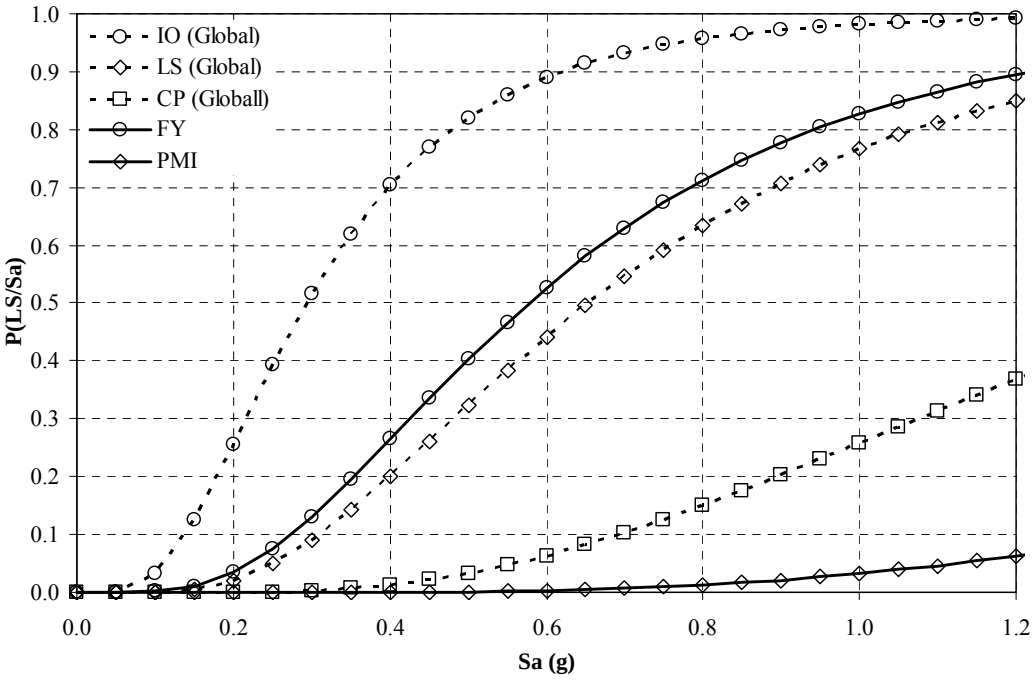

(b) Critical response push-over analysis

Fig. 6.25. Fragility curves for Retrofit 1 based on additional quantitative limits

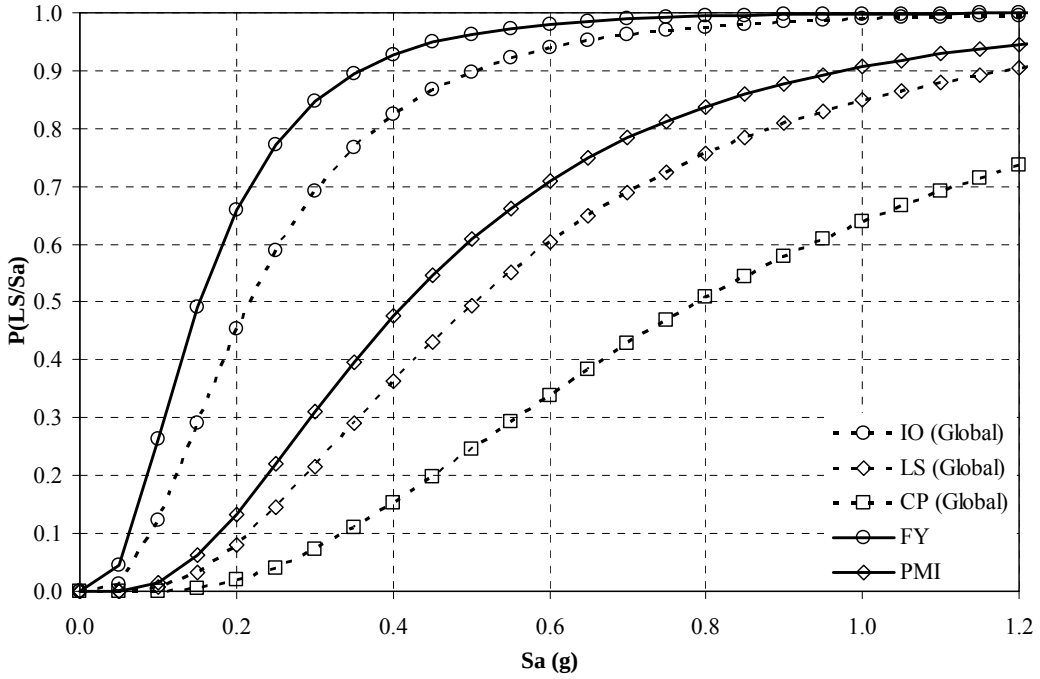

(a) Regular push-over analysis

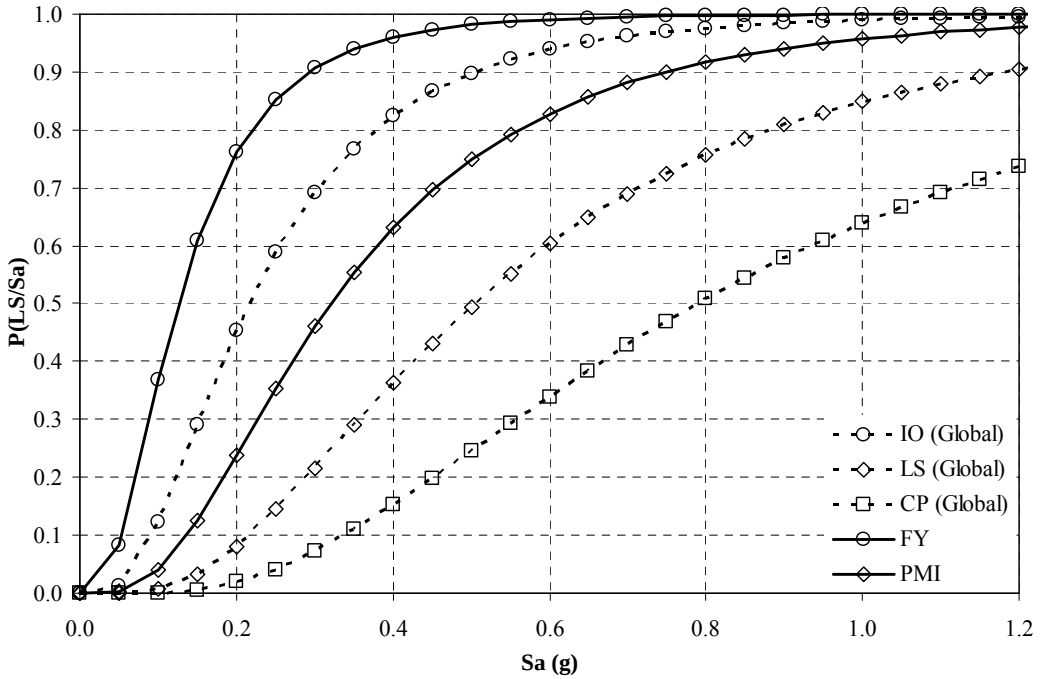

(b) Critical response push-over analysis

Fig. 6.26. Fragility curves for Retrofit 2 based on additional quantitative limits

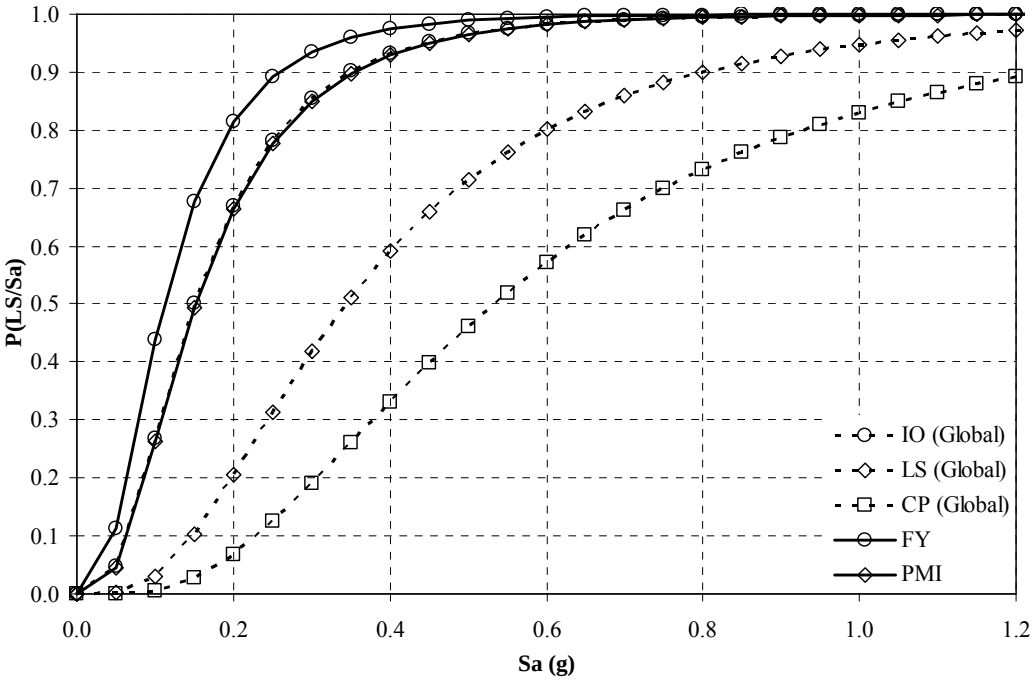

(a) Regular push-over analysis

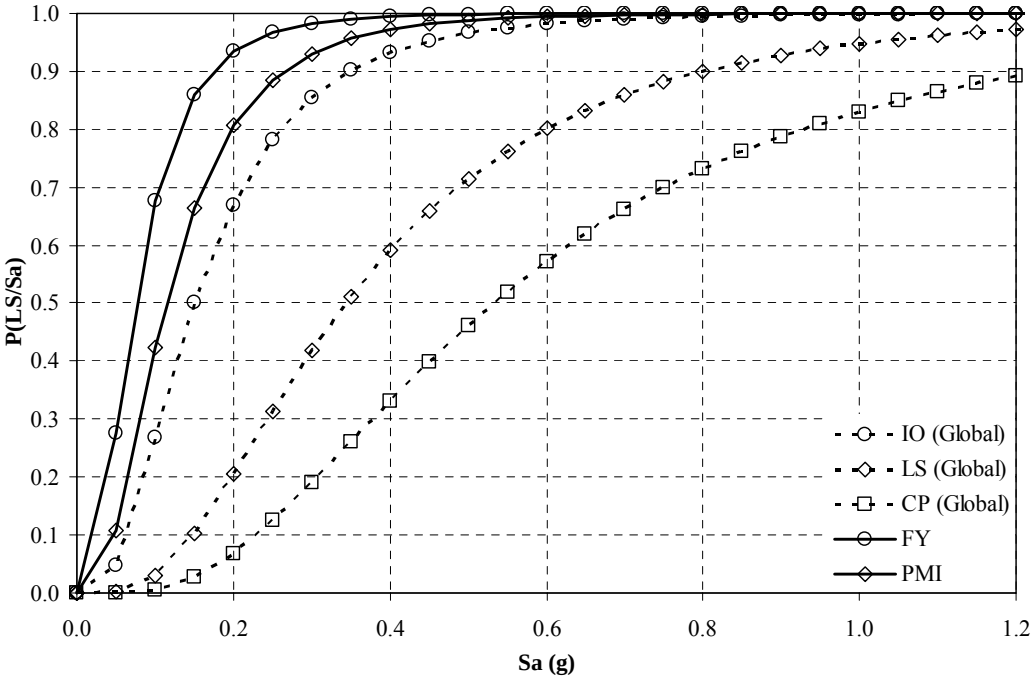

(b) Critical response push-over analysis

Fig. 6.27. Fragility curves for Retrofit 3 based on additional quantitative limits

Table 6.18 summarizes the probability of exceeding PMI limit state corresponding to a spectral acceleration value for additional quantitative limits with a critical response push-over analysis.

Table 6.18. Probability of exceeding PMI limit state with a critical response push-over analysis

Structure	Spectral acceleration (S_a)						
	0.0	0.2	0.4	0.6	0.8	1.0	1.2
Unretrofitted	0	0.901	0.990	0.998	1	1	1
Retrofit 1	0	0	0	0.004	0.014	0.036	0.069
Retrofit 2	0	0.266	0.674	0.860	0.937	0.969	0.984
Retrofit 3	0	0.831	0.977	0.995	0.999	1	1

Fig. 6.28 shows the fragility curves for each limit state based on additional quantitative limits with a critical response push-over analysis. As shown in Fig. 6.28, the probabilities of exceeding each limit state for the addition of shear walls and RC column jackets were reduced while those for the confinement of column plastic hinge zones were the same with the unretrofitted structure.

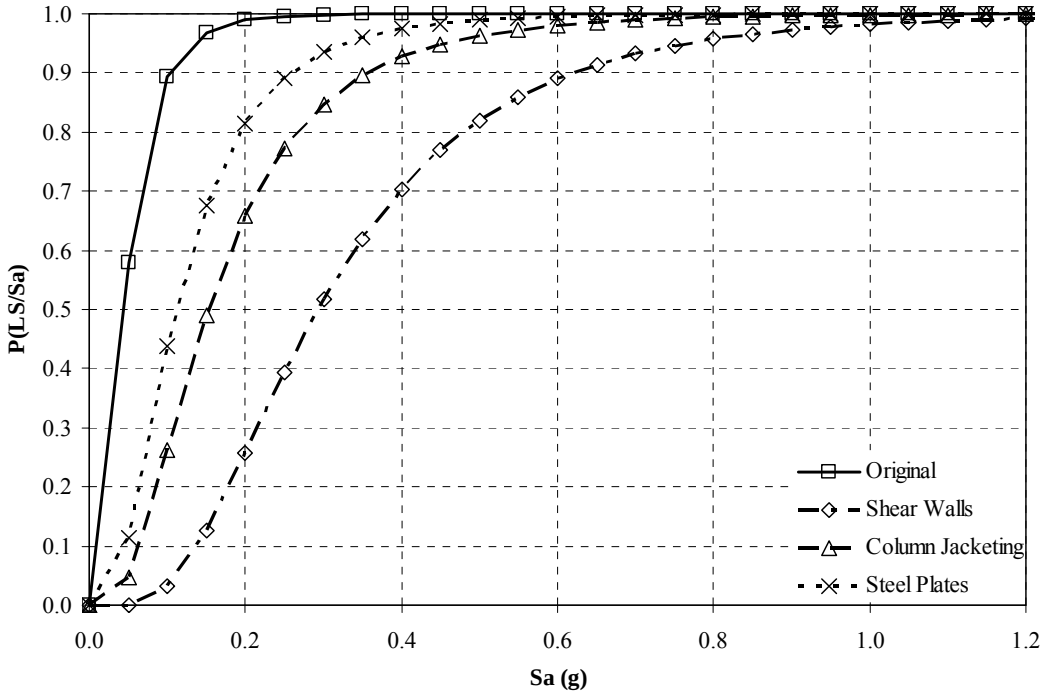

(a) FY

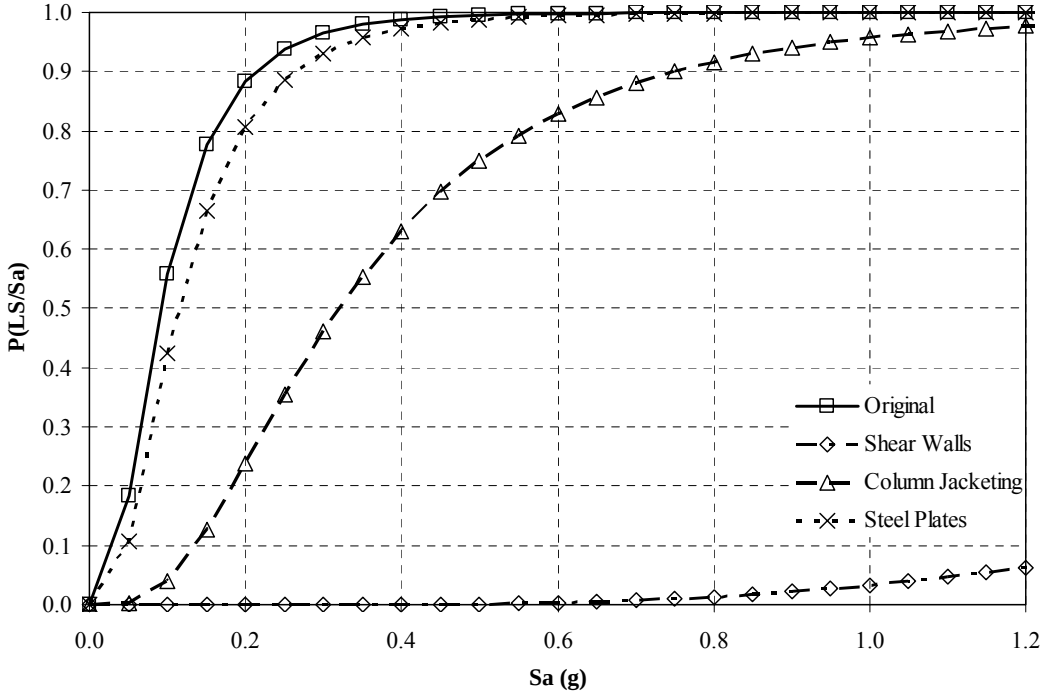

(b) PMI

Fig. 6.28. Comparisons of quantitative limits fragility curves for each limit state

6.7 Summary

In this section, the analysis of the retrofitted case study building was described and compared with that of the unretrofitted structure. Based on the analytical results, fragility curves for the retrofitted structure were developed using the FEMA 356 performance criteria and additional limit states. The fragility curves developed based on FEMA global-level drift limits and member-level plastic rotation limits were compared with those for the unretrofitted structure. In addition to this, additional quantitative limit states, described by Wen et al. (2003), were determined and compared to the limits based on the FEMA 356 criteria.

7 SUMMARY, CONCLUSIONS AND RECOMMENDATIONS

7.1 Summary

Through structural analyses, the seismic performance of a reinforced concrete (RC) flat-slab building structure was evaluated and three retrofit techniques were selected and applied to the structure. In addition, the effectiveness of the applied retrofit techniques was assessed through the development of probabilistic fragility curves. The case study building was designed to be representative of those constructed in St. Louis, Missouri and Memphis, Tennessee in the mid-1980s. This building was designed according to the load requirements in the ninth edition of the *Building Officials and Code Administrators (BOCA) Basic/National Code* (BOCA 1984). The design of structural components was carried out according to the provisions of the *American Concrete Institute (ACI) Building Code Requirements for Reinforced Concrete, ACI 318-83* (ACI Comm. 318 1983). The case study building is a five-story RC flat-slab building and an overall height of 20.4 m (67 ft.) with a perimeter moment resisting frame.

Because there is not adequate recorded strong motion to characterize the seismicity for specific locations in the Mid-America region, synthetic ground motions developed by Wen and Wu (2000) for St. Louis, Missouri and Memphis, Tennessee were used for dynamic time history analysis. Two different approaches for modeling and analyzing the case study building were evaluated: a fiber model using the ZEUS-NL program and a macro-model using the DRAIN-2DM program. In addition, two structural analysis methods, nonlinear static analysis and nonlinear dynamic analysis, were used to predict the seismic behavior of the building under lateral demands. Based on a comparison of results from two structural nonlinear analysis programs (ZEUS-NL and DRAIN-2DM), the ZEUS-NL program was selected for additional analytical studies to evaluate the expected seismic performance of the structure for the St. Louis and Memphis synthetic ground motions.

Based on the analytical results, seismic evaluations were conducted using FEMA 356 performance criteria. FEMA 356 suggests two approaches for seismic evaluation: global-level and member-level with acceptance criteria provided for three performance levels (Immediate Occupancy, Life Safety and Collapse Prevention). For the global-level evaluation, the maximum interstory drifts for each story were determined based on the results of nonlinear dynamic analysis. According to FEMA 356, the Basic Safety Objective (BSO) is defined as LS performance for the Basic Safety Earthquake 1 (BSE-1) earthquake hazard level and CP performance for the BSE-2 earthquake hazard level. BSE-1 is defined as the smaller of an event corresponding to 10% probability of exceedance in 50 years (10% in 50 years) and 2/3 of BSE-2, which is the 2% probability of exceedance in 50 years (2% in 50 years) event.

According to the FEMA 356 global-level (drift) criteria, the structure met the BSO recommended by FEMA 356 for both the 10% and 2% probabilities of exceedance in 50 years ground motions for St. Louis and Memphis. However, for the member-level evaluation which used plastic rotation limits for each member, a number of structural components including beams, columns and slabs did not satisfy the FEMA 356 BSO of Collapse Prevention (CP) for the 2% probability of exceedance in 50 years Memphis motions.

Based on the seismic evaluation results, three seismic retrofit techniques were applied to enhance the seismic performance of the structure: addition of shear walls, addition of RC column jackets, and confinement of the column plastic hinge regions using externally bonded steel plates. The retrofits were selected to impact the major structural response parameters: stiffness, strength and ductility. The shear walls were added to the two central bays of the exterior frame, loading to an increase in the global stiffness and strength of the structure. Column jacketing was applied to the columns that did not satisfy with FEMA 356 member-level (plastic hinge) limits and increased the strength and stiffness of the structure. The addition of external steel plates confined the

plastic hinge zones at the ends of vulnerable columns to increase ductility. Nonlinear static and dynamic analyses were performed to predict the seismic behavior of the retrofitted structure. Based on the analytical results, a seismic evaluation was conducted.

Finally, fragility curves were developed for the both retrofitted and unretrofitted structures. The fragility curves developed based on FEMA global-level drift limits and member-level plastic rotation limits were compared. In addition to this, additional quantitative limit states, suggested by Wen et al. (2003), were determined and compared to the limits based on the FEMA 356 criteria. These included first yield (FY), plastic mechanism initiation (PMI) and strength degradation (SD). The drift limits corresponding to the FEMA 356 member-level criteria and additional quantitative limits were determined from traditional push-over analysis and a critical response (story-by-story) push-over analysis suggested by Dooley and Bracci (2001).

7.2 Conclusions

The following conclusions were made based on the results of this study:

1. The comparison of analytical results from nonlinear analysis using ZEUS-NL (fiber model) and DRAIN-2DM (macro model) showed good agreement, especially at lower load magnitudes. However, for nonlinear static analysis, ZEUS-NL provided more reasonable results to predict the inelastic behavior of the structure including P-delta effects. For nonlinear dynamic analysis, the maximum building drift and maximum base shear were similar for the two analysis programs.

2. A comparison between nonlinear static (push-over) and nonlinear dynamic analysis gave good agreement of global response. In particular, for lower amplitudes of motion, the global responses were relatively similar.

3. For seismic evaluation using the FEMA 356 criteria, it was found that the predicted response of the case study building for the St. Louis motions was within the BSO limits. For the Memphis motions, different outcomes occurred when the global-level performance criteria were used versus the member-level criteria. Based on the global-level criteria, the BSO was satisfied for both the 10% in 50 years and 2% in 50 years events. However, for the member-level criteria, a number of members did not meet the BSO of CP for the 2% in 50 years event.

4. Three retrofit techniques were applied to the case study building to impact the major structural response parameters. For all retrofits, the seismic performance of the structure was enhanced based on the analytical results from both the nonlinear static and nonlinear dynamic analyses.

5. Fragility curves using the FEMA global-level criteria were developed for both the unretrofitted and retrofitted case study buildings. Addition of shear walls and RC column jackets reduced the probability of exceeding each limit state. However, for the case of the structure retrofitted by confining with steel plates, the global-level fragility curves were almost same as those for the unretrofitted structure.

6. The drift limits based on member-level criteria were determined with two different definitions of limit states using push-over analysis. As a result, drift limits based on FEMA 356 member-level (plastic rotation) criteria did not match well with the FEMA 356 global-level (drift) limits. This is because limits for structures depend on many structural characteristics, such as details of reinforcement and level of confinement (ductility).

7. The formation of story mechanisms was also considered to determine the most critical limit state values. This procedure provided the most vulnerable cases of failure and drift limits for each story.

7.3 Recommendations for Future Research

The work in this thesis has been limited to a five-story reinforced concrete flat-slab structural frame system. Hence, the structural fragility curves are not generic to this type of structural system because many structural configurations are possible. Some of the future research needs related to seismic fragility and retrofitting are listed below:

1. This study could be extended to other types of structures, including steel, masonry, composite and other concrete structures to develop fragility curves. In addition to this, further research to verify performance criteria for limit states would be beneficial. For instance, additional experimental and analytical studies to match the limit states with actual damage data for developing more general fragility curves are encouraged.

2. It would be useful to consider the performance of nonstructural members when the limit states are defined.

3. An assessment model that evaluates not only the structural performance but also economic or social impacts of damage would be useful. Then vulnerability functions associated with a specified economic or social impact should be developed.

4. More specific derivation of fragility curves corresponding to each retrofit scheme would be useful. For instance, the optimal values of design parameters for a

specific retrofitting method would influence the effectiveness of the retrofit techniques.

REFERENCES

Abrams, D.P., Elnashai, A.S. and Beavers, J.E. (2002), "A New Engineering Paradigm: Consequence-Based Engineering," Linbeck Lecture Series in Earthquake Engineering: Challenges of the New Millennium, University of Notre Dame's Linbeck Distinguished Lecture Series, Notre Dame, IN.

Aycardi, L.E., Mander, J.B. and Reinhorn, A.M. (1994), "Seismic Resistance of Reinforced Concrete Frame Subasseblages," *ACI Structural Journal*, 91, (5), 559-560.

ACI Committee 318 (1983), *Building Code Requirements for Reinforced Concrete* (ACI 318-83), American Concrete Institute, Detroit, MI.

ACI Committee 318 (2002), *Building Code Requirements for Reinforced Concrete* (ACI 318-02), American Concrete Institute, Farmington, MI.

AISC (2001), *Manual of Steel Construction: Load and Resistance Factor Design* (3rd edition), American Institute of Steel Construction, Chicago, IL.

Al-Haddad, M.S. and J.K. Wight (1986). "Feasibility and consequences of moving beam plastic hinging zones for earthquake resistant design of R/C buildings," *Report No. UMCE 86-1*, Department of Civil Engineering, University of Michigan, Ann Arbor, MI.

Altin, S., Ersoy, U. and Tankut, T. (1992), "Hysteretic Response of Reinforced-Concrete Infilled Frames," *Journal of Structural Engineering*, 118, (8), 2133-2150.

ASCE (2000), *Prestandard and Commentary for the Seismic Rehabilitation of Buildings (FEMA 356)*, prepared by American Society of Civil Engineers for the Federal Emergency Management Agency, Washington, D.C.

ATC (1996), *Seismic Evaluation and Retrofit of Concrete Buildings (ATC-40)*, prepared by Applied Technology Council, Redwood City, CA.

Badoux, M. and Jirsa, J.O. (1990), "Steel Bracing of RC Frame for Seismic Retrofitting," *Journal of Structural Engineering*, 116, (1), 55-74.

BOCA (1984), *Building Officials and Code Administrators (BOCA) Basic/National Code/1984*, Building Officials and Code Administrators International, Inc., Country Club Hills, IL.

Bracci, J.M., Reinhorn, A.M. and Mander, J.B. (1995), "Seismic Retrofit of RC Frame Buildings Designed for Gravity Loads: Performance of Structural Model," *ACI Structural Journal*, 92, (6), 771-723.

Bush, T.D., Jones, E.A. and Jirsa, J.O. (1991), "Behavior of RC Frame Strengthened Using Structural Steel Bracing," *Journal of Structural Engineering*, 117, (4), 1115-1126.

Constantinou, M.C., Kartoum, A. and Kelly, J.M. (1992), "Analysis of Compression of Hollow Circular Elastomeric Bearings," *Engineering Structures*, 14, (2), 103-111.

Dooley, K.L. and Bracci, J.M. (2001), "Seismic Evaluation of Column-to-Beam Strength Ratios in Reinforced Concrete Frames," *ACI Structural Journal*, 98, (6), 843-851.

Dumova-Jovanoska E. (2000), "Fragility Curves for Reinforced Concrete Structures in Skopje (Macedonia) Region," *Soil Dynamics and Earthquake Engineering*, 19, 455-466.

Elnashai, A.S., Papanikolaou, V. and Lee, D.H. (2002), "ZEUS-NL User Manual," University of Illinois at Urbana-Champaign / Mid-America Earthquake Center.

Elnashai, A.S. and Pinho, R. (1998), "Repair and Retrofitting of RC Walls Using Selective Techniques," *Journal of Earthquake Engineering*, 2, (4), 525-568.

Elnashai, A.S., Pinho, R. and Antoniou (2000), "INDYAS – A Program for Inelastic Dynamic Analysis of Structures," *Research Report ESEE/00-2,* Engineering Seismology and Earthquake Engineering Section, Imperial College, London.

Elnashai, A.S. and Salama, A.I. (1992), "Selective Repair and Retrofitting Techniques for RC Structures in Seismic Regions," *Research Report ESEE/92-2,* Engineering Seismology and Earthquake Engineering Section, Imperial College, London.

Farhey, D.N., Adin, M.A. and Yankelevsky, D.Z. (1993), "Repair of RC Column-Flat Slab Joints," *Proc., 17th Regional European Seminar on Earthquake Engineering,* Haifa, Israel, 459-469.

FEMA (1997a), *NEHRP Guidelines for the Seismic Rehabilitation of Buildings (FEMA 273)*, prepared by the Building Seismic Safety Council for the Federal Emergency Management Agency, Washington, D.C.

FEMA (1997b), *NEHRP Commentary on the Guidelines for Seismic Rehabilitation of Buildings (FEMA 274)*, prepared by the Building Seismic Safety Council for the Federal Emergency Management Agency, Washington, D.C.

Fu, Y. (1996), "Frame Retrofit by Using Viscous and Viscoelastic Dampers," *Proc., 11th World Conference on Earthquake Engineering*, Acapulco, Mexico (CD-Rom).

Gates, W.E., Hart, G.C., and Crouse, C.B. (1990), "Vibration Studies of an Existing Building for Base Isolation Retrofit," *Proc., 4th U.S. National Conference on Earthquake Engineering,* Palm Springs, CA, 3, 559-568.

Goel, S.C. and Masri, A.C. (1996), "Seismic Strengthening of an RC Slab-Column Frames with Ductile Steel Bracing," *Proc., 11th World Conference on Earthquake Engineering*, Acapulco, Mexico (CD-Rom).

Gulkan, P. and Sozen, M.A. (1999), "Procedure for Determining Seismic Vulnerability of Building Structures," *ACI Structural Journal*, 96, (3), 336-342.

Harries, K., Ricles, J., Sause, R., Pessiki, S. and Walkup, L. (1998), "Seismic Retrofit of Non-Ductile Reinforced Concrete Building Columns Using FRPC Jackets," *Proc., 6th U.S. National Conference on Earthquake Engineering,* Seattle, WA (CD-Rom).

Hart, J.F. (2000), "Analysis of a Typical Midwestern Structure Subjected to Seismic Loads," University Undergraduate Research Fellow Program Senior Honor Thesis, Department of Civil Engineering, Texas A&M University, College Station, TX.

Hassan, A.F. and Sozen, M.A. (1997), "Seismic Vulnerability Assessment of Low-Rise Buildings in Regions with Infrequent Earthquakes," *ACI Structural Journal*, 94, (1), 31-39.

Hueste, M.B.D. and Wight, J.K. (1997), "Evaluation of a Four-Story Reinforced Concrete Building Damaged During the Northridge Earthquake," *Earthquake Spectra*, 13, (3), 387-414.

Hueste, M.B.D. and Wight, J.K. (1999), "Nonlinear Punching Shear Failure Model for Interior Slab-column Connections," *Journal of Structural Engineering*, 125, (9), 997-1008.

Hwang, H.M. and Huo, J.-R. (1994), "Generation of Hazard-Consistent Fragility Curves for Seismic Loss Estimation Studies," *Technical Report NCEER-94-0015*, National Center for Earthquake Engineering Research, State University of New York at Buffalo, Buffalo, NY.

Hwang, H.M. and Huo, J.-R. (1996), "Simulation of Earthquake Acceleration Time Histories," *Technical Report*, Center for Earthquake Research and Information, University of Memphis, Memphis, TN.

IES (1998), Visual Analysis V3.5, Integrated Engineering Software, Inc., Bozeman, MT.

Inukai, M. and Kaminosono, T. (2000), "Seismic Performance of an existing RC frame retrofitted by Precast Prestressed Concrete Shear Walls," *Proc., 12th World Conference on Earthquake Engineering*, Auckland, New Zealand (CD-Rom) .

Jirsa, J.O. and Kreger, M. (1989), "Recent Research on Repair and Strengthening of Reinforced Concrete Structures," *Proceedings, ASCE Structures Congress*, San Francisco, CA, 1, 679-688.

Kannan, A.E. and Powell, G.H. (1973), "A General Purpose Computer Program for Dynamic Analysis of Inelastic Plane Structures," *Report No. EERC 73-6*, Earthquake Engineering Research Center, University of California, Berkeley, CA.

Kawamura, S., Sugisaki, R., Ogura, K., Maezawa, S., Tanaka, S., and Yajima, A. (2000), "Seismic Isolation Retrofit in Japan," *Proc., 12th World Conference on Earthquake Engineering*, Auckland, New Zealand (CD-Rom).

Krawinkler, H. (1999), "Challenges and Progress in Performance-Based Earthquake Engineering*," International Seminar on Seismic Engineering for Tomorrow – In Honor of Professor Hiroshi Akiyama*, Tokyo, Japan.

Kunisue, A., Koshika, N., Kurokawa Y., Sakamoto M., Suzuki N., and Tagami J. (2000), "Retrofitting Method of Existing Reinforced Concrete Buildings Using Elasto-Plastic Steel Dampers," *Proc., 12th World Conference on Earthquake Engineering*, Auckland, New Zealand (CD-Rom).

Lew, H.S. and Kunnath, S.K. (2002), "Assessment of Structural Systems Evaluation Methods Based on Local Seismic Demands," Innovations in Design with Emphasis on Seismic, Wind, and Environmental Loading; Quality Control and Innovations in Materials/Hot-Weather Concreting (SP-209), *ACI 5th International Conference*, Cancun, Mexico.

Lombard, J., Humar, J.L. and Cheung, M.S. (2000), "Seismic Strengthening and Repair of Reinforced Concrete Shear Walls," *Proc., 12th World Conference on Earthquake Engineering*, Auckland, New Zealand (CD-Rom).

Luo, Y. and Durrani, A.J. (1994), "Seismic Retrofit Strategy for Non-Ductile Flat-Plate Connections," *Proc., 5th U.S. National Conference on Earthquake Engineering,* Chicago, IL, 3, 627-636.

Mander, J.B., Priestley, M.J. and Park, R. (1988), "Theoretical Stress-Strain Model for Confined Concrete," *Journal of Structural Engineering*, 114, (8), 1804-1826.

Martinez-Cruzado, J.A., Qaisrani, A.-N., and Moehle, J.P. (1994), "Post-tensioned Flat-Plate Slab-Column Connections Subjected to Earthquake Loading," *Proc., 5th U.S. National Conference on Earthquake Engineering,* Chicago, IL, 2, 139-148.

McKeown, F.E. (1982), "Overview and discussion," Investigations of the New Madrid, Missouri, Earthquake Region, *USGS Professional Paper 1236*, 1-14, Washington, D.C.

Miranda, E. and Bertero, V.V. (1990), "Post-tensioning Techniques for Seismic Upgrading of Existing Low-Rise Buildings," *Proc., 4th U.S. National Conference on Earthquake Engineering,* Palm Springs, CA, 3, 393-402.

Moehle, J.P. (2000), "State of Research on Seismic Retrofit of Concrete Building Structures in the US," *US-Japan Symposium and Workshop on Seismic Retrofit of Concrete Structures,* Tokyo, Japan.

Munshi, J.A. (1998), "Energy Dissipation of Viscoelastically Damped Reinforced Concrete Systems," *Proc., 6th U.S. National Conference on Earthquake Engineering,* Seattle, WA (CD-Rom).

Nuttli, O.W. (1982), "Damaging Earthquakes of the Central Mississippi Valley," Investigations of the New Madrid, Missouri, Earthquake Region, *USGS Professional Paper 1236*, 15-20, Washington, D.C.

Park, Y.J., Ang, A.H.-S. and Wen, Y.K. (1985), "Seismic Damage Analysis of Reinforced Concrete Buildings," *Journal of Structural Engineering*, 111, (4), 740-757.

Paulay, T. and Priestley, M.J.N. (1992), *Seismic Design of Reinforced Concrete and Masonry Buildings*, Wiley, NY.

Pekcan, G., Mander, J.B., and Chen, S.S. (1995), "The Seismic Response of a 1:3 Scale Model R.C. Structure with Elastomeric Spring Dampers," *Earthquake Spectra*, 11, (2), 249-267.

Pincheira, J.A. (1992), "Seismic Strengthening of Reinforced Concrete Frames Using Post-Tensioned Bracing Systems," Ph.D. Dissertation, Department of Civil Engineering, University of Texas at Austin, Austin, TX.

Pincheira, J.A. and Jirsa, J.O. (1995), "Seismic Response of RC Frames Retrofitted with Steel Braces or Walls," *Journal of Structural Engineering*, 121, (8), 1225-1235.

Powell, G.H. (1973), "DRAIN-2D, User's Guide," *Report No. EERC 73-22*, Earthquake Engineering Research Center, University of California, Berkeley, CA.

Raffaelle, G.S. and J.K. Wight (1992), "R/C Eccentric Beam-Column Connections Subjected to Earthquake-Type Loading," *Report No. UMCEE 92-18*, Department of Civil Engineering, University of Michigan, Ann Arbor, MI.

Reinhorn, A.M., Barron-Corverra, R. and Ayala, A.G. (2002), "Global Spectral Evaluation of Seismic Fragility of Structures," *Proc., 7th U.S. National Conference on Earthquake Engineering,* Boston, MA (CD-Rom).

SEAOC (1995), *Vision 2000 a Framework for Performance-Based Engineering*, Structural Engineers Association of California, Sacramento, CA.

Shama, A.A., Mander, J.B. and Chen, S.S. (2002), "Seismic Investigation of Steel Pile Bents: II. Retrofit and Vulnerability Analysis," *Earthquake Spectra*, 18, (1), 143-160.

Shedlock, K.M. and Johnston, A.C. (1994), "Introduction – Investigation of the New Madrid Seismic Zone," Investigations of the New Madrid, Missouri, Earthquake Region, *USGS Professional Paper 1538*, pp. A1-A5, Washington, D.C.

Shinozuka, M., Feng, M.Q., Lee, J. and Naganuma, T. (2000a), "Statistical Analysis of Fragility Curves," *Journal of Engineering Mechanics*, 126, (12), 1224-1231.

Shinozuka, M., Feng, M.Q., Kim, H.-K. and Kim, S.-H. (2000b), "Nonlinear Static Procedure for Fragility Curve Development," *Journal of Engineering Mechanics*, 126, (12), 1287-1295.

Soubra, K.S., J.K. Wight and A.E. Naaman (1992), "Fiber reinforced concrete joints for precast construction in seismic areas," *Report No. UMCEE 92-2*, Department of Civil Engineering, University of Michigan, Ann Arbor, MI.

Tang, X. and Goel, S.C. (1988), "DRAIN-2DM technical notes and user's guide," *Research Report UMCE 88-1*, Department of Civil Engineering, University of Michigan, Ann Arbor, MI.

Tena-Colunga, A., Gomez-Soberon, C., and Munoz-Loustaunau, A. (1997), "Seismic Isolation of Buildings Subjected to Typical Subduction Earthquake Motions for the Mexican Pacific Coast," *Earthquake Spectra*, 13, (3), 505-532.

Teran-Gilmore, A., Bertero, V.V., and Youssef, N. (1995), "Seismic Rehabilitation of Framed Buildings Infilled with Unreinforced Masonry Walls Using Post-tensioned Steel Braces," *UCB/EERC-95/06*, Berkeley, Earthquake Engineering Research Center (EERC), University of California, Berkeley.

Thermou, G. and Elnashai, A.S. (2002), "Performance Parameters and Criteria for Assessment and Rehabilitation," Seismic Performance Evaluation and Retrofit of Structures (SPEAR), *European Earthquake Engineering Research Network Report*, Imperial College, UK.

Trifunac, M.D. and Brady, A.G. (1975), "A Study on the Duration of Strong Earthquake Ground Motion," *Bulletin of the Seismological Society of America*, 65, (3), 581-626.

Wen, Y.K., Ellingwood, B.R., Veneziano, D. and Bracci, J.M. (2003), "Uncertainty Modeling in Earthquake Engineering," *Mid-America Earthquake (MAE) Center Project FD-2 Report*, 12 Feb. 2003, Urbana, IL.

Wen, Y.K., Ellingwood, B.R. and Bracci, J.M. (2004), "Vulnerability Functions," *Mid-America Earthquake (MAE) Center Project DS-4 Report*, submitted for review, Feb. 2004, Urbana, IL.

Wen, Y.K. and Wu, C.L. (2000), "Generation of Ground Motions for Mid-America Cities," Mid-America Earthquake (MAE) Center, 27 Jan. 2000. http://mae.ce.uiuc.edu/newsite/research/rr-1/gmotions/index.html

Wen, Y.K. and Wu, C.L. (2001), "Uniform Hazard Ground Motions for Mid-America's Cities," *Earthquake Spectra*, 17, (2), 359-384.

Yang, G., Spencer Jr., B.F., Carlson, J.D. and Sain, M.K. (2002), "Large-Scale MR Fluid Dampers: Modeling and Dynamic Performance Considerations," *Engineering Structures*, 24, 309-323.

APPENDIX A DYNAMIC ANALYSIS RESULTS (DRIFT OF THE UNRETROFITTED CASE STUDY BUILDING)

As mentioned in Section 5.3.2, dynamic analysis results using ZEUS-NL for St. Louis, Missouri and Memphis, Tennessee are provided.

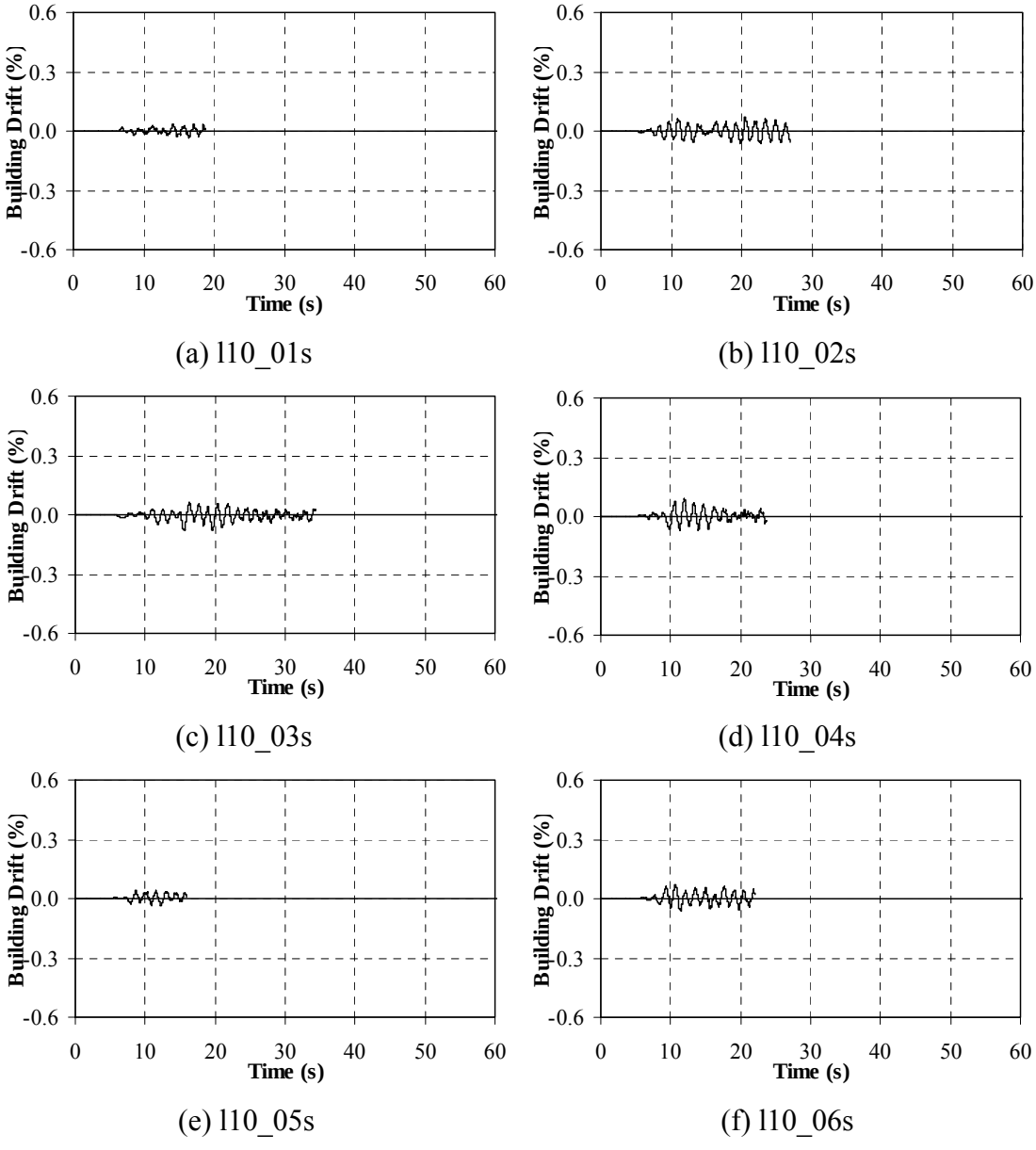

Fig. A.1. Building drift time histories for 10% in 50 years St. Louis Motions

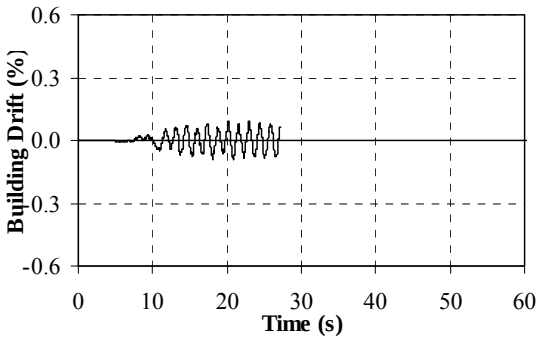

(g) l10_07s

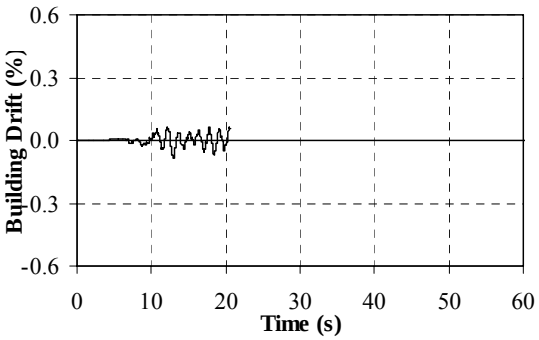

(h) l10_08s

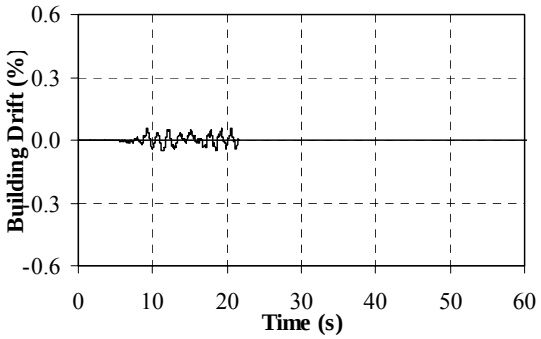

(i) l10_09s

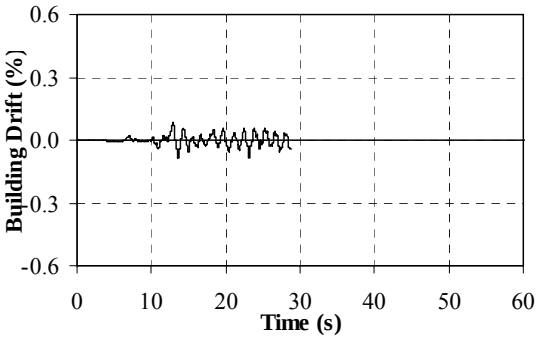

(j) l10_10s

Fig. A.1. Continued

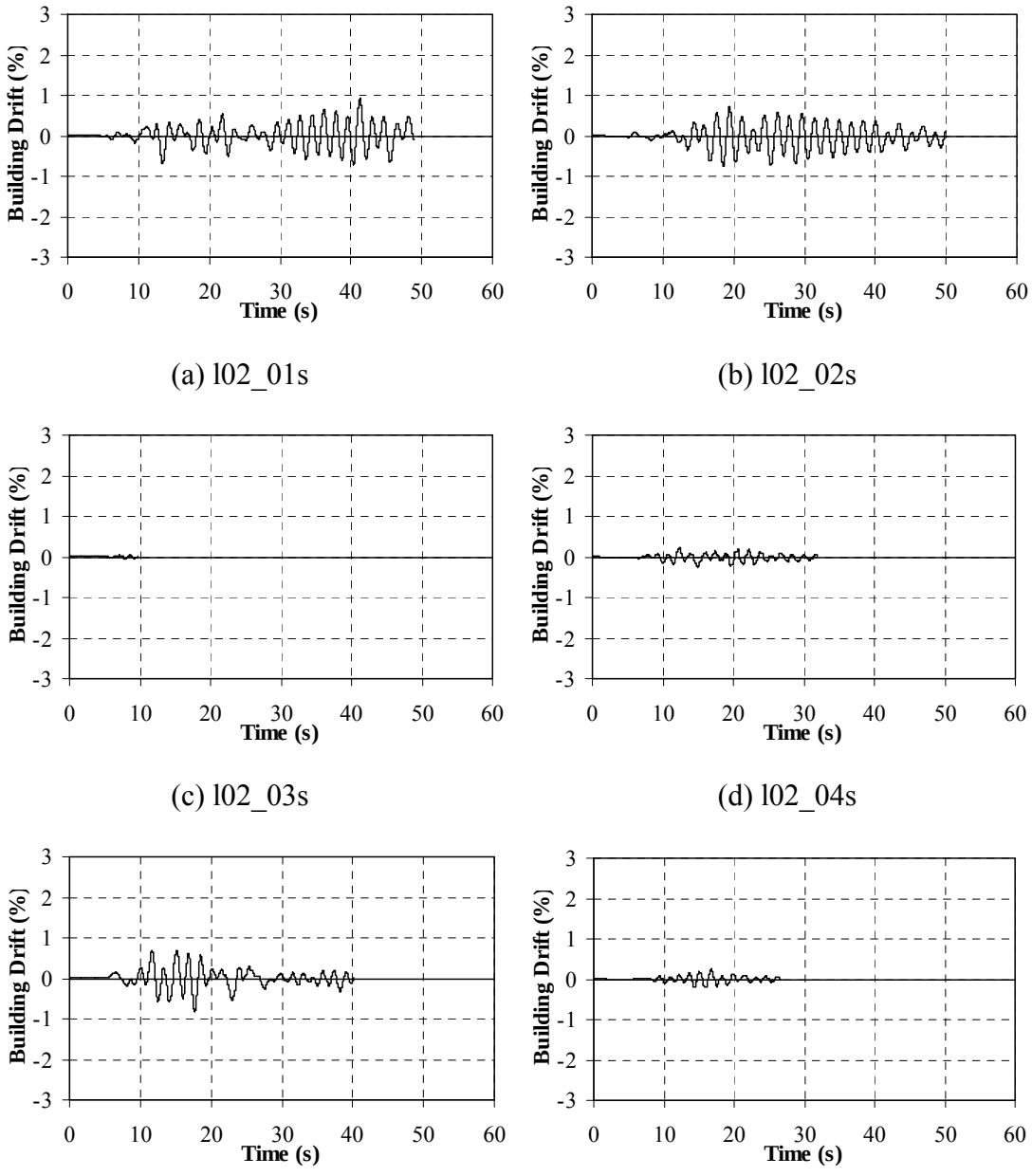

Fig. A.2. Building drift time histories for 2% in 50 years St. Louis Motions

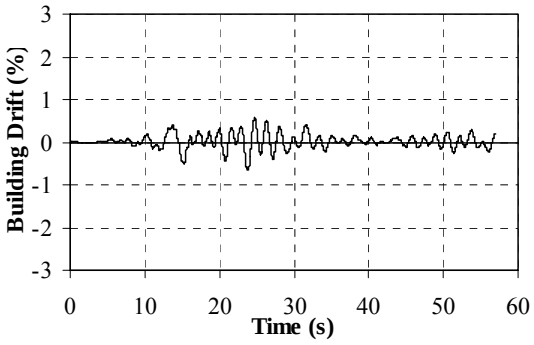

(g) l02_07s

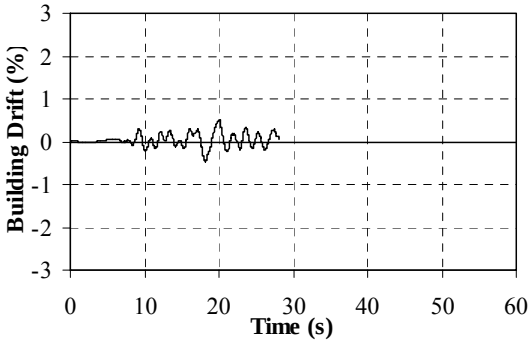

(h) l02_08s

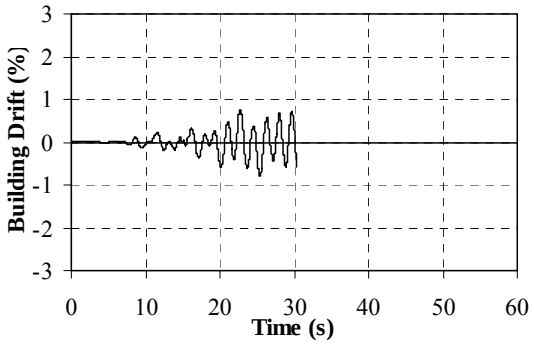

(i) l02_09s

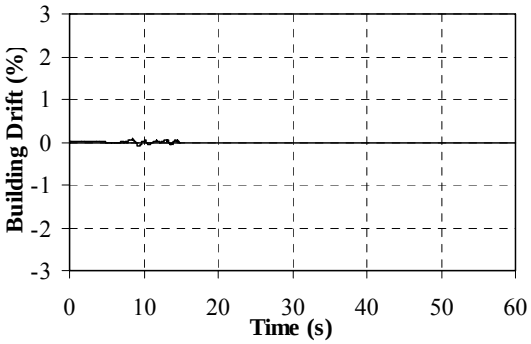

(j) l02_10s

Fig. A.2. Continued

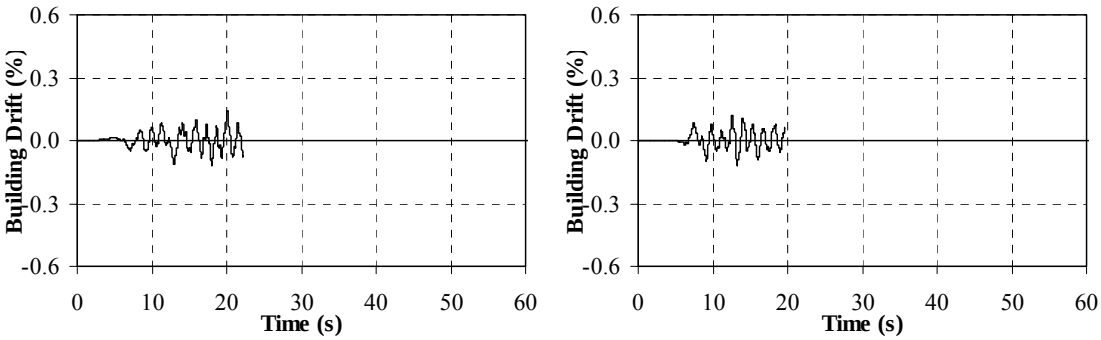

(a) m10_01s

(b) m10_02s

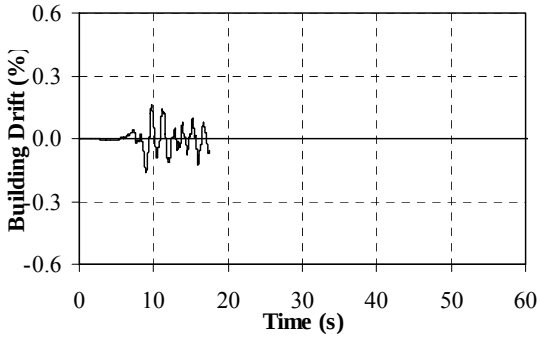

(c) m10_03s

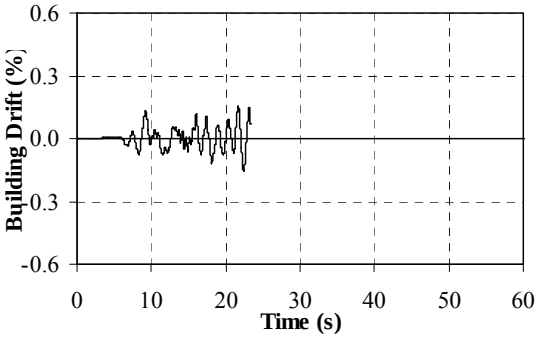

(d) m10_04s

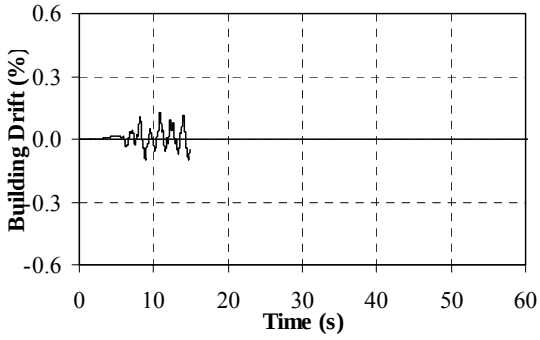

(e) m10_05s

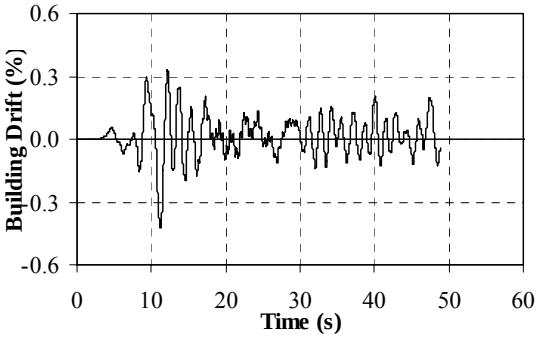

(f) m10_06s

Fig. A.3. Building drift time histories for 10% in 50 years Memphis Motions

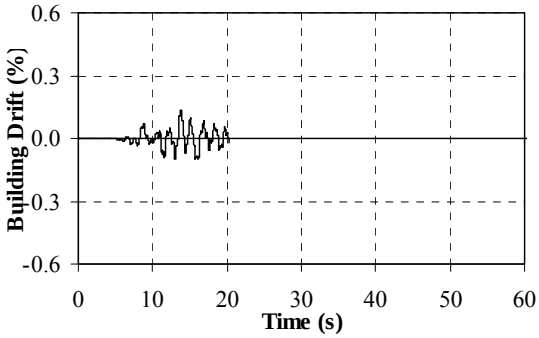

(g) m10_07s

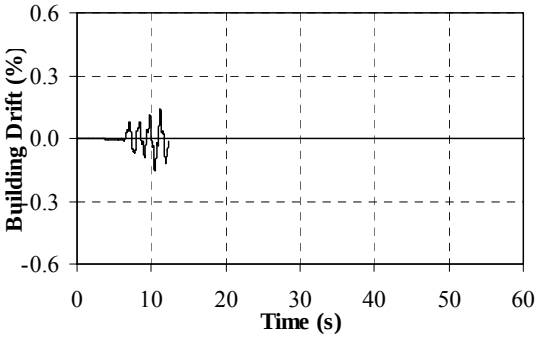

(h) m10_08s

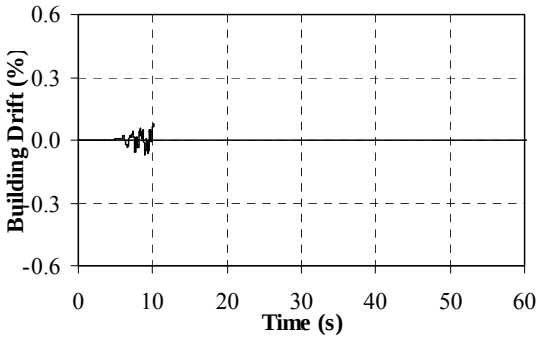

(i) m10_09s

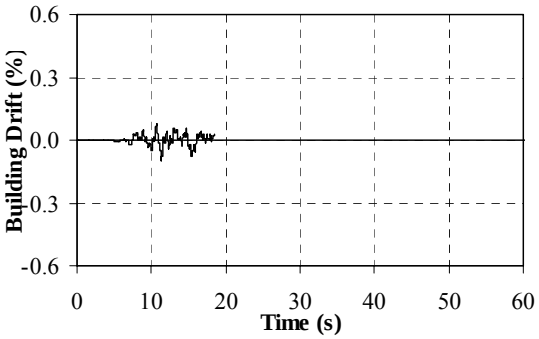

(j) m10_10s

Fig. A.3. Continued

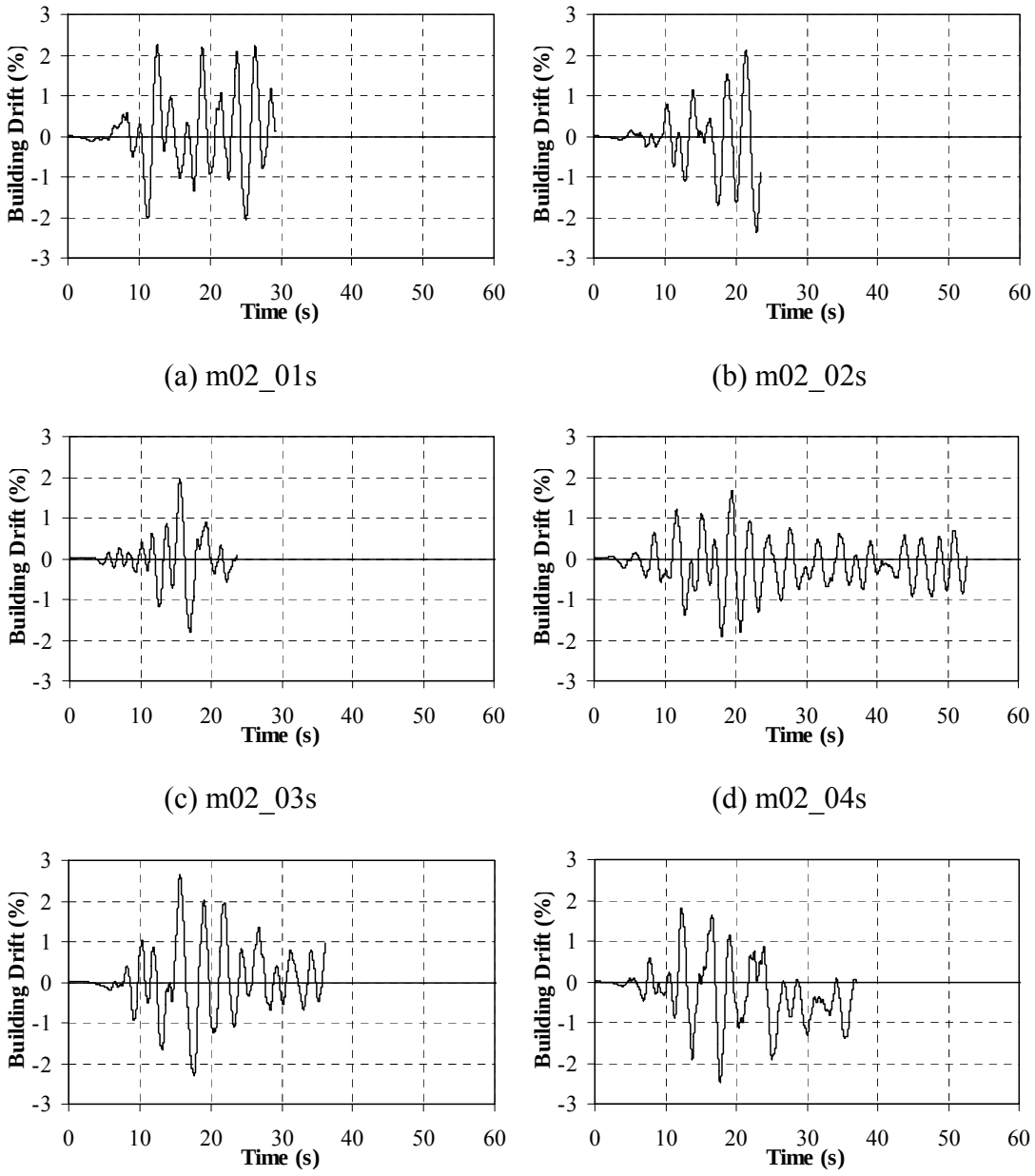

Fig. A.4. Building drift time histories for 2% in 50 years Memphis Motions

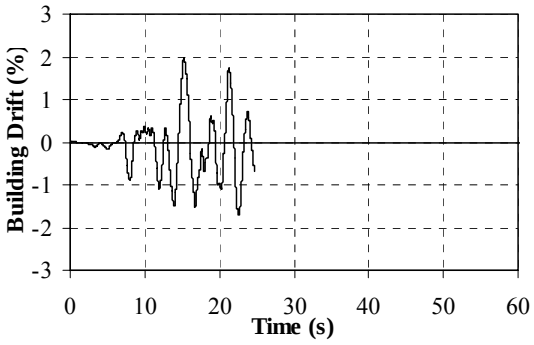

(g) m02_07s

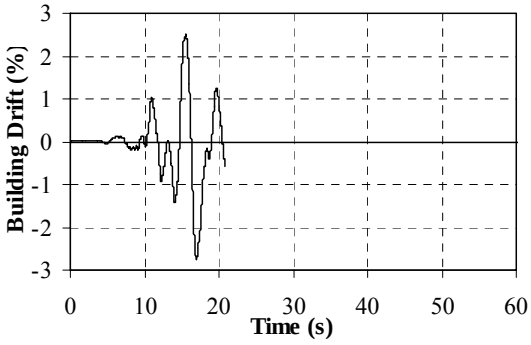

(h) m02_08s

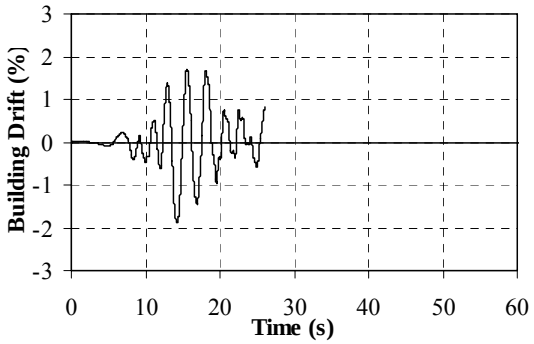

(i) m02_09s

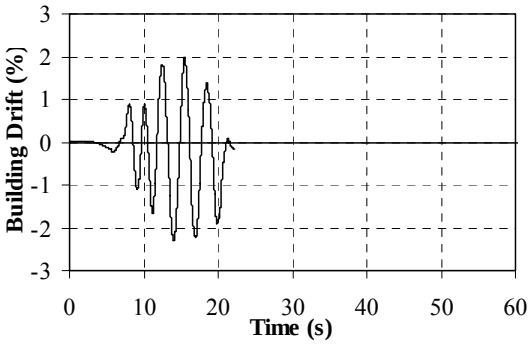

(j) m02_10s

Fig. A.4. Continued

VITA

Jong-Wha Bai was born in Seoul, Korea, on January 21, 1976. He studied at Yonsei University in Seoul, where he received the degree of Bachelor of Science in civil engineering in 2000. After graduation he enrolled in the master's program in civil engineering at Texas A&M University, where he has worked as a research assistant. He worked with Dr. Hueste and his research was focused on seismic retrofitting and evaluation for reinforced concrete (RC) structures as a part of the Mid-America Earthquake (MAE) Center project. He graduated in May 2004 with a M.S. degree in civil engineering from Texas A&M University (College Station, Texas). He can be contacted through the following addresses:

Jong-Wha Bai

3950 Highway 71 East #926
Bastrop, TX 78602

E-mail: jongwhabai@tamu.edu